DEFINING BIOMARKERS OF FRAILTY IN THE KIDNEY: IMPLICATIONS FOR ENDOBIOTIC AND XENOBIOTIC METABOLISM IN MICE

by

Maddison Hodgins

Submitted in partial fulfilment of the requirements
for the degree of Master of Science

at

Dalhousie University
Halifax, Nova Scotia
August 2023

Dalhousie University is located in Mi'kma'ki, the
ancestral and unceded territory of the Mi'kmaq.
We are all treaty people.

DEDICATION PAGE

I dedicate this thesis to my family, including all grandparents, aunts, uncles, cousins, parents, siblings, and pets. Phone calls and visits don't come often enough, but when they do, I am reminded of how supported I am.

Mom and dad, thank you for being my constant source of motivation, inspiration, and unconditional love.

TABLE OF CONTENTS

LIST OF TABLES

LIST OF FIGURES

ABSTRACT

Frailty describes individuals with increased susceptibility to adverse health outcomes. The frailty index (FI) quantifies frailty by measuring deficit accumulation. This project aimed to characterize the molecular signature of frailty in the mouse kidney to (a) identify biomarkers for frailty and (b) investigate the impacts of frailty on kidney metabolism. Age-matched female mice with high and low FI scores were selected for RNA sequencing (RNA-Seq). Seven metabolic genes were differentially expressed upon comparing high FI to low FI mice, these included: *Ugt1a9/10*, *Cyp4a12a/b*, *Akr1c18*, *Pla2g12b*, and *Hdc*. Quantitative polymerase chain reaction (qPCR) was used to measure expression of these genes in mice with a gradient of FI scores. Finally, metabolic gene expression was examined in mice treated with the angiotensin-converting-enzyme (ACE) inhibitor, enalapril, which has been shown to attenuate FI scores. These data suggest that renal xenobiotic and endobiotic metabolism may be altered by frailty, but further work is necessary.

LIST OF ABBREVIATIONS USED

°C	Degrees Celsius
20-HETE	20-Hydroxyeicosatetraenoic acid
20α-HSD	20-Alpha-Hydroxysteroid Dehydrogenase
AA	Arachidonic Acid
ACE	Angiotensin
ADR	Adverese Drug Reaction
AKD	Acute Kidney Diseases and Disorders
AKI	Acute Kidney Injury
AKR	Aldo-Keto Reductase
ANOVA	Analysis Of Variance
ANS	Angiotensin II, Nephrectomy, and Salt
Ark1c18	Aldo-Keto Reductase Family 1, Member C18
BAM	Binary Alignment Map
bp	Base Pair
BUN	Blood Urea Nitrogen
cDNA	Complementary Deoxyribonucleic Acid
CKD	Chronic Kidney Disease
CPM	Counts Per Million
Cq	Quantification Cycle
CRP	C-Reactive Protein
CVD	Cardiovascular Disease

CYP450	Cytochrome P450
Cyp4a12a	Cytochrome P450, Family 4, Subfamily a, Polypeptide 12a
Cyp4a12b	Cytochrome P450, Family 4, Subfamily a, Polypeptide 12b
DEMG	Differentially Expressed Metabolic Gene
DNA	Deoxyribonucleic Acid
DO	Diversity Outbred
EDTA	Ethylenediaminetetraacetic Acid
EET	Epoxyeicosatrienoic Acid
eGFR	Estimated Glomerular Filtration Rate
FDR	False Discovery Rate
FI	Frailty Index
FP	Frailty Phenotype
gDNA	Genomic Deoxyribonucleic Acid
GFR	Glomerular Filtration Rate
GO	Gene Ontology
GSH	Glutathione
GSSG	Oxidized Glutathione
h	Hours
H2AX	H2A Histone Family Member X
Hdc	Histidine Decarboxylase
HDL	High-Density Lipoprotein
HETE	Hydroxyeicosatetraenoic Acid

Hprt	Hypoxanthine Guanine Phosphoribosyl Transferase
IGF-1	Insulin-Like Growth Factor 1
IL-10	Interleukin-10
IL-18	Interleukin-18
IL-6	Interleukin-6
KEGG	Kyoto Encyclopedia of Genes and Genomes
kg	Kilogram
L	Liter
Limma	Linear Models for Microarray and RNA-Seq Data
LN_2	Liquid Nitrogen
Log_2CPM	Log_2 Counts Per Million
Log_2FC	Log_2 Fold-Change
Lp-PLA_2	Lipoprotein Phospholipase A_2
mg	Milligram
min	Minutes
mL	Milliliter
MMP	Maximal Mappable Prefixes
mo.	Month
mRNA	Messenger Ribonucleic Acid
MS_{error}	Mean Square Error
NADPH	Nicotinamide Adenine Dinucleotide Phosphate
NCBI	National Center for Biotechnology Information

ng	Nanogram
nm	Nanometer
ns	Not Significant
PC	Principal Component
PCA	Principal Component Analysis
PCR	Polymerase Chain Reaction
pFDR	Positive False Discovery Rate
PLA_2	Phospholipase A_2
Pla2g12b	Phospholipase A_2, group XIIB
Ppia	Peptidylprolyl Isomerase A
Q_a	Critical Q Value
qPCR	Quantitative Polymerase Chain Reaction
RIN	Ribonucleic Acid Integrity Number
RNA	Ribonucleic Acid
RNA-Seq	Ribonucleic Acid Sequencing
rRNA	Ribosomal Ribonucleic Acid
RT-PCR	Reverse Transcriptase Polymerase Chain Reaction
SD	Standard Deviation
sec	Seconds
SNP	Single Nucleotide Polymorphism
STAR	Spliced Transcripts Alignment to a Reference
TAE	Tris-Acetate-Ethylenediaminetetraacetic Acid

TE	Tris-Ethylenediaminetetraacetic Acid
TMM	Trimmed Mean of M-Values
TNF- α	Tumour Necrosis Factor - Alpha
UDP	Uridine 5'-Diphospho-Glucuronosyltransferase
UGT	Uridine 5'-diphosphate
Ugt1a10	Uridine 5'-Diphospho-Glucuronosyltransferase 1 Family, Polypeptide A10
Ugt1a9	Uridine 5'-Diphospho-Glucuronosyltransferase 1 Family, Polypeptide A9
α	Alpha
Δ	Delta
µg	Microgram
µL	Microliter
µM	Micromolar

ACKNOWLEDGEMENTS

I would like to acknowledge all of the individuals who were involved in the completion of this work. Firstly, I am grateful for the help of Dr. Tobias Karakach, Dr. Karla Valenzuela, and all other members of the Karakach lab. The infinite support from my lab mates cannot go unrecognized, nor can their friendship. Next, I would like to acknowledge our collaborators at the National Research Council, including Jeff Gallant, Qing Liu, and Sonia Leclerc for their technical expertise. I would like to extend a huge thank you to Dr. Evelyn Teh at NRC (Halifax) for her ongoing guidance, inside and outside of the lab. Her commitment to the Bioanalyzer will not be forgotten. Furthermore, I would like to thank my committee members, Dr. Susan Howlett and Dr. Morgan Langille, for their dedication and advocacy throughout this project. Thank you to the Howlett lab members for their assistance, most notably to Peter Nicholl for both his technical support and softball managerial skills. I would like to thank Dr. Stefan Heinze for his wisdom, seemingly endless expertise, and consistent willingness to help. Additionally, I would like to mention Alex Young for his assistance with some tricky mathematics and for always having his door open. Thank you to all other Dalhousie faculty, staff, and students whose advice and encouragement has been deeply appreciated. The relationships that I have formed throughout this degree have been invaluable. I would like to acknowledge the Faculty of Medicine for assisting in funding this project through the 2022 FOM Graduate Studentship Award. Finally, I would like to extend a most heartfelt thank you to all of my friends and family, without whom none of this would have been possible.

CHAPTER 1 INTRODUCTION

1.1 General Overview

Frailty is an emerging public health crisis in Canada. More than 1.6 million Canadians are frail today, and this number is expected to increase to over two million in the next 10 years [1]. Frail individuals are more susceptible to adverse health outcomes, including falls, dementia, disability, and death [2–5]. Furthermore, frailty increases the likelihood of hospitalization, placement in nursing homes, and an overall decline in quality of life [6–8]. The implications of frailty for frail individuals, their families, and the health care system necessitate a better understanding of this syndrome.

Frailty is thought to manifest via a complex interplay of various mechanisms, including declining proteostasis, hormone dysregulation, deteriorating metabolism, inflammation, deoxyribonucleic acid (DNA) damage, and cellular senescence [9]. Furthermore, environmental exposures can exacerbate the development of frailty [9]. Although frailty is an increasingly important area of research, it is a difficult concept to study since it arises from a combination of mechanisms that are still unclear.

There is no gold-standard method for quantifying frailty [9]. Two main approaches for measuring frailty exist, but these measurements mainly rely on observational variables [10,11]. Thus, there is a need for validated frailty biomarkers. Molecular markers could enable earlier detection of frailty and may elucidate the causes of frailty originating at the cellular level [12]. Several biomarker candidates for frailty have been proposed, but none have been validated for use in clinical settings [13].

Frailty is characterized by a decreased physiological reserve across multiple organ systems [14]. However, an organ-specific approach may be useful in the study of frailty as it could reveal the molecular manifestation related to declining organ function. Moreover, understanding the effects of frailty in individual organs could permit the development of interventions to prevent organ deterioration and/or restore organ function [15]. Kidney function is particularly

susceptible to age- and frailty-related decline [16–18]. Despite this, the molecular mechanisms of frailty in the kidney have yet to be uncovered.

The main aim of this thesis is to associate transcriptional differences in the kidney with frailty. Broader goals include elucidating mechanisms in the kidney related to the pathogenesis of frailty and the proposition of frailty biomarkers.

1.2 Defining frailty, its implications for the health system, and current knowledge

Our understanding and definitions of frailty have changed over the past two decades, but the term is generally used to describe individuals with increased vulnerability to adverse health outcomes [19]. Frailty can explain the disconnect between chronological and biological age in which frail individuals appear weaker than their age-matched counterparts [20]. Frail individuals are more vulnerable to acute stressors and may experience a disproportionate change in health status in response to a minor infection, minor illness, or new drug [14]. Broadly speaking, this vulnerability results from impaired homeostatic mechanisms and functional decline across multiple physiological systems, which weaken the adaptive capacity of an individual [14,21].

Frailty presents challenges for public health and health policies. As our population ages, the study of frailty and its recognition in clinical environments becomes increasingly important [22]. Although frailty exists outside of the geriatric population, it is a common syndrome among older adults and understanding its causes and consequences is critical for managing the health needs of this growing group. Many studies attempt to understand the implications of frailty on the healthcare system and how healthcare can be better adapted to care for frail individuals with complex multi-system problems [22].

Given the detrimental effects of frailty on the healthcare system, there is also significant interest in identifying strategies to treat and manage frailty. The research in this area is broad, with a 2019 review of primary care interventions for frailty categorizing interventions into the following groups: physical exercise, health education, nutrition supplementation, home visits,

hormone supplementation, and counselling [23]. To date, there is no standard treatment option for frailty. Indeed, exercise regimens appear to be consistently successful, but it has yet to be determined which intervention is most effective [22]. Pharmacological interventions have also been considered for treating frailty. For example, the use of angiotensin-converting enzyme (ACE) inhibitors, commonly used to treat hypertension, have been used in observational studies and randomized control trials as potential interventions for reducing frailty [24–26]. ACE inhibitors have been shown to delay the loss of muscle strength in elderly women with hypertension [25]. Additionally, the ACE inhibitor perindopril was shown to improve exercise capacity in elderly people with functional impairment [26]. More recently, Keller et al. found that chronic treatment with enalapril, an ACE inhibitor, was able to reduce frailty in C57BL/6 mice [27]. Overall, the development of frailty interventions is expected to become increasingly important as frailty becomes more prevalent.

Despite the field of frailty growing steadily for the past 20 years, determining the most appropriate way to define and measure frailty remains an active area in frailty research [28–30]. Studying frailty requires a measure that considers social, psychological, cognitive, and physical health domains [31]. Therefore, much research has been dedicated to developing and refining multidimensional assessments that can capture these aspects of frailty [32–34]. Preclinical frailty models have more recently been developed and will enable more extensive frailty research [35].

A large portion of research has been devoted to understanding what might predict the development of frailty. It is well-established that old age greatly increases the chances of becoming frail [14]. However, frailty has also been associated with various chronic diseases in younger people and people with non-age-related diseases [36]. In the literature, frailty is often assessed in patients with liver disease, cardiovascular disease, chronic kidney disease, neurodegenerative disorders, cancer, and diabetes, among many others [37–42]. In addition to disease and old age, there are various psychological, social, environmental, and lifestyle factors which can influence the development of frailty [43,44]. The identification of risk factors for frailty is an area of research that continues to grow.

Another substantial area in frailty research aims to elucidate its biological mechanisms. There is no one cause of frailty, but attempts have been made to uncover some of the molecular underpinnings. Examples of mechanisms implicated in frailty are inflammation, DNA damage, decreased metabolism, hormone dysregulation, altered protein production, epigenetic alterations, and impaired stem cell regeneration [9]. Some studies look at the molecular manifestation of frailty specific to certain organs such as the brain, heart, and skeletal muscle [45–50]. The study of molecular mechanisms is likely to be even more popular with the progression of omics platforms, which permit studies of how frailty impacts the genome, epigenome, transcriptome, proteome, and metabolome.

1.3 Frailty versus aging

Aging and frailty are concepts often used interchangeably in descriptions of deteriorating health and decreased resilience. Both frailty and aging are described as functional impairments and can be used to predict mortality. However, while the likelihood of becoming frail increases with chronological age, the two are not the same [14].

Aging is a process characterized by progressive impairment in the functioning of cells, tissues, and organs, which eventually leads to death [51]. Aging involves the accumulation of deleterious changes which can occur as a result of development, genetic defects, environmental exposures, and disease [51]. Deterioration of molecular structures and cellular pathways reduces functional capacity, impairing homeostatic and homodynamic abilities [52]. Impairments in biological mechanisms, including apoptosis, senescence, and inflammation, can also contribute to the aging process [52]. Aging is most often measured chronologically, in which one's chronological age refers to the amount of time passed. Chronological age can be used to give an estimate of the number of age-related changes that may have accumulated and predict life expectancy [51].

Frailty is a state of accelerated aging in which an individual faces increased vulnerability to stressors and poor health outcomes compared to individuals of the same chronological age [14]. Frailty is commonly discussed in the context of aging, given that it is common in older adults. However, frailty can occur in younger individuals, particularly those with chronic health

conditions, such as human immunodeficiency virus, cancer, and cardiovascular disease (CVD) [36]. Frailty is, therefore, not an inevitable consequence of chronological aging but rather a syndrome that may occur throughout the aging process.

While chronological age can, in some instances, be used as a proxy measure of an individual's health status, the onset and rate at which aging progresses are highly varied between people, even with the same degree of exposure [36]. Frailty considers this heterogeneity amongst individuals of the same age. Additionally, unlike chronological age, the concept of frailty is dynamic because an individual can transition in and out of a frail state. Frailty is, therefore, a more functional measurement than chronological age and may be a better estimation of resilience. To conclude, frailty is indicative of biological age rather than chronological age, giving a more meaningful measure of one's health status.

1.4 Measuring frailty

Although numerous definitions and assessments for frailty exist, two models are most commonly used to operationalize frailty [14]. The first is the Frailty Phenotype (FP), from Fried and colleagues, in which frailty is viewed as a clinical syndrome defined by specific phenotypic presentations. For this model, five criteria are assessed: unintentional weight loss, weakness, low energy, slowness, and low physical activity [10]. Using this measure, individuals who score well across all categories are considered "robust". Individuals who score poorly in 1 or 2 categories are termed "prefrail", and individuals scoring poorly in 3 or more categories are said to be "frail" [10].

The second model is the Frailty Index (FI), from Rockwood and colleagues, which looks at frailty as a non-specific and multifactorial state characterized by the accumulation of various health deficits [11,53]. Health-related deficits can include signs, symptoms, laboratory abnormalities (e.g. urea and creatinine), and functional impairments [11]. The FI is calculated as a ratio of the number of deficits present to the total number of deficits considered [54]. The individual variables measured must cover a range of systems. Typically, variables are coded so that 0 indicates the absence of a deficit, 1 indicates presence, and 0.5 represents an intermediate state [54]. Once all

variables are summed, they can be divided by the total number of deficits being assessed to yield an FI where a value closer to 1 is very frail and a value close to 0 is non-frail.

The FI requires a more comprehensive clinical assessment compared to the FP in order to evaluate all the deficits [55]. However, the FI is a continuous measure, whereas the FP is discrete. Therefore, the FI can more precisely identify individuals of varying degrees of frailty and discriminate between those with moderate and severe frailty [14]. To maintain the continuous measure of the FI while minimizing patient participation, Howlett et al. investigated a modification of the FI, called the FI-lab, which would incorporate blood tests and routine physical assessments [12]. The FI-lab successfully identifies older adults with an increased risk of death, a conclusion that warranted further research regarding appropriate biomarkers for routine blood tests [12]. Blodgett et al. showed that an FI-lab constructed of only laboratory test values, pulse pressure, and blood pressure could predict increased mortality risk [56]. In this study, the FI-lab enabled the identification of frailty using subclinical health deficits as opposed to those that are clinically visible. The laboratory markers used for the FI-lab included measures such as albumin, bicarbonate, blood urea nitrogen, C-reactive protein (CRP), and creatinine. This FI-lab was proposed as a method to detect frailty earlier by using signs of aging at a cellular level [56]. As the field of frailty biomarker discovery grows, more markers could be used in combination for a biomarker-based FI. *Table 1.1* contrasts the frailty measures discussed, identifying the advantages and disadvantages of each.

Table 1.1. Contrasting frailty measures

Frailty Measure	How Frailty is Quantified	Key Advantage	Key Disadvantage
Frailty Phenotype (FP)	Assessment of 5 criteria	Ease of use	Discrete measure
Frailty Index (FI)	Ratio of health deficit accumulation	Continuous measure	Requires comprehensive assessment
Laboratory-marker Frailty Index (FI-Lab)	Ratio of health deficit accumulation using mainly laboratory markers	Continuous measure requiring minimal patient participant	Lack of validated biomarkers for frailty

1.5 Preclinical models of frailty

Frailty is frequently assessed as an outcome or prognostic measure of a disease or chronic condition in human populations. However, preclinical models provide the opportunity to investigate the mechanisms and potential interventions for frailty more extensively. The mouse is a commonly used model in aging research. Advantages of the mouse model include its short lifespan and the fact that they share genetic, metabolic, and physiologic similarities with humans [57]. Additionally, rat and canine models for frailty have been developed [35]. As with humans, preclinical models also employ the FI and FP approaches.

The FP approach has been applied to wild-type C57BL/6 male mice in which grip strength, walking speed, physical activity, and endurance were assessed [58]. The same FP measure was used in Fisher 344 rats by Miller et al. [59]. The FP assessment in dogs was developed by Hua et al. in which canines were assessed across five criteria: muscular weakness, exhaustion, activity levels, nutrition, and mobility [60]. Genetically modified C57BL/6-based homozygous interleukin-10 (IL-10) knockout mice (IL-$10^{tm/tm}$) have been used as a model to study frailty [61]. These mice had an age-associated increase in the pro-inflammatory cytokine interleukin-6 (IL-6) and age-associated changes in gene expression related to mitochondrial function and apoptosis [35,61]. Although frailty was not assessed in these mice, the IL-$10^{tm/tm}$ mice developed weakness, weight loss, low activity, muscle changes, and inflammation characteristic of the FP [35,61]. Generally, the FP approach in preclinical models is predominantly a physical measure of frailty and fails to consider other multi-system variables such as body composition and ocular deficits [35].

The FI approach has also been applied to animal models. The FI was initially used in C57BL/6 mice in which 31-items derived from four groups (basic metabolic status, activity levels, hemodynamic measures, and body composition) were used to assess deficit accumulation [62]. A simplified 8-item index was also created, but the few variables assessed were only related to physical frailty [62]. The clinical FI measured 31 items from the musculoskeletal, integumentary, vestibulocochlear/auditory, ocular/nasal, digestive/urogenital, and respiratory systems, in addition to signs of discomfort in C57BL/6 mice [63]. The clinical FI was also used in Fisher 344 rats, measuring 27 items across nine categories [64]. Finally, a variation of the human FI-lab was

created by Kane et al., which measured common laboratory markers in C57BL/6 mice [65]. An advantage of the FI approach versus the FP is that the whole body is considered to obtain a multi-system measure of frailty [35].

Sex differences in frailty are evident in human populations; although females have higher frailty scores, they tend to live longer [35]. However, in preclinical frailty models, sex-differences are less clear. Limited studies have found no difference between sexes [62,66]. Generally, studies using the FI assessment in mice have found that females are frailer than males [27,63,67]. Additionally, female mice were frailer than males in a study using the FP approach [68]. Yet, Herrera et al. concluded that FI scores were higher in male mice than female mice, and a study using the FI-lab in mice showed that males were frailer than females [65,69]. Sex differences could depend on animal strain and the frailty approach used, but there is evidence to suggest that sex differences do exist in preclinical models of frailty [35,70].

1.6 Biomarkers for frailty

Biomarkers are biological characteristics which can be objectively measured to give some insight into the physiological state of an organism [71]. Measurement of biomarkers can be valuable for detecting the presence or severity of a disease. Identifying and detecting biomarkers that reflect frailty-associated molecular changes could allow for early recognition of frailty before clinically detectable signs emerge. Fluctuations in the levels of such molecular markers may allow us to predict severity and implement appropriate interventions throughout the progression of frailty. A panel of biomarkers, used like the FI-lab, could facilitate the diagnosis of frailty.

Reliable biomarkers for frailty have yet to be validated for use in clinical practice, but there are some candidates that have been associated with various frailty measures [13]. These molecules can be broadly grouped into inflammatory, immune, endocrine, oxidative stress, epigenetic, and genetic markers [72,73]. Additionally, a group of common markers that can be assessed during blood collection have been associated with frailty [72]. The following paragraphs

give an overview of biomarkers that appear in the literature frequently but are not an exhaustive list of all biomarkers that have been studied in relation to frailty.

Inflammatory markers have been the most extensively studied biomarkers since inflammation has been implicated as a potential mechanism of frailty [72]. Generally, chronic inflammation is characterized by increased pro-inflammatory cytokines such as CRP, tumour necrosis factor-α (TNF-α), and interleukin-6 (IL-6) [73]. CRP is made in the liver and released by macrophages and T-cells. Predominantly, increased CRP has been associated with frailty [74–76]. TNF-α, mainly produced by activated macrophages, is found to be increased with frailty [74,75]. Likewise, IL-6 is also said to be elevated with frailty [74,75,77]. While CRP, TNF-α, and IL-6 appear to increase with frailty, associations were less clear in longitudinal studies, which warrants further research [72]. The immune system is vulnerable to dysfunction in response to stressors such as acute illness, infections, and inflammation. With the inability to properly regulate immune function, an individual would be particularly susceptible to adverse health outcomes and could be considered frail [73]. It is, therefore, unsurprising that immune biomarkers related to frailty have been identified. Increased white blood cell count, neutrophil count, monocyte count, and neopterin levels have been related to higher frailty [74,77–80]. Conversely, increased lymphocyte count and increased albumin were associated with lower levels of frailty [74,75,81].

In addition to common immune and inflammatory markers, markers related to hormones and oxidative stress have been studied. Dysregulation of the endocrine system is expected in frail individuals as homeostasis becomes impaired and the risk of frailty increases [73]. Low vitamin D levels have been shown to increase the incidence of frailty [76]. Low testosterone in males is said to be associated with higher frailty [82,83]. On the other hand, increased estradiol is associated with frailty in women [84]. Hormones related to glucose and insulin dynamics have also been measured. Adiponectin, involved in the regulation of glucose, and leptin, a hormone involved in hunger regulation, are both increased with frailty [85,86]. Growth hormones such as insulin-like growth factor 1 are involved in the maintenance of skeletal muscle, bone mass, and strength [73]. Unsurprisingly, frailty is more prevalent among people with lower levels of IGF-1[79,87]. Dysregulation of thyroid hormones can lead to weight loss and fatigue [73]. Reduction in free triiodothyronine has been associated with frailty [88]. Additionally, frailty incidence has been

associated with the accumulation of oxidative damage, which leads to physiologic dysregulation [10,89]. Isoprostanes are compounds formed from the peroxidation of fatty acids. The isoprostanes malondialdehyde and 4-hydroxynonenal were found to be increased with frailty [90–92]. Thiols are antioxidants integral to preventing and protecting cells from oxidative stress. Total thiol levels were reduced with frailty [93]. Glutathione (GSH) is one thiol which plays a large role in detoxification reactions. Oxidation of GSH to oxidized glutathione (GSSG) reflects a state of oxidative stress and affects cell survival. Although there was no change to GSH levels, GSSG was found to decline with frailty; thus, the GHS/GSSG ratio increased with frailty [92]. Protein carbonylation and derivatives of reactive oxygen metabolites are other markers for oxidative stress and were found to increase with frailty [93,94]. Likewise, 8-hydroxy-2'-deoxyguanosine, which signifies oxidative damage to DNA, showed a positive association with frailty [93].

Genetic and epigenetic studies are becoming more popular, and indeed the relationship between frailty and various genomic alterations is an emerging body of work. Single nucleotide polymorphisms (SNPs) are variants at a single position in DNA. SNPs of genes such as CRP, transcobalamin-2, interleukin-12 , and interleukin-18 (IL-18) have been associated with an increased risk of developing frailty [95–98]. Telomeres are repetitive nucleotide sequences that "cap" the internal regions of chromosomes. The association between telomere length and frailty is heavily debated. Some studies have found a relationship between frailty and the length of leukocyte telomeres, while others did not find any association [74,99–103]. In addition to genetic biomarkers, epigenetic markers, which involve changes to DNA that modify gene expression, have also been investigated. A global decrease in DNA methylation and methylation of CpG islands with high GC content has been observed with frailty [104,105]. One marker of DNA damage is phosphorylation at the C-terminal of the variant core histone, H2A histone family member X (H2AX) [106]. Increased phosphorylation of H2AX was seen with frailty [106].

Finally, there are common markers for frailty that can be measured via standard blood tests. Tissue plasminogen activator, fibrinogen, D-dimer, and factor VIII are involved in blood coagulation and thrombosis [72]. In general, an increase in all three markers was seen with frailty, although increased fibrinogen was not observed longitudinally [81,107–109]. Creatinine, a breakdown product of creatine and an indicator of low muscle mass, was decreased with frailty [109]. Total

cholesterol and low-density lipoprotein cholesterol levels were also reduced in frailty [82]. Lipoprotein phospholipase A_2 (Lp-PLA_2) and cystatin C can be quantified in the bloodstream; the former is often used to assess cardiovascular risk, and the latter serves as a marker of kidney function. Both Lp-PLA_2 and cystatin C were found to increase with frailty [90,109]. The protein klotho, a receptor for fibroblast growth factor-23, has been well-studied in relation to aging. Klotho has been shown to decrease with age, and high levels of klotho in blood plasma were associated with a lower risk of frailty [110,111].

Overall, there are several biomarker candidates for frailty related to a wide range of physiological systems and mechanisms. While promising, none of the biomarkers detailed above are universally recognized. The lack of biomarker validation can be attributed to several challenges and limitations.

1.7 Limitations to biomarker discovery

A common limitation of biomarker studies is a failure to match for variables such as sex, diet, lifestyle, and activity [112]. Furthermore, there has been inadequate ethnic and regional representation as most studies have been conducted throughout Europe and the Americas [113]. Another major limitation in frailty biomarker discovery is that many are considered markers of aging [20]. Therefore, fluctuations of some markers related to frailty could be associated with age, independent of the presence of frailty. Similarly, biomarker discovery for frailty is limited by a lack of specificity. For instance, IL-6 is a promising candidate. However, it is linked to inflammation and can be increased by various pathologic conditions, including autoimmune and inflammatory disorders. Therefore, it is not necessarily specific to frailty [114,115]. There is also a lack of consistency in sample collection and preparation, assessment tools, and omics technologies [112]. Frailty research is challenged by the lack of a universal definition and standard measure. In the literature, several biomarkers have been studied using the FP rather than the FI or vice versa. These factors limit the applicability of the biomarkers discovered to date [112].

Future studies should be more extensive and longitudinal to allow for follow-up and increase biomarkers' reliability [112]. Biases should be minimized by grouping and matching based

on demographic factors [112]. Integrating data from multiple omics methods (E.g. proteomics and metabolomics) could further increase the reliability of biomarkers [112]. Ideally, a successful biomarker or panel of biomarkers would be able to predict and distinguish the progression of frailty (prefrail from frail, or from low FI from moderate FI) and would be associated with clinical outcomes of frailty such as disability, quality of life, and mortality [20]. Since frailty biomarkers are often associated with other comorbidities a panel of frailty biomarkers will likely be used to address the issue of specificity [20,72]. In the longer term, biomarkers need to be trialled in a clinical setting to determine their reliability and diagnostic ability outside of the original populations [113]. More research will be required to determine the accuracy, specificity, and sensitivity of such biomarkers [112].

Another focus of future work should be mechanistic studies aimed at identifying the key pathways dysregulated with frailty [116]. Most of the existing literature has examined blood-based biomarkers for frailty. While these are convenient and non-invasive measures for clinical use, they do not necessarily clarify the molecular basis of frailty. A potential route for prospective studies would be to investigate the molecular manifestation of frailty in individual organ systems, allowing for additional mechanistic insight and highlighting specific altered pathways. This may be an opportunity to discover novel biomarkers for frailty where the components (proteins and metabolites) of dysregulated pathways could be correlated with frailty and measured in peripheral fluids, such as blood or urine, for diagnostic purposes.

1.8 Pathogenesis of frailty in organs and systems

Although frailty is often said to involve multi-system dysregulation and multi-organ dysfunction, little is known about how frailty manifests in physiological systems or impacts organ structure and function. The immune and musculoskeletal systems are perhaps two of the best studied systems regarding the pathogenesis of frailty, while the heart and brain are extensively studied organs. However, this is not to say that the mechanisms have been fully uncovered. While understanding the manifestation of frailty on individual organs and systems would be advantageous, it is challenging to study the effects of frailty in organs and systems independently, given that frailty involves a complex interplay of various systems.

One of the main topics in frailty research regarding the immune system is the concept of inflammaging. Briefly, inflammaging is characterized by immune dysregulation and a chronic pro-inflammatory state [117]. Inflammaging has been proposed as a marker of accelerated aging, and frailty is said to be a risk factor [118]. In this sense, one of the major impacts of frailty on the immune system seems to be a pathological upregulation of pro-inflammatory markers.

In terms of the musculoskeletal system, sarcopenia is frequently considered the physical manifestation of frailty [50]. Sarcopenia is a syndrome in which an individual experiences loss of muscle mass and strength [50]. Cesari et al. found that frailty was associated with lower muscle density and muscle mass as well as higher fat mass [45]. This study hypothesized that frailty-related differences in body composition were driven by an underlying chronic inflammatory status [45]. However, the associations were unchanged when adjusting for IL-6, CRP, and TNF-α concentrations [45]. Therefore, frailty appears to manifest in the musculoskeletal system through changes in body composition, but these changes seem to occur independent of systemic inflammation [45].

Structural and functional abnormalities appear to be a part of the manifestation of frailty in the brain. Kant et al. found that frailty is associated with cortical brain infarcts and reduced total brain volume and grey matter volume [47]. Another study observed that frail individuals have reduced functional connectivity between posterior regions of the parietal cortex and portions of the frontoparietal regions [49]. Thus, brain connectivity alterations are thought to contribute to the pathogenesis of frailty in the brain [49].

There are various frailty-related structural and functional changes in the heart. For example, sinoatrial node function was impaired with frailty due to electrical remodelling, including changes to electrical conduction and action potential morphology [48]. Fibrosis in the sinoatrial node was also associated with frailty in a mouse model of aging [48]. A mouse model assessing the impact of frailty on ventricular structure and function showed that cardiac hypertrophy and contractile dysfunction increase with age and are graded by frailty [46].

The pathogenesis of frailty in a select group of systems and organs has been summarized. However, there is limited literature classifying the basis of frailty elsewhere. The kidney is an underrepresented organ in this field of frailty research. This is concerning given that it is a vital organ with several excretory and regulatory roles necessary to sustain life.

1.9 Kidney anatomy and function

1.9.1 Basic kidney anatomy

The kidney is a highly vascular organ which carries out several roles crucial for maintaining homeostasis [119]. The nephrons are the functional units of the kidney. Each kidney contains approximately 1 million nephrons [119]. The microscopic structure of the nephron is complex but can be split into two parts, the glomerulus and the tubule system [119]. The glomerulus is a cluster of capillaries supplied by the afferent arteriole and ending with the efferent arteriole. It is surrounded by the cup-like Bowman's capsule, which leads to a segmented tubule system. Adjacent to the Bowman's capsule is the proximal convoluted tubule, which leads to the loop of Henle. The loop of Henle has ascending and descending limbs which flow to the distal convoluted tubule and end with the collecting tube and collecting duct [119]. The kidney has an outer layer, the cortex, and an inner layer, the medulla [119]. The collecting ducts of nephrons collectively open in the renal pelvis, part of the medulla [120]. *Figure 1.1* depicts the basic anatomy of the kidney [119].

Figure 1.1. Basic anatomy of the kidney.
This figure was adapted from Moinuddin & Dhanda [119]. **A.** Coronal section of the right kidney. **B.** Section of a kidney showing the position of nephrons.

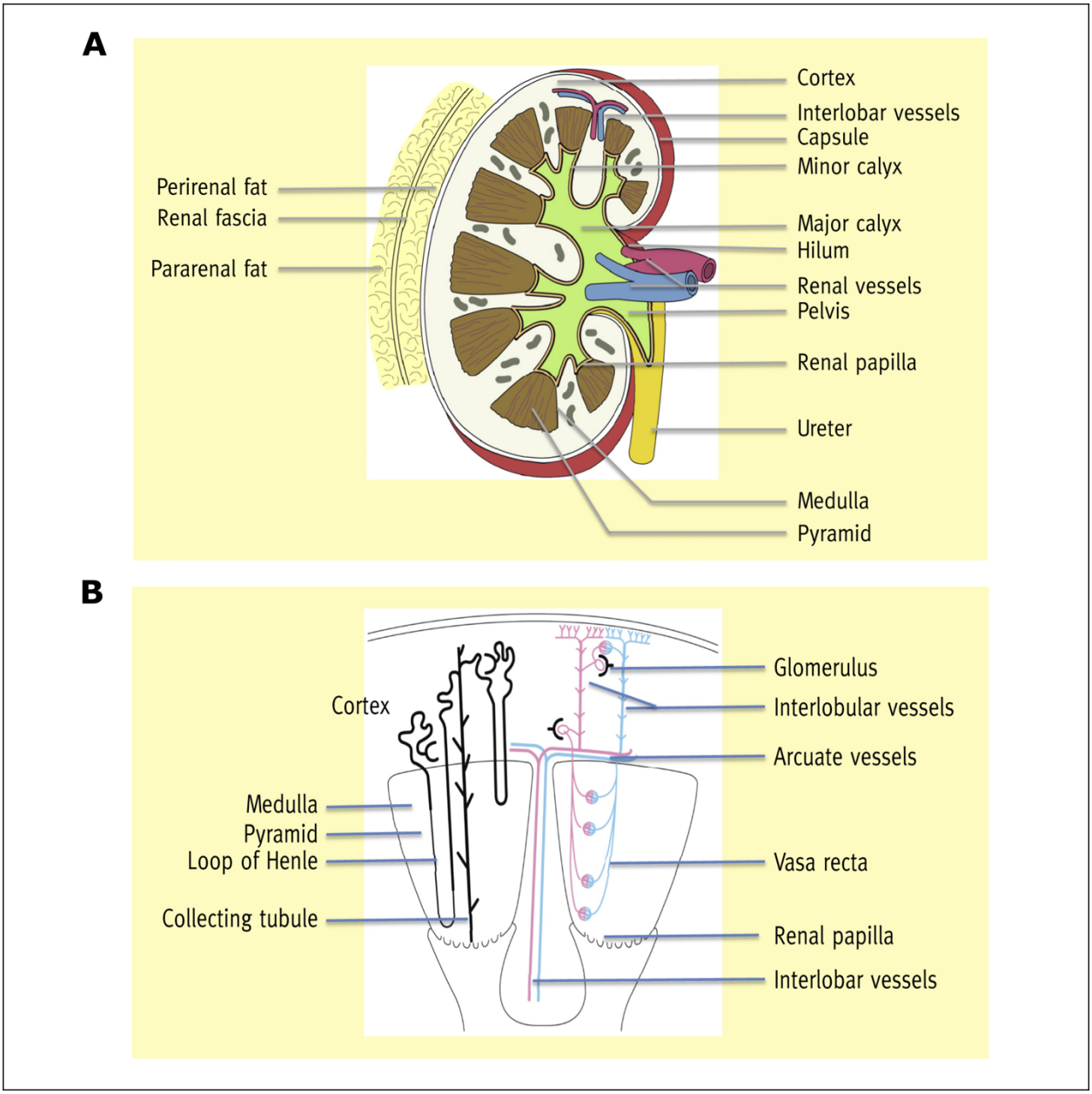

1.9.2 General kidney function

Renal function can be classified into five major groups: controlling fluid volume, maintaining acid-base balance, preserving electrolyte homeostasis, eliminating waste products, and acting as an endocrine organ [121]. The structure of the kidney permits these functions.
Maintenance of the volume and composition of extracellular fluids by the kidney is achieved by glomerular filtration. This filtration occurs across the capillaries of the glomerulus. The glomerular filtration barrier is composed of fenestrated endothelial cells, a basement membrane, and highly differentiated epithelial cells known as podocytes [120]. Water, small solutes, and low-molecular-weight proteins permeate the barrier and become the filtrate. In the tubules of the nephron, the filtrate is modified as fluids, ions, and molecules are reabsorbed and eliminated, influencing the composition of the urine [120]. Urine excretion can also be altered in response to various hormones, such as antidiuretic hormone [122]. Elimination of waste products can also occur throughout this process as organic molecules and drug metabolites can be secreted via transporters in the proximal tubule [120].

1.9.3 Common measures of kidney function

Glomerular filtration rate (GFR) and albuminuria are two methods of assessing renal function [123]. The best measure of kidney function is the GFR. Inulin is a substance used to directly measure GFR and is considered the gold-standard [124]. However, establishing the true GFR is impractical in clinical environments because it is time-consuming and relies on expensive exogenous markers, like inulin [124]. Instead, an estimated glomerular filtration rate (eGFR) can be determined to diagnose and monitor patients with chronic kidney disease (CKD). The eGFR relies on blood-based markers to approximate the kidney's filtering ability [125]. eGFR can be measured indirectly using endogenous markers such as blood urea nitrogen (BUN), serum creatinine, and serum cystatin C.

Urea was the initial marker for kidney function after urea was found to accumulate in the blood and decrease in the urine of those with diseased kidneys [126]. Then, in the early 1900s, BUN was introduced as a new measure [126]. BUN is still used to date as a measure of kidney function,

but it is considered suboptimal [125]. While increased BUN can be indicative of poor kidney function, its concentration can also be altered by extraneous factors, such as protein intake and gastrointestinal bleeding [125]. In the mid-1900s, serum creatinine was used preferentially over BUN, and it continues to be a widely used assessment of kidney function [125]. Creatinine is formed at a relatively constant rate, is freely filtered by the glomerulus, and is not reabsorbed. Although secreted at variable rates, creatinine-based equations have been created to account for this variation to estimate GFR. Serum cystatin C is a newer marker used to estimate GFR. It is like creatinine in that it is produced at a consistent rate and is freely filtered. However, cystatin C may be more reliable for determining the eGFR because its concentration appears to be regulated independently of age, sex, and muscle mass [127]. Other protein markers of eGFR include β2-Microglobulin and β-trace proteins which have similar advantages to cystatin C, though these markers require further validation [125].

Another method of assessing and staging kidney disease is albuminuria. Albuminuria refers to the abnormal presence of albumin in the urine due to kidney damage [123]. Albuminuria is used to assess kidney disease progression and has been associated with an increased risk of death [128].

In general, GFR is indicative of one of the most critical roles of the kidney: the ability to filter blood. GFR is the most useful measure for measuring renal function and diagnosing kidney diseases, but it is less informative in terms of metabolic impairments in the kidney [124].

1.10 The metabolic capacity of the kidney

Among the other physiological activities carried out by the kidneys, there is a notable capacity for the metabolism of xenobiotics (including drugs and non-drug exogenous substances) and endobiotics (endogenous substances).

The liver is universally regarded as the organ that contributes the most to the metabolism of drugs and xenobiotics, while the kidneys are responsible for their elimination [129]. Clearance of drugs via the kidneys occurs by a combination of glomerular filtration, tubular secretion, reabsorption, and the actions of renal transporters [130]. The kidneys have long been recognized for

their role in the elimination of drugs. Still, there is mounting evidence pointing to the existence of renal drug-metabolizing enzymes, including cytochrome P450s (CYP450s) and uridine 5'-diphospho-glucuronosyltransferases (UGTs) [130]. CYP450s carry out oxidative metabolism, part of phase I of biotransformation [129]. Renal glucuronidation is a major detoxification pathway. It is part of phase II biotransformation and occurs by UGTs [129]. Renal CYP450s and UGTs play a minor role compared to major drug-metabolizing organs like the liver, but they are undoubtedly significant to renal physiology and function [130].

Furthermore, renal CYP450s and UGTs play a role in endobiotic metabolism. Some subfamilies of CYP450s are responsible for the hydroxylation of fatty acids [131]. For example, renal CYP450 enzymes convert arachidonic acid to hydroxyeicosatetraenoic acids (HETEs). Subsequent glucuronidation of HETEs by UGTs modulates their biological activity and aids their elimination from the kidney [131]. More research is needed to better understand the metabolic potential of the kidney and the role of renal enzymes in the metabolism of endogenous substances, drugs, and exogenous non-drug chemicals.

1.11 The impact of age on kidney function

Aging affects all organs in the body, but the kidney is particularly susceptible to age-associated changes to structure and function, which may lead to renal pathologies. Changes to the kidney throughout the lifespan can predispose the kidney to injury via altered hemodynamics, oxidative stress, apoptosis, autophagy, inflammation, and decreased repair mechanisms [17]. Age-related micro-anatomical changes to the kidney include glomerulosclerosis, tubular atrophy, interstitial fibrosis, and hardening of small arteries in the kidney, which injures nephrons (nephrosclerosis) [132]. Several macro-anatomical changes to the kidney also occur with age. As aging progresses, there is an associated decline in kidney cortical volume. As the number of functional nephrons declines with age, there is a compensatory hypertrophic response from the remaining nephrons [132]. However, when hypertrophy of functional nephrons can no longer compensate for the effects of nephrosclerosis, there is a loss of total kidney volume. This loss of total volume becomes accelerated after approximately 50 years of age [132]. Additionally, kidney parenchymal cysts become larger and more abundant with old age [132]. In general, because of

structural and functional changes, the aged kidney is susceptible to podocyte injury, apoptosis, altered reabsorption in the tubules, altered urinary concentration, changes to the production of kidney-derived molecules and hormones, changes to the permeability of the glomeruli, and decreased GFR [132]. GFR is known to decrease with age, although the rate of decline has been debated in the literature and is often dependent on the measure used [125,133–135].

There are several conditions that involve impairment of kidney function. However, two major functional impairments are acute kidney injury (AKI) and CKD. AKI is defined as a sudden loss in the excretory function of the kidney [136]. AKI belongs to a broader spectrum of acute kidney diseases and disorders (AKDs) [136]. AKDs are characterized by a progressive deterioration in kidney function or persistent kidney dysfunction and are associated with a loss of kidney cells and nephrons [136]. AKDs can therefore lead to CKD, which is defined by persistent structural abnormalities, urine abnormalities, or impaired excretory function, suggesting a loss of functional nephrons [137]. A GFR of less than 60 mL/min/1.73 m^2 or albuminuria $\geq$ 30 mg per 24 hours for more than three months is used to diagnose CKD [138]. There is a bidirectional relationship between AKI and CKD where AKI can lead to the progression of CKD, and on the other hand, CKD is a risk factor for the development of AKI [139].

Old age is a significant risk factor for the development of CKD. Both men and women experience decreased renal function with age, and CKD is a very common clinical problem in the older population [140]. Furthermore, the risk of AKI increases with age and is especially prevalent in older adults [17]. CKD, comorbid conditions (including diabetes mellitus, hypertension, heart failure, and atherosclerosis), and medication use are common amongst the older population and contribute to the risk of AKI [17].

As renal structure changes throughout the aging process and kidney function declines, there is an impact on renal drug clearance. The number of functional glomeruli decreases, renal permeability declines, nephrosclerosis increases, renal blood flow decreases, and tubular function becomes impaired [141]. Therefore, the aging process can be expected to influence pharmacokinetics [141]. As renal function deteriorates, the clearance of drugs and drug metabolites is decreased, thus increasing drug plasma concentration and extending the drug's half-life [141]. Therefore, older

individuals are more susceptible to nephrotoxicity and adverse drug reactions (ADRs) [141,142]. In fact, the frequency of ADRs is said to be between three to ten times greater in older people compared to the younger population [142].

While the implications of age-related kidney dysfunction on drug clearance have been well-characterized, it is not known how renal metabolism is altered with age. Activity and content of CYP450 and UGT enzymes can decline with age, so alterations to the metabolism of both endogenous and exogenous substances by the kidney could be expected [143,144].

1.12 The impact of frailty on kidney function

The kidney has not been widely investigated in terms of frailty research. Typically, research surrounding frailty and the kidney focuses on assessing frailty in populations with CKD. It has been established that frailty is prevalent in kidney disease patients [18]. Increased frailty prevalence is associated with decreased GFR, so there is likely to be a link between CKD and frailty [18]. In a longitudinal study of older people, frailty status was associated with declining eGFR [16]. Considering that GFR is the most important marker of kidney function, frailty undoubtedly causes kidney dysfunction in some capacity. Although frailty-related impairments in renal function have been observed, the mechanisms that contribute to the development of kidney dysfunction with frailty have not been determined [18]. Furthermore, it is unknown how frailty impacts metabolic pathways in the kidney.

Although frailty is distinct from aging, age is highly associated with frailty. Therefore, age-related changes in the kidney could provide some insight into how the kidney might deteriorate with the progression of frailty. For instance, since drug clearance is reduced and susceptibility to ADRs is increased as a result of age-related structural and functional changes, a similar effect might be seen in frail individuals. Inhibition of renal CYP450s and UGTs might also be expected with frailty, contributing to the dysfunction of xenobiotic and endobiotic metabolic pathways. To speculate further, other manifestations of frailty in the kidney might predispose an individual to hypertension, metabolic syndrome, or diabetes, for example, since the kidney is related to their pathology and CKD is a risk factor for these conditions [145,146]. Adding to the complexity of frailty

research is the bi-directional relationship between frailty and disease. Hypertension, metabolic syndrome, diabetes, and other kidney dysfunction could be the result of pre-existing frailty, or the existence of these conditions could cause the development of frailty.

In general, there are few studies targeting the basis of frailty in the kidney, and there are no validated frailty biomarkers originating from kidney tissue. Further, there is a significant gap in the literature assessing how frailty manifests in the kidney at a molecular level.

1.13 Rationale, hypothesis, and objectives

Age-related structural, functional, and metabolic changes in the kidney have been identified. However, there is minimal literature looking at similar changes in relation to frailty. Characterizing the molecular basis of frailty in the kidney will provide a mechanistic explanation of how structural, functional, and metabolic dysfunction arises. Furthermore, the molecular aspect will allow for the discovery of novel biomarkers, including transcripts, proteins, and metabolites, that could be linked to the development of frailty in the kidney.

The use of molecular markers could allow for the detection of frailty prior to the observable manifestations of frailty. Identifying a panel of biomarkers that can be measured in peripheral fluids, such as blood or urine, could complement existing frailty tools for clinical use. Earlier detection could lead to the prevention and/or reversal of frailty. While frailty more frequently occurs in the geriatric population, young people can also be frail. A young person may not typically be subjected to a frailty assessment, but with a simple and non-invasive measure, frailty could more frequently be diagnosed in younger populations.

Mechanistic studies of frailty in the kidney would have implications for both clinical practice and future research. Identifying the molecular signature of frailty in the kidney could contribute to the practice of personalized medicine. With a better understanding of how renal function is impacted by frailty, clinicians could be better informed for designing suitable treatment plans. The consequences of frailty on metabolic processes in the kidney, such as drug metabolism, could be evaluated and used to determine the most appropriate medication prescription and dosage.

Research aiming to describe the mechanism of frailty in the kidney could promote further work proposing healthy aging interventions and discovering novel drug targets.

Hypothesis

Biomarkers associated with frailty can be identified by examining the differential patterns of gene expression in the kidneys of mice with varying degrees of frailty.

Objectives

1. Evaluate transcriptional differences in the kidneys of age-matched mice with low and high FI via RNA-Seq.

2. Validate the expression of differentially expressed metabolic genes identified via RNA-seq in the kidneys of age-matched mice with a range of low, intermediate, and high FI using qPCR.

3. Evaluate whether enalapril-mediated reduction of FI is related to variability in the expression of the differentially expressed metabolic genes related to frailty.

CHAPTER 2 MATERIALS AND METHODS

2.1 Model of study

The tissue used throughout this thesis was obtained from female C57BL/6J mice provided by Dr. Howlett (Pharmacology, Dalhousie University). Mice had been allowed to age over a period of study and were euthanized using pentobarbital sodium (200-300mg/kg ip) and heparin (100 units) to inhibit blood coagulation. Organs (kidneys and livers) were harvested and stored at -80 °C. Kidney tissue was collected in order to investigate the molecular basis of frailty in this organ. Livers were collected to be used as control tissue.

Three cohorts of mice were used throughout this thesis. Two of the cohorts were comprised of control/untreated mice that were allowed to age naturally without any intervention. The other cohort was comprised of mice from a study in which enalapril treatment was used. Conditions for the mice belonging to each of these three cohorts are described below.

Mice belonging to the control/untreated cohorts were group-housed in individually vented caging systems (Allentown Inc; 21 °C; 35% humidity) and kept on a 12h light/dark cycle in the Carlton Animal Care Facility at Dalhousie University. Mice had free access to food (ProLab RMH 3000, Purina LabDiet, Aberfoyle, Ontario, Canada) and water in their cages.

Mice from the enalapril-treated cohort were aged for approximately nine months and then started on the study [27]. Animals were kept in a 12h light/dark cycle with 1-5 mice per box. Mice were permitted *ad libitum* access to food and water. Initially, animals were fed Prolab RMH3000 (LabDiet, MO). Once the experiment began, mice were given Standard Grain-Based Control Rodent Diet with bacon-flavor (#F4059; Bio-Serve, Frenchtown, NJ) containing either enalapril (280 mg/kg) or no drug. Food and drug intake was estimated twice per month.

For all cohorts, animal protocols were approved by the Dalhousie University Committee on Laboratory Animals and studies were performed in accordance with the guidelines of the

Canadian Council on Animal Care (CCAC, Ottawa, ON: Vol 1, 2nd edition, 1993; revised March 2017).

2.2 Frailty assessment

End-point FI values for each mouse were collected by an external investigator using the Mouse Frailty Assessment Form© from Whitehead and colleagues [63]. The 31-item index evaluated deficits related to the integumentary, physical/musculoskeletal, vestibulocochlear/auditory, ocular/nasal, digestive/urogenital, and respiratory systems, as well as general discomfort. For each parameter, a "0" was assigned if a deficit was absent, a 0.5 was assigned for a mild deficit, and a "1" was assigned for a severe deficit. In addition, body weight and body surface temperatures were collected. For these variables, scores were given according to how much the mouse's weight and temperature varied from a reference mean. Reference means were obtained from a within-group calculation of mean and standard deviation. If values differed from the reference by less than ±1 standard deviation (SD), mice were given a 0 for that variable. Values that differed between ±1 SD and ±2 SD were given 0.25, between ±2 SD and ±3 SD were given 0.5, between ±3 SD and ±4 SD were given 0.75. For values that differed by more than ± 4 SD, they received the maximum score of 1. After totalling the scores for all 31 deficits, the FI was calculated by dividing the total by the number of deficits assessed. This generated an FI value between 0 and 1, where a higher number was indicative of a frailer mouse.

2.3 Samples used

2.3.1 RNA-Seq cohort selection

A total of eight female mice from the Howlett Lab tissue bank were selected for an exploratory ribonucleic acid sequencing (RNA-Seq) study based on their FI scores. If the investigators who conducted the FI scoring noted any observable kidney growths or abnormalities, those mice were not included in this study.

Boxplots were created to assess the distribution of the ages and FI scores of the mice used (Figure 2.3.1). Boxplots show the minimum and maximum values as well as the upper and lower

quartiles, in which 25% of values fall above or below, respectively. The median represents the midpoint of the data. Whiskers represent the upper and lower 25% of values. The interquartile range represents the middle 50% of values. Mice with extreme FI values were chosen, generating two groups of four mice each (Figure 2.3.1 A). The mice in both groups were selected to be of similar age to look at frailty decoupled from aging (Figure 2.3.1 B).

Mean values and standard deviations were also calculated to assess the centre and spread of the extreme FI groups. The first was a low FI group which had an average FI of 0.22 ± 0.01 and an average age of 25.90 ± 1.01 months. The second group was comprised of high FI mice with a mean FI of 0.46 ± 0.04 and an age of 25.50 ± 0.64 months. The ages of mice in the entire cohort ranged from 24.6 - 26.7 months. The average age of the whole cohort was 25.67 ± 0.81 months.

Figure 2.3.1. FI scores differ between high and low FI groups, but age is approximately the same.
Boxplots indicating **A.** Individual FI values of eight mice are plotted according to their respective FI group (low FI: n = 4, high FI: n =4). **B.** Ages (in months) of individual mice are plotted. Mice have been divided according to their FI group.

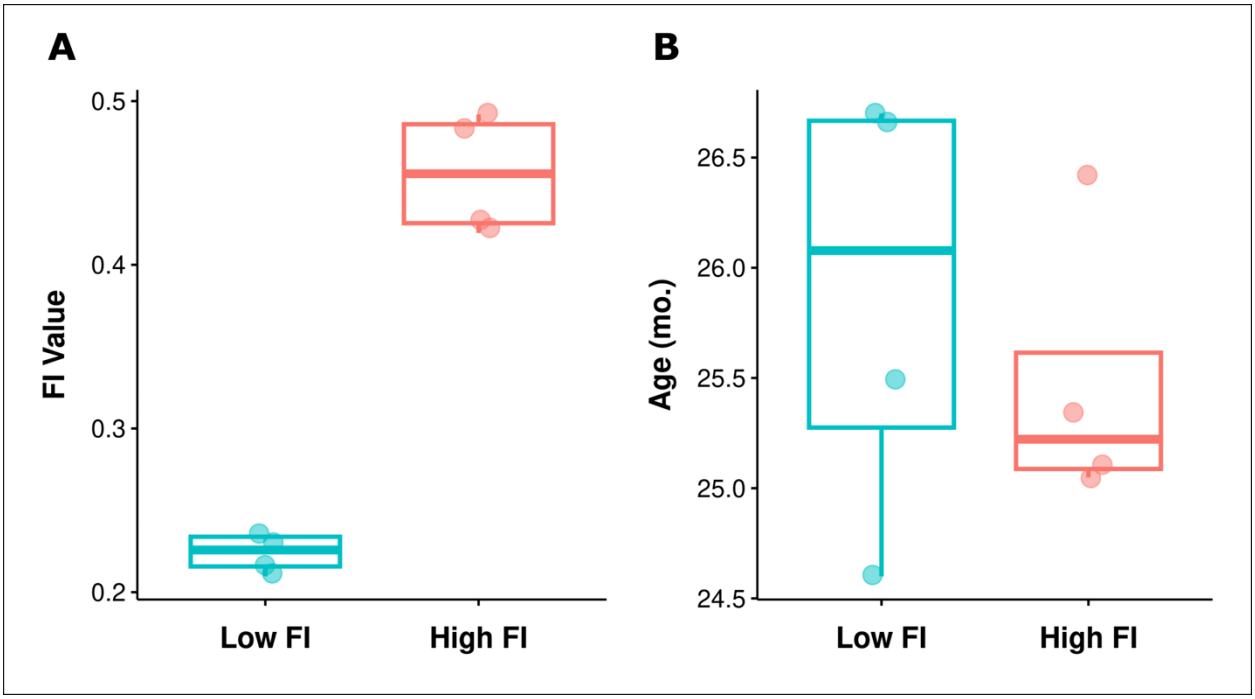

2.3.2 qPCR cohort selection

Kidney tissue from 16 female mice provided by Dr. Howlett was used for quantitative polymerase chain reaction (qPCR) experiments. A continuum of FI values was used to observe trends in gene expression as FI increased. The goal was to create a calibration curve in which gene expression can be used to predict FI.

Nine new mice with intermediate FI values were selected and divided amongst three mid FI groups, with three mice per group. Additionally, the high and low FI mice from the RNA-Seq cohort were also included in the qPCR cohort, with the exception of one sample. This sample, which belonged to the high FI group, had insufficient ribonucleic acid (RNA) remaining for qPCR assays. New RNA from the same kidney was extracted, but the sample was eventually excluded due to differences in sample preparation. Therefore, only seven of the eight RNA samples from the RNA-Seq cohort were used for qPCR.

The entire qPCR cohort was comprised of n = 16 samples divided into a low FI group (n = 4), three mid FI groups (n = 3 each), and a high FI group (n = 3). Descriptive statistics, including mean and standard deviation, were determined for the groups. The average FI score of the low FI group was 0.22 ± 0.01 and the average age was 25.90 ± 1.01 months. Mid FI 1 had a mean FI of 0.33 ± 0.00 and a mean age of 25.20 ± 0.24 months. The mean FI and age of Mid FI 2 were 0.37 ± 0.00 and 24.90 ± 0.54 months, respectively. The average FI score for Mid FI 3 was 0.40 ± 0.00 while the average age was 25.40 ± 0.69. Finally, the average FI for the high group was 0.47 ± 0.04 and the average age was 25.60 ± 0.73 months. Overall, the mean age of the entire qPCR cohort was 25.44 ± 0.70 months.

As with the original RNA-Seq study, mice belonging to the qPCR cohort were approximately the same age to control for the effect of chronological age. Boxplots were generated to observe the distribution of FI values and ages (Figure 2.3.2). While the FI values differed between the FI groups (Figure 2.3.2 A), the ages of mice in all FI groups were approximately the same, ranging from 24.43 – 26.7 months (Figure 2.3.2 B).

Figure 2.3.2. FI scores are different between groups, but age is approximately the same. **A.** Individual FI values of 16 mice are plotted according to their respective FI group (low FI: n =4, mid FI 1: n =3, mid FI 2: n=3, mid FI 3: n =3, high FI: n=3). **B.** Ages (in months) of individual mice are plotted. Mice have been divided according to their FI group.

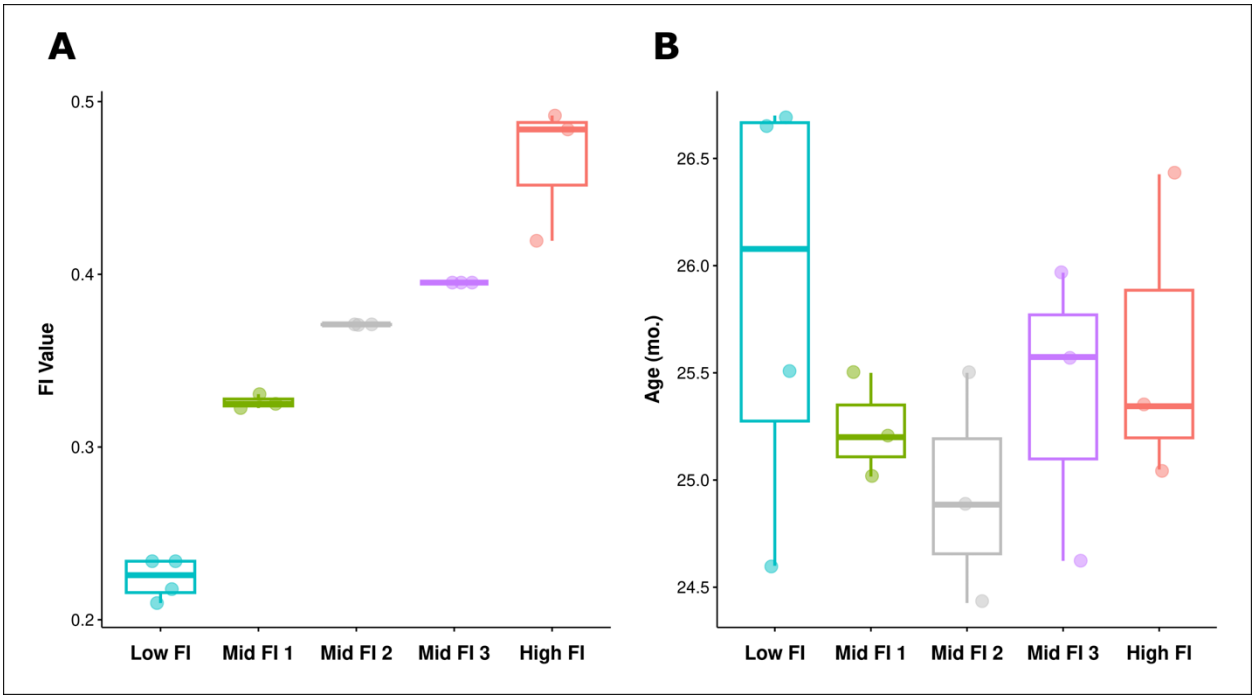

2.3.3 Enalapril study

Kidney tissue from 11 female mice provided by Dr. Howlett was used for qPCR experiments. These mice belonged to a previous trial which explored the potential for enalapril to attenuate frailty [27]. The control group consisted of five mice, and the treated group had six. All mice were considered middle-aged. Mice were allowed to age naturally for nine months, at which point the experiment began, and they received enalapril over the course of four months. Across four months of treatment, the mean enalapril dose was 29.7 ± 1.7 mg/kg/day for females [27]. The experimental design is depicted in *Figure 2.3.3*. Significant differences in average FI scores between the control and drug group were assessed using a t-test.

Figure 2.3.3. Enalapril study timeline in middle-aged female mice.
Timeline depicting the experimental design for the enalapril study from Keller et al. [27]. The final FI assessment occurred after four months of enalapril treatment when the mice were 13 months of age. At 13 months, the kidneys were harvested for further experimentation. FI = Frailty index.

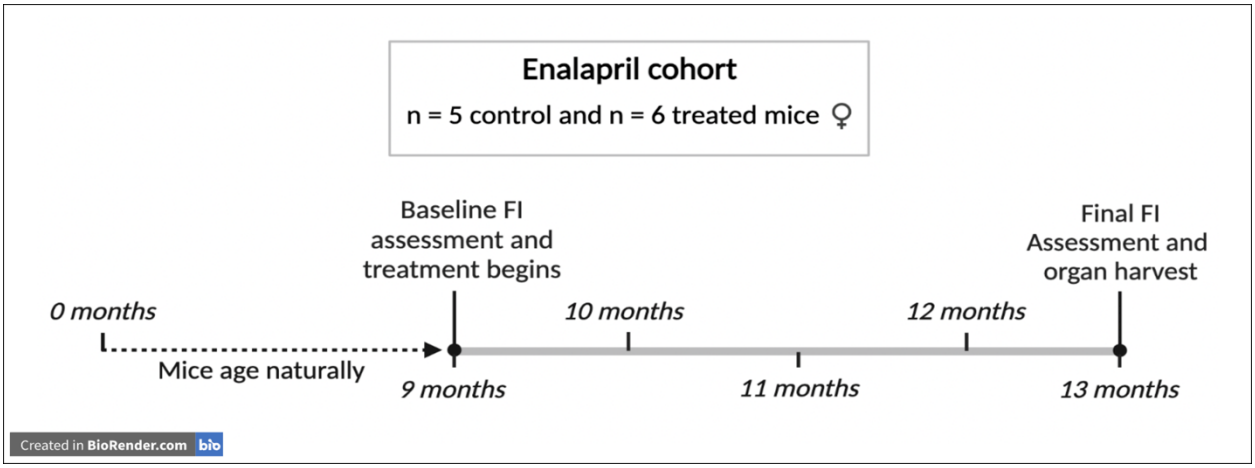

2.3.4 Takemon et al. transcriptomics dataset

Takemon and colleagues produced transcriptomic data from mouse kidneys at six months, 12 months, and 18 months of age [147]. Kidney tissue was obtained from 188 diversity outbred (DO) mice, 93 females and 95 males [147]. Expression of 22,259 genes was detected via RNA-Seq using a 100-base pair (bp) single-end Illumina HiSeq 2500, and the raw data was made publicly available [148]. For the purposes of this thesis, data from the 93 female mice evaluated in this study (33 mice at six months of age, 31 mice at 12 months of age, and 29 mice at 18 months of age) were used to observe the transcriptional changes that occur in the aging kidney. Raw messenger RNA (mRNA) counts were downloaded as a comma-separated value file to be used for future analysis [148].

2.4 Tissue pulverization

Intact kidneys, which had been stored at -80°C, were weighed and then cryopulverized using a mortar and pestle as described below. The mortar and pestle were chilled with liquid nitrogen (LN_2) prior to pulverization. An individual kidney was placed in the mortar with LN_2 and tapped gently with the pestle to create small pieces. These pieces were then ground into a fine powder. LN_2 was replenished as necessary throughout the process to ensure tissue remained frozen. The homogenized ground tissue was then transferred using a spatula to a 2 mL cryotube which was chilled on dry ice. The powdered tissue was stored at -80 °C until used. The mortar, pestle, and spatula were bleached, sprayed with RNaseZap™ RNase Decontamination Solution (Thermo Fisher Scientific, Cat. No. AM9780), and then rinsed with distilled water between each use.

2.5 Total RNA extraction

Two different RNA extraction protocols were carried out. A Zymo kit was used to isolate RNA to be used for RNA-Seq. Subsequently, a Qiagen kit was used to extract RNA to be used for qPCR assays. Both methods are described below.

2.5.1 Zymo extraction

To isolate RNA using the Zymo Direct-zol™ RNA MiniPrep Plus kit (Cedarlane, Cat. No. R2070), 40-50 mg of pulverized tissue was weighed and added to a nuclease-free two mL centrifuge tube followed by the addition of 800 µL of QIAzol lysis reagent (Qiagen, Cat. No. 79306). The tissue was lysed using a combination of vortexing and mechanical disruption with a mini pestle. Once the tissue was sufficiently lysed, the tubes were centrifuged (IEC Micromax) at 13,000 x g for one min. The supernatant was transferred to a new two mL centrifuge tube, and the pellet was discarded. Then, 800 µL of anhydrous ethanol (Commercial Alcohols, Car. No. P006EAAN) was added to the tube and contents were mixed by pipetting up and down. The mixture was transferred, 700 µL at a time, to the Zymo-Spin™ IIICG Column, which had been placed in a fresh collection tube. The column was centrifuged between each transfer at 13,000 x g for 30 sec, discarding the flow through. The column was washed by adding 400 µL of RNA wash buffer and centrifuging at 13,000 x g for 30 sec. Treatment with DNase I (provided in the kit) was completed by adding 5 µL of DNase to 75 µL of DNA Digestion Buffer and mixing. The DNase I mixture was added to the column and incubated at room temperature for 15 min. Twice, 400 µL of Direct-zol™ RNA PreWash was added to the column and centrifuged at 13,000 x g for 30 sec, discarding the flow-through in between. A final wash was performed by adding 700 µL of RNA Wash Buffer to the column and centrifuging at 13,000 x g for one min. Then, the column was transferred to a new nuclease-free tube. To elute the RNA, 50 µL of DNase/RNase-Free Water was added to the column and centrifuged at 13,000 x g for 30 sec.

2.5.2 Qiagen extraction

To isolate RNA using the RNeasy Mini kit (Qiagen, Cat. No.74104), 10-20 mg of pulverized tissue was weighed and added to a nuclease-free two mL microcentrifuge tube. Before proceeding with the manufacturer's directions, ten µL of 2-mercaptoethanol (Millipore Sigma, Cat. No. M7154) was added for every 1 mL of RNA lysis buffer, and four volumes of anhydrous ethanol was added to the secondary RNA wash buffer. Additionally, anhydrous ethanol was diluted to 70% using nuclease-free water (Thermo Fisher Scientific, Cat. No. AM9935). To begin, tissue was disrupted in 600 µL of RNA lysis buffer by pipetting up and

down and homogenizing with a mini pestle. The lysate was centrifuged at 8,000 x g for five min. For samples that were poorly lysed, an additional 200 µL of RNA lysis buffer was added, passed through a 20-gauge syringe 15 times, and spun again at 8,000 x g for three min. The supernatant was removed and added to a new two mL nuclease-free microcentrifuge tube. One volume of 70% ethanol was added to the lysate and was mixed by pipetting. The mixture was then transferred in 700 µL portions to an RNeasy Mini spin column, which was placed in a collection tube. The column was centrifuged at 8,000 x g for 15 sec, discarding the flow-through between transfers. Then, 350 µL of RNA wash buffer was added to the column and centrifuged at 8,000 x g for 15 sec, discarding the flow-through. Ten µL of DNase I was mixed with 70 µL of DNase digestion buffer from the RNase-Free DNase set (Qiagen, Cat. No. 79254) and was centrifuged briefly at 8,000 x g. The DNase I mixture was added to the column and left to incubate at room temperature for 15 min. Next, 350 µL of RNA wash buffer was added to the column, and it was centrifuged at 8,000 x g for 15 sec. Twice, 500 µL of secondary RNA wash buffer was added to the column. The column was centrifuged at 8,000 x g for 15s after the first addition and for two min after the second addition. The column was then placed in a new 2 mL collection tube and was spun at 8,000 x g for one min to dry the membrane. To elute, the column was placed in a 1.5 mL collection tube, and 50 µL of RNase-free water was added. After waiting five min, the column was spun at 8,000 x g for one min. The flow-through was removed and passed through the column again by centrifuging for 8,000 x g for another minute.

2.5.3 Quantification of RNA concentration using NanoDrop

To quantify RNA concentration, one to two µL of eluted RNA was read on a NanoDrop (Thermo Fisher Scientific, ND-1000) using DNase/RNase-free water as a blank. After obtaining concentrations, 260/280 ratios, and 260/230 ratios, the RNA was stored at -80°C for future use.

2.6 RNA sequencing

2.6.1 Assessment of RNA concentration and quality using Bioanalyzer

RNA concentration and quality were assessed on an Agilent 2100 Bioanalyzer. The RNA 6000 Pico Kit (Agilent, Cat. No. 5067-1513) was used according to the manufacturer's directions. Before use, the RNA ladder was heat denatured for two min at 70°C and then cooled on ice. Ninety µL of RNase-free water was added to the vial and mixed by vortexing. Aliquots were stored at -80 °C. To prepare the gel, 550 µL of RNA 6000 Pico gel matrix was placed in a spin filter and spun in a centrifuge for ten min at 1500 x g. The gel was aliquoted in 65 µL volumes and stored at 4 °C. Prior to running the Bioanalyzer, the ladder was thawed, kept on ice and all reagents were allowed to equilibrate to room temperature for 30 min. To prepare for the assay, the Bioanalyzer electrodes were cleaned by closing the lid over a chip containing 350 µL of RNaseZap for one min and then 350 µL of RNase-free water for ten sec. The lid was opened and left to dry for ten sec. To prepare the gel-dye matrix for use, the RNA 6000 Pico dye concentrate was vortexed for ten sec and spun down. One µL of the dye concentrate was added to a 65 µL aliquot of the filtered gel. The contents of the tube were vortexed to mix thoroughly. Next, the tube was spun for ten minutes at 13,000 x g at room temperature. To load the gel-dye mix, a new RNA chip was placed on the chip priming station. Nine µL of gel-dye mix was pipetted into the bottom of the RNA chip. On the chip priming station, the plunger was positioned at the 1 mL mark. The priming station was closed, and the plunger of the syringe was depressed until it was held by the clip. After 30 sec, the plunger was released and moved back to the 0.3 mL mark. After five sec, the plunger was slowly pulled to the 1 mL mark. The priming station was opened, and nine µL of gel-dye matrix was pipetted in gel-dye wells. Nine µL of RNA 6000 Pico conditioning solution and five µL of RNA 6000 Pico marker were added to wells on the chip. One µL of RNA Pico ladder was loaded into the ladder well. Then, one µL of each sample was added to the sample wells, and the chip was vortexed for one min at 2400 rpm (IKA Basic Vortex Mixer). The chip was placed into the Bioanalyzer, the lid was closed, and the "Eukaryote Total RNA Pico" assay was run. RNA integrity values (RIN) were determined by calculating the 18S to 28S band ratio [149]. RIN values were used to assess RNA quality.

2.6.2 Quantification of RNA concentration using gel electrophoresis

Electrophoresis separation of RNA was performed by preparing a 1.2% agarose gel using 1.2 g of UltraPure™ Agarose-1000 (Thermo Fisher Scientific, Cat. No. 16550100)

dissolved in 100 mL of 1X Tris-acetate-ethylenediaminetetraacetic acid buffer (TAE buffer: Tris-base, glacial acetic acid, EDTA). The melted agarose was poured into a gel tray with a comb in place. Once the gel was prepared, four µL of RiboRuler High Range RNA Ladder (Thermo Scientific, Cat. No. SM1821) was added. Four µL of RNA sample was mixed with five µL of 2X RNA Loading Dye Solution (Thermo Fisher Scientific, Cat. No. R0641) and one µL of ethidium bromide. The samples were heat denatured for five min at 65 °C and then chilled on ice for five min before loading. Electrophoresis was performed at 50 Volts for 60-90 min. The ChemiDoc™ XRS+ Imaging System (BioRad) was used for RNA visualization and imaging.

2.6.3 Ribosomal RNA depletion

Estimations of RNA concentration via NanoDrop, Bioanalyzer, and RNA gel electrophoresis were used to determine how samples would be diluted prior to ribosomal RNA (rRNA) depletion and library preparation. The ribosomal component of each RNA sample was depleted using the NEBNext® rRNA Depletion Kit (New England BioLabs, Cat. No. E7405L) following the manufacturer's directions. Briefly, samples were diluted to 400 ng of RNA in 11 µL of nuclease-free water in a 200 µL thin-walled polymerase chain reaction (PCR) tube. The RNA/probe hybridization reaction master mix containing two µL of NEBNext® v2 rRNA Depletion Solution and two µL of NEBNext® Probe Hybridization Buffer per RNA sample was assembled on ice in a 1.5 mL tube. Four µL of the master mix was dispensed into each tube of RNA, mixed thoroughly by pipetting up and down, and spun in a mini centrifuge. The tubes were placed in a thermal cycler (Applied Biosystems™, SimpliAmp™) with a heated lid set to 105 °C. The thermocycler program was as follows: 95 °C for 2 min, ramp down to 22 °C at a rate of 0.1 °C/sec, and then hold at 22 °C for five min. After the program was complete, the tubes were spun down and placed on ice. Next, the RNase H digestion reaction was prepared on ice. The RNase H master mix contained two µL of NEBNext® RNase H Reaction Buffer, two µL of NEBNext ®Thermostable RNase H, and one µL of nuclease-free water per RNA sample. The master mix was mixed thoroughly by pipetting, then spun down, and five µL was dispensed into each RNA sample. The sample tubes were mixed, spun, and incubated in the thermocycler for 30 min at 50 °C with a heated lid set to 55 °C. After, the tubes were centrifuged and placed on ice.

The samples were treated with DNase I again to eliminate any trace of DNA. For this, the master mix containing five µL of DNase I Reaction Buffer, 2.5 µL of NEBNext® DNase I, and 22.5 µL of nuclease-free water per RNA sample was prepared on ice. After mixing and spinning, 30 µL of the DNase I master mix was added to each tube of RNA. The tubes were mixed by pipetting, spun, and incubated in the thermocycler for 30 min at 37 °C with a heated lid set to 40 °C. The samples were then spun and placed on ice. Next, the RNA samples were purified using NEBNext® RNA Sample Purification Beads. RNA samples were transferred to fresh 1.5 mL tubes, and 90 µL of beads were added to each RNA sample, then samples were mixed by pipetting. RNA samples were incubated on ice for 15 min to allow the RNA to bind to the beads. Next, the tubes were placed on a magnetic rack, allowing the beads and supernatant to separate. Once the solution became clear, the supernatant was carefully removed and discarded, ensuring the beads were not disturbed. While the tubes were on the magnetic rack, 200 µL of 80% ethanol prepared from anhydrous ethanol was added to each tube and incubated at room temperature for 30 sec, then the supernatant was removed and discarded. This wash was repeated once. Residual ethanol was removed, and the beads were allowed to air dry for five min by leaving the tube lids open, being sure to avoid over-drying the beads (ensuring they were glossy and dark brown). Tubes were removed from the rack, and the RNA was eluted with seven µL of nuclease-free water. This was accomplished by mixing and then incubating for two min at room temperature. The tubes were transferred back to the magnetic rack and left for about two min until the solution cleared. Five µL of supernatant containing the RNA was removed and transferred to a 200 µL nuclease-free tube. Tubes were immediately placed on ice and stored at -80 °C until proceeding with library preparation.

2.6.4 Library preparation

Library preparation of rRNA-depleted samples was completed using the NEBNext® Ultra II Directional RNA Library Prep Kit for Illumina (New England BioLabs, Cat. No. E7765S) according to the manufacturer's directions. All reactions were carried out on ice unless stated otherwise. Beginning with RNA fragmentation and priming, the master mix was prepared by adding four µL of NEBNext® First Strand Synthesis Reaction Buffer, one µL of Random Primers, and five µL of nuclease-free water per RNA sample to a 1.5 mL tube. The master mix

was mixed thoroughly by pipetting, and five µL was dispensed into each rRNA-depleted sample. The contents of each sample tube were mixed and then placed in the thermocycler at 94 °C for 8 min as per the directions for partially degraded RNA (RIN = 2 to 7). The priming master mix was assembled by combining 8 µL of NEBNext® Strand Specificity Reagent and two µL of NEBNext® First Strand Synthesis Enzyme Mix per sample in a 1.5 mL tube and mixing thoroughly. Ten µL of the master mix was added to the primed RNA samples, pipetting to mix. Samples were incubated in a thermocycler with a pre-heated lid (80 °C) for 10 min at 25 °C, 15 min at 42 °C, 15 min at 70 °C, and then held at 4 °C. The second strand synthesis master mix was prepared by adding eight µL of NEBNext® Second Strand Synthesis Reaction Buffer with Deoxyuridine Triphosphate Mix (included in the kit), four µL of NEBNext® Second Strand Synthesis Enzyme Mix, and 48 µL of nuclease-free water per sample to a 1.5 mL tube and mixing thoroughly. Sixty µL of the master mix was added to the first strand synthesis product. Tubes were incubated for one hour at 16 °C without the heated lid. After incubation, RNA samples were transferred to new 1.5 mL tubes.

The newly made complementary DNA (cDNA) was purified by adding 144 µL of NEBNext® Sample Purification Beads to the samples. Tubes were vortexed and then incubated for five min at room temperature. The tubes were spun briefly to collect the sample, then placed on a magnetic rack to separate the beads from the supernatant. Once the solution cleared, the supernatant was removed and discarded, leaving the cDNA bound to the beads. Eighty % ethanol was prepared fresh from anhydrous ethanol, and 200 µL was added to each tube and was left to incubate for 30 sec at room temperature. The supernatant was discarded, and the wash step was repeated. Beads were allowed to air dry for five min on the rack with the tube lid open. Next, tubes were removed from the magnetic rack, and DNA was eluted by adding 53 µL of 0.1X Tris-EDTA (TE) buffer (provided in the kit). Beads were vortexed, spun down at high speed, and incubated for two min at room temperature. Tubes were placed back on the rack, allowing the solution to clear. Fifty µL of the supernatant was removed and transferred to a new 200 µL nuclease-free tube. Purified cDNA was stored at -20 °C overnight before carrying out the end prep reaction on the following day.

The end prep reaction includes end repair and dA-tailing. End repair involves the conversion of fragmented DNA to blunt-ended DNA with 5′ phosphates and 3′-hydroxyls. dA-tailing prevents concatemer formation during the subsequent ligation steps by incorporating a non-templated deoxyadenosine monophosphate on the 3′ end of a blunt DNA fragment. The end prep reaction master mix contained seven µL of NEBNext® Ultra II End Prep Reaction Buffer and three µL of NEBNext® Ultra II End Prep Enzyme Mix per cDNA sample. The master mix was mixed, and ten µL was dispensed into each sample. After mixing and spinning down, samples were incubated in a thermocycler with the heated lid set to 80 °C. The program was run for 30 min at 20 °C, and 30 min at 65 °C, and then the samples were held at 4 °C. Next, the ligation reaction was carried out. For 400 ng input of RNA, the NEBNext® Adaptor was diluted five-fold with the Adaptor Dilution Buffer. The ligation master mix was prepared by adding and mixing 1 µL of NEBNext® Ligation Enhancer and 30 µL of NEBNext® Ultra II Ligation Master Mix for each sample. Then, 2.5 µL of the diluted adaptor was added to the samples. This was followed by the addition of 31 µL of the ligation master mix, and then the samples were mixed thoroughly by pipetting. After spinning, the tubes were incubated in the thermocycler for 15 min at 20 °C. Following this, three µL of the USER Enzyme was added. Then, tube contents were mixed, and the tubes were incubated for 15 min at 37 °C with a heated lid set to 50 °C.

The ligation reaction was purified using NEBNext® Sample Purification Beads. First, the ligation reactions were transferred to new 1.5 mL tubes. Then, 87 µL of beads were added to each tube, vortexing the contents, and incubated at room temperature for ten min. Tubes were spun and placed on the magnetic rack. After allowing the solution to clear for approximately five min, the supernatant was collected and discarded. Next, 200 µL of 80% ethanol was added to each tube and left to incubate for 30 sec at room temperature. The supernatant was removed and discarded. This wash step was repeated a second time before removing all residual ethanol and air drying the beads for five min. Tubes were removed from the magnetic rack, and DNA was eluted using 17 µL of 0.1X TE. The tubes were vortexed and incubated for two min at room temperature, then placed on the rack to allow the solution to clear. Without disturbing the bead pellet, 15 µL of supernatant was transferred to a clean PCR tube.

PCR enrichment was completed using NEBNext® Multiplex Oligos for Illumina® (New England BioLabs, Cat. No. E7335S). Twenty-five µL of NEBNext® Ultra II Q5 Master Mix and five µL of Universal PCR Primer/i5 Primer per sample were added to a 1.5 mL tube and mixed. Thirty µL of the master mix and five µL of unique primer (Index (X) Primer/i7 Primer) was added to each of the samples. Samples were placed in a thermocycler with a heated lid set to 105°C for PCR amplification. The program included one cycle at 98 °C for 30 sec, 11 cycles at 98 °C for 10 sec and 65 °C for 75 sec, one cycle at 65 °C for 5 min, and ended by holding at 4 °C. The PCR reaction was transferred to 1.5 mL tubes, and 45 µL of NEBNext® Sample Purification Beads were added to each tube, vortexing to mix. Tubes were incubated for five min at room temperature, spun, and then placed on the magnetic rack. The beads were allowed to separate from the supernatant for five min; then the supernatant was removed and discarded without disturbing the beads. While they were on the magnetic rack, 200 µL of 80% ethanol was added to each tube and incubated at room temperature for 30 sec before discarding the supernatant. This wash was repeated once. Residual ethanol was removed, and the beads were allowed to air dry for five min by leaving the tube lids open, avoiding over-drying the beads. Tubes were removed from the rack, and DNA was eluted with 23 µL of 0.1X TE; then, the contents were mixed by pipetting, spun down, and incubated for two min at room temperature. Next, tubes were transferred back to the magnetic rack and left for about two min until the solution cleared. Twenty µL of supernatant containing the DNA library was removed and transferred to a new PCR tube.

2.6.5 DNA library quality check using Bioanalyzer

DNA quality was assessed on an Agilent 2100 Bioanalyzer. The DNA 1000 Kit (Agilent, Cat. No. 5067-1504) was used according to the manufacturer's directions. Before the assay, the Bioanalyzer electrodes were cleaned by closing the lid over a chip containing 350 µL of deionized water for ten sec. The lid was opened and left to dry for ten sec. To prepare the gel-dye matrix, the DNA dye concentrate, and DNA gel matrix were allowed to equilibrate to room temperature. The dye concentrate was vortexed and spun down. Twenty-five µL of the dye concentrate was added to a DNA gel matrix vial and vortexed. The gel-dye matrix was added to the top of a spin filterer which was centrifuged for 15 min at room temperature at 2500 x g. A

new DNA chip was placed on the chip priming station. Nine µL of gel-dye mix was pipetted into the bottom of the DNA chip. The plunger on the chip priming station was positioned at the 1 mL mark. Then, the chip priming station was closed, and the plunger of the syringe was depressed until it was held by the clip. After 60 sec, the plunger was released and moved back to the 0.3 mL mark. After five sec, the plunger was slowly pulled to the one mL mark. The priming station was opened, and nine µL of gel-dye matrix was pipetted into the wells of the chip. Five µL of DNA marker was added to the ladder well and to each of the 12 sample wells. One µL of DNA ladder (supplied) was added to the ladder well, and one µL of the DNA library samples was added to the sample wells. One µL of deionized water was added to the unused wells. The chip was vortexed for 60 sec at 2400 rpm (IKA Basic Vortex Mixer). Finally, the chip was placed into the Bioanalyzer, the lid was closed, and the "DNA 1000" assay was run. The electropherogram was checked to verify a narrow distribution with a peak size of approximately 200 bp.

2.6.6 DNA library quality check using qPCR

The concentration of the DNA libraries was assessed via qPCR using the NEBNext® Library Quant Kit for Illumina® (New England BioLabs, Cat. No. E7630S) according to the manufacturer's directions. Briefly, reagents were thawed and mixed. The NEBNext® Library Quant Buffer Mix was prepared by adding 100 µL of Primer Mix to the 1.5 mL tube of Master Mix. The 10X NEBNext® Library Quant Dilution Buffer was diluted 1:10 with nuclease-free water (Thermo Fisher Scientific, Cat. No. AM9935) and was mixed by vortexing. An initial 1:1,000 dilution of each library sample was prepared by adding one µL of the sample to 999 µL of 1X Dilution Buffer. Two serial dilutions were completed for each sample (1:10,000, 1:10,000) using the 1:1,000 dilution. For the PCR reaction, four µL of the DNA standards (NEBNext® Library Quant DNA Standards) or four µL of diluted library sample was added to 16 µL of Master Mix (with primers). The DNA standards and library sample reactions were run in triplicate. A no-template control was made with four µL of 1X dilution buffer and 16 µL of Master Mix (with primers). Reactions were mixed by pipetting. The plate was sealed and centrifuged at approximately 3000 x g for two min. The qPCR assay was run in a LightCycler 480 (Roche Diagnostics Canada) with the SYBR setting. The cycling conditions included an initial denaturation cycle at 95 °C for 1 min, then 35 cycles at 95 °C for 15 sec and 63 °C for 45

sec. To analyze the data, concentrations of the six NEBNext® Library Quant DNA standards were annotated. The concentrations of the diluted libraries (in triplicate) were obtained using the standard curve generated by the DNA standards. The average concentration of the 1:10,000 and 1:100,000 triplicate dilutions was calculated. Concentrations were adjusted using the average size of the DNA library and normalizing using the standard fragment size (399 bp). The concentration of the undiluted library stock was determined by multiplying by the appropriate dilution factor.

2.6.7 Sequencing and mapping

Libraries were sequenced on an Illumina Nextseq550 platform using a high-output flow cell (Illumina, Cat. No. 20024907), yielding up to 60 million reads per sample. Unmapped reads were received from the sequencing facility (National Research Council, Ottawa) in FASTQ format. These raw sequence reads were mapped to the mm10 mouse genome using a splice-aware algorithm, Spliced Transcripts Alignment to a Reference (STAR) [150]. The STAR algorithm works by searching for Maximal Mappable Prefixes (MMPs), the longest sequences that exactly match one or more locations of the reference genome [150]. Different parts of a read are mapped in separate portions which are referred to as seeds [151]. Therefore, the first MMP is seed1. Then, the unmapped portion of a read will then be considered, and the next longest sequence in that read, which matches the genome (the next MMP), will be seed2. STAR stitches together separate seeds to create a complete read. Seeds are stitched through a process of clustering based on proximity and scoring based on the number of mismatches and gaps [150]. Unlike other methods, STAR uses local alignment eliminating the need for a trimming step [152]. When it is not able to find an exact sequence match, MMPs are extended. If extensions do not provide a good alignment, poor-quality reads, and adaptor sequences are soft-clipped by STAR [152]. The aligned Binary Alignment Map (BAM) files were exported from STAR, and then counts were quantified by HTSeq using ENSEMBL GrCm39.109 gene coordinates [153,154]. HTSeq gives a read count associated with a gene by reporting how many aligned reads overlap its exons [154]. A file containing raw counts was exported for further analysis.

2.7 RNA-Seq data analysis and statistics

Raw mRNA counts from my RNA-Seq study and from Takemon et al. were analyzed using RStudio *Bioconductor* packages and code written in-house [155]. Briefly, the RNA-Seq data files (containing raw counts and ENSEMBL gene identifiers) and the sample metadata files were imported into RStudio. Counts per million (CPM) were obtained by dividing raw counts by the sum of the library (total library size) and multiplying by 1 million. Genes were filtered by the following criteria: (a) Only genes with at least 0.5 CPM in at least two of the samples were kept for further analysis, and (b) only genes whose expression summed to be greater than or equal to one when added across all samples were kept. Normalization factors were calculated and used for the weighted trimmed mean of M-values (TMM). TMM trims off the most highly variable genes and uses the normalization factor to adjust for library size [156]. CPM was then transformed into Log_2 counts per million (Log_2CPM).

2.7.1 Frailty analysis

Analysis of my data began with principal component analysis (PCA). PCA allows for the visualization of sample similarity in two-dimensional space by reducing a large dataset to a smaller one containing only the most important information. This is achieved by computing a covariance matrix and determining the principal components (PCs) which represent directions of the data which explain the most variance. Genes were sorted based on their variance, and the top 3000 most variable coding and non-coding genes from the kidney (Appendix A) were used for PCA plots. Ninety-five % confidence ellipses were constructed around a group mean point and were used to visually indicate the certainty with which a sample can be said to belong to its respective FI group.

A list of all known mouse metabolic genes was retrieved from the Kyoto Encyclopedia of Genes and Genomes (KEGG) database and was converted to ENSEMBL identifiers [157]. The genes in the RNA-Seq data file were matched to the complete list of mouse metabolic genes. From this point forward, analyses were completed using all metabolism-related genes, beginning with another PCA. Then, a linear model was constructed according to the Linear Models for Microarray and RNA-Seq Data (Limma) user guide [158]. The voom transformation was applied to

the normalized and filtered counts based on the previously constructed design matrix. The design matrix was specified for a single explanatory variable and excluded an intercept term [159]. Following this, a differential expression analysis was carried out via the Limma pipeline [160]. To determine differentially expressed genes, a moderated t-statistic was used. This is like an ordinary t-statistic, but it uses a Bayesian model to moderate the standard errors across genes by taking the ratio of the $\log_2$ Fold-Change (Log_2FC) to the standard error [158]. P-values were generated from the moderated t-statistic, and adjusted p-values were calculated using Benjamini and Hochberg's false discovery rate (FDR) [161]. Volcano plots were created by plotting $-\log_{10}$ of the adjusted p-values against the Log_2FC of the metabolic genes. Differentially expressed metabolic genes (DEMGs) were determined using an arbitrary Log_2FC cut-off of ≥ 2. A heatmap was used to visualize changes in DEMG expression and relationships between the samples. Z-score normalization was carried out on the Log_2 normalized read counts across samples for each gene. Z-scores were computed for each row by subtracting the mean expression value and dividing by the standard deviation. One minus Pearson correlation distance with average linkage was used to compute distances between samples, and clustering was performed using Euclidean distance with Ward's linkage. Following this, the TMM-normalized Log_2CPM of the DEMGs was used to create boxplots showing gene expression according to FI group. Statistical differences in gene expression between high and low FI groups were evaluated using a t-test. The DEMGs were also used for Gene Ontology (GO) enrichment analysis. The gene list of interest (containing the seven DEMGs) was mapped to the GO database to determine which GO terms are significantly enriched in the gene list compared to the background genes. The background genes used included all coding and non-coding genes that were identified in the mouse kidney via RNA-Seq. A one-sided Fisher's exact test was used to determine which GO attributes were enriched. P-values, adjusted p-values, and q-values were reported. P-values were calculated using a hypergeometric distribution:

$$p = 1 - \sum_{i=0}^{k-1} \frac{\binom{M}{i}\binom{N-M}{n-i}}{\binom{N}{n}}$$

Here, N represents the number of background genes, M is the number of genes annotated to the gene set of interest, n is the number of genes in the list of interest, and k is the number of genes from the list of interest that are annotated to the gene set. The FDR correction was applied

to adjust p-values for multiple comparisons. The q-value is an analogue of the FDR known as the positive false discovery rate (pFDR) [162]. Q-values represent the rate of false positives.

2.7.2 Aging analysis

After filtering and normalizing the Takemon et al. data, analysis involved creating boxplots in which gene expression, in Log_2CPM, was plotted against age, in months. Statistical differences in mean mRNA expression with age were determined using a one-way Analysis of Variance (ANOVA). Since the sample sizes of each group were unequal, the Tukey-Kramer post-hoc test was used. First, absolute mean differences were calculated between each pairwise comparison. Next, a critical Q value (Q_α) was determined from a Studentized Range Distribution according to the number of treatments and degrees of freedom. The critical range was determined using the following calculation, which assumes the groups have equal variance:

$$Critical\ range = Q_\propto \sqrt{\frac{\frac{MS_{error}}{n_i} + \frac{MS_{error}}{n_j}}{2}}$$

MS_{error} is the mean square error, and n_i and n_j denote the sample size of each group. Finally, the critical range was compared to the absolute mean differences. If the absolute mean difference was greater than the critical range, it was concluded with 95% confidence that there was a significant difference between the groups compared.

2.8 Quantitative polymerase chain reaction

2.8.1 Primers used in this study

Peptidylprolyl isomerase A (*Ppia*) and Hypoxanthine guanine phosphoribosyl transferase (*Hprt*) were chosen as reference genes, given their stability in C57BL/6NCrSlc female mouse gonads [163]. Primer sequences for *Hdc, Akr1c18, Ugt1a9, Ugt1a10, Cyp4a12a/b, Ppia, and Hprt* were publicly available on the *OriGene* website (Table 2.1) [164]. Sequences for *Pla2g12b* were obtained from a previously published study (Table 2.1) [165]. Primers had approximately the same melting temperature (~60 °C). Sequences were submitted to the National Center for

Biotechnology Information (NCBI) Primer-BLAST database to ensure there were no unintended targets [166]. Primers were purchased from *Integrated DNA Technologies.* Primers were resuspended in an appropriate amount of molecular-grade water to make a 100 µM stock solution. Tubes were vortexed and spun down. Ten µL of forward and 10 µL of reverse primer stock were combined with 80 µL of molecular-grade water for a 10 µM solution containing both the forward and reverse primers.

Table 2.1. Primers used in this study

Gene	Sequence	Amplicon size (bp)	Source
Hdc	For: 5'-GAGTACGCTGACTCCTTCACCT-3' Rev: 5'- CAGAGTTGGCATGTCGGAGGTA-3'	142	OriGene
Akr1c18	For: 5'-CAGTGGATCTCTGTGACACATGG-3' Rev: 5'- CTGGTTGCACACAGGCTTGTAC-3'	149	OriGene
Pla2g12b	For: 5'-GGTGTCGATATGGAAAGGCG-3' Rev: 5'- AACACTTGGTCATTGCTGGG-3'	135	Ming et al.[165]
Ugt1a9	For: 5'-TTGGTGGGATCAACTGCCTCCA-3' Rev: 5'- CGGAATCTCTGAGACCATGGATC-3'	122	OriGene
Ugt1a10	For: 5'-GACAGACCTCTTTAGCCCAGTG-3' Rev: 5'- CCAGAGGCGTTGACATAGGCTT-3'	165	OriGene
Cyp4a12a/b	For: 5'-CAGAGTGTCCTCTAATGGCTGC-3' Rev: 5'- GATGTCCAGGAAATCCAATCGCC-3'	154	OriGene
Ppia	For: 5'-CATACAGGTCCTGGCATCTTGTC-3' Rev: 5'- AGACCACATGCTTGCCATCCAG-3'	112	OriGene
Hprt	For: 5'-CTGGTGAAAAGGACCTCTCGAAG-3' Rev: 5'-CCAGTTTCACTAATGACACAAACG-3'	146	OriGene

2.8.2 Genomic DNA removal

Genomic DNA (gDNA) contaminants were removed by treating RNA samples with the RapidOut DNA Removal Kit (Thermo Fisher Scientific, Cat. No. K2981). Before proceeding with the manufacturer's directions, total RNA samples were diluted to 100 ng/µL with molecular-grade water based on the concentrations obtained from the NanoDrop. In a 1.5 mL tube, 17 µL of RNA sample, 1 µL of DNase I, and 2 µL of 10X DNase buffer with magnesium chloride were combined and vortexed. The samples were incubated for 30 min at 37 °C. DNase Removal Reagent (provided) was vortexed until it was completely resuspended before adding 1 µL to each reaction. Tubes were left to incubate at room temperature for 2 min, mixing gently 2-3 times. Tubes were centrifuged at 1000 x g for 1 min to pellet the DNase Removal Reagent. The supernatant containing the cleaned RNA sample was transferred to a new PCR tube.

2.8.3 Reverse transcription

Total RNA was reverse transcribed using iScript Reverse Transcription Supermix for reverse transcription polymerase chain reaction (BioRad, Cat. No. 1708841). To confirm that the concentration of the RNA samples surpassed the lower limits of the kit (50 ng/µL), seven samples were selected at random to read on the Nanodrop. Then, cDNA was generated as per the manufacturer's recommendations by adding 4 µL of iScript Reverse Transcriptase Supermix and 6 µL of molecular-grade water to 10 µL of RNA template. To generate a no-reverse transcriptase control reaction, five RNA samples were randomly selected and combined with 4 µL of iScript Reverse Transcription Supermix and 10 µL of molecular-grade water. The reaction mixes were then incubated in a thermocycler for 5 min at 25 °C, 20 min at 46 °C, and 1 min at 95 °C. cDNA sample concentration was measured using a NanoDrop, and samples were diluted with molecular-grade water to 50 ng/µL accordingly. The amount of molecular-grade water added to the cDNA samples was averaged to determine what volume to add to the no-reverse transcriptase controls.

2.8.4 qPCR reaction

For qPCR, the SensiFAST SYBR No-ROX Kit (FroggaBio, Cat. No. BIO-98005) was used according to the manufacturer's instructions. Reactions were carried out on 384-well PCR microplates (Axygen, Cat. No. 321-73-071). First, master mixes of the appropriate volume for the number of samples being tested were assembled. The master mixes contained the forward and reverse primer solution for each gene which had been previously prepared. To an individual well, 5 µL of SYBR, 0.8 µL of 10 µM forward and reverse primer mix, and 2.2 µL of molecular-grade water were added. Eight µL of the master mix for each gene was dispensed, and then two µL of the cDNA templates were added to the corresponding wells. Every plate had a positive control (cDNA from tissue known to express the gene of interest), no-reverse transcriptase control, and no-template control for each gene. All reactions were completed in triplicate. The plate was covered in film and centrifuged (Beckman Coulter, Allegra 25R) at 2,000 x g for one min. The reactions took place in a Roche LightCycler 480 (Roche Diagnostics Canada) with polymerase activation at 95 °C for two min followed by 40 cycles of 95 °C for five sec, 60-65 °C for 10 sec, and 72 °C for 10 sec. Fluorescence was measured at the end of each cycle.

2.8.5 Primer efficiencies

To assess primer binding, positive control tissue was used for primer efficiency calculations. First, it was determined which organ expressed the genes of interest and reference genes. Male mouse kidneys and livers were used since they have been shown to express these genes [167]. Kidney tissue from male C57BL/6J mice was used as a positive control for *Ppia, Ugt1a9, Ugt1a10,* and *Cyp4a12a/b* genes, while liver tissue from male C57BL/6J mice was used for *Hprt, Hdc, Akr1c18,* and *Pla2g12b.*

RNA extracted from the positive control tissues was diluted to 100 ng/µL using molecular-grade water. gDNA was removed, and the clean RNA concentration was determined on a NanoDrop. Reverse transcriptase and no-reverse transcriptase reactions were carried out for both tissues as previously described. cDNA concentration was measured on a NanoDrop before diluting the samples to 500 ng/µL using molecular-grade water. A 1:10 serial dilution was performed to give 500, 50, 5, 0.5, and 0.05 ng/µL of cDNA. Each dilution, a no-reverse transcriptase control, and no template control for every gene was plated in triplicate and read in a

LightCycler with the same program as above. Raw quantification cycle values (Cqs) from each triplicate were averaged. If Cq values were inconsistent and/or close to 35, the point was eliminated and not used in the subsequent slope calculations. Log_{10} values were calculated for each dilution where 500 ng/µL can be considered first value and be treated as "1". The "slope" function in Microsoft Excel was used to compute the slope of the regression between the Log_{10} values and the average Cqs. Primer efficiency was calculated using the following formula:

$$Efficiency\ (\%) = \left(10^{-1/Slope} - 1\right) \times 100$$

Primer efficiency is expressed as a percentage, where 90-110% efficiency is generally considered acceptable [168].

2.8.6 qPCR data analysis and statistics

Raw Cq values from all experiments were averaged, discarding any deviating values, to generate a single Cq value for each gene of interest and reference gene. Delta Cq (ΔCq) values were calculated by subtracting the Cq of the gene of interest from the mean Cq of the two reference genes. The mean number of mRNA molecules present for the gene of interest relative to the reference genes was determined by transforming the ΔCq values using the formula $2^{\Delta Cq}$. The transformed values were representative of the relative mRNA abundance for each treatment group. The data were presented as a fold-change relative to mRNA abundance for low FI samples, which were considered the reference group. A Log_2 transformation was applied to fold-change data, generating Log_2FC values.

When statistical significance between two FI groups was assessed, a t-test was used. Statistical differences between more than two FI groups were evaluated using an ANOVA, and post-hoc analysis was completed using the Tukey-Kramer method.

2.9 DNA gel electrophoresis

2.9.1 Agarose gel electrophoresis for qPCR product quantification

Electrophoresis of DNA was performed by preparing a 1.5% agarose gel using 1.5 g of Froggarose (FroggaBio, Cat. No A87-500G) dissolved in 100 mL of 0.5X TAE buffer. Five µL of Invitrogen™ SYBR™ Safe DNA Gel Stain (Thermo Scientific, Cat. No. S33102) was added to the melted agarose before pouring into a gel tray with a comb in place. Once the gel was prepared, three µL of 1Kb plus DNA Ladder (FroggaBio, Cat. No. DM015-R500) was loaded. To test the products of the qPCR reactions, sample triplicates were mixed together for a total of 30 µL. Five µL of 6X loading dye (New England BioLabs, Cat. No. B7024S) was added before loading 10 µL of the mixture into each well. Samples were subjected to electrophoresis at 100 Volts for 30 min. The G:Box Imaging System (Syngene) was used for DNA visualization and imaging.

2.9.2 Quantification of qPCR product in ImageJ

DNA bands were quantified in ImageJ by modifying a protocol typically used for the quantification of Western Blots [169]. First, the picture of the DNA gel was transformed to greyscale. In ImageJ, the measurement criteria were specified by selecting only "Grey Mean Value". The gel image was imported into ImageJ, and a region of interest was defined by drawing a rectangular frame over the largest band. Once the frame was properly sized, the selection was named with the gene of interest and saved. Bands representing the reference genes were also selected so they could be used as a loading control. For each gene, measurements were taken beginning, with the first lane and using the region of interest for that band in all other lanes. Additionally, a background measurement was taken by placing the frame somewhere around the band where there were no stains on the image. Measurements for each gene were recorded and exported into a spreadsheet in Microsoft Excel. Once all measurements were collected, the pixel density was inverted by calculating 255 – X, where X is the value collected from ImageJ. Next, the net value was calculated by subtracting the inverted background from the inverted band/loading control value. Once the net bands and loading controls were computed, the ratio of the net band over the net loading control (reference gene) was calculated. The final values were a relative quantification expressed as a ratio of the net band to net loading control. The values for each sample were averaged to produce a mean value for the low and high FI groups. A fold-change value was obtained by dividing the mean of the high FI group by the mean

of the low FI reference group. Fold-change values were generated to compare results to qPCR. Statistical differences between gel and qPCR results were evaluated using a t-test.

CHAPTER 3 RESULTS

Chapter three has been broken down into five sections that assess the objectives proposed in this thesis. In the first section, I optimized RNA extraction techniques to be used for subsequent experiments, including RNA-Seq and qPCR. The second section outlines the results of an exploratory RNA-Seq study and proposes differentially expressed metabolic genes (DEMGs), which may be associated with a high clinical FI (Objective 1). In the third section, I show that the differentially expressed genes identified are unique to frailty and do not fluctuate with age. Section four includes qPCR results in which differential metabolic gene expression is validated in groups of mice with extreme and intermediate FI values (Objective 2). Finally, section five aims to quantify frailty-related metabolic genes in mice treated with enalapril (Objective 3).

3.1 RNA extraction standardization

The overall goal of this project was to identify genes that could be associated with the clinical FI in a mouse model. To measure gene expression, total RNA was extracted from mouse kidney tissue and used for molecular techniques. To optimize RNA extractions, several isolation procedures were investigated using different kits, various starting tissue amounts and protocol adjustments. Nanodrop measurements were used to assess RNA yield. Nanodrop 260/280 and 260/230 ratios were also used as they are indicators of RNA purity. Protein and phenol contaminants can cause abnormal shifts in the 280 nm wavelength region. An optimal 260/280 ratio is ~2.0 [170]. Abnormalities in the 230 nm region usually indicate regent contamination. An optimal 260/230 ratio ranges from 2.0-2.2 [170].

The results of the various RNA extractions are summarised in *Table 3.1*. The first kit used was the Zymo Direct-zol™ RNA MiniPrep Plus kit. I began by using 12 mg, 26 mg, and 40 mg of kidney tissue. The RNA yield was 0.47, 0.19, and 0.97 ng/mg of tissue, respectively (Table 3.1). The 260/280 and 260/230 ratios from the extractions indicated contamination with proteins and/or reagents. While performing these extractions, I noted that lysing kidney tissue was challenging due to its fibrotic composition, likely reducing the RNA yield. A subsequent

extraction with 20 mg of tissue was completed, ensuring that the kidney was lysed sufficiently prior to loading the column by using a mini pestle. This extraction was more successful than the previous, with 260/230 and 260/280 ratios closer to the optimal ranges. Additionally, 8.31 ng of RNA was produced per mg of tissue (Table 3.1). To further improve RNA yield, an additional proteinase K step was added to the Zymo kit protocol. Proteinase K is a reagent used to inactivate nucleases that degrade RNA and digest unwanted proteins that contaminate nucleic acid preparations. Unexpectedly, proteinase K digestion reduced the RNA yield to 4.00 ng of RNA per mg of tissue. Still, excess tissue clogging the spin column was thought to decrease the RNA yield and contaminate the sample. Alternatively, to reduce tissue buildup in the column, an additional centrifugation step was performed after the tissue lysis, prior to loading the sample in the spin column. Adding a centrifugation step produced better results than Proteinase K (Table 3.1). The 260/280 and 260/230 ratios from this isolation were near the optimal values, and the RNA yield increased to 11.24 ng per mg of tissue (Table 3.1). Ultimately, the Zymo kit with an additional centrifugation step was used to prepare RNA samples for RNA-Seq.

An alternative RNA extraction kit from Qiagen, the RNeasy Mini, was also investigated. RNA was extracted from 10 mg and 19 mg of kidney tissue, yielding 21.31 and 14.37 ng/mg of RNA, respectively. Furthermore, the 260/280 and 260/230 ratios were close to the accepted values, indicating that there was no substantial contamination (Table 3.1). Therefore, using the Qiagen kit as per the manufacturer's instructions was deemed acceptable and was used to prepare RNA samples for qPCR experiments.

Table 3.1. Variables considered when selecting an RNA extraction protocol

Starting Tissue	RNA Extraction Method	Total RNA Concentration (ng/μL)	RNA/Tissue ratio (ng/mg)	260/280	260/230
12 mg	Zymo Direct-zol™ RNA MiniPrep Plus	5.59	0.47	1.40	2.23
26 mg	Zymo Direct-zol™ RNA MiniPrep Plus	4.82	0.19	1.32	1.24
40 mg	Zymo Direct-zol™ RNA MiniPrep Plus	38.70	0.97	1.42	1.16
20 mg	Zymo Direct-zol™ RNA MiniPrep Plus (using mini pestle)	166.22	8.31	2.04	2.11
20 mg	Zymo Direct-zol™ RNA MiniPrep Plus (adding digestion with Proteinase K)	79.95	4.00	2.02	2.16
20 mg	Zymo Direct-zol™ RNA MiniPrep Plus (additional centrifugation)	224.85	11.24	2.00	2.19
10 mg	Qiagen RNeasy Mini	213.05	21.31	2.12	2.27
19 mg	Qiagen RNeasy Mini	272.94	14.37	2.08	2.21

3.2 High versus low FI comparison via RNA-Seq

3.2.1 Selection of RNA samples for sequencing

Two RNA extractions were performed using kidneys from each of the eight mice in the RNA-Seq cohort. To determine which preparation would be used for sequencing, RNA sample quality and concentration were considered. RNA quality was assessed via Bioanalyzer by generating a RIN for each sample. The RIN gives an estimate of RNA degradation and is calculated based on the ratio of 28S:18S rRNA [149]. This generated a value ranging from 1-10, where a lower value indicates a more highly degraded RNA sample [149]. Typically, samples should have a RIN of about 7-8 to be used for sequencing [171]. However, none of the RNA extractions from any of my samples yielded a RIN within this range (Table 3.2.1). RIN calculations rely on rRNA indicators which have a low correlation with RNA integrity [172]. Furthermore, the RIN is not a direct measure of mRNA, which is the genetic material used to construct sequencing libraries [173]. Therefore, I proceeded with sample selection based on RNA concertation without considering the RIN.

RNA concentration was assessed via Nanodrop and Bioanalyzer reading(s). When Nanodrop and Bioanalyzer concentrations varied greatly for some samples, an RNA agarose gel was used to quantify the concentration of RNA by comparing band intensity to an RNA standard ladder. For example, RNA preparation 1 and 2 of sample 111-1 had inconsistent concentration readings (Table 3.2.1). Since there was disagreement between the Bioanalyzer and Nanodrop in the first preparation (111-1 (1)), it was subjected to RNA agarose gel separation. Using the RNA gel, the sample concentration was estimated to be ~ 200 µg/µL. Therefore, 111-1 (1) was chosen for sequencing. The same approach was used for selecting samples F429 (2), 110 (2) and 103 (2). The first preparation of sample 111-8 had a consistent concentration across the Bioanalyzer and Nanodrop with an average of 256.60 µg/µL, which was deemed high enough to use for sequencing. The Bioanalyzer and Nanodrop concentration readings for sample 115 (1) were relatively high, averaging 433.59 ng/µL. Therefore, despite the variation in readings between the individual methods (Nanodrop: 398.35 ng/µL and Bioanalyzer: 468.82 ng/µL), the lower concentration of 398.35 ng/µL was assumed. Samples OF2 (1) and F82620 (1) both had

consistent concentration estimations from the Bioanalyzer and Nanodrop. OF2 (1) was more than 250 ng/µL, and F82620 (1) was more than 150 ng/µL, so these samples were selected for sequencing. Overall, the RNA concentrations of the samples selected for RNA-seq ranged from 75 ng/µL to 398.35 ng/µL (Table 3.2.1).

The RNA samples selected for RNA-Seq had low RINs, so cDNA library construction was completed according to guidelines for partially degraded RNA (RIN = 2-7). When a quality check was performed for the DNA libraries, the Bioanalyzer report showed that the size of the majority of the DNA in each sample was > 200 bp (Appendix B). The Illumina NextSeq550 sequencing system allows for read lengths of up to 2 × 75 bp when using a high-output flow cell. Given that the sequencer does not read very long fragments, the quality of the DNA libraries was deemed acceptable for RNA-Seq.

Table 3.2.1. RNA-Seq sample quality and concentration

Sample (Extraction #)	Nanodrop concentration (ng/µl)	Bioanalyzer concentration(s) (ng/µl)	Bioanalyzer RIN	Gel Concentration (ng/µL)
111-1 (1)*	270.54	453.86	3.10	200
111-1 (2)	187.76	61.98/12.08	4/5.50	
111-8 (1)*	258.64	254.56	NA	
111-8 (2)	164.39	48.86/13.98	2.40/2.30	
OF2 (1)*	289.40	280.78	NA	
OF2 (2)	75.44	25.69/8.92	3.10/2.60	
F429 (1)	161.84	184.67	NA	
F429 (2)*	218.42	42.84	2.70	75
115 (1)*	398.35	468.82	2.30	
115 (2)	401.72	37.09	2.30	
110 (1)	174.13	151.97	5.60	
110 (2)*	254.47	11.30	NA	125
103 (1)	188.56	479.16	2.70	
103 (2)*	376.40	26.39	2.70	125
F82620 (1)*	174.51	165.57	NA	
F82620 (2)	84.69	10.07	3.40	

*Indicates RNA samples selected for RNA-Seq

3.2.2 Principal component analysis

After mapping raw sequence reads and filtering low-count genes, 20,034 coding and non-coding genes from the kidney tissue were identified by RNA-Seq. Gene counts were normalized, at which point PCA was used to simplify the complex dataset computing PCs that account for the greatest variation in the data. PCA scores plots show the clustering of samples based on their similarity.

I identified the top 3000 most variable gene transcripts from the kidney (Appendix A). To visualize the clustering of high FI and low FI mice, emphasizing maximal variation in gene expression, I created scores plots with the top 3000 genes. In doing so, 76.6% of the cumulative variance was explained by the first three PCs. Thus, looking at PCs one through three would reduce the dimensionality of my RNA-Seq data and enable me to plot the relationship between my samples in a 2-dimensional space. PCs 1, 2, and 3 explained 51.5%, 13.2%, and 11.9% of the variance, respectively. Frailty information was projected on the plot to visualize the grouping of high (red) and low (blue) FI samples. Visualizing PC1 and PC2 created groups in which 95% confidence ellipses of high and low FI samples overlapped considerably (Figure 3.2.1 A). However, plotting PC2 and PC3 produced groups of high and low FI samples in which the ellipses overlapped less, and FI groups could be distinguished across PC3 (Figure 3.2.1 B). Therefore, genes highly associated with the third PC could potentially be associated with frailty.

Having looked at the entire transcriptome, I was interested in further investigating metabolic changes that occurred in the kidneys of mice with high FIs. To determine if metabolic genes could explain a greater proportion of variance, I calculated principal components using only genes related to metabolism. All 1,447 metabolic genes identified were used to carry out PCA. Cumulatively, 80.6% of the variance was explained by PCs one, two, and three. These PCs were used to generate scores plots. Grouping of samples according to FI was observed across the first two dimensions. PC1 and PC2 accounted for 55.9% and 14.8% of the variation, respectively (Figure 3.2.2 A). The third PC only explained 9.9% of the variance. Plotting the second and third PCs resulted in overlapping 95% confidence ellipses and close proximity of samples belonging to the opposing FI group (Figure 3.2.2 B). Based on the better differentiation of FI groups across

dimensions 1 and 2 (Figure 3.2.2 A), frailty was more likely to be related to genes associated with PC1 and PC2.

Figure 3.2.1. The total transcriptomes of high and low FI mice are fundamentally different. Total RNA from eight mouse kidneys was sequenced. The RNA-Seq samples were projected into 2-dimensional space based on the top 3000 most variable genes extracted from the total kidney transcriptomics dataset using PCA. **A.** PC2 vs PC1 scores plot. PC1 explains 51.5% variance, and PC2 explains 13.2%. There is some overlap of high FI (red dots) and low FI (blue dots) samples. This is highlighted by the superimposed 95% confidence ellipses. **B.** PC3 vs PC2 scores plot. 13.2% of explained by PC2 while 11.9% is explained by PC3. There is minimal overlap of 95% confidence ellipses, and high FI (red dots) and low FI (blue dots) samples are grouped together.

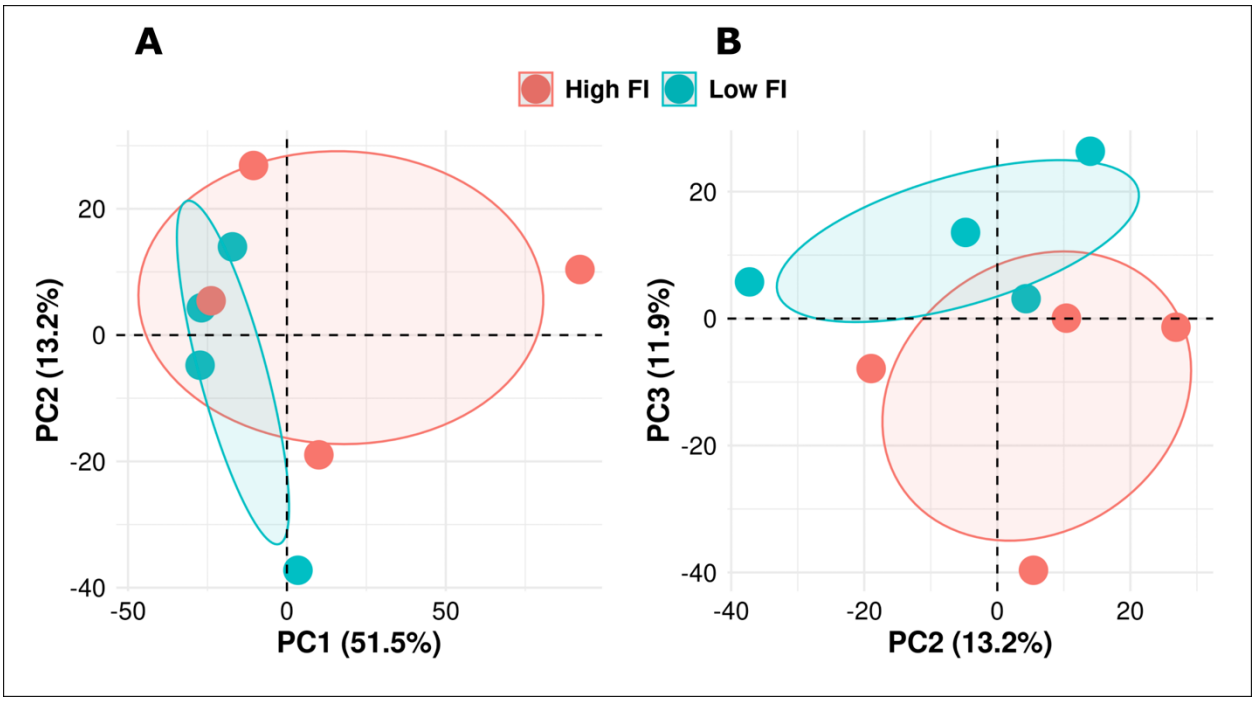

Figure 3.2.2. The metabolic transcriptomes of high and low FI mice are fundamentally different.
Total RNA from eight mouse kidneys was used for RNA-Seq. The samples were projected into a plane based on the expression of 1,447 kidney metabolic genes using PCA. **A.** PC2 vs PC1 scores plot. PC1 explains 55.9% variance, and PC2 explains 14.8%. There is little overlap between high FI (red dots) and low FI (blue dots) samples. The superimposed 95% confidence ellipses highlight the distinction between FI groups. **B.** PC3 vs PC2 scores plot. 14.8% of explained by PC2 while 9.9% is explained by PC3. There is considerable overlap of 95% confidence ellipses. High FI (red dots) and low FI (blue dots) samples are not clearly grouped.

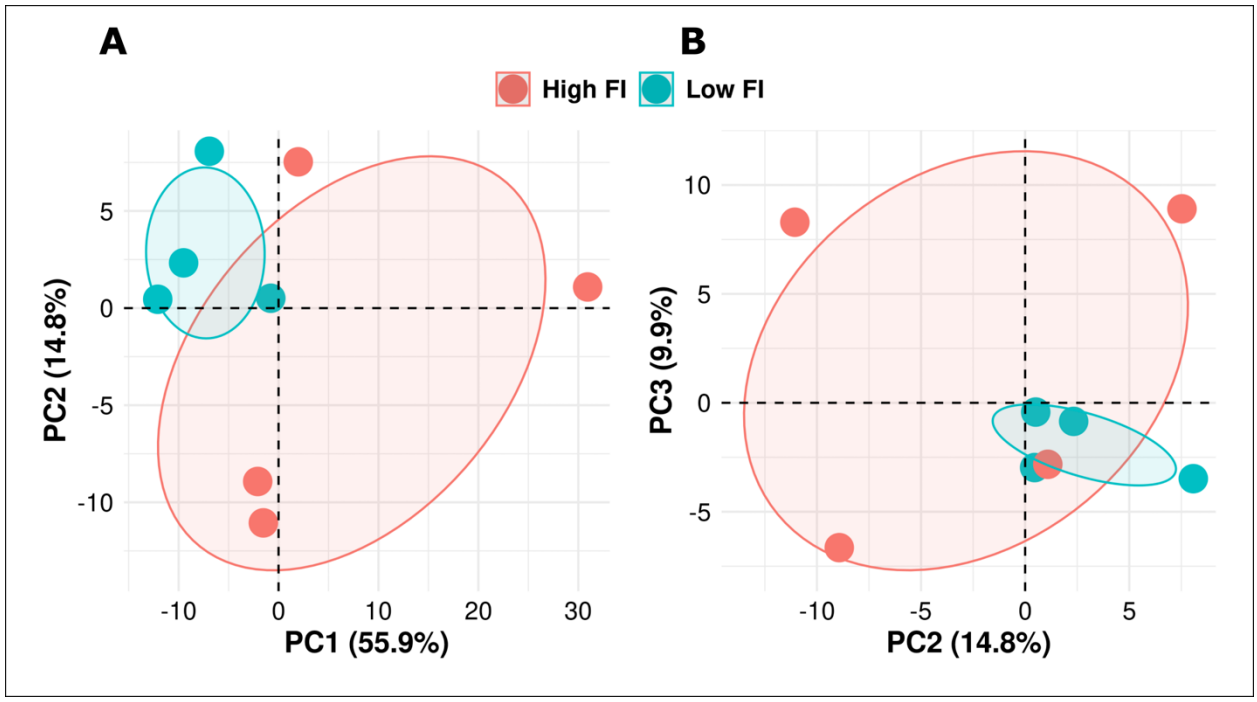

3.2.3 Differential expression analysis

After conducting PCA, I determined that the first three PCs calculated for the metabolic genes explained a greater proportion of variance between the high FI and low FI samples than the first three PCs calculated for the entire transcriptome (80.6% versus 76.6%). Therefore, further analyses were carried out with only the 1,447 genes that were identified as being involved in metabolism. First, a differential expression analysis was carried out to quantify and highlight significant changes in gene expression between the high FI and low FI groups. This was accomplished by conducting a moderated t-test, obtaining a p-value, and adjusting for false discovery. A volcano plot was created to identify the differentially expressed genes. The volcano plot appeared atypical because the $-\log_{10}$ of the FDR-adjusted p-value for all genes was close to zero (Figure 3.2.3 A). The adjusted p-values indicated a lack of statistical significance in the expression of metabolic genes between the high and low FI groups, although many genes met the arbitrary $|\text{Log}_2\text{FC}|$ cut-off of ≥ 1 (Figure 3.2.3 A). Fold change alone can be used for the identification of differentially expressed genes; it is calculated relative to a control (in this case, low FI) and can sometimes provide a more biologically meaningful interpretation [174]. Therefore, a more stringent cut-off of $|\text{Log}_2\text{FC}| \geq 2$ was set to identify a small panel of genes that differed more greatly in their expression in the high FI mice compared to the low FI mice. Using this cut-off, seven DEMGs were identified. These DEMGs were four times up or downregulated in high FI compared to low (Figure 3.2.3 B, Table 3.2.2). Furthermore, all seven DEMGs belonged to the subset of 3000 genes from the entire transcriptome that were said to be the most variable (Appendix A).

The seven DEMGs identified include uridine 5'-diphosphate (UDP) glucuronosyltransferase 1 family, polypeptide A9 (*Ugt1a9*), UDP glycosyltransferase 1 family, polypeptide A10 (*Ugt1a10*), cytochrome P450, family 4, subfamily a, polypeptide 12a (*Cyp4a12a*), and cytochrome P450, family 4, subfamily a, polypeptide 12b (*Cyp4a12b*), histidine decarboxylase (*Hdc*), aldo-keto reductase family 1, member C18 (*Akr1c18*), and phospholipase A_2, group XIIB (*Pla2g12b*) (Table 3.2.4).

I created a heatmap to visualize the expression of the DEMGs across high and low FI samples (Figure 3.2.4). Expression patterns indicated that *Hdc, Akr1c18, Ugt1a9, Ugt1a10,* and *Pla2g12b* are downregulated in the high FI group compared to the low FI group, whereas *Cyp4a12a* and *Cyp4a12b* are upregulated. These patterns are relatively consistent for each gene across the various samples within each FI group (Figure 3.2.4).

To verify these trends in gene expression, I plotted $\log_2$ counts per million (Log_2CPM) of each gene for individual samples according to their FI group using the filtered and normalized counts data from RNA-Seq (Figure 3.2.5). Statistical significance in expression differences between the high and low FI groups was assessed using a t-test. *Ugt1a9* and *Ugt1a10* were both significantly downregulated in the high FI group (Figure 3.2.5 A-B). The average expression of *Ugt1a9* was -2.02 ± 0.622 Log_2CPM in the high FI group versus 0.59 ± 0.44 Log_2CPM in the low FI group. The high FI group had an average of 0.70 ± 1.48 Log_2CPM for *Ugt1a10* compared to 3.53 ± 1.08 Log_2CPM for the low FI group. Similarly, *Hdc*, *Pla2g12b*, and *Akr1c18* were also significantly downregulated in the frailer group (Figure 3.2.5 E-G). The mean expression of *Hdc* was 7.14 ± 0.86 Log_2CPM in the high group versus 9.15 ± 0.35 Log_2CPM in the low group. Expression of *Pla2g12b* was -2.46 ± 0.93 Log_2CPM in the high group, while the low FI group was averaged at -0.26 ± 1.03 Log_2CPM. The average expression of *Akr1c18* was 3.15 ± 1.55 Log_2CPM for the high FI group and 5.68 ± 0.70 Log_2CPM for the low FI group. However, the expression of both cytochrome genes was increased in the high FI group. *Cyp4a12a* was significantly upregulated, with 2.34 ± 0.26 Log_2CPM being the average expression of the high group and 0.33 ± 0.72 Log_2CPM the average of the low group (Figure 3.2.6 C). The mean expression of *Cyp4a12b* was also significantly higher in the high FI group (2.79 ± 0.12) than in the low FI group (0.31 ± 0.78, Figure 3.2.5 D). High FI mice showed *Hdc, Akr1c18, Ugt1a9, Ugt1a10,* and *Pla2g12b* downregulation, whereas *Cyp4a12a* and *Cyp4a12b* were upregulated. Taking these data together, there were significant differences in the expression of seven metabolic genes between very frail and a less frail mice.

Figure 3.2.3. Seven metabolic genes are differentially expressed after applying and fold-change cut-off.
Volcano plots in which $\log_2$ fold change (Log_2FC) quantifies how much expression of each gene has changed in the high FI group relative to the low FI group. The y-axis is the $-\log_{10}$ of the False Discovery Rate (FDR)-adjusted p-value ($-Log_{10}$ P adj) that was obtained via the moderated t-test and corrected for multiple testing. Individual metabolic genes are represented by dots. **A.** Grey dots indicate genes that are not significantly differentially expressed ($p < 0.05$) and did not meet the set $|Log_2FC|$ cut-off of ≥ 1. Red dots indicate genes that are not significant ($p < 0.05$) but have a $|Log_2FC|$ of ≥ 1. **B.** A more stringent $|Log_2FC|$ cut-off of ≥ 2 has been applied. Grey dots indicate genes that are not significant ($p < 0.05$) and do not meet the set Log_2FC cut-off. Red dots with labelled gene names indicate non-significant genes with a $|Log_2FC| \geq 2$.

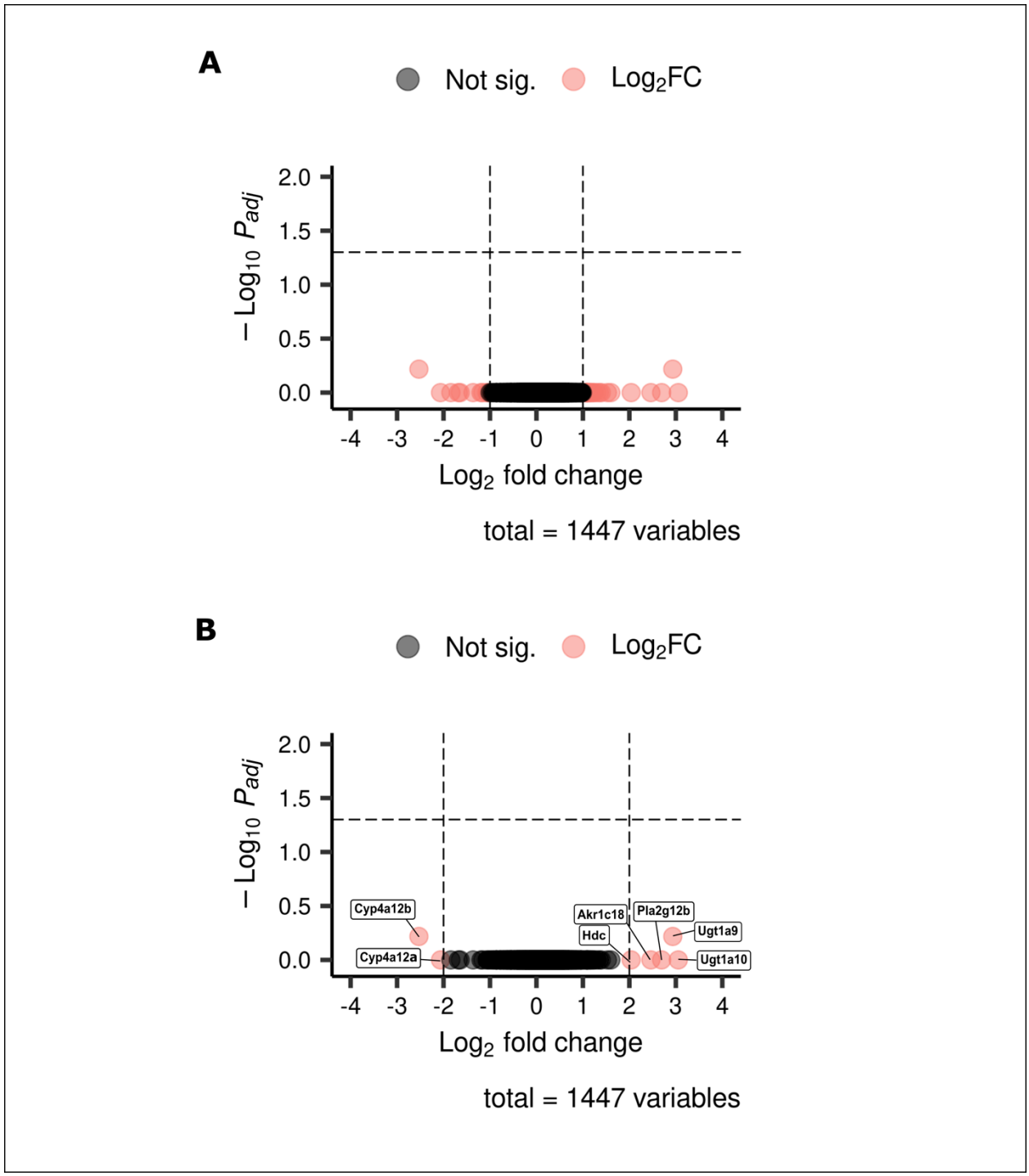
A
Not sig.
Log2FC
2.0
1.5
1.0
0.5
0.0
− Log10 Padj
-4
-3
-2
-1
0
1
2
3
4
Log2 fold change
total = 1447 variables
B
Not sig.
Log2FC
2.0
1.5
1.0
0.5
0.0
− Log10 Padj
Cyp4a12b
Cyp4a12a
Akr1c18
Hdc
Pla2g12b
Ugt1a9
Ugt1a10
-4
-3
-2
-1
0
1
2
3
4
Log2 fold change
total = 1447 variables

Table 3.2.2. Differential expression report

Gene	Log_2FC	Average Expression (Log_2CPM)	t	P-Value	Adjusted P-Value
Cyp4a12b	-2.529589	1.5228398	-4.570247	0.0005714427	0.6061950
Ugt1a9	2.934064	-0.8632502	4.318760	0.0008378645	0.6061950
Cyp4a12a	-2.064811	1.3031535	-3.096998	0.0059336080	0.9999998
Ugt1a10	3.052852	2.0838066	2.498864	0.0165464973	0.9999998
Hdc	2.039145	8.1436027	2.369284	0.0201865494	0.9999998
Pla2g12b	2.694692	-1.6276266	2.134420	0.0303649874	0.9999998
Akr1c18	2.463428	4.4078491	2.126876	0.0305275506	0.9999998

t: outcome of the moderated t-test.

P-value: p-value from moderated t-test.

Adjusted p-value: false discovery rate (FDR) adjusted p-value.

Figure 3.2.4. Top-most differentially expressed metabolic genes.
Heatmap of the most differentially expressed genes (defined as $Log_2FC| \geq 2$) in the high FI versus low FI comparison across eight samples from RNA-Seq. Each column corresponds to a sample, and each row corresponds to a specific gene. A z-score normalization was performed on the log_2 normalized read counts across samples for each gene. Z-scores were computed for each row by subtracting the mean expression value and dividing by the standard deviation. The z-score was used to plot the heatmap (blue = downregulated, red = upregulated).

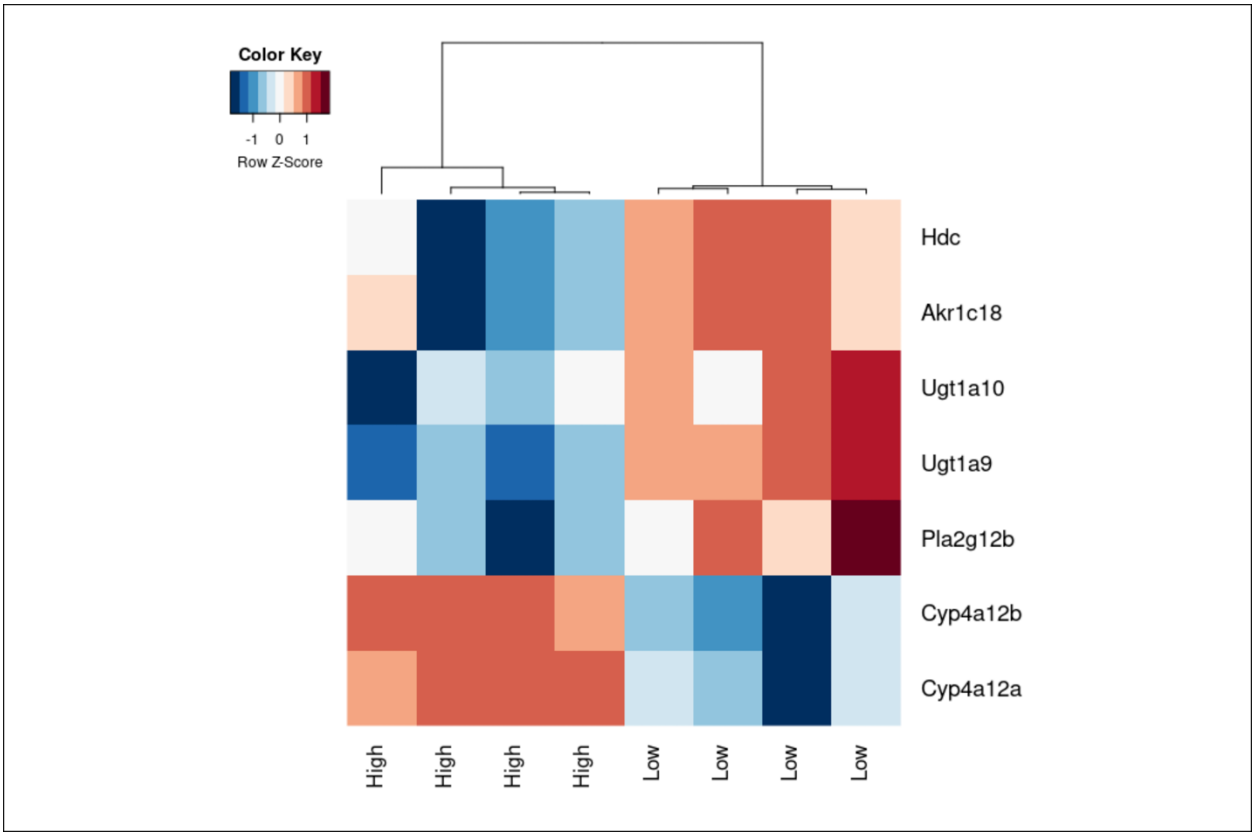

Figure 3.2.5. Metabolic genes are differentially expressed in FI groups.
Expression of metabolic genes shown as Log2CPM. Individual mice are plotted and grouped according to FI. Unpaired t-tests have been carried out, comparing the mean expression in high and low FI groups. **A.** Expression of uridine 5'-diphospho-glucuronosyltransferase 1 family, polypeptide A9 (*Ugt1a9*). ***p < = 0.001. **B**. Uridine 5'-diphospho-glucuronosyltransferase 1 family, polypeptide A10 (*Ugt1a10*) expression. *p <= 0.05. **C**. Expression of cytochrome P450, family 4, subfamily a, polypeptide 12a (*Cyp4a12a*). **p <= 0.01. **D.** Expression of cytochrome P450, family 4, subfamily a, polypeptide 12b (*Cyp4a12b*). **p <= 0.01. **E.** Histidine decarboxylase (*Hdc*) expression. *p <= 0.05. **F.** Phospholipase A_2, group XIIB (*Pla2g12b*) expression. *p <= 0.05. **G.** Expression of aldo-keto reductase family 1, member C18 (*Akr1c18*). *p <= 0.05.

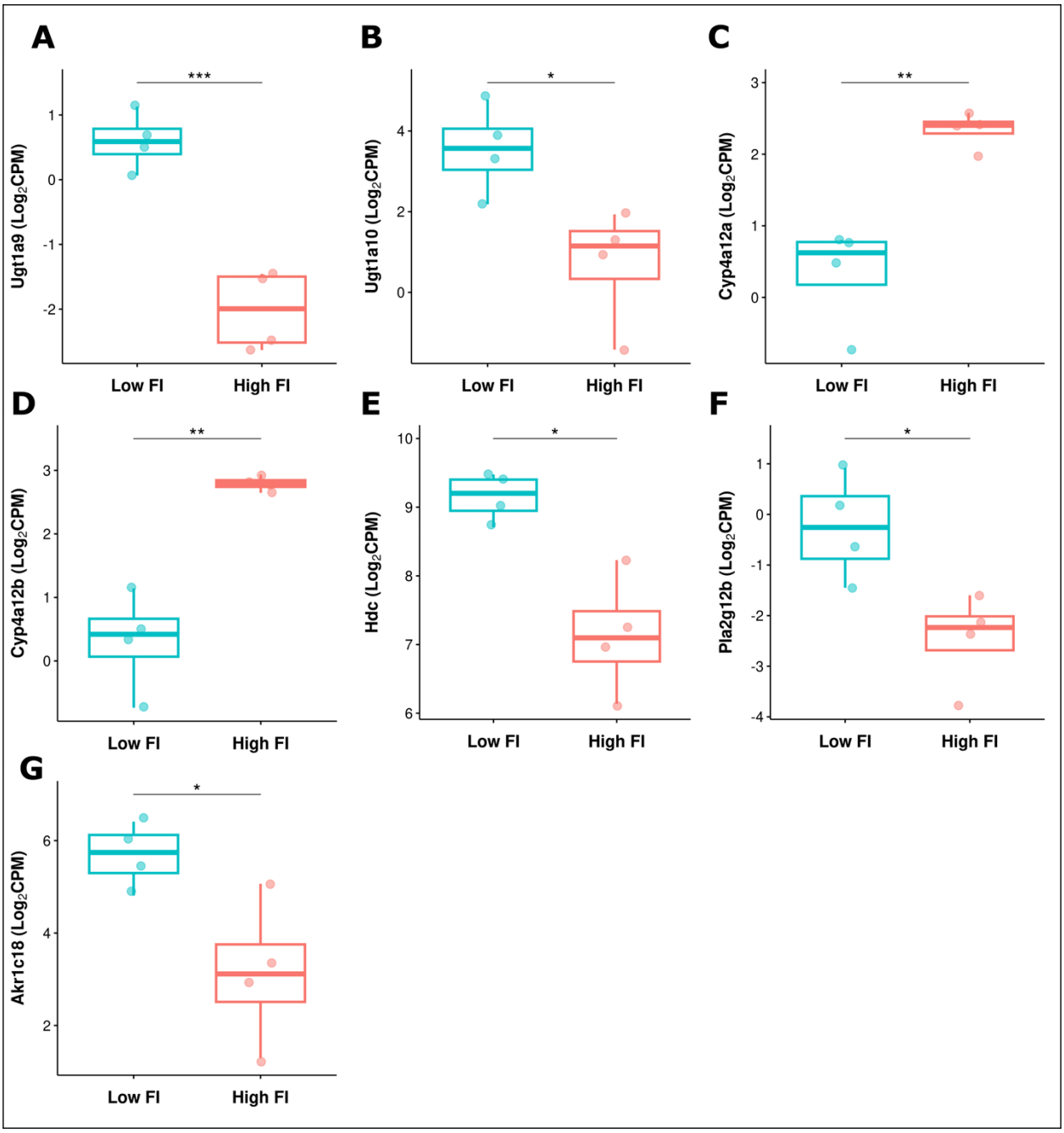
A
***
Ugt1a9 (Log2CPM)
1
0
-1
-2
Low FI
High FI
B
*
Ugt1a10 (Log2CPM)
4
2
0
Low FI
High FI
C
**
Cyp4a12a (Log2CPM)
3
2
1
0
Low FI
High FI
D
**
Cyp4a12b (Log2CPM)
3
2
1
0
Low FI
High FI
E
*
Hdc (Log2CPM)
10
9
8
7
6
Low FI
High FI
F
*
Pla2g12b (Log2CPM)
1
0
-1
-2
-3
-4
Low FI
High FI
G
*
Akr1c18 (Log2CPM)
6
4
2
Low FI
High FI

3.2.4 Functional analysis

To elucidate the biological significance of the expression levels of metabolic genes observed in high FI mice, I conducted a GO enrichment analysis. A GO enrichment analysis can be used to determine whether a set of functional attributes (molecular function, biological processes, or cellular components) are enriched in relation to an overall population of genes with respect to a particular gene set of interest. I used the seven DEMGs identified via RNA-Seq as the gene set of interest, referencing the entire kidney transcriptome as a set of background genes (14, 929 genes). Having defined these parameters, I used a GO analysis to identify which biological processes may be over-represented in the gene set of interest (my DEMGs), as these pathways would be considered "enriched".

The top 15 most enriched biological processes with the results of the statistical test applied are shown in *Table 3.2.3*. *Cyp4a12a* and *Cyp4a12b* were significantly enriched in the omega-hydrolase P450 pathway, lauric acid metabolism, medium chain fatty acid metabolism, linoleic acid metabolism, icosanoid biosynthesis, and arachidonic acid metabolic processes. Therefore, these pathways may be altered by changes in the expression of *Cyp4a12a* and *Cyp4a12b* and could be impacted by frailty. Additionally, the cytochrome genes and *Akr1c18* were significantly enriched in unsaturated fatty acid metabolism, icosanoid metabolism, and olefinic compound metabolism. *Akr1c18* alone was implicated in progesterone and C21 steroid hormone catabolism. Cellular glucuronidation, uronic acid metabolism, and glucuronate metabolic processes were significantly enriched by *Ugt1a9* and *Ugt1a10*. Lastly, *Hdc* was significantly enriched in histamine biosynthesis. Overall, these 15 metabolic pathways may be altered by a high degree of frailty as they were significantly enriched by the altered expression of the DEMGs identified from RNA-Seq. The top three enriched biological processes with the highest gene count (Figure 3.2.6) are interesting because dysregulation of such pathways could affect lipid metabolism in the kidney.

Table 3.2.3. Summary of Gene Ontology enrichment analysis

GO Description	Gene Ratio	BgRatio	Gene ID	p-value	Adjusted p-value	q Value
Omega-hydroxylase P450 pathway	2/7	5/14929	*Cyp4a12a/ Cyp4a12b*	1.883328e-06	0.0001567520	3.716265e-05
Lauric acid metabolic process	2/7	6/14929	*Cyp4a12a/ Cyp4a12b*	2.824361e-06	0.0001567520	3.716265e-05
Unsaturated fatty acid metabolic process	3/7	92/14929	*Cyp4a12a/ Cyp4a12b/ Akr1c18*	7.786667e-06	0.0002613883	6.196973e-05
Icosanoid metabolic process	3/7	98/14929	*Cyp4a12a/ Cyp4a12b/ Akr1c18*	9.419399e-06	0.0002613883	6.196973e-05
Olefinic compound metabolic process	3/7	108/14929	*Cyp4a12a/ Cyp4a12b/ Akr1c18*	1.261802e-05	0.0002712790	6.431461e-05
Cellular glucuronidation	2/7	13/14929	*Ugt1a9/ Ugt1a10*	1.466373e-05	0.0002712790	6.431461e-05
uronic acid metabolic process	2/7	18/14929	*Ugt1a9/ Ugt1a10*	2.873136e-05	0.0003543535	8.400983e-05
Glucuronate metabolic process	2/7	18/14929	*Ugt1a9/ Ugt1a10*	2.873136e-05	0.0003543535	8.400983e-05
Medium-chain fatty acid metabolic process	2/7	18/14929	*Cyp4a12a/ Cyp4a12b*	2.873136e-05	0.0003543535	8.400983e-05
Linoleic acid metabolic process	2/7	19/14929	*Cyp4a12a/ Cyp4a12b*	3.210435e-05	0.0003563583	8.448513e-05
Icosanoid biosynthetic process	2/7	42/14929	*Cyp4a12a/ Cyp4a12b*	1.608195e-04	0.0016228149	3.847356e-04
Arachidonic acid metabolic process	2/7	45/14929	*Cyp4a12a/ Cyp4a12b*	1.847904e-04	0.0017093116	4.052422e-04

GO Description	Gene Ratio	BgRatio	Gene ID	p-value	Adjusted p-value	q Value
Histamine biosynthetic process	1/7	1/14929	*Hdc*	4.688861e-04	0.0034697568	8.226071e-04
Progesterone catabolic process	1/7	1/14929	*Akr1c18*	4.688861e-04	0.0034697568	8.226071e-04
C21-steroid hormone catabolic process	1/7	1/14929	*Akr1c18*	4.688861e-04	0.0034697568	8.226071e-04

Gene Ratio: Ratio of genes of interest that are annotated in a GO biological process.

BgRatio: Ratio of all genes that are annotated in a GO biological process.

Gene ID: List of gene symbols belonging to each GO biological process.

p-value: p-value calculated by hypergeometric distribution.

Adjusted p-value: false discovery rate (FDR) adjusted p-value.

q - value: positive false discovery rate (pFDR) analogue of the p-value.

Figure 3.2.6. Potentially dysregulated biological processes in frailty.
Results of a Gene Ontology (GO) enrichment analysis. Fifteen biological processes that were over-represented in a list of seven differentially expressed metabolic genes (DEMGs) have been shown. GO biological process descriptions are shown on the y-axis. Gene count is shown on the x-axis, representing the sum of genes belonging to each GO biological process. Bars are coloured according to the false discovery rate (FDR)-adjusted p-value.

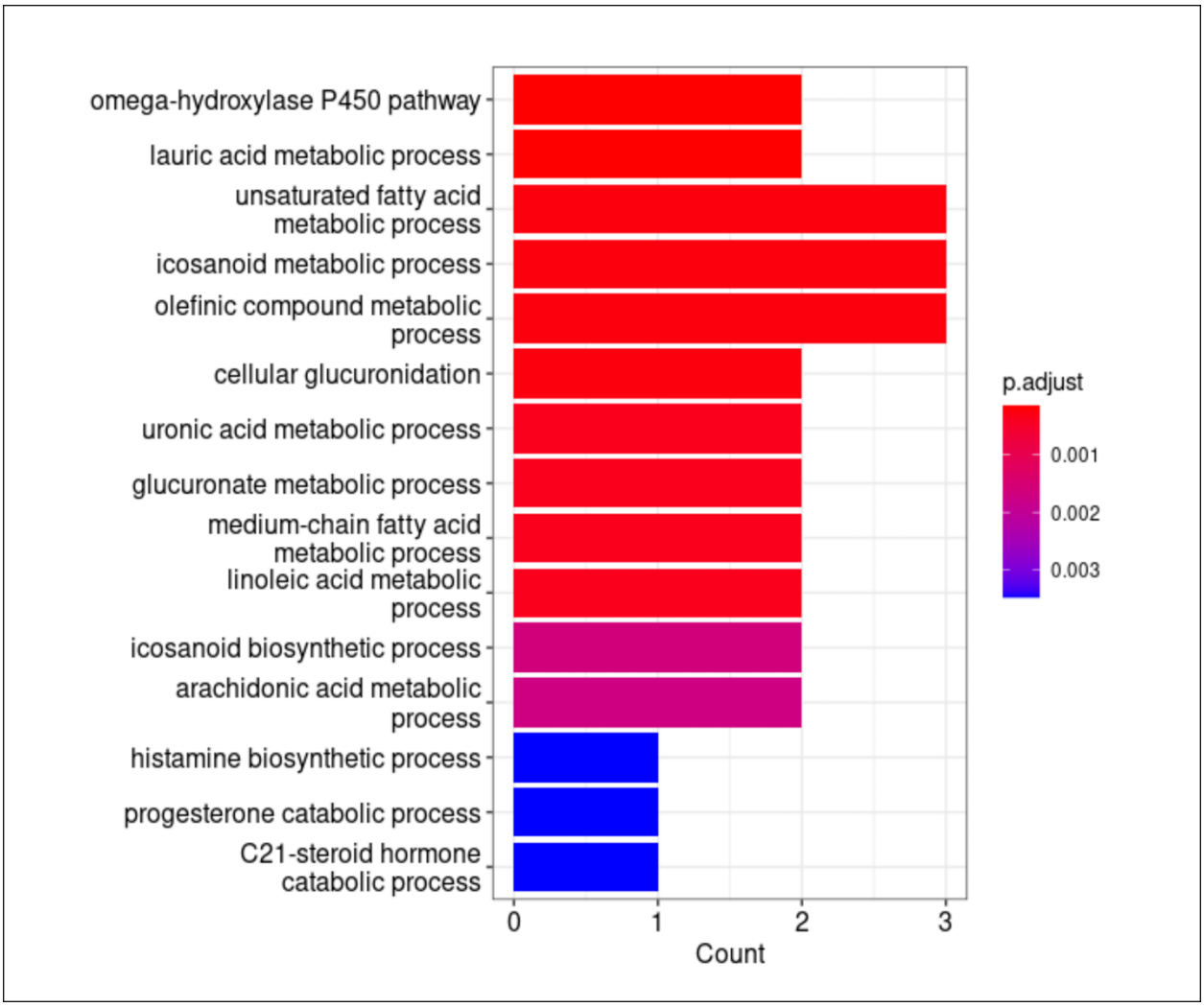

3.3 Analysis of aging data

Based on my data, seven DEMGs appeared to be associated with frailty in a group of age-matched female mice. I was interested in confirming that the expression of these genes did not vary with age. To validate this, I used a publicly available transcriptomics dataset. Takemon et al. completed RNA-Seq using kidney tissue from genetically diverse mice, generating gene expression data for 93 female Diversity Outbred (DO) mice 6 months (n = 33), 12 months (n = 31), and 18 months (n = 29) of age [147].

I identified the seven DEMGs from the 19,492 genes in the Takemon et al. dataset (Figure 3.3.1) and plotted their expression as a function of age. It was found that the expression of *Ugt1a9*, *Ugt1a10*, *Cyp4a12a*, *Cyp4a12b, Hdc*, and *Akr1c18* was stable across all age groups, with no significant differences identified between 6, 12, and 18 months. However, the expression of *Pla2g12b* was significantly different at the 95% confidence level when comparing the 6 month group to 12 months and 18 months (Figure 3.3.1 F). Therefore, there is reason to believe that six (*Ugt1a9*, *Ugt1a10*, *Cyp4a12a*, *Cyp4a12b, Hdc*, and *Akr1c18*) of my seven metabolic DEMGs are associated with frailty independent of age in female mice. However, these results must be interpreted with caution as the DEMGs were found in C57BL/6 mice and the aging data was obtained from DO mice. Thus, the results could be impacted by differences between inbred strains (C57BL/6) and outbred strains (DO), which are thought to have greater phenotypic variability [175]. Differences in behaviour, immune function, anatomy, and organ function between strains could limit the ability compare the expression of DEMGs identified in C57BL/6 mice to the expression of those same genes in DO mice [175].

Figure 3.3.1. Expression of six metabolic genes that are differentially expressed in frailty is not altered with age.
Boxplots showing the expression of seven metabolic genes using gene counts obtained from a publicly available dataset. Gene count is shown in Log2CPM. Individual mice are plotted and grouped according to age (in months). One-way ANOVAs have been carried out, comparing the mean expression of each gene across all three age groups. **A.** Expression of uridine 5'-diphospho-glucuronosyltransferase 1 family, polypeptide A9 (*Ugt1a9*). p = 0.46. **B**. Uridine 5'-diphospho-glucuronosyltransferase 1 family, polypeptide A10 (*Ugt1a10*) expression. p = 0.55. **C**. Expression of cytochrome P450, family 4, subfamily a, polypeptide 12a (*Cyp4a12a*). p = 0.19. **D.** Expression of cytochrome P450, family 4, subfamily a, polypeptide 12b (*Cyp4a12b*). p =0.43. **E.** Histidine decarboxylase (*Hdc*) expression. p = 0.73. **F.** Phospholipase A_2, group XIIB (*Pla2g12b*) expression. *p <= 0.05, ***p < = 0.001. **G.** Expression of aldo-keto reductase family 1, member C18 (*Akr1c18*). p = 0.55.

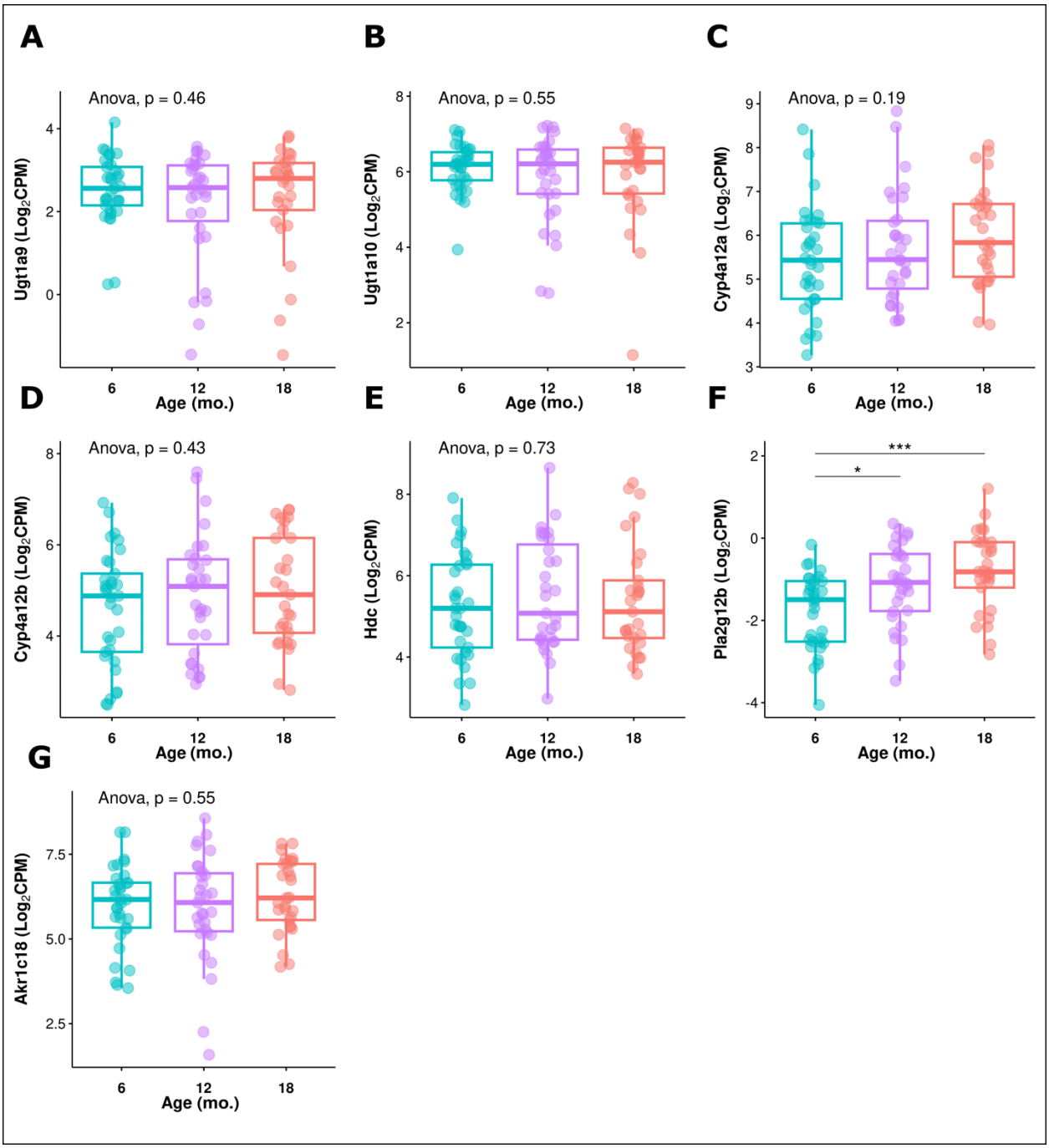
A
Anova, p = 0.46
Ugt1a9 (Log2CPM)
Age (mo.)
B
Anova, p = 0.55
Ugt1a10 (Log2CPM)
Age (mo.)
C
Anova, p = 0.19
Cyp4a12a (Log2CPM)
Age (mo.)
D
Anova, p = 0.43
Cyp4a12b (Log2CPM)
Age (mo.)
E
Anova, p = 0.73
Hdc (Log2CPM)
Age (mo.)
F
***
*
Pla2g12b (Log2CPM)
Age (mo.)
G
Anova, p = 0.55
Akr1c18 (Log2CPM)
Age (mo.)

3.4 Validation of differentially expressed genes with qPCR

Having identified seven genes of interest which may be associated with high FI in female mice using RNA-Seq, I wanted to validate my findings using an orthogonal method (a different method used to measure the same attributes). To do this, I completed a series of qPCR experiments which aimed to measure the expression of the DEMGs (*Ugt1a9*, *Ugt1a10*, *Cyp4a12a*, *Cyp4a12b, Hdc*, *Pla2g12b*, and Akr1c18) in a novel group of mice. The exploratory RNA-Seq study used mice with extremely high and low FI values, but qPCR involved new mice with intermediate FI scores. I aimed to create a standard curve in which expression of the DEMGs could be used to predict a mouse's FI value.

3.4.1 Reference gene selection and primer efficiencies for qPCR

The seven metabolic DEMGs with a $|Log_2FC| \geq 2$ from RNA-Seq were considered genes of interest for qPCR assays. Primers were designed to be specific *Ugt1a9*, *Ugt1a10*, *Hdc*, *Pla2g12b*, and *Akr1c18.* However, the primers used for the cytochrome P450 genes (*Cyp4a12a* and *Cyp4a12b*) were not specific for the individual isoforms; thus, they were measured together as *Cyp4a12a/b*.

In addition to these genes, suitable reference genes needed to be selected for the qPCR experiments. At the time of this study, there were no published papers discussing the stability of reference genes in female mouse kidneys and/or appropriate reference genes for frailty research in mice. Previous literature suggested that *Ppia* and *Hprt* expression was stable in developing female mouse gonads. To determine if these genes would be a good choice, I visualized how their expression changed using my RNA-Seq data to ensure they did not fluctuate with frailty (Figure 3.4.1). Indeed, expression of both *Ppia* and *Hprt* was not significantly different between FI groups. Furthermore, I used the aging RNA-Seq data from Takemon et al. to assess whether their expression changed dramatically with age. The comparison of 6 month to 12 month and 12 month to 18 month-old female mice showed that *Ppia* and *Hprt* expression in the kidneys was not significantly different (Figure 3.4.2). *Ppia* expression was also not significantly different between 6 months and 18 months. However, the expression of *Hprt* was significantly different in

the 6 month to 18 month comparison. Overall, *Ppia* and *Hprt* expression did not vary significantly between mice that were 6 months apart in age (Figure 3.4.2). The mice used in the qPCR cohort were no more than 2.3 months apart in age, so the effect of age was considered negligible. Therefore, *Ppia* and *Hprt* were selected as reference genes for my study.

To determine the amplification efficiency of my primers, I constructed a standard curve. Ideally, the Cq values of a 10-fold dilution should be 3.3 cycles apart, which would correspond to 100% efficiency. In general, 90-110% efficiency is considered optimal [176]. *Table 3.4* shows that all primers for the genes of interest and reference genes fell within this range.

Figure 3.4.1. Reference genes expression is stable with frailty in mice.
Expression of reference genes shown as Log2CPM. Individual mice are plotted and grouped according to FI. Unpaired t-tests have been carried out, comparing the mean expression in high and low FI groups. **A.** Expression of Peptidylprolyl isomerase A (Ppia). ns = not significant p>0.05. **B.** Expression of Hypoxanthine guanine phosphoribosyl transferase (Hprt). ns = not significant p>0.05.

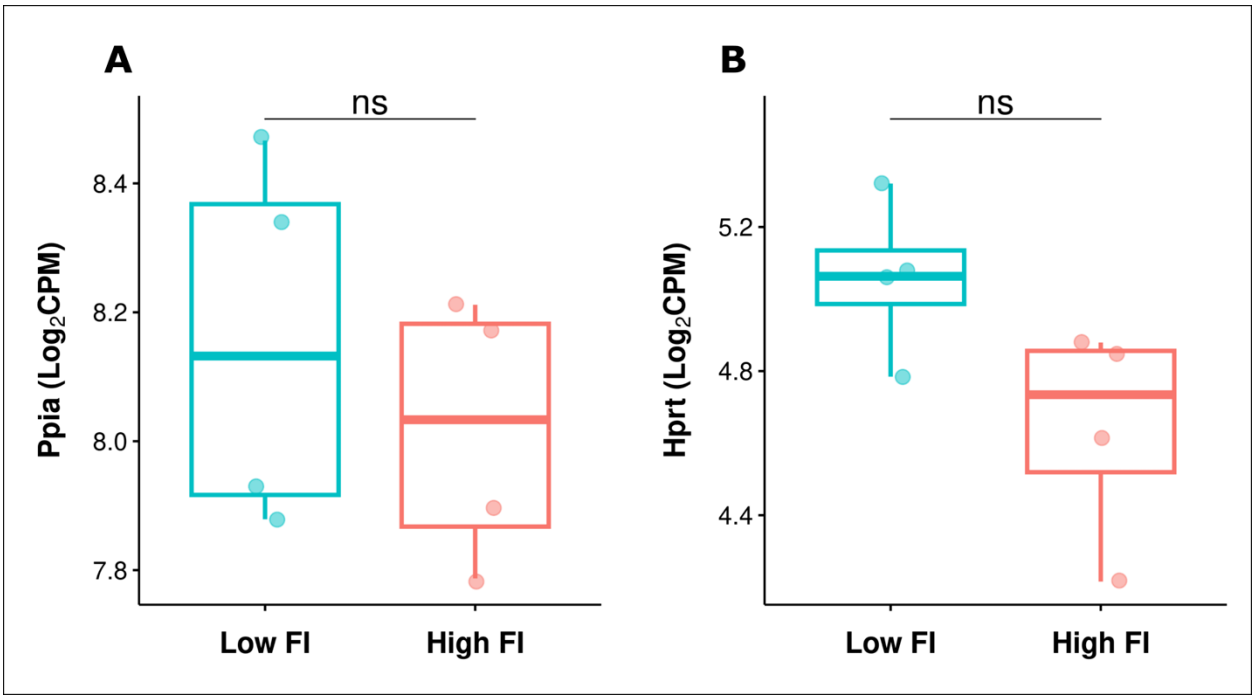

Figure 3.4.2. Reference gene expression does not fluctuate in mice within a 6 month age range.
Expression of reference genes using gene counts obtained from a publicly available dataset. Gene count is shown in Log2CPM. Individual mice are plotted and grouped according to age (in months). One-way ANOVAs have been carried out, comparing the mean expression of each gene across all three age groups. **A.** Expression of Peptidylprolyl isomerase A (*Ppia*). p = 0.67. **B.** Expression of Hypoxanthine guanine phosphoribosyl transferase (*Hprt*). *p <= 0.05, ns = not significant p>0.05.

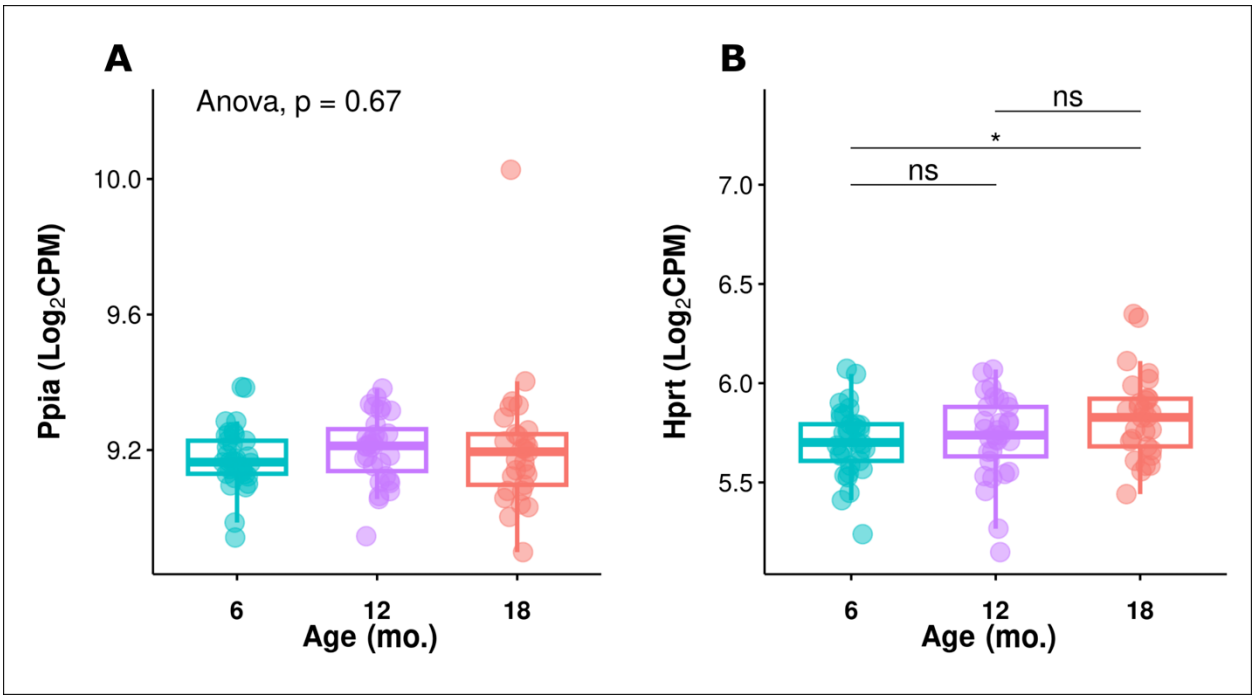

Table 3.4. Primer efficiencies

Primer	Efficiency (%)
Hdc	106.6
Akr1c18	102.3
Pla2g12b	103.5
Ugt1a9	107.5
Ugt1a10	105.7
Cyp4a12a/b	105.4
Ppia	105.9
Hprt	97.1

3.4.2 Quantification of frailty-related DEMG expression with qPCR

To verify the expression patterns of the DEMGs using qPCR, I plotted the Log_2FC of each gene for individual samples. First, I looked at gene expression in the same mice from RNA-Seq, so boxplots were made using only the high and low FI mice (Figure 3.4.3). Fold-change was calculated with respect to the low FI group. Significant differences in gene expression between the two groups were determined using a t-test.

None of the DEMGs tested were significantly different in high FI mice compared to low FI mice using qPCR data. However, the general trends appeared to be consistent with RNA-Seq for most of the DEMGs (Figure 3.4.3). As with RNA-Seq, expression of *Hdc*, *Pla2g12b*, and *Akr1c18* in the high FI group was decreased compared to the low FI group (Figure 3.4.3 D-F). Also akin to the RNA-Seq results, *Cyp4a12a/b* appeared to be upregulated in the high FI group relative to the low FI group (Figure 3.4.3 C). However, unlike the RNA-Seq findings, trends in *Ugt1a9* and *Ugt1a10* expression appeared to be reversed. Whereas the UGT genes were significantly decreased in the high FI group relative to the low FI group in the RNA-Seq results (Figure 3.2.5 A-B), the qPCR trends suggested that *Ugt1a9* and *Ugt1a10* are more highly expressed in the high FI group when compared to the low FI group (Figure 3.4.3 A-B).

I was also interested in determining whether DEMG expression could be graded with an FI score. Therefore, I evaluated the expression of these genes in low FI mice, three groups of mid FI mice, and a group of high FI mice via qPCR. Significant expression differences between the five groups were determined using a one-way ANOVA.

Aside from a significant difference in the expression of *Ugt1a9* between the mid FI 2 and high FI group, no other significant differences for any DEMG across any of the FI groups were found (Figure 3.4.4). Therefore, rather than comparing means, I noted the general trends in gene expression with increasing FI. For *Hdc*, *Pla2g12b*, and *Akr1c18,* although the expression in the high FI group was decreased compared to the low FI group, the mid FI groups were more variable (Figure 3.4.4 D-F). For example, *Hdc* expression decreased gradually from low FI to mid FI 1 and from mid FI 1 to mid FI 2. Yet, expression from mid FI 2 to mid FI 3 increased

again before decreasing from mid FI 3 to high FI (Figure 3.4.4 D). Similar inconsistencies were identified in the general trends of *Pla2g12b* and *Akr1c18* (Figure 3.4.4 E-F). Although *Cyp4a12a/b* expression was greater in the high FI group relative to the low, expression of these genes did not increase gradually as FI increased. Rather, *Cyp4a12a/b* expression decreased from low FI to mid FI 1, increased from mid FI 1 to mid FI 2, decreased from mid FI 2 to mid FI 3, and increased from mid FI 3 to the high FI group (Figure 3.4.4 C). Interestingly, while *Ugt1a9* and *Ugt1a10* were found to be upregulated in high FI mice, their expression decreased gradually from the low FI group to the mid FI 2 group and then increased from mid FI 2 to high FI (Figure 3.4.4 A-B).

In summary, there was apparent variability in gene expression amongst the samples in the qPCR cohort. As expected, the expression patterns of *Hdc, Pla2g12b, Akr1c18,* and *Cyp4a12a/b* identified by RNA-Seq were also observed via qPCR when comparing high to low FI groups. Yet, the differences between the high and low FI groups were non-significant. In a continuum of mid FIs, expression of *Ugt1a9* and *Ugt1a10* appeared to decrease and then gradually increase again as FI increased.

In general, there were no obvious trends when considering the mid FI groups. Perhaps the most remarkable finding was that differential expression of *Ugt1a9* and *Ugt1a10* in the high and low FI groups determined using qPCR showed the opposite trend as RNA-Seq (Figure 3.2.5, Figure 3.4.3) .

To further investigate the discrepancy in *Ugt1a9* and *Ugt1a10* expression, I ran a DNA agarose gel to examine the intensity of the bands produced by the UGT gene qPCR products in the high FI and low FI samples. Figure *3.4.5* shows that the agarose gel results mirror that of qPCR, where no significant differences exist between the two quantification methods. Therefore, I concluded complications in data acquisition via the Lightcycler likely do not explain this disagreement.

Figure 3.4.3. Expression of six metabolic genes in high and low FI mice.
Expression of metabolic genes determined via qPCR and shown in terms of $\log_2$ fold-change (Log_2FC) relative to the low FI group. Individual mice are plotted and grouped according to FI group. Unpaired t-tests have been carried out, comparing the mean expression in high and low FI groups. ns = not significant $p>0.05$. **A.** Expression of uridine 5'-diphospho-glucuronosyltransferase 1 family, polypeptide A9 (*Ugt1a9*). **B**. Uridine 5'-diphospho-glucuronosyltransferase 1 family, polypeptide A10 (*Ugt1a10*) expression. **C.** Expression of cytochrome P450, family 4, subfamily a, polypeptide 12a/b (*Cyp4a12a/b*). **D.** Histidine decarboxylase (*Hdc*) expression. **E.** Phospholipase A_2, group XIIB (*Pla2g12b*) expression. **F.** Expression of aldo-keto reductase family 1, member C18 (*Akr1c18*).

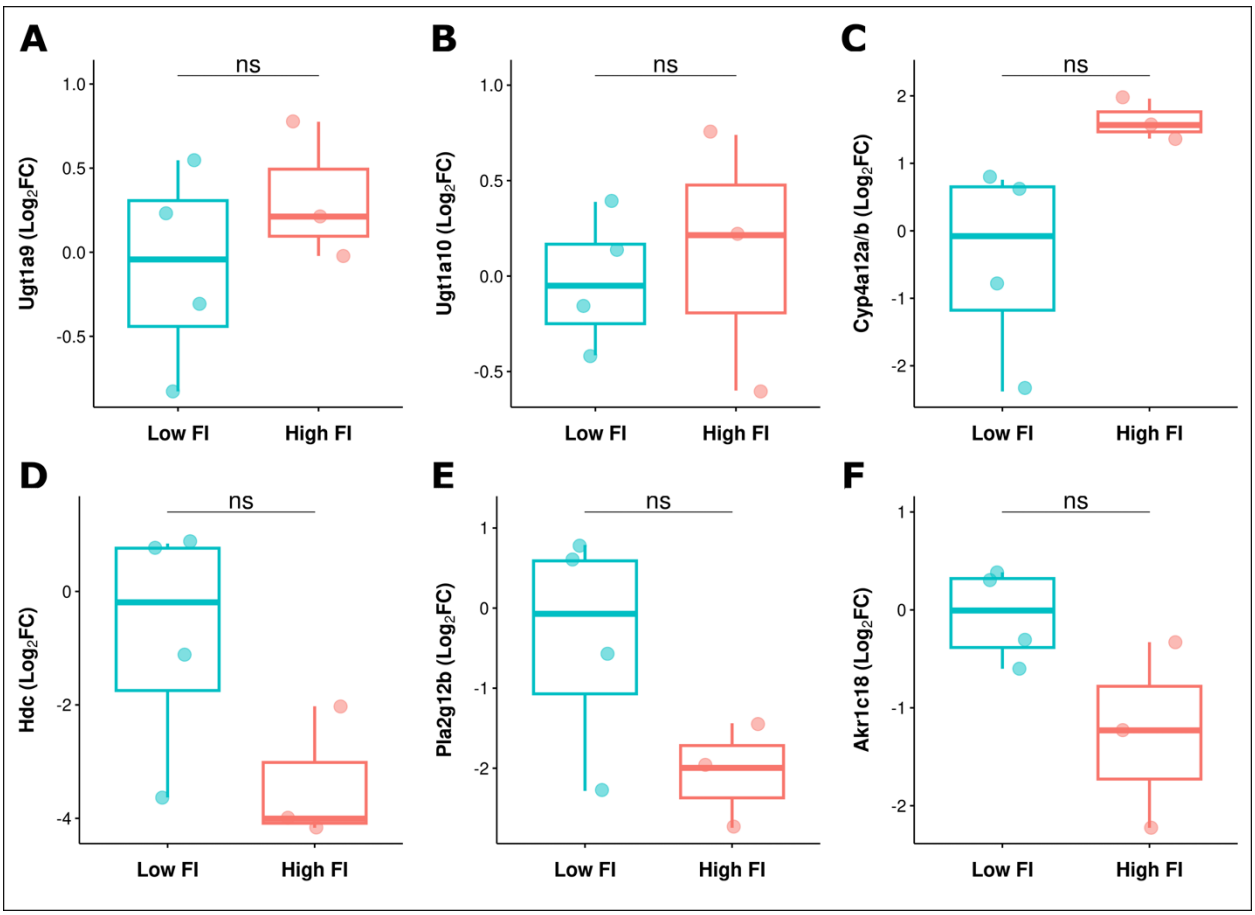

Figure 3.4.4. Expression of six metabolic genes across a gradient of FIs.
Expression of metabolic genes determined via qPCR and shown in terms of log_2 fold-change (Log_2FC) relative to the low FI group. Individual mice are plotted and are grouped according to FI group. One-way ANOVAs have been carried out, comparing the mean expression of each gene across all five FI groups. **A.** Expression of uridine 5'-diphospho-glucuronosyltransferase 1 family, polypeptide A9 (*Ugt1a9*). *p <= 0.05. **B**. Uridine 5'-diphospho-glucuronosyltransferase 1 family, polypeptide A10 (*Ugt1a10*) expression. p = 0.14. **C.** Expression of cytochrome P450, family 4, subfamily a, polypeptide 12a/b (*Cyp4a12a/b*). p =0.15. **D.** Histidine decarboxylase (*Hdc*) expression. p = 0.15. **E.** Phospholipase A_2, group XIIB (*Pla2g12b*) expression. p = 0.55. **F.** Expression of aldo-keto reductase family 1, member C18 (*Akr1c18*). p = 0.15.

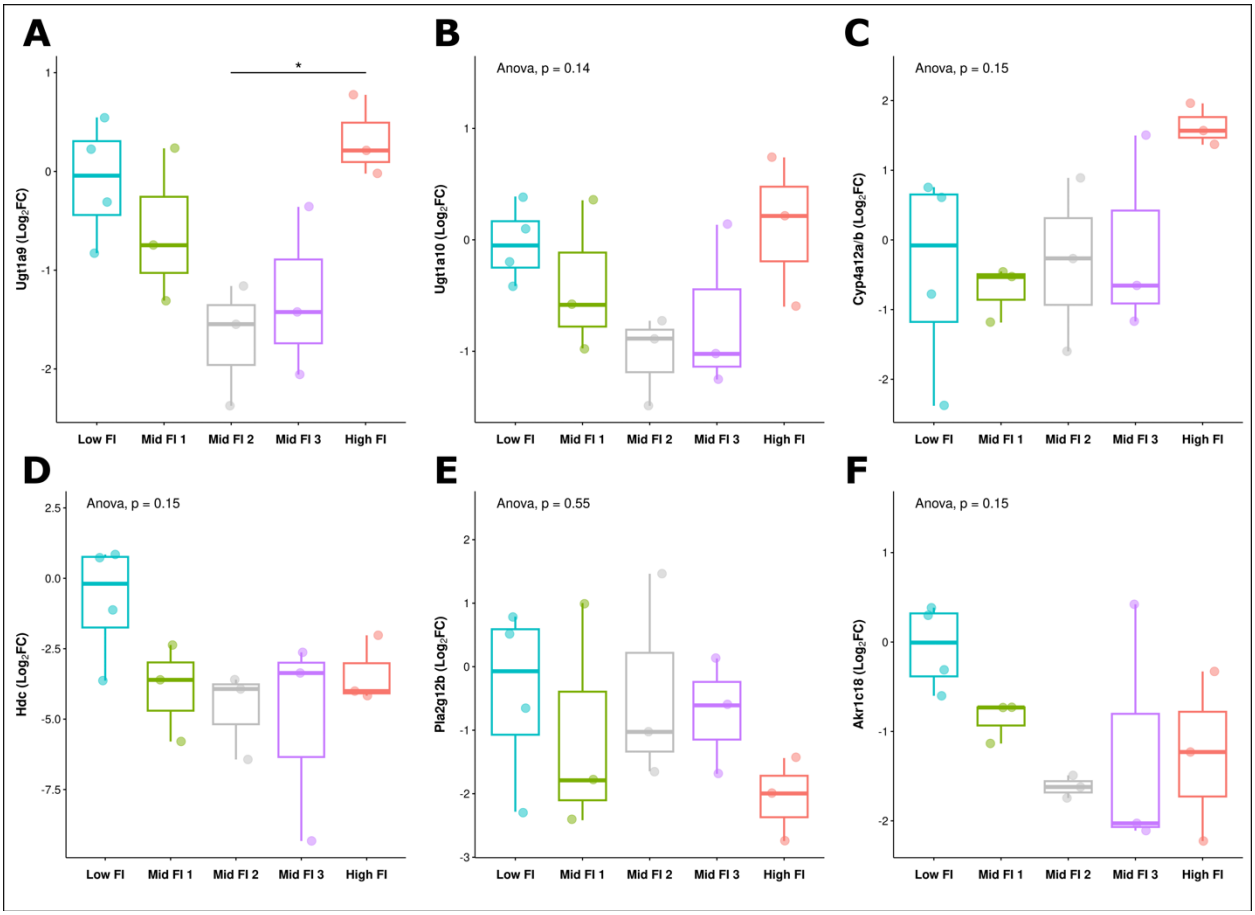

Figure 3.4.5. No significant differences exist between two methods of quantifying *Ugt1a9* and *Ugt1a10* qPCR products.
Boxplots comparing the quantification of qPCR products determined via two methods: DNA gel (indicated by Gel) and qPCR instrument (indicated by qPCR). Low FI (left) and high FI samples (right) are shown. Uridine 5'-diphospho-glucuronosyltransferase 1 family, polypeptide A9 (*Ugt1a9*) product (top) and Uridine 5'-diphospho-glucuronosyltransferase 1 family, polypeptide A10 (*Ugt1a10*) product (bottom) were quantified by either method. Expression is given as $\log_2$ fold-change (Log_2FC) relative to the low FI group. Unpaired t-tests have been carried out. ns = not significant $p>0.05$.

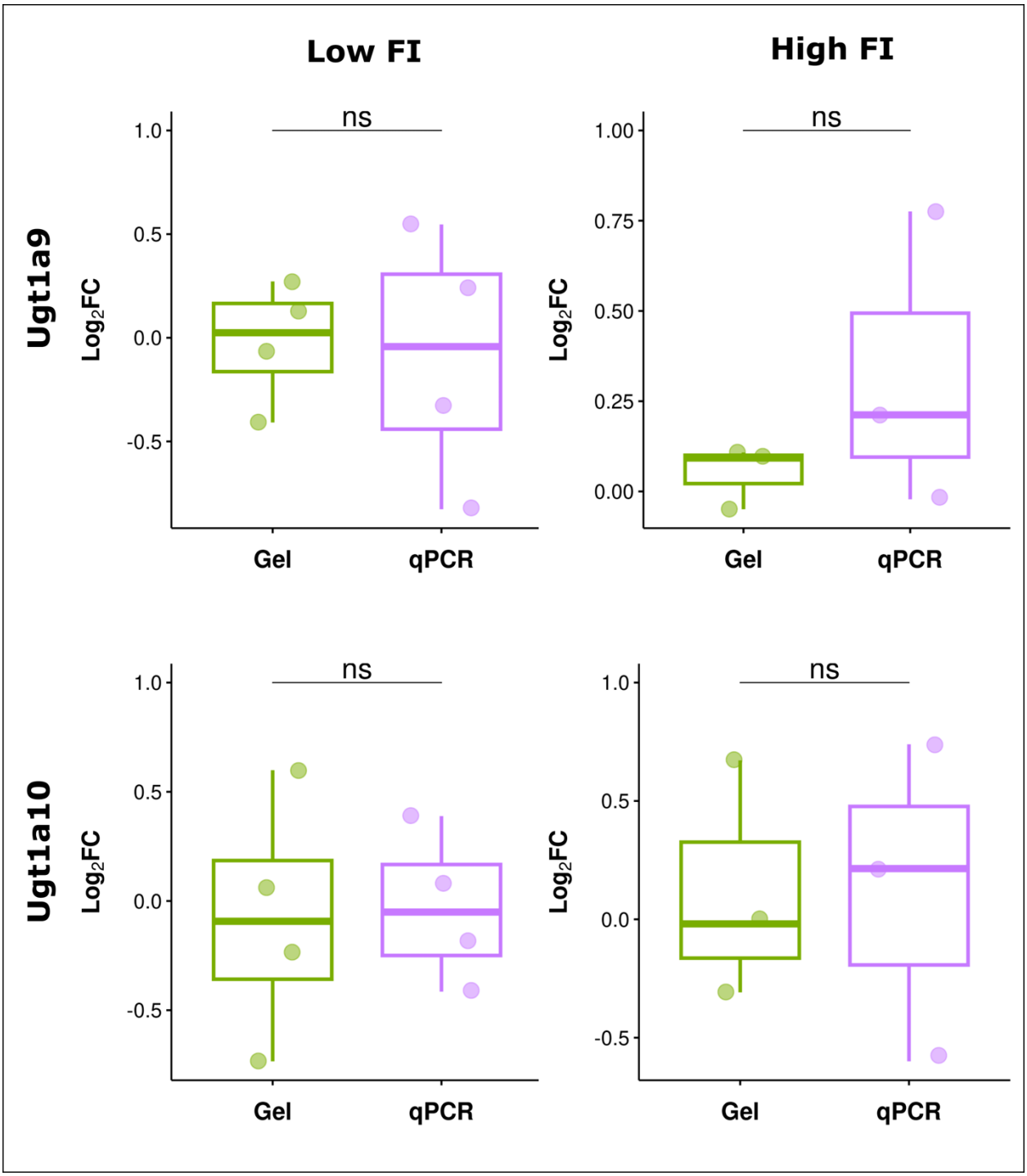
Low FI
High FI
Ugt1a9
Ugt1a10
Log2FC
ns
1.0
0.5
0.0
-0.5
1.00
0.75
0.50
0.25
0.00
Gel
qPCR

3.5 Measuring DEMGs in enalapril-treated mice using qPCR

3.5.1 Enalapril cohort

Enalapril, an angiotensin-converting enzyme (ACE) inhibitor, is a drug commonly used to treat hypertension and has previously been shown to attenuate frailty [27]. A significant reduction in FI scores was observed in middle-aged female mice treated with enalapril, independent of the long-term effects on blood pressure [27]. The mechanism by which enalapril exerts its effects and reduces frailty in middle-aged female mice is unknown. I wanted to investigate whether the renal DEMGs identified as being associated with frailty were altered by treatment with enalapril.

To do this, I extracted RNA from the kidneys of mice which belonged to the cohort of middle-aged females from the published study [27]. Mice were ~9 months old at the beginning of enalapril treatment and were treated over the course of 4 months. The cohort I used for qPCR was comprised of 11 mice in total. FI values for the enalapril-treated (n = 6) and control mice (n =5) were collected in the previous study by another investigator and were used for this thesis. Using FI data from Keller et al., I confirmed that there was a significant reduction in FI in the treated group compared to the control group (Figure 3.5.1). The mean FI of the control group was 0.23 ± 0.03, while the average of the treated group was 0.16 ± 0.02. Like the RNA-Seq and qPCR cohorts above, mice belonging to the enalapril cohort were approximately the same age (41.1 weeks). Therefore, changes in gene expression could be attributed to frailty, independent of age.

Figure 3.5.1. Enalapril-treated mice have significantly lower FI.
Individual FI scores of 11 mice from the enalapril cohort are plotted according to their respective treatment group (Control: n = 5, Enalapril-treated: n = 6). Unpaired t-test. **p <= 0.01.

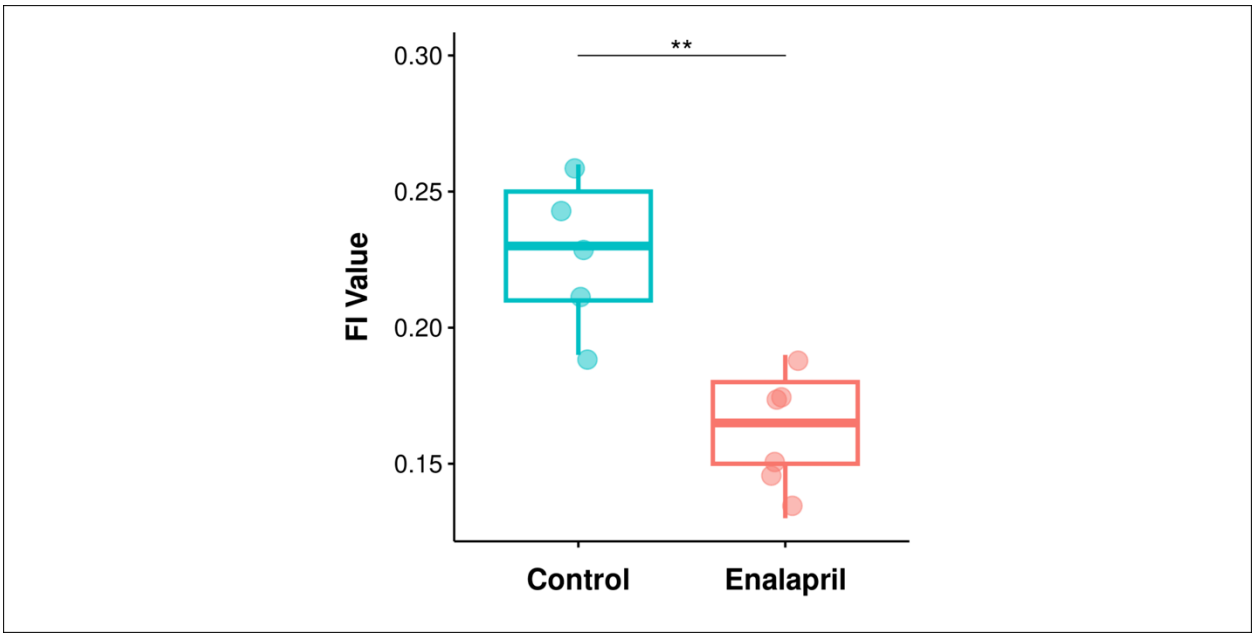

3.5.2 Assessing whether frailty-DEMGs are altered by enalapril

To assess fluctuations in DEMG (*Ugt1a9, Ugt1a10, Cyp4a12a/b, Hdc, Pla2g12b,* and *Akr1c18*) expression resulting from enalapril treatment, qPCR was used, with *Ppia* and *Hprt* as reference genes. The Log_2FC for each gene was calculated, comparing gene expression in the enalapril-treated group relative to the untreated control group (Figure 3.5.2). There was considerable variability in Log_2FC values for many of the genes. Notably, the average Log_2FC of Cyp4a12a/b in the control group was -0.247, with a standard deviation of 0.966 (Figure 3.5.2 C). Similarly, the average expression of Pla2g12b in the enalapril group was $Log_2FC = -1.02 \pm 1.05$ (Figure 3.5.2 E). Therefore, it is difficult to make conclusions about these genes.

Expression of *Ugt1a9, Ugt1a10, Pla2g12b,* and *Akr1c18* (Figure 3.5.2 A-B, E-F) appears to trend downwards with enalapril treatment, while *Cyp4a12a/b* and *Hdc* trend upwards (Figure 3.5.2 C-D). However, no significant differences were identified between the control and treated groups for any of the genes. Overall, the DEMGs identified by RNA-seq in highly frail mice did not appear to play a role in the mechanism by which enalapril reduces FI. Of note, the FIs of mice in this cohort were 0.16 ± 0.02 for the enalapril group and 0.23 ± 0.03 for the control (Figure 3.5.1). In contrast, the RNA-Seq cohort in which the DEMGs were initially identified had more extreme FIs (low FI group: 0.22 ± 0.012 and high FI group: 0.46 ± 0.04) (Figure 3.2.1). The lack of significant results in the enalapril-treated groups could be due to less prominent differences in the FI values of these mice compared to the cohort's extreme FI groups where the DEMGs were identified.

Figure 3.5.2. Metabolic genes of interest are not involved in the mechanism that causes FI reduction in enalapril-treated mice.
Expression of metabolic genes determined via qPCR and shown in terms of log_2 fold-change (Log_2FC). Individual mice are plotted and grouped according to treatment, either enalapril (n = 6) or untreated control (n = 5). Expression is relative to the untreated control group. Unpaired t-tests have been carried out, comparing the mean expression of each gene between groups. ns = not significant $p > 0.05$. **A.** Expression of uridine 5'-diphospho-glucuronosyltransferase 1 family, polypeptide A9 (*Ugt1a9*). **B**. Uridine 5'-diphospho-glucuronosyltransferase 1 family, polypeptide A10 (*Ugt1a10*) expression. **C.** Expression of cytochrome P450, family 4, subfamily a, polypeptide 12a/b (*Cyp4a12a/b*). **D.** Histidine decarboxylase (*Hdc*) expression. **E.** Phospholipase A_2, group XIIB (*Pla2g12b*) expression. **F.** Expression of aldo-keto reductase family 1, member C18 (*Akr1c18*).

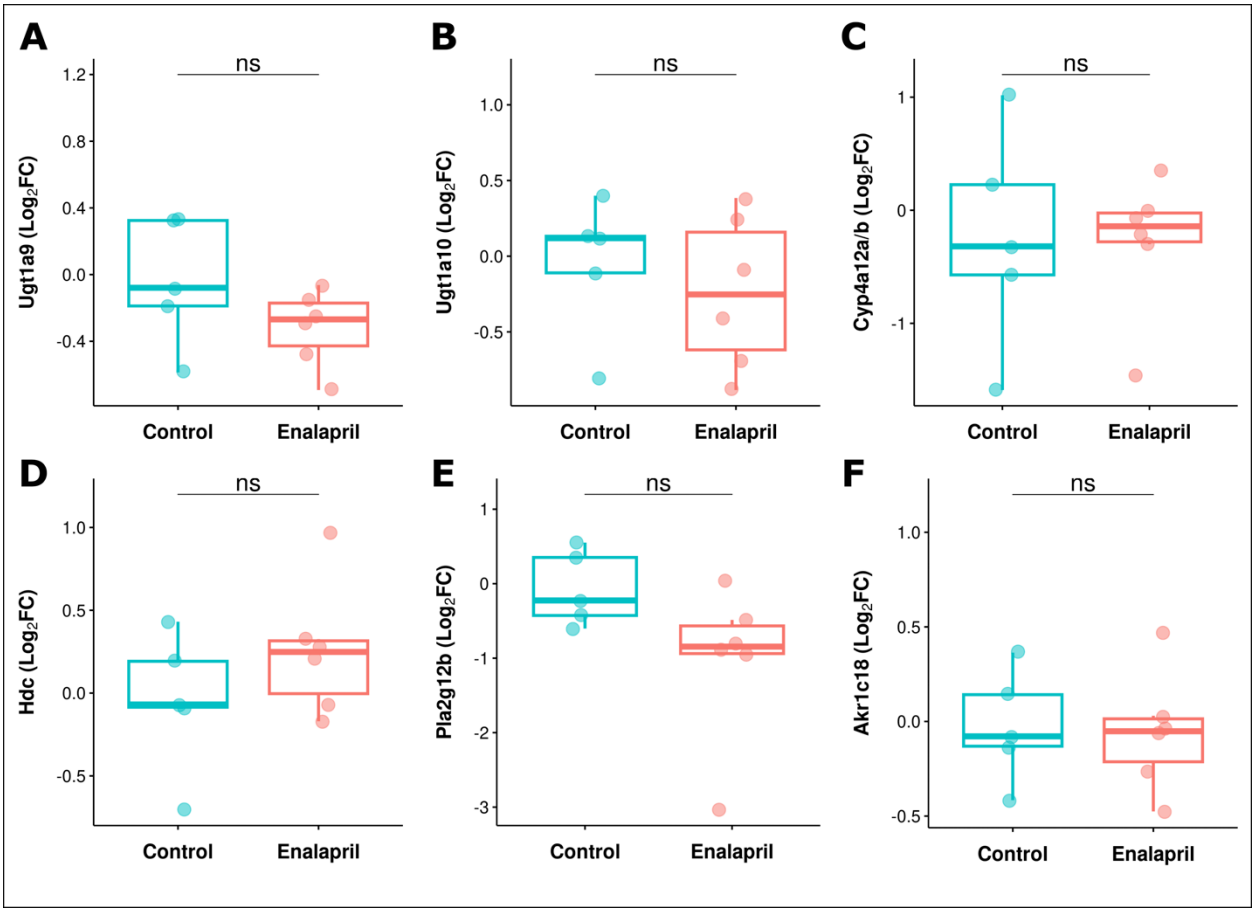

CHAPTER 4 DISCUSSION

The molecular basis of frailty has yet to be uncovered in the literature. In particular, the genes, proteins, and metabolites involved in the manifestation of frailty in the kidney have not been established. I hypothesized that biomarkers associated with frailty could be identified by examining the differential patterns of gene expression in the kidneys of mice with varying degrees of frailty. To test this hypothesis, I conducted an exploratory study to identify genes in the kidney that were differentially expressed with frailty. RNA-Seq was used to quantify transcriptional differences in mice with high and low FIs. I identified seven DEMGs related to frailty, independent of chronological age. I used qPCR to validate the expression of these genes in groups of mice with low, mid, and high FI scores. Finally, I used qPCR to assess whether the ACE inhibitor enalapril attenuates frailty by a mechanism related to the DEMGs associated with frailty.

4.1 Frailty and metabolism

RNA-Seq allowed for the identification of coding and non-coding gene transcripts in the female mouse kidney. Analysis of the total transcriptome distinguished high FI from low FI mice. However, metabolic transcripts alone differentiated the two groups more effectively, as evidenced by the greater proportion of variance explained by the first three PCs. Therefore, I performed a differential expression analysis on the metabolic genes and found seven interesting candidates, which I called DEMGs. Although these genes had an FDR value > 0.05, they were four or more times up or downregulated in the high FI group compared to the low FI group ($|\text{Log}_2\text{FC}| \geq 2$). The DEMGs identified were *Ugt1a9*, *Ugt1a10*, *Cyp4a12a*, *Cyp4a12b, Hdc*, *Pla2g12b*, and *Akr1c18.* When t-tests were conducted using the filtered and normalized Log_2CPM gene counts, *Ugt1a9*, *Ugt1a10*, *Hdc*, *Pla2g12b*, and *Akr1c18* were found to be significantly downregulated in the high FI group compared to low FI. Conversely, *Cyp4a12a* and *Cyp4a12b* were significantly upregulated in high FI versus low FI. Therefore, variations in these DEMGs may be associated with frailty.

The seven DEMGs were used to conduct a functional analysis, generating a list of biological processes potentially dysregulated with frailty. Notably, the omega-hydroxylase P450 pathway, glucuronate metabolic process, and arachidonic acid metabolic process were enriched by the frailty-associated DEMGs. These metabolic pathways were supported by supplementary research into the function of each individual gene.

When frailty and metabolism are discussed in the literature, this is often done in the context of diabetes mellitus and muscle metabolism. For instance, one study found dysregulated glucose metabolism to be related to frailty in older women [177]. Another study associated frailty with insulin resistance in obese individuals [178]. Cardiometabolic disorders can include cardiovascular disease, diabetes mellitus, and metabolic syndrome [179]. Tang et al. found that frail individuals are at increased risk of developing cardiometabolic disorders, and frailty severity increases with the occurrence of cardiometabolic disorders [180]. Thus, there appears to be a relationship between frailty and a metabolic phenotype that could contribute to diabetes. In terms of muscle metabolism, frailty has been shown to exacerbate age-related alterations in protein metabolism [181]. Frailty is associated with an increase in muscle protein catabolism and a decrease in muscle mass [181]. Frailty and sarcopenia, which is a syndrome characterized by muscle loss, are considered highly overlapping conditions [182]. Aside from these more commonly studied metabolic dysfunctions, frailty has been investigated, albeit minimally, in association with energy metabolism. Dysregulated carnitine shuttle and vitamin E pathways were observed in frail individuals, and it was concluded that lipid metabolism might deteriorate with frailty [183].

While there is evidence of some association between frailty and metabolism, frailty is often measured as an outcome of metabolic disorders and disease. This begs the question of whether frailty predisposes an individual to dysregulated metabolism or whether dysregulated metabolism is a contributor to the pathogenesis of frailty. This study raises the same question but aims to fill a large gap in the literature by characterizing metabolism in the kidney and its link to frailty.

4.2 Frailty DEMGs are independent of age and have not been previously implicated in kidney diseases

One challenge in identifying biomarkers for frailty is separating frailty from age. Frailty and age are closely related concepts, and frailty tends to increase with age [14]. However, I wanted to identify a panel of potential biomarkers related to frailty independent of chronological age. To achieve this, the low and high FI mice chosen for RNA-Seq were approximately the same age. To confirm that fluctuations in the DEMGs were not related to age, I assessed their expression in a publicly available kidney transcriptomics dataset. Takemon et al. measured gene expression in the kidneys of aging DO mice at 6, 12, and 18 months of age [147]. I evaluated the expression of the frailty DEMGs in the female mice from the Takemon et al. dataset. *Pla2g12b* expression was significantly different between 6 months and 12 months as well as 6 months to 18 months. However, no difference was detected between 12 and 18 months. Interestingly, the expression of *Ugt1a9*, *Ugt1a10*, *Cyp4a12a*, *Cyp4a12b, Hdc*, and *Akr1c18* was not significantly different at any age. These results suggest that most of the DEMGs identified here are associated with frailty but not age.

Even though CKD and cancers of the kidney can contribute to frailty, an individual can be frail in the absence of these diseases [18,184]. Therefore, I wanted to identify biomarkers specific to frailty that could be used in the frail population more generally. Mice with observable damage to the kidney or the presence of tumors were excluded from this study. Furthermore, the FI measure did not include any direct measures of kidney function. To investigate whether my biomarkers were previously implicated in other diseases, I compared the DEMGs found to previously reported biomarkers for CKD and cancer in the literature.

CKD biomarkers can be categorized as markers of kidney function, tubulointerstitial injury, glomerular injury, endothelial dysfunction, oxidative stress, inflammation, fibrosis, cardiovascular dysfunction, and metabolic disorders [185]. Examples of these markers include cystatin C, liver-type fatty acid-binding protein, nephrin, F2-isoprostanes, IL-18, transforming growth factor beta 1, and apolipoprotein A-IV [185]. In terms of kidney cancers, aquaporin-1 and adipophilin appear to be useful markers for those originating in the proximal tubule [186]. Another study attempted to identify metabolites in the urine of kidney cancer patients. Possible biomarkers included quinolinate, 4-hydroxybenzoate, and gentisate, among others [187]. Plasma

kisspeptin-10, urinary expression of microRNA 15a, serum prolyl hydroxylase domain-containing protein 3, and plasma kidney injury molecule are a group of potential markers for renal cell carcinoma [188]. In any case, none of the biomarkers for CKD or kidney cancer that I found in the literature appeared to overlap with the frailty DEMGs.

Although mice with observable abnormalities of the kidney were excluded from this study, it is possible that the mice included could have unknowingly had diseased kidneys. The FI measure does not directly relate to kidney function and rather reflects the functioning of multiple systems. Thus, it is a promising measure for associating kidney markers with frailty rather than with diseases specific to the kidney. None of the frailty DEMGs appear to be established biomarkers for kidney diseases.

4.3 Metabolic genes are dysregulated in frail mice

4.3.1 Histidine decarboxylase (*Hdc*) is downregulated in frail mice

Hdc encodes the histidine decarboxylase protein (HDC), orthologous to *HDC* in humans, which participates in the histamine biosynthetic and histidine catabolic processes [189]. Expression of *Hdc* is high in the ovary and lung of adult mice [167].

Histamine, the product of *Hdc* activity, has been implicated in allergic and non-allergic inflammatory responses and is commonly induced during the late and chronic phases of inflammation [190]. Renal histamine and *Hdc* have not been extensively investigated [191]. However, histamine seems to play a part in both the physiological and pathological functions of the kidney via the actions of its receptors, H1, H2, H3, and H4 [191]. There is some literature suggesting that the role of histamine in the kidney is to modulate renal hemodynamics (by mediating renal blood flow and vascular resistance) and to participate in urine formation [192–195].

Neither *Hdc* nor histamine appear to have a documented association with frailty. In my study, the RNA-Seq analysis, later validated by qPCR, showed that *Hdc* was downregulated in kidneys from high FI mice compared to low FI mice. This was an unexpected finding given that

frailty has been associated with a chronic pro-inflammatory state, and histamine is generally produced during chronic inflammation. One might expect *Hdc* to be increased with frailty. However, histamine could actually have a protective quality in the kidney. Noguchi et al. found that plasma histamine levels are elevated in an angiotensin II, nephrectomy, and salt (ANS) model of cardiac dysfunction [196]. Interestingly, when HDC was knocked out in the ANS model, cardiac and kidney dysfunction increased [196]. In the same study, an H3 agonist was found to ameliorate cardiorenal damage [196]. There is additional literature suggesting that agonists of the H3 receptors may exert protective effects in the kidney and heart [197,198]. Therefore, the downregulation of *Hdc* and its product, histamine, may have a more complex role in frailty that warrants further studies.

4.3.2 Aldo-keto reductase family 1, member C18 (Akr1c18) is downregulated in frail mice

In mice, *Akr1c18* encodes aldo-keto reductase family 1, member C18 (AKR1C18) [199]. The AKR1C18 protein possesses 20-alpha-hydroxysteroid dehydrogenase (20α-HSD) activity which is relevant for parturition and progesterone catabolism [200]. The aldo-keto reductase (AKR) family catalyzes progesterone to 20α-hydroxy-4-pregnen-3-one, an inactive metabolite [200]. *Akr1c18* expression is particularly high in the adult adrenal glands and ovaries but also in the kidneys of mice [167,201]. The mouse AKR1C18 protein is most similar to aldo-keto reductase family 1 members C1 to 4 (AKR1C1, AKR1C2, AKR1C3, AKR1C4) in humans [201].

In humans, endogenous substrates of AKR1C1-C4 enzymes are steroids and prostaglandins [202]. AKR1C1 has 20α-HSD activity, while AKR1C2 has 3α-hydroxysteroid dehydrogenase type 3 activity, and has been implicated in the transportation of bile acids [203–205]. AKR1C3 catalyzes the prostaglandins H_2 to PGF2α and D_2 to 9α,11β-PGF2α. Additionally, AKR1C3 has 17β-hydroxysteroid dehydrogenase activity, which allows for the conversion of estrone to estradiol and androstanedione to testosterone [206,207]. Frailty has been previously associated with decreased testosterone in males and increased estradiol in females [82–84]. It is interesting that AKR1C18, the mouse ortholog of human AKR1C3, was found to be downregulated with frailty in mice. Decreased AKR1C18 activity could suggest that the

production of estradiol and testosterone from their respective precursors is impaired. Reduced testosterone with frailty aligns with previous studies in humans, but decreased estradiol does not [82–84]. Finally, AKR1C4 has 3α-hydroxysteroid dehydrogenase type 1 activity [205]. In addition to their hydroxysteroid dehydrogenase activity, the family of AKR enzymes is known for their ability to reduce carbonyl-containing compounds, contributing to the metabolism of exogenous substrates [202,208]. AKRs participate in phase I of drug metabolism by functionalizing carbonyl groups, enabling phase II reactions [209]. Several drugs are known to be metabolized by the AKR1C isoforms [202].

AKRs have been extensively studied in association with a variety of cancers in human populations. Imbalances in the production and inactivation of steroids have been implicated in the development of hormonally dependent breast, prostate, endometrial, and ovarian cancers [210,211]. Indeed, alterations in human *AKR1C1-AKR1C4* expression seem to play a role in the development of these cancers [212–215].

While a link between AKR1Cs and cancer has been established, a literature search of AKRs and frailty does not yield any results. My RNA-seq and qPCR validation show *Akr1c18* is downregulated in frailty. In frail mice, decreased *Akr1c18* may confer impairments in the ability to transform drugs into their functionalized metabolites. Given the role of AKRs in the conversion of exogenous and endogenous compounds, a link between frailty, *Akr1c18* expression, and metabolism should be further explored.

4.3.3 Phospholipase A_2 group XIIB (*Pla2g12b*) is downregulated in frail mice

Pla2g12b encodes the phospholipase A2, group XIIB protein (PLA2G12B), orthologous to human *PLA2G12B* [216]. This gene is largely expressed in the adult placenta, small intestine, and large intestine, among other tissues in mice [167]. Broadly, phospholipase A_2 (PLA_2) enzymes are involved in the homeostasis of cellular membranes, lipid digestion, host defense, and the production of lipid mediators [217]. PLA_2s possess the ability to catalyze substrate phospholipids, producing lysophospholipids and fatty acids, such as arachidonic acid (AA) and oleic acid [218].

However, the *Pla2g12b* isoform has a mutation at its active site which suggests it is catalytically inactive [217]. Instead, it is thought to act as a ligand for receptors that have yet to be identified [217].

A study involving knockout mice showed that the accumulation of triglycerides, cholesterol, and fatty acids in the livers of *Pla2g12b*$^{-/-}$ animals led to the development of severe hepatosteatosis [219]. Furthermore, mice with mutations in *Pla2g12b* experienced reductions in serum levels of total cholesterol, non-high-density lipoprotein (HDL) cholesterol, and triglyceride levels [220]. The mutation also caused lipid accumulation in the liver [220]. Thus, *Pla2g12b* seems to have some role in lipid metabolism despite its catalytic inactivity. In fact, a recent study used biochemical, genetic, and imaging techniques to better characterize the function of *Pla2g12b* in model systems, including mice, zebrafish, and larvae [216]. *Pla2g12b* was shown to interact with apolipoprotein-B, microsomal triglyceride transfer protein, calcium, and the endoplasmic reticulum membrane [216]. Others have shown that *Pla2g12b* is a master regulator of lipids between luminal lipid droplets and triglycereide-rich lipoproteins, and alterations to *Pla2g12b* expression resulted in a reduction of serum lipoproteins [219,221,222].

Lp-PLA$_2$s contribute to lipid metabolism in the blood, thereby regulating vascular inflammation [223]. Notably, elevated Lp-PLA$_2$ levels have been associated with increased frailty odds and slower gait speed [90]. Perhaps there is an interesting link between genes encoding members of the PLA$_2$ superfamily, such as *Pla2g12b* and frailty.

My RNA-Seq and subsequent qPCR validation showed *Pla2g12b* to be downregulated with frailty, which was unexpected given previous literature suggesting Lp-PLA$_2$ is increased with frailty. However, the *Pla2g12b* isoform in mice likely has an alternative function compared to other genes encoding PLA$_2$s considering its mutation. *Pla2g12b* has been implicated in lipid metabolism, and there is evidence to support that in *Pla2g12b* knockouts or mutant models, lipids accumulate in the liver [219,220]. Therefore, it could be interesting to explore the impact of downregulated *Pla2g12b* and dysregulated lipid metabolism on renal function. Lipid accumulation in the renal parenchyma can damage the tubules and glomerulus [224]. Additionally, structural and functional changes to podocytes, proximal tubule cells, and mesangial cells can be brought about by the accumulation of fats in the kidney, thus affecting nephron function [224,225]. If

Pla2g12b is downregulated with frailty, it is possible that kidney function could deteriorate due to lipid accumulation and subsequent structural damage. Still, additional research is needed to verify this and better understand the relationship between the phospholipase A_2 group XIIB genes, their proteins, and frailty.

4.3.4 Cytochrome P450, family 4, subfamily a, polypeptide 12a and 12b (*Cyp4a12a* and *Cyp4a12b*) are upregulated in frail mice

The *Cyp4a12a* gene encodes cytochrome P450, family 4, subfamily a, polypeptide 12a (CYP4A12A), and the *Cyp4a12b* gene encodes cytochrome P450, family 4, subfamily a, polypeptide 12b (CYP4A12B) [226]. These genes have biased expression in the embryonic liver and adult genital fat pad of mice [167]. Previous studies have shown that the expression of *Cyp4a12* genes is specific to males and is androgen-related, with *Cyp4a12* isoforms being expressed at very low or undetectable levels in the female mouse kidney [226–228]. The cohort used here was comprised of females only and unexpectedly showed overexpression of both renal *Cyp4a12a and Cyp4a12b* in high FI mice. Interestingly, testosterone treatment has been shown to increase *Cyp4a12* RNA expression in the kidneys of female mice [227]. Since *Cyp4a12* expression is androgen-sensitive, varying blood testosterone levels across different mouse strains provide one possible explanation for the discrepancy in these findings [226,229]. Expression of the *Cyp4a14* gene, another member of the *Cyp4a* family, was found to be dependent on age and decreased in the male mouse kidney upon reaching sexual maturity [228]. In a similar fashion, *Cyp4a12*s could also be age-dependent, which could be another explanation for low or undetectable levels in female mouse kidneys.

CYP4A12A and CYP4A12B belong to a large family of CYP450 enzymes. They participate in the metabolism of endogenous substances, including vitamins and fatty acids, and also have the ability to metabolize xenobiotics to detoxified products or reactive intermediates [230]. The *Cyp4a12a and Cyp4a12b* genes are orthologous to human *CYP4A11* and *CYP4A22,* which encode the CYP4A11 and CYP4A22 proteins, respectively [231,232]. The *Cyp4a* subfamily encodes CYP450s with omega-hydroxylase activity [230]. This activity enables the catalysis of

endogenous fatty acids, such as AA, to 19- and 20-hydroxyeicosatetraenoic acids (19- and 20-HETE) [233]. Of the CYP4A proteins, CYP4A12s exhibit the greatest capacity for producing 20-HETE [226,228]. However, of CYP4A12A and CYP4A12B, the former is the predominant 20-HETE synthase [234,235]. The equivalent human CYP isoforms mainly responsible for renal 20-HETE synthesis are CYP4A11 and CYP4F2 [232,236]. In addition to their endobiotic metabolism abilities, the CYP450 enzymes are well-known for their role in phase I of biotransformation where they metabolize drugs via oxidation reactions [237]. It is important to note that the role of renal CYP450s is less significant compared to that of hepatic CYP450s, which can be attributed to the lower organ weight and microsome yield of the kidney [131,238].

Expression of CYP4A enzymes was found to be upregulated in a variety of human cancer tumour samples [239]. Furthermore, it has been speculated that altered expression of renal CYP4As could be related to hypertension due to its involvement in AA metabolism [240–242]. Twenty-HETE, the product of CYP4A11 activity in humans and CYP4A12A activity in mice, has been widely studied with regard to its conflicting anti-/pro-hypertensive roles. On one hand, 20-HETE regulates the reabsorption of sodium into the tubules of the kidney [243]. By inhibiting sodium reabsorption and promoting natriuresis, 20-HETE can have anti-hypertensive properties [243]. A variant of the human CYP4A11 isoform has been linked with hypertension in humans. This variant conferred reduced 20-HETE synthase activity and was associated with hypertension, highlighting the anti-hypertensive properties of 20-HETE [232]. On the other hand, 20-HETE regulates vascular tone and is a potent vasoconstrictor [244,245]. This increase in vascular resistance leads to the development of hypertension [246]. Although the hypertensive effects are debated, more often than not in the literature, elevated 20-HETE is implicated in the pathogenesis of hypertension [247]. Additionally, 20-HETE has been implicated in the pathogenesis of stroke, cystic renal disease, CKD, and diabetes mellitus, among other diseases [247–251].

Given that the *Cyp4a12a* and *Cyp4a12b* genes were identified as being upregulated in frail mice, further exploration into their roles in metabolism is needed. Research surrounding renal CYP450s is lacking [131]. In particular, there is limited information about xenobiotic substrates of renal CYP450s [131]. Therefore, it is unknown exactly how alterations in the expression of renal *Cyp4a* genes will affect drug metabolism. Furthermore, there has been no

evidence yet to support a link between either *Cyp4a12a* or *Cyp4a12b* and frailty, nor is there a documented relationship between *CYP4A11* and frailty in humans. Nevertheless, it has been established that the proteins encoded by these genes are involved in endobiotic metabolism and contribute to the production of 20-HETE. Ultimately, impaired hydroxylase activity caused by altered *Cyp4a* expression could alter xenobiotic and endobiotic metabolic pathways in the kidney, necessitating a further understanding of renal CYP4A dysfunction in relation to frailty.

4.3.5 UDP glycosyltransferase 1 family, polypeptide A9 and A10 (*Ugt1a9* and *Ugt1a10*) are downregulated in frail mice

In mice, the *Ugt1a9* gene encodes Uridine 5'-diphospho-glucuronosyltransferase (UDP) 1 family, polypeptide A9 (UGT1A9), while the *Ugt1a10* gene encodes UDP glycosyltransferase 1 family, polypeptide A10 (UGT1A10) [252]. *Ugt1a9* and *Ugt1a10* are typically expressed in the adult mouse kidney and liver [167]. The protein products of *Ugt1a9* and *Ugt1a10* belong to the UGT superfamily. UGT enzymes are involved in glucuronidation reactions in which compounds are detoxified through conjugation to glucuronic acid [253]. Endogenous substrates of UGTs include steroids, bilirubin, testosterone, and estradiol [253]. Additionally, UGTs have xenobiotic substrates such as drugs and flavonoids [253].

The *Ugt1a9* and *Ugt1a10* genes do not appear to be previously studied with respect to frailty. However, human orthologs have been examined in the context of cancer. Mouse UGT1A9 has 80% homology with human UGT1A9, while mouse UGT1A10 has 77-78% homology with UGT1A9 in humans [254,255]. Downregulated expression of *UGT1A9* mRNA has been observed in human renal cell carcinoma tissue [256]. Another study found that in humans, renal drug metabolism by UGTs was diminished in neoplastic kidneys compared to normal tissues [257]. This reduced capacity for glucuronidation observed in kidney tumor samples coincided with a reduction in UGT1A9 mRNA and protein expression [257]. Given these findings, reduced expression of the *UGT1A9* gene and its protein appears to be a recurring pattern in cancers of the kidney.

UGT enzymes have been studied in terms of their role in phase II of drug biotransformation and in detoxification reactions [258]. These enzymes conjugate UDP-glucuronic acid to endo- and xeno-biotics to increase their water solubility and aid their elimination via bile or urine [258]. Localization of UGT1A9 in the kidneys appears to provide a detoxification mechanism. This limits the exposure and response to drugs acting in the kidney, thereby reducing the chances of damage by nephrotoxic compounds [130]. In humans, the *UGT1A9* isoform, encoding the UGT1A9 protein, is abundantly expressed in the kidney and has been recognized for its role in the glucuronidation of drugs, arachidonic acid, prostaglandins, and leukotrienes [131]. Furthermore, UGT1A9 plays a substantial role in endobiotic metabolism. UGT1A9 is a contributor to the metabolism of 20-HETE, the product of AA catabolism [259]. In fact, glucuronidation by UGT1A9 is thought to be the main pathway for the inactivation and excretion of 20-HETE via the urine [259,260]. Overall, UGTs terminate the biological actions of exogenous substances and serve as a clearance pathway for various compounds [261].

The RNA-Seq results from the present study suggest that downregulation of *Ugt1a9* and *Ugt1a10* expression occurred with frailty. Therefore, high FI mice could experience decreased glucuronidation, impairments to detoxification, and reduced clearance of endogenous and endogenous compounds. However, qPCR showed that *Ugt1a9* and *Ugt1a10* expression was upregulated with frailty. Variations in UGT expression would be interesting to study given the potential for frailty-related deteriorations in xenobiotic and endobiotic metabolism. However, expression of the UGT genes in frail mice requires further research considering the inability to validate my findings in the present study.

4.4 DEMGs do not explain enalapril-mediated attenuation of frailty

Keller et al. investigated the protective effects of the ACE inhibitor enalapril and its ability to mitigate the age-dependent increase in frailty [27]. In this study, middle-aged (9 month old) female mice were treated with enalapril over the course of four months [27]. Significant reductions in FI scores were observed in this group after three months of treatment and at four months when the treatment concluded [27]. The authors hypothesized that the effects of enalapril on pro-inflammatory and anti-inflammatory cytokines might provide a mechanistic explanation

for how enalapril reduces frailty [27]. Yet, enalapril did not significantly alter inflammatory cytokines at this early age, suggesting there is an alternative mechanism [27].

I was interested in determining whether the frailty-associated DEMGs could be related to the attenuation of frailty by enalapril. I theorized that enalapril-treated mice achieved a lower FI by means of the same DEMGs that were up or downregulated in the high versus low FI comparison. To answer this question, I measured DEMG expression in middle-aged female control and enalapril-treated mice. If the enalapril mechanism was related to the frailty DEMGs, I would have expected to observe a significant difference in the expression of those genes in the treated compared to the untreated mice. This would suggest that a lower FI could be achieved by restoring DEMG expression levels. However, no significant differences in the DEMGs between control and enalapril-treated mice were observed. It was concluded that in middle-aged female mice, enalapril likely does not attenuate frailty by a mechanism related to the frailty DEMGs.

One possible explanation for the lack of significant differences in DEMG expression between the enalapril and control group was that the middle-aged mice were not very frail. At the end of treatment, the average FI of the control mice used in the enalapril cohort was 0.23 ± 0.03 while the average FI for the treated mice was 0.16 ± 0.02. Ultimately, the FI scores of the middle-aged females from the enalapril cohort were not very high. Rather, their scores were comparable to the low FI group from the RNA-Seq cohort. Since the DEMGs were initially obtained from a study which compared very old mice with high FI scores (0.46 ± 0.04) to those with low FI scores (0.22 ± 0.012), significant differences in those genes might not be expected in a cohort of mice where all of the FI scores are relatively low. It is possible that significant differences in DEMG expression might not occur until frailty progresses further. Therefore, enalapril-treatment may only appear to restore DEMG expression once the mice become frail enough for the genes to be differentially expressed.

I have associated four of the frailty DEMGs with AA metabolism and the production of the 20-HETE metabolite. Frailty appears to be related to dysfunctions in the production and elimination of 20-HETE due to the up or downregulation of *Cyp4a12a, Cyp4a12b, Ugt1a9*, and *Ugt1a10.* Moreover, 20-HETE has been implicated in the development of hypertension [247].

Fortuitously, the ACE inhibitor enalapril attenuates frailty and is commonly used to treat hypertension. However, in the initial study from Keller et al., enalapril was found to attenuate frailty in middle-aged and older female mice independent of effects on blood pressure [27]. At both six weeks and 4 months of treatment, there were no significant differences in systolic or diastolic blood pressure readings between or within the control and enalapril-treated groups [27].

Although differences in blood pressure readings were not observed with enalapril treatment, measuring differences in 20-HETE levels in control and treated groups might be of interest. In fact, 20-HETE has been said to activate ACE expression [235]. Furthermore, 20-HETE production in outer medullary microsomes was previously quantified after treatment with the ACE inhibitors captopril and enalapril [262]. Captopril increased 20-HETE production by 100%, while enalapril caused a 143% increase [262]. Perhaps the molecular mechanism of enalapril could manifest via a marker such as 20-HETE. Levels of 20-HETE, a product of AA metabolism related to *Cyp4a12a*, *Cyp4a12b*, *Ugt1a9*, and *Ugt1a10*, could be associated with enalapril-mediated reduction of frailty scores. Furthermore, quantification of 20-HETE could indicate whether enalapril causes changes in cardiovascular function related to the attenuation of frailty. This would be an interesting outcome since Keller et al. did not observe measurable differences in blood pressure with enalapril treatment [27].

4.5 Limitations of this study

After identifying seven genes which were differentially expressed in the high versus low FI groups via RNA-Seq, I aimed to measure their expression in a more extensive range of FIs using qPCR. The goal was to create a calibration curve in which the proposed frailty-associated DEMGs could be graded by FI, allowing for the prediction of a mouse's FI according to their expression. Based on qPCR assays, the expression of *Hdc, Pla2g12b, and Akr1c18* did appear to gradually decrease with FI, which was concordant with the RNA-Seq. However, these trends were not statistically significant and were not necessarily consistent with increasing FI. Expression of *Cyp4a12a/b* in the intermediate FI groups was unclear and did not appear to follow an upward or downward trend. Yet, qPCR did validate the expression patterns of *Hdc, Pla2g12b, Akr1c18, and Cyp4a12s* that were seen with RNA-Seq when comparing high FI to

low FI. Because the expression of the DEMGs with a range of low, intermediate, and high FIs did not produce significant or consistent trends, these genes may not be ideal biomarkers for discriminating gradual changes in FI and may be limited for use in distinguishing extreme high and low FI scores.

There were also two limitations to using the qPCR result to quantify the expression of *Ugt1a9* and *Ugt1a10* expression. First, the patterns exhibited by these genes were interesting because their expression seemed to decrease from low FI to mid FI but then increased gradually from mid FI to high FI. Therefore, *Ugt* genes would not be reliable for the detection of a range of FI values. Secondly, the expression of *Ugt1a9* and *Ugt1a10* in the high FI and low FI groups displayed an opposite trend between methods. The RNA-Seq results showed *Ugt* downregulation in high FI, whereas qPCR showed upregulation with high FI. In a study comparing differential gene expression correlations from RNA-Seq and qPCR, 80-85% of genes were found to be concordant between the two methods [263]. However, 1.8% of the 13,045 genes considered were called "severely non-concordant" because their fold-changes differed substantially between qPCR and RNA-Seq [263]. Perhaps this could contribute to the discrepancies in my data. qPCR relies on a number of factors for a successful assay. These include but are not limited to: accurate quantification of the gene amplicon, selection of appropriate reference genes, and design of primers that are specific for a target gene. Technical issues with quantifying the amplicon were ruled out after conducting a DNA agarose gel which confirmed no differences between qPCR and the gel method. Reference gene selection was carried out based on the stable expression of both *Ppia* and *Hprt* with increasing age and frailty. Primer sequences were input into the NCBI Primer-BLAST tool to ensure there was no off-target binding. Nevertheless, it is possible that with several *Ugt* isoforms, non-specific binding could have occurred and led to the overestimation of *Ugt* expression via qPCR [166]. In my RNA-Seq data, eight isoforms belonging to the *Ugt1a* family were identified (*Ugt1a1, Ugt1a2, Ugt1a5, Ugt1a6a, Ugt1a6b, Ugt1a7c, Ugt1a9,* and *Ugt1a10*). Since these transcripts were quantified in the kidney samples, it is possible that non-specific binding with the *Ugt1a9* and *Ugt1a10* qPCR primers could have occurred. Further confirmation of *Ugt* gene expression could be evaluated via protein quantification methods. However, for the purpose of this thesis, I accepted the RNA-Seq results over qPCR because RNA-Seq evaluates individual gene expression relative to the entire

transcriptome, does not rely on primers, and is capable of identifying alternatively spliced isoforms.

Considering the documented sex differences in mouse models of frailty, this study was conducted using exclusively female mice [27,63,65,67,69,70]. Therefore, the findings are limited to females, and they may not be reproducible in male mice. Studies of the molecular basis of frailty in male mice are needed to alleviate this limitation and allow for translation to both sexes in the human population.

An additional limitation was the fact that this study only looked for frailty biomarkers in a single strain of inbred mice, C57BL/6J. The mouse FI was validated for use in C57BL/6J mice [66]. These mice are commonly used in aging research because of the availability of phenotypic and genotypic information [66]. However, C57BL/6J mice have a relatively long lifespan compared to other short lived strains such as DBA/2J and BALB/cJ [66,264]. Mice with reduced lifespans could show different features of aging compared to mice with longer lifespans [265]. Interestingly, Kane et al. found that age- and diet-matched male DBA/2J mice had higher FI scores than C57BL/6J mice, suggesting strain differences [66]. Thus, the frailty-associated DEMGs identified in this study may not necessarily be generalizable to other mouse strains with shorter lifespans.

Another limitation of this study was that it included only a single omics measure. RNA-Seq was used to profile the transcriptome, consisting of all coding and non-coding RNA molecules. Protein-coding metabolic genes were identified as being differentially expressed, and a number of hypotheses about the metabolic aspects of frailty were formed based on the assumption that mRNA expression directly correlates with protein abundance. However, mRNA does not solely dictate protein levels. Rather, protein abundance is largely determined by translational and post-translational events [266]. Takemon et al. found that with age, mRNA cannot be used to reliably predict the direction of change of a protein [147]. In part, this could be due to a loss of proteostasis that transpires with age [147]. Proteostasis is characterized by protein aggregation, protein unfolding, oxidative damage, post-translational modifications, and alterations in the rate of protein turnover [267]. Similar to age, proteostasis is a hallmark of frailty [9].

This study was further limited by not having access to blood pressure or 20-HETE measurements from the high and low FI mice used. Even without protein levels data, speculation regarding altered endobiotic metabolism could have been substantiated with these measurements, which might have provided a link to hypertension.

4.6 A model of altered metabolism in the kidneys of frail mice

4.6.1 Endobiotic metabolism

One of the pathways identified in the GO enrichment analysis was the metabolism of the endogenous molecule AA. AA is a component of membrane phospholipids [268]. AA can be mobilized from the cell membrane by PLA_2 and phospholipase C during times of cellular stress, generating free AA [268]. AA can be metabolized into several different products via three pathways [268]. Prostaglandins and thromboxanes can be produced by the cyclooxygenase pathway [268]. The lipoxygenase pathway creates leukotrienes and lipoxins [268]. Finally, AA can be metabolized via the CYP450 pathway to generate epoxyeicosatrienoic acids (EETs) or HETEs (Figure 4.1) [268].

In my study, the *Cyp4a12a* gene encoding a CYP450 enzyme was found to be upregulated in the kidneys of mice with high FI. *Cyp4a12b* was also shown to be overexpressed in the frail mouse kidney, but CYP4A12A has a greater ability to metabolize AA to 20-HETE via its omega-hydroxylase activity [234,235]. Therefore, increased expression of *Cyp4a12a* in frail mice could increase the catabolism of AA, leading to increased production of the 20-HETE metabolite.

Renal UGTs can metabolize CYP450-derived metabolites from AA catabolism [131]. UGT1A9 plays a key role in the detoxification process and is part of the primary pathway by which 20-HETE is eliminated [259]. UGT1A9 produces the glucuronidated form of the AA metabolite, 20-HETE glucuronide, which is eliminated via the urine in this form (Figure 4.1) [259]. My RNA-Seq results showed that *Ugt1a9* and *Ugt1a10* were downregulated in high FI mice. If

the downregulation of these genes led to reduced expression of the UGT1A9 enzyme, 20-HETE might not be cleared as effectively in frail mice.

In very frail mice, overexpression of *Cyp4a12a* could increase the production of 20-HETE from free AA. Simultaneously, the downregulation of *Ugt1a9* and *Ugt1a10* could lead to less effective detoxification. Taken together, an accumulation of 20-HETE in the kidney could be associated with frailty (Figure 4.1). Twenty-HETE has been shown to increase vascular tone and vasoconstriction, potentially leading to hypertension [244–246]. Furthermore, 20-HETE is involved in the regulation of blood flow to various organs, such as the brain and kidney [269]. Considering the aforementioned alterations in gene expression, accumulation of 20-HETE could be associated with frailty in mice. This also provides a potential link between frailty and hypertension, although this is not to say that one causes the other. Rather, the accumulation of 20-HETE and the development of hypertension could contribute to the pathogenesis of frailty by increasing the risk of end-organ damage or comorbid conditions [270,271].

4.6.2 Xenobiotic metabolism

The metabolism of drugs is primarily carried out by the liver, whereas the kidney is responsible for their excretion [237]. Hydrophilic drugs are more easily excreted via the kidneys than hydrophobic drugs. Biotransformation reactions take place, generally in the liver, to increase the hydrophilicity of hydrophobic drugs prior to their elimination [237]. Biotransformation can be divided into phase I and phase II metabolism, though both phases do not always occur sequentially. Molecules can directly enter phase II metabolism without the occurrence of phase I and can be excreted after phase I without the occurrence of phase II [237]. Phase I metabolism entails the oxidation, reduction, or hydrolysis of a drug or exogenous molecule (Figure 4.1) [237]. These modifications create or reveal polar functional groups to create a functionalized metabolite [237]. During phase II metabolism, polar groups are conjugated to molecules to generate water-soluble metabolites (Figure 4.1) [237]. Drug metabolites can be renally excreted, though bile is another significant method of elimination [237].

In my study, renal *Cyp4a12a* and *Cyp4a12b* were significantly overexpressed in the kidneys of frail mice. Assuming CYP4A12 abundance is upregulated as a result of increased mRNA expression, CYP450 enzyme activity in the kidney could increase. Hepatic CYP450 enzymes are mainly responsible for phase I metabolism [237]. Nevertheless, if renal CYP4A12 activity were to contribute to phase I reactions, biotransformation may occur more rapidly. This could increase the functionalization of drug metabolites to aid their elimination [272]. However, bioactivation could increase the production of and exposure to toxic drug metabolites [272].

The RNA-Seq data showed *Akr1c18* expression is downregulated in frail mice. AKR enzymes also play a part in phase I drug metabolism as they carry out nicotinamide adenine dinucleotide phosphate (NADPH)-dependent reduction of carbonyl groups (Figure 4.1) [209]. This process functionalizes the carbonyl group and allows for phase II conjugation reactions to aid drug elimination [209]. AKRs detoxify aldehyde and ketone substrates since they form alcohols, which are less reactive products. However, reduced chemical reactivity does not necessarily mean reduced biological activity [202]. Sometimes, the products of AKR reduction reactions can be bioactivated, forming reactive molecules [202]. In this sense, AKR enzymes can contribute to both the detoxification and bioactivation of drugs. Hence, reduced *Akr1c18* expression and resulting downregulation of AKR1C18 in frail mice may alter phase I of the biotransformation process.

Phase II of biotransformation can be completed by glucuronidation, catalyzed by UGT enzymes (Figure 4.1) [237]. This process of converting lipophilic compounds results in the production of a polar metabolite with increased hydrophilicity [261]. This generally terminates the biological effects of the parent drug compound and eases its elimination and clearance [261]. In other instances, the drug may be converted to a highly reactive metabolite with increased pharmacological activity or toxicity [261]. Thus, fluctuations in the expression of UGTs could have interesting implications for drug metabolism. Since the RNA-Seq results indicated that *Ugt1a9* and *Ugt1a10* expression is downregulated in high FI mice, the enzymatic activity of their respective proteins may be reduced. Detrimental effects of this could include a reduced ability to detoxify and clear drugs by glucuronidation with frailty.

Overall, variable expression of genes encoding CYP450s, AKRs, and UGTs could have several implications for the metabolism of endogenous and exogenous compounds in frail mice (Figure 4.1). Metabolism of xenobiotics, including drugs, environmental pollutants, and plant constituents, could be impaired with frailty [273]. The therapeutic effect of a drug may be reduced if CYP450 activity is increased because pharmacologically active compounds could be rendered inactive more readily via oxidation reactions [274]. Alternatively, chemically reactive metabolites could be produced more readily by CYP450s, increasing the production of harmful compounds [274]. Furthermore, enhanced CYP450 activity could cause an administered prodrug to be converted to its active form at a faster rate, causing an enhanced therapeutic effect [274]. Reduced expression of enzymes with detoxification properties, such as AKRs and UGTs, could result in the inability to clear drug metabolites and lengthen the exposure to potentially toxic compounds [202,261]. Another possible consequence of decreased AKR activity could be a reduction in the therapeutic effect of a prodrug since a pharmacologically active product could be formed at a slower rate. Metabolism of endobiotics, particularly AA, may lead to the accumulation of 20-HETE. Since 20-HETE has been associated with hypertension, there may be a relationship between changes in blood pressure and frailty [247].

In general, these results need to be interpreted with caution as hepatic enzymes have a significantly greater metabolic capacity, particularly with regard to the metabolism of drugs [131]. Additionally, inferences regarding enzyme activity have been made based on gene expression. More research is needed to understand the functionality of renal enzymes, their contribution to biotransformation, and their role in AA metabolism before a definitive conclusion is made regarding dysfunctional xenobiotic and endobiotic metabolism in frail mice.

Figure 4.1. A model of altered endobiotic and xenobiotic metabolism in a frail mouse. **A.** Arachidonic acid is mobilized from the plasma membrane and converted to 20-Hydroxyeicosatetraenoic acid (20-HETE) by cytochrome P450. UDP-glucuronosyltransferases conjugate glucuronic acid to 20-HETE to aid in elimination. However, increased *Cyp4a12a* and decreased *Ugt1a9/10* expression in frail mice results in the accumulation of the unconjugated form of 20-HETE. **B.** Drug metabolism can occur through phase I and/or phase II metabolism. Phase I involves oxidation reactions carried out by cytochrome P450s or reduction reactions by aldo-keto reductases to create a polar functionalized metabolite. Phase II involves conjugation reactions, usually carried out by UDP-glucuronosyltransferases. *Cyp4a12a/b* expression is upregulated while *Akr1c18* and *Ugt1a9/10* expression is downregulated, leading to dysregulated drug metabolism in the frail mouse.

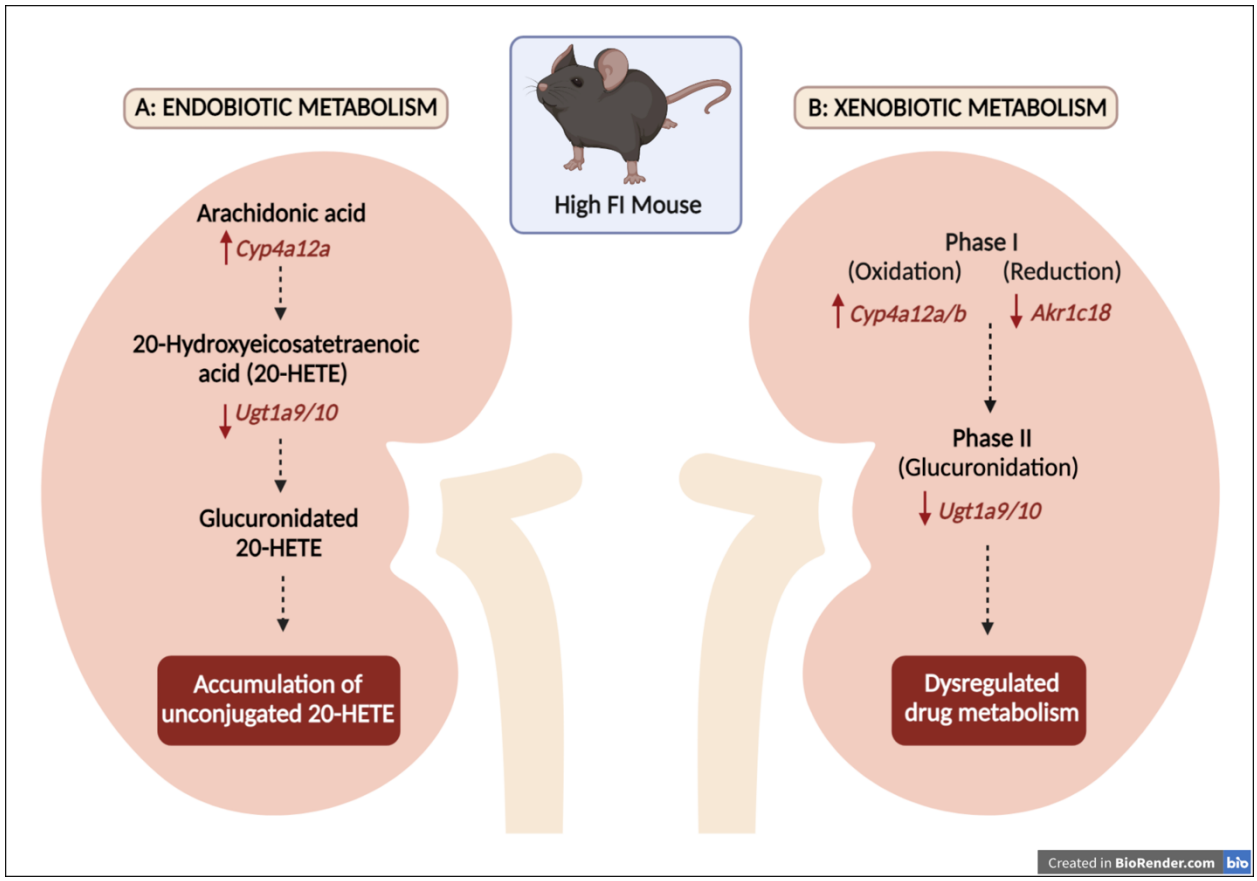

4.7 Implications of this study

4.7.1 Frailty biomarkers for clinical use

One of the main goals of this study was to identify novel biomarkers for frailty which originate in the mouse kidney. The DEMGs identified were done so using kidney tissue. In order to translate the results of this study to a clinical setting, the kidney-based biomarkers would need to be related to markers which could be measured non-invasively, such as in the urine or blood. To enable this, I associated the DEMGs with several dysregulated metabolic pathways, such as AA metabolism. As an example, I identified 20-HETE as a key metabolite in the AA pathway, which has the potential to accumulate in frail mice. Twenty-HETE can be measured in the urine and, therefore could undergo further testing to assess its feasibility as a biomarker for frailty [275]. Peripheral measurement of the vital components (Eg. enzymes and metabolites) of other pathways which are dysregulated with frailty could allow for the identification of additional frailty biomarkers. The broader implication of this work is that kidney-based biomarkers could be added to a panel of other FI-associated biomarkers that, when measured, could enable the pre-emptive detection of frailty prior to the emergence of observable health deficits.

4.7.2 Molecular basis of frailty

In addition to providing potential biomarkers for frailty, this study provides insights into the molecular basis of frailty. Currently, mechanistic explanations for how frailty occurs are lacking. Having elucidated metabolic pathways which may be altered with frailty, I have revealed a potential contributing mechanism through which frailty manifests in the kidney. Of course, it remains to be known whether frailty develops as a result of alterations to metabolic pathways or if frailty causes metabolic dysfunction to occur. Regardless, dysfunctional pathways have been identified, enabling target discovery for frailty interventions. Pharmacological treatments or non-pharmacological interventions related to these pathways could be developed to prevent frailty, promote healthy aging, or reverse the effects of frailty in the kidney and other organs.

4.7.3 Pharmacokinetic considerations

Since I proposed that drug metabolism may be altered in frailty, this research could have interesting implications for pharmacokinetics. In general, frail individuals are susceptible to ADRs [276]. However, this study may provide new insights as to how exactly the kidney changes with frailty, becoming less resilient and predisposing frail individuals to ADRs. Absorption, distribution, metabolism, and excretion of drugs can be highly influenced by drug-metabolizing enzymes. Altered CYP450s, AKRs, and UGTs could impact the ability of the kidney to metabolize drugs and transform them into their active or inactive forms. Therefore, pharmacokinetic considerations may need to be made for a frail individual where drug efficacy could be altered, or exposure to toxic metabolites may be increased. For example, if a drug is known to be metabolized by a renal CYP450 enzyme whose function is frailty-dependent, a more optimal drug might be prescribed. Moreover, frailty-associated alterations to UGT expression and activity could affect the ability of the kidney to clear drug metabolites from the body. In this case, drug dosing might need to be adjusted to account for these changes. In summary, this study might lead to further work that aims to elucidate the pharmacokinetic impacts of frailty. This could allow for the personalization of medical treatment based on frailty status and, ultimately, the reduction of ADRs in frail individuals. However, more research is needed as renal enzymes may not contribute significantly to both phase I and II of drug metabolism.

4.7.4 Polypharmacy

Dysfunctional drug metabolism may be a result of frailty itself, but it could also be related to the prevalence of polypharmacy in the frail population. Indeed, my study suggests that frailty is associated with molecular changes in the kidney that could lead to altered drug metabolism. However, polypharmacy (the use of multiple medicines) is prevalent in frail older people and can lead to altered metabolism and the occurrence of ADRs [276,277]. Related to my study, multiple drugs are metabolized by the AKR1C, CYP4A, and UGT1A9 isoforms in humans. Many drugs have been labelled as inducers or inhibitors of these enzymes, which enhance or interfere with their activity and increase vulnerability to ADRs and drug-drug

interactions [272,278–281]. This further complicates pharmacokinetics in frail individuals because polypharmacy can exacerbate the impairments in renal metabolism explored here.

4.8 Future directions

Further work pertaining to this study should aim to measure the 20-HETE metabolite in urine as it is an attractive candidate biomarker for frailty. Measurements of this metabolite should be obtained in mice with varying degrees of frailty to determine if it is a reliable marker and if it is sensitive enough to be associated with graded changes in the FI.

Protein abundance data for each of the corresponding DEMGs should be acquired using measures of protein expression such as Western blotting or proteomics. This would confirm the expression trend for each protein in frail mice. My study was limited to only gene expression, which does not necessarily correlate with protein expression. Furthermore, protein measurements could confirm how UGTs are altered with frailty, as the RNA-Seq and qPCR results differed in my study. Phosphoproteomics may be the most favourable method since it quantifies protein and provides additional information about protein activity based on phosphorylation status.

Finally, future work looking to uncover the metabolic effects of frailty should focus on the liver. The liver is another highly metabolic organ, especially given its large role in the metabolism of drugs. This study was limited to the manifestation of frailty in the kidney, but metabolic dysfunction related to frailty should also be assessed in the liver to get a sense of how hepatic enzymes may be impacted in frail individuals. Undoubtedly, frailty-related changes in the liver would also have important implications for endobiotic and xenobiotic metabolism. Additionally, the liver could be used to propose additional biomarkers for the detection of frailty.

4.9 Concluding remarks

The prevalence of frailty continues to grow worldwide, especially with our aging population. Pre-emptive detection of frailty might ease the strain on healthcare systems by treating frailty sooner or potentially reversing its effects through various interventions. Currently,

the main methods used to assess frailty are the FI and FP, which rely on mostly observable variables. To allow for earlier identification of frail individuals, techniques that rely mainly on laboratory test values, such as the FI-lab, have been developed. However, there are no biomarkers for frailty that have been validated for use clinically.

Considering the lack of reliable biomarkers, I aimed to associate differentially expressed genes in the kidney with the pre-existing clinical FI for mice. Using RNA-Seq, I evaluated transcriptional differences in the kidneys of female mice with extremely low and high FI scores. Seven frailty-associated DEMGs were identified (*Ugt1a9*, *Ugt1a10*, *Cyp4a12a*, *Cyp4a12b, Hdc*, *Pla2g12b*, and *Akr1c18*), and most of their expression trends in low and high FI mice were validated with qPCR. Furthermore, expression of the majority of the DEMGs was found to be associated with frailty, independent of chronological age.

Pharmacological interventions for frailty are an area of increasing interest. To provide a potential mechanistic explanation for how the ACE inhibitor enalapril attenuates frailty in middle-aged female mice, expression of the frailty DEMGs was measured in treated and untreated mice. However, enalapril did not appear to exert its effects by a mechanism related to these metabolic genes.

The DEMGs identified highlight dysregulated metabolic pathways in the kidneys of frail mice. This study provides new information regarding the implications of frailty on xenobiotic and endobiotic metabolism in the kidney. However, more work is needed to better characterize the effects of frailty on specific metabolic enzymes. In the future, the quantification of proteins and metabolites related to dysregulated metabolic pathways in the blood or urine could enable non-invasive detection of frailty. Validation of these biomarkers for use in clinical settings would allow for routine testing for frailty, including in younger people who can be afflicted by frailty as well.

In closing, this thesis characterizes the molecular effects of frailty in the kidney and paves the way for a broader understanding of this state. Ultimately, more research is necessary to validate the DEMGs described here. My research contributes important insights that, in the long

term, could help determine how we can better care for individuals with complex multi-system problems to ease the global burden of frailty.

APPENDIX A TOP 3000 MOST VARIABLE GENES

ENSMUSG00000064359	ENSMUSG00000031428	ENSMUSG00000020808
ENSMUSG00000093896	ENSMUSG00000030156	ENSMUSG00000071203
ENSMUSG00000058626	ENSMUSG00000104887	ENSMUSG00000039092
ENSMUSG00000095429	ENSMUSG00000028195	ENSMUSG00000022667
ENSMUSG00000066170	ENSMUSG00000030562	ENSMUSG00000095891
ENSMUSG00000096715	ENSMUSG00000027513	ENSMUSG00000029659
ENSMUSG00000068105	ENSMUSG00000043613	ENSMUSG00000016179
ENSMUSG00000024673	ENSMUSG00000027792	ENSMUSG00000057110
ENSMUSG00000030724	ENSMUSG00000004707	ENSMUSG00000019929
ENSMUSG00000014030	ENSMUSG00000049580	ENSMUSG00000087141
ENSMUSG00000040026	ENSMUSG00000009356	ENSMUSG00000039339
ENSMUSG00000098814	ENSMUSG00000032487	ENSMUSG00000063683
ENSMUSG00000029306	ENSMUSG00000062727	ENSMUSG00000052271
ENSMUSG00000096833	ENSMUSG00000029380	ENSMUSG00000066512
ENSMUSG00000018623	ENSMUSG00000085017	ENSMUSG00000047511
ENSMUSG00000047842	ENSMUSG00000109877	ENSMUSG00000022186
ENSMUSG00000096422	ENSMUSG00000069855	ENSMUSG00000091028
ENSMUSG00000104375	ENSMUSG00000031098	ENSMUSG00000035274
ENSMUSG00000076596	ENSMUSG00000050097	ENSMUSG00000012889
ENSMUSG00000032053	ENSMUSG00000051220	ENSMUSG00000011008
ENSMUSG00000095127	ENSMUSG00000109096	ENSMUSG00000029162
ENSMUSG00000076550	ENSMUSG00000024694	ENSMUSG00000110221
ENSMUSG00000076666	ENSMUSG00000052133	ENSMUSG00000074639
ENSMUSG00000063388	ENSMUSG00000068085	ENSMUSG00000086174
ENSMUSG00000094546	ENSMUSG00000028068	ENSMUSG00000021898
ENSMUSG00000009246	ENSMUSG00000040345	ENSMUSG00000023243
ENSMUSG00000096074	ENSMUSG00000049265	ENSMUSG00000020275
ENSMUSG00000022304	ENSMUSG00002076165	ENSMUSG00000071177
ENSMUSG00000048031	ENSMUSG00000049037	ENSMUSG00000036896
ENSMUSG00000003379	ENSMUSG00000119459	ENSMUSG00000022025
ENSMUSG00000105128	ENSMUSG00000015401	ENSMUSG00000055421
ENSMUSG00000094509	ENSMUSG00000085058	ENSMUSG00000083392
ENSMUSG00000030468	ENSMUSG00000107029	ENSMUSG00000047143
ENSMUSG00000103995	ENSMUSG00000026104	ENSMUSG00000080823
ENSMUSG00000094006	ENSMUSG00000039653	ENSMUSG00000090555
ENSMUSG00000095771	ENSMUSG00000034206	ENSMUSG00000090939
ENSMUSG00000095204	ENSMUSG00000119142	ENSMUSG00000016206

ENSMUSG00000008193
ENSMUSG00000094433
ENSMUSG00000030577
ENSMUSG00000076532
ENSMUSG00000105096
ENSMUSG00000032484
ENSMUSG00000095335
ENSMUSG00000042474
ENSMUSG00000065968
ENSMUSG00000050635
ENSMUSG00000076587
ENSMUSG00000014686
ENSMUSG00000096767
ENSMUSG00000076555
ENSMUSG00000027748
ENSMUSG00000031710
ENSMUSG00000001027
ENSMUSG00000086324
ENSMUSG00000105646
ENSMUSG00000040405
ENSMUSG00000105547
ENSMUSG00000086211
ENSMUSG00000104927
ENSMUSG00000004110
ENSMUSG00000096459
ENSMUSG00000032758
ENSMUSG00000096020
ENSMUSG00000094088
ENSMUSG00000079222
ENSMUSG00000110682
ENSMUSG00000096410
ENSMUSG00000076612
ENSMUSG00000030592
ENSMUSG00000005364
ENSMUSG00000022416
ENSMUSG00000095642
ENSMUSG00000026011
ENSMUSG00000059994
ENSMUSG00000076731
ENSMUSG00000053469
ENSMUSG00000050014
ENSMUSG00000099375
ENSMUSG00000117465
ENSMUSG00000037466
ENSMUSG00000021614
ENSMUSG00000005410
ENSMUSG00000095304
ENSMUSG00000022385
ENSMUSG00000044229
ENSMUSG00000057191
ENSMUSG00000084796
ENSMUSG00000022947
ENSMUSG00000063730
ENSMUSG00000002033
ENSMUSG00000028262
ENSMUSG00000040258
ENSMUSG00000026068
ENSMUSG00000030867
ENSMUSG00000035365
ENSMUSG00000020264
ENSMUSG00000035910
ENSMUSG00000056531
ENSMUSG00000032532
ENSMUSG00000113136
ENSMUSG00000097651
ENSMUSG00000052125
ENSMUSG00000026979
ENSMUSG00000049988
ENSMUSG00000035686
ENSMUSG00000044199
ENSMUSG00000006310
ENSMUSG00000042385
ENSMUSG00000025386
ENSMUSG00000026301
ENSMUSG00000013418
ENSMUSG00000032094
ENSMUSG00000080440
ENSMUSG00000065778
ENSMUSG00000001494
ENSMUSG00000026407
ENSMUSG00000033777
ENSMUSG00000086564
ENSMUSG00000110141
ENSMUSG00000093580
ENSMUSG00000079263
ENSMUSG00000031298
ENSMUSG00000027347
ENSMUSG00000102235
ENSMUSG00000080768
ENSMUSG00000103931
ENSMUSG00000049588
ENSMUSG00000110720
ENSMUSG00000029260
ENSMUSG00000040613
ENSMUSG00000063268
ENSMUSG00000020062
ENSMUSG00000046245
ENSMUSG00000063193
ENSMUSG00000056145
ENSMUSG00000080538
ENSMUSG00000099875
ENSMUSG00000062859
ENSMUSG00000100774
ENSMUSG00000037443
ENSMUSG00000107760
ENSMUSG00000022221
ENSMUSG00000087364
ENSMUSG00000079491
ENSMUSG00000037010
ENSMUSG00000046598
ENSMUSG00000070690
ENSMUSG00000107092
ENSMUSG00000045094
ENSMUSG00000117023
ENSMUSG00000094915
ENSMUSG00000033767
ENSMUSG00000078122
ENSMUSG00000015316
ENSMUSG00000047583
ENSMUSG00000082956

ENSMUSG00000085786	ENSMUSG00000023393	ENSMUSG00000090186
ENSMUSG00000015314	ENSMUSG00000006398	ENSMUSG00000026726
ENSMUSG00000056978	ENSMUSG00000018983	ENSMUSG00000049152
ENSMUSG00000079794	ENSMUSG00000047976	ENSMUSG00000116639
ENSMUSG00000094335	ENSMUSG00000086891	ENSMUSG00000028356
ENSMUSG00000076605	ENSMUSG00000074771	ENSMUSG00000118026
ENSMUSG00000110439	ENSMUSG00000016942	ENSMUSG00000006462
ENSMUSG00000105606	ENSMUSG00000070691	ENSMUSG00000074183
ENSMUSG00000040592	ENSMUSG00000033177	ENSMUSG00000027330
ENSMUSG00000098021	ENSMUSG00000117988	ENSMUSG00000070298
ENSMUSG00000009350	ENSMUSG00000038550	ENSMUSG00000092528
ENSMUSG00000016529	ENSMUSG00000074968	ENSMUSG00000036905
ENSMUSG00000105906	ENSMUSG00000086040	ENSMUSG00000046593
ENSMUSG00000104713	ENSMUSG00000030218	ENSMUSG00000116999
ENSMUSG00000076606	ENSMUSG00000119563	ENSMUSG00000015850
ENSMUSG00000079192	ENSMUSG00000022805	ENSMUSG00000108753
ENSMUSG00000090165	ENSMUSG00000024481	ENSMUSG00000023120
ENSMUSG00000019982	ENSMUSG00000080365	ENSMUSG00000027496
ENSMUSG00000054072	ENSMUSG00000004552	ENSMUSG00000079563
ENSMUSG00002076091	ENSMUSG00000041449	ENSMUSG00000089995
ENSMUSG00000079190	ENSMUSG00000030945	ENSMUSG00000039246
ENSMUSG00000092618	ENSMUSG00000082260	ENSMUSG00000036353
ENSMUSG00000040809	ENSMUSG00000051985	ENSMUSG00000029868
ENSMUSG00000040627	ENSMUSG00000028172	ENSMUSG00000063796
ENSMUSG00000076562	ENSMUSG00000109564	ENSMUSG00000026676
ENSMUSG00000094694	ENSMUSG00000083979	ENSMUSG00000074006
ENSMUSG00000076569	ENSMUSG00000025877	ENSMUSG00000068086
ENSMUSG00000043243	ENSMUSG00000027073	ENSMUSG00000023073
ENSMUSG00000043773	ENSMUSG00000061356	ENSMUSG00000076928
ENSMUSG00000095079	ENSMUSG00000117313	ENSMUSG00000033987
ENSMUSG00000076580	ENSMUSG00000022053	ENSMUSG00000031700
ENSMUSG00000079362	ENSMUSG00000037379	ENSMUSG00000046093
ENSMUSG00000041202	ENSMUSG00000018865	ENSMUSG00000046805
ENSMUSG00000029417	ENSMUSG00000045291	ENSMUSG00000000567
ENSMUSG00000076522	ENSMUSG00000105239	ENSMUSG00000004105
ENSMUSG00000076695	ENSMUSG00000072944	ENSMUSG00000049758
ENSMUSG00000076578	ENSMUSG00000118524	ENSMUSG00000106634
ENSMUSG00000047798	ENSMUSG00000031444	ENSMUSG00000027533
ENSMUSG00000076672	ENSMUSG00000112307	ENSMUSG00000024617
ENSMUSG00000093894	ENSMUSG00000105954	ENSMUSG00000037108

ENSMUSG00000104452
ENSMUSG00000078680
ENSMUSG00000026822
ENSMUSG00000092021
ENSMUSG00000076556
ENSMUSG00000014453
ENSMUSG00000023078
ENSMUSG00000076939
ENSMUSG00000044453
ENSMUSG00000052477
ENSMUSG00000015854
ENSMUSG00000037922
ENSMUSG00000096883
ENSMUSG00000026390
ENSMUSG00000015437
ENSMUSG00000095700
ENSMUSG00000073628
ENSMUSG00000096577
ENSMUSG00000000248
ENSMUSG00000078922
ENSMUSG00000076617
ENSMUSG00000020279
ENSMUSG00000056071
ENSMUSG00000021214
ENSMUSG00000076934
ENSMUSG00000095007
ENSMUSG00000096100
ENSMUSG00000060807
ENSMUSG00000073631
ENSMUSG00000030263
ENSMUSG00000076549
ENSMUSG00000049608
ENSMUSG00000070530
ENSMUSG00000111862
ENSMUSG00000076937
ENSMUSG00000073538
ENSMUSG00000076619
ENSMUSG00000093861
ENSMUSG00000095197
ENSMUSG00000037337
ENSMUSG00000040522
ENSMUSG00000091002
ENSMUSG00000052087
ENSMUSG00000026220
ENSMUSG00000043461
ENSMUSG00000114441
ENSMUSG00000077714
ENSMUSG00000085873
ENSMUSG00000040751
ENSMUSG00000030589
ENSMUSG00000042529
ENSMUSG00000069308
ENSMUSG00000066687
ENSMUSG00000026012
ENSMUSG00000073421
ENSMUSG00000069307
ENSMUSG00000025001
ENSMUSG00000032322
ENSMUSG00000037035
ENSMUSG00000040675
ENSMUSG00000030147
ENSMUSG00000069303
ENSMUSG00000097108
ENSMUSG00000018899
ENSMUSG00000047420
ENSMUSG00000037725
ENSMUSG00000045102
ENSMUSG00000031382
ENSMUSG00000023262
ENSMUSG00000022901
ENSMUSG00000097993
ENSMUSG00000109913
ENSMUSG00000079553
ENSMUSG00000074489
ENSMUSG00000023274
ENSMUSG00000048498
ENSMUSG00000029195
ENSMUSG00000020051
ENSMUSG00000024866
ENSMUSG00000023505
ENSMUSG00000020234
ENSMUSG00000112061
ENSMUSG00000074628
ENSMUSG00000036887
ENSMUSG00000005057
ENSMUSG00000102692
ENSMUSG00000018927
ENSMUSG00000103992
ENSMUSG00000042404
ENSMUSG00000031362
ENSMUSG00000026458
ENSMUSG00000104488
ENSMUSG00000027875
ENSMUSG00000032356
ENSMUSG00000040940
ENSMUSG00000092243
ENSMUSG00000099773
ENSMUSG00000021367
ENSMUSG00000026630
ENSMUSG00000022014
ENSMUSG00000034987
ENSMUSG00000045842
ENSMUSG00000027639
ENSMUSG00000069516
ENSMUSG00000117117
ENSMUSG00000066491
ENSMUSG00000024899
ENSMUSG00000064109
ENSMUSG00000098934
ENSMUSG00000110218
ENSMUSG00000003882
ENSMUSG00000059430
ENSMUSG00000113195
ENSMUSG00000018211
ENSMUSG00000090171
ENSMUSG00000116919
ENSMUSG00000094281
ENSMUSG00000110697
ENSMUSG00000105960
ENSMUSG00000073492

ENSMUSG00000067341
ENSMUSG00000020401
ENSMUSG00000038421
ENSMUSG00000030798
ENSMUSG00000050578
ENSMUSG00000058773
ENSMUSG00000098973
ENSMUSG00000028270
ENSMUSG00000079033
ENSMUSG00000095351
ENSMUSG00000079543
ENSMUSG00000094689
ENSMUSG00000076563
ENSMUSG00000046591
ENSMUSG00000078853
ENSMUSG00000095787
ENSMUSG00000026581
ENSMUSG00000108317
ENSMUSG00000104213
ENSMUSG00000034785
ENSMUSG00000094728
ENSMUSG00000025938
ENSMUSG00000024526
ENSMUSG00000047880
ENSMUSG00000005716
ENSMUSG00000095612
ENSMUSG00000032564
ENSMUSG00000114294
ENSMUSG00000068606
ENSMUSG00000074483
ENSMUSG00000078921
ENSMUSG00000076583
ENSMUSG00000026984
ENSMUSG00000090252
ENSMUSG00000037548
ENSMUSG00000076608
ENSMUSG00000094872
ENSMUSG00000052013
ENSMUSG00000076508
ENSMUSG00000056054
ENSMUSG00000065714
ENSMUSG00000000628
ENSMUSG00000031613
ENSMUSG00000073980
ENSMUSG00000046402
ENSMUSG00000060509
ENSMUSG00000063632
ENSMUSG00000026602
ENSMUSG00000107134
ENSMUSG00000026167
ENSMUSG00000004371
ENSMUSG00000025479
ENSMUSG00000091898
ENSMUSG00000040747
ENSMUSG00000025422
ENSMUSG00000090338
ENSMUSG00000099762
ENSMUSG00000119476
ENSMUSG00000069270
ENSMUSG00000069305
ENSMUSG00000008845
ENSMUSG00000079507
ENSMUSG00000001506
ENSMUSG00000070392
ENSMUSG00000095547
ENSMUSG00000021123
ENSMUSG00000097053
ENSMUSG00000044254
ENSMUSG00000021176
ENSMUSG00000119011
ENSMUSG00000030935
ENSMUSG00000064342
ENSMUSG00000097012
ENSMUSG00000024965
ENSMUSG00000038642
ENSMUSG00000036469
ENSMUSG00000114457
ENSMUSG00000042029
ENSMUSG00000030074
ENSMUSG00000073411
ENSMUSG00000097399
ENSMUSG00000090256
ENSMUSG00000069581
ENSMUSG00000022584
ENSMUSG00000111709
ENSMUSG00000112023
ENSMUSG00000029283
ENSMUSG00000117573
ENSMUSG00000015843
ENSMUSG00000033880
ENSMUSG00000109587
ENSMUSG00000050994
ENSMUSG00000029910
ENSMUSG00000025089
ENSMUSG00000118384
ENSMUSG00000030270
ENSMUSG00000027797
ENSMUSG00000020167
ENSMUSG00000025429
ENSMUSG00000092674
ENSMUSG00000071658
ENSMUSG00000020684
ENSMUSG00000087319
ENSMUSG00000086596
ENSMUSG00000054717
ENSMUSG00000046207
ENSMUSG00000029608
ENSMUSG00000085412
ENSMUSG00000054013
ENSMUSG00000045009
ENSMUSG00000052572
ENSMUSG00000029304
ENSMUSG00000058022
ENSMUSG00000080777
ENSMUSG00000018381
ENSMUSG00000026365
ENSMUSG00000099241
ENSMUSG00000038738
ENSMUSG00000092837
ENSMUSG00000062296

ENSMUSG00000095450	ENSMUSG00000039699	ENSMUSG00000032661
ENSMUSG00000036198	ENSMUSG00000018819	ENSMUSG00000087232
ENSMUSG00000094075	ENSMUSG00000024675	ENSMUSG00000109684
ENSMUSG00000051596	ENSMUSG00000037913	ENSMUSG00000117771
ENSMUSG00000025432	ENSMUSG00000081596	ENSMUSG00000044156
ENSMUSG00000062007	ENSMUSG00000034394	ENSMUSG00000055978
ENSMUSG00000094087	ENSMUSG00000033213	ENSMUSG00000028341
ENSMUSG00000051111	ENSMUSG00000064225	ENSMUSG00000039518
ENSMUSG00000006469	ENSMUSG00000024330	ENSMUSG00000022378
ENSMUSG00000076614	ENSMUSG00000064901	ENSMUSG00000039488
ENSMUSG00000071068	ENSMUSG00000045751	ENSMUSG00000111116
ENSMUSG00000079455	ENSMUSG00000068227	ENSMUSG00000011179
ENSMUSG00000072109	ENSMUSG00000074604	ENSMUSG00000020159
ENSMUSG00000116868	ENSMUSG00000055866	ENSMUSG00000065118
ENSMUSG00000030093	ENSMUSG00000090307	ENSMUSG00000074469
ENSMUSG00000076655	ENSMUSG00000022034	ENSMUSG00000107605
ENSMUSG00000044117	ENSMUSG00000052316	ENSMUSG00000036246
ENSMUSG00000018168	ENSMUSG00000038252	ENSMUSG00000071550
ENSMUSG00000079808	ENSMUSG00000024660	ENSMUSG00000066180
ENSMUSG00000061100	ENSMUSG00000021640	ENSMUSG00000022603
ENSMUSG00000066677	ENSMUSG00000031698	ENSMUSG00000021879
ENSMUSG00000010142	ENSMUSG00000073403	ENSMUSG00000049122
ENSMUSG00000017002	ENSMUSG00000040253	ENSMUSG00000068114
ENSMUSG00000021457	ENSMUSG00000057425	ENSMUSG00000030789
ENSMUSG00000038379	ENSMUSG00000029563	ENSMUSG00000003410
ENSMUSG00000076609	ENSMUSG00000042116	ENSMUSG00000023216
ENSMUSG00000094918	ENSMUSG00000069274	ENSMUSG00000004791
ENSMUSG00000041538	ENSMUSG00000038665	ENSMUSG00000081657
ENSMUSG00000003484	ENSMUSG00000036944	ENSMUSG00000038704
ENSMUSG00000076677	ENSMUSG00000057103	ENSMUSG00000079293
ENSMUSG00000044201	ENSMUSG00000085713	ENSMUSG00000089542
ENSMUSG00000021613	ENSMUSG00000030495	ENSMUSG00000104508
ENSMUSG00000095630	ENSMUSG00000080712	ENSMUSG00000039463
ENSMUSG00000079298	ENSMUSG00000026117	ENSMUSG00000117879
ENSMUSG00000076613	ENSMUSG00000026395	ENSMUSG00000111583
ENSMUSG00000076604	ENSMUSG00000109492	ENSMUSG00000110084
ENSMUSG00000096594	ENSMUSG00000030256	ENSMUSG00000036764
ENSMUSG00000031004	ENSMUSG00000096937	ENSMUSG00000110086
ENSMUSG00000032783	ENSMUSG00000029862	ENSMUSG00000036602
ENSMUSG00000095300	ENSMUSG00000048922	ENSMUSG00000111417

ENSMUSG00000033576
ENSMUSG00000030142
ENSMUSG00000054999
ENSMUSG00000049133
ENSMUSG00000036422
ENSMUSG00000076618
ENSMUSG00000096965
ENSMUSG00000063021
ENSMUSG00000040264
ENSMUSG00000105909
ENSMUSG00000067577
ENSMUSG00000067149
ENSMUSG00000026955
ENSMUSG00000095609
ENSMUSG00000009646
ENSMUSG00000031494
ENSMUSG00000111258
ENSMUSG00000109675
ENSMUSG00000090175
ENSMUSG00000021356
ENSMUSG00000058470
ENSMUSG00000022422
ENSMUSG00000037138
ENSMUSG00000094797
ENSMUSG00000043931
ENSMUSG00000098975
ENSMUSG00000025279
ENSMUSG00000076577
ENSMUSG00000095250
ENSMUSG00000067144
ENSMUSG00000091694
ENSMUSG00000118428
ENSMUSG00000035818
ENSMUSG00000035186
ENSMUSG00000107420
ENSMUSG00000017400
ENSMUSG00000079071
ENSMUSG00000033220
ENSMUSG00000093954
ENSMUSG00000031283
ENSMUSG00000105212
ENSMUSG00000022613
ENSMUSG00000096852
ENSMUSG00000039055
ENSMUSG00000002020
ENSMUSG00000091199
ENSMUSG00000067235
ENSMUSG00000052026
ENSMUSG00000030167
ENSMUSG00000095616
ENSMUSG00000006403
ENSMUSG00000099974
ENSMUSG00000117294
ENSMUSG00000050069
ENSMUSG00000041324
ENSMUSG00000038540
ENSMUSG00000046378
ENSMUSG00000076615
ENSMUSG00000052821
ENSMUSG00000110027
ENSMUSG00000038508
ENSMUSG00000102439
ENSMUSG00000042078
ENSMUSG00000097039
ENSMUSG00002075746
ENSMUSG00000053318
ENSMUSG00000043439
ENSMUSG00000050974
ENSMUSG00000065701
ENSMUSG00000036083
ENSMUSG00000096878
ENSMUSG00000022057
ENSMUSG00000018008
ENSMUSG00000026786
ENSMUSG00000058147
ENSMUSG00000069306
ENSMUSG00000075478
ENSMUSG00000036655
ENSMUSG00000094306
ENSMUSG00000022229
ENSMUSG00000036908
ENSMUSG00000045868
ENSMUSG00000028159
ENSMUSG00000091255
ENSMUSG00000105199
ENSMUSG00000020044
ENSMUSG00000078606
ENSMUSG00000032087
ENSMUSG00000006574
ENSMUSG00000085709
ENSMUSG00000027820
ENSMUSG00000020312
ENSMUSG00000086513
ENSMUSG00000028167
ENSMUSG00000028845
ENSMUSG00000089281
ENSMUSG00000102737
ENSMUSG00000018507
ENSMUSG00000098055
ENSMUSG00000040860
ENSMUSG00000032281
ENSMUSG00000019876
ENSMUSG00000039899
ENSMUSG00000053490
ENSMUSG00000005986
ENSMUSG00000022906
ENSMUSG00000074896
ENSMUSG00000029055
ENSMUSG00000084830
ENSMUSG00000001444
ENSMUSG00000116702
ENSMUSG00000060586
ENSMUSG00000079038
ENSMUSG00000113980
ENSMUSG00000030513
ENSMUSG00000040552
ENSMUSG00000102091
ENSMUSG00000077704
ENSMUSG00000045763
ENSMUSG00000044244

ENSMUSG00000095981	ENSMUSG00000054598	ENSMUSG00000027636
ENSMUSG00000001131	ENSMUSG00000020734	ENSMUSG00000050382
ENSMUSG00000020897	ENSMUSG00000044288	ENSMUSG00000044626
ENSMUSG00000109482	ENSMUSG00000025498	ENSMUSG00000051379
ENSMUSG00000051378	ENSMUSG00000032589	ENSMUSG00000056608
ENSMUSG00000029368	ENSMUSG00000021702	ENSMUSG00000063297
ENSMUSG00000026009	ENSMUSG00000020676	ENSMUSG00000018925
ENSMUSG00000043592	ENSMUSG00000114456	ENSMUSG00000066682
ENSMUSG00000012443	ENSMUSG00000090273	ENSMUSG00000032452
ENSMUSG00000078597	ENSMUSG00000027322	ENSMUSG00000107668
ENSMUSG00000071715	ENSMUSG00000000204	ENSMUSG00000060176
ENSMUSG00000073529	ENSMUSG00000098318	ENSMUSG00000024066
ENSMUSG00000086695	ENSMUSG00000044485	ENSMUSG00000028713
ENSMUSG00000009185	ENSMUSG00000112358	ENSMUSG00000004098
ENSMUSG00000050600	ENSMUSG00000028758	ENSMUSG00000038011
ENSMUSG00000095794	ENSMUSG00000063354	ENSMUSG00000036634
ENSMUSG00000095589	ENSMUSG00000023267	ENSMUSG00000079037
ENSMUSG00000047592	ENSMUSG00000085683	ENSMUSG00000101555
ENSMUSG00000033676	ENSMUSG00000000386	ENSMUSG00000055373
ENSMUSG00000076607	ENSMUSG00000083457	ENSMUSG00000089906
ENSMUSG00000050357	ENSMUSG00000030683	ENSMUSG00000062038
ENSMUSG00000044816	ENSMUSG00000079419	ENSMUSG00000004341
ENSMUSG00000079363	ENSMUSG00000057897	ENSMUSG00000025993
ENSMUSG00000029204	ENSMUSG00000026669	ENSMUSG00000117391
ENSMUSG00000057606	ENSMUSG00000022366	ENSMUSG00000109574
ENSMUSG00000030041	ENSMUSG00000079547	ENSMUSG00000025153
ENSMUSG00000052889	ENSMUSG00000097233	ENSMUSG00000062908
ENSMUSG00000022686	ENSMUSG00000029322	ENSMUSG00000084274
ENSMUSG00000005268	ENSMUSG00000096768	ENSMUSG00000104350
ENSMUSG00000079800	ENSMUSG00000026697	ENSMUSG00000034028
ENSMUSG00000066363	ENSMUSG00000032184	ENSMUSG00000086825
ENSMUSG00000030111	ENSMUSG00000073208	ENSMUSG00000074259
ENSMUSG00000082292	ENSMUSG00000119132	ENSMUSG00000013846
ENSMUSG00000037474	ENSMUSG00000005087	ENSMUSG00000024176
ENSMUSG00000116380	ENSMUSG00000101167	ENSMUSG00000115009
ENSMUSG00000019893	ENSMUSG00000020037	ENSMUSG00000029762
ENSMUSG00000031264	ENSMUSG00000042345	ENSMUSG00000039853
ENSMUSG00000048782	ENSMUSG00000094230	ENSMUSG00000026188
ENSMUSG00000094777	ENSMUSG00000048534	ENSMUSG00000051439
ENSMUSG00000094248	ENSMUSG00000103966	ENSMUSG00000020108

ENSMUSG00000053303
ENSMUSG00000105986
ENSMUSG00000096336
ENSMUSG00000086804
ENSMUSG00000097636
ENSMUSG00000101211
ENSMUSG00000113007
ENSMUSG00000022780
ENSMUSG00000035699
ENSMUSG00000000861
ENSMUSG00000069301
ENSMUSG00000118670
ENSMUSG00000027863
ENSMUSG00000026579
ENSMUSG00000079494
ENSMUSG00000002068
ENSMUSG00000068101
ENSMUSG00000046031
ENSMUSG00000095092
ENSMUSG00000094874
ENSMUSG00000008318
ENSMUSG00000115363
ENSMUSG00002075524
ENSMUSG00000094420
ENSMUSG00000045273
ENSMUSG00000021091
ENSMUSG00000100301
ENSMUSG00000104371
ENSMUSG00000039252
ENSMUSG00000061947
ENSMUSG00000020914
ENSMUSG00000102660
ENSMUSG00000026285
ENSMUSG00000085129
ENSMUSG00000114279
ENSMUSG00000094345
ENSMUSG00000000244
ENSMUSG00000049539
ENSMUSG00000027843
ENSMUSG00000027219
ENSMUSG00000053113
ENSMUSG00000058589
ENSMUSG00000118361
ENSMUSG00000039546
ENSMUSG00000031821
ENSMUSG00000057228
ENSMUSG00000037649
ENSMUSG00000119520
ENSMUSG00000036832
ENSMUSG00000037020
ENSMUSG00000028044
ENSMUSG00000113680
ENSMUSG00000118815
ENSMUSG00000031756
ENSMUSG00000083397
ENSMUSG00000106180
ENSMUSG00000026770
ENSMUSG00000028976
ENSMUSG00000030254
ENSMUSG00000073879
ENSMUSG00000098206
ENSMUSG00000059305
ENSMUSG00000084391
ENSMUSG00000051498
ENSMUSG00000031389
ENSMUSG00000088008
ENSMUSG00000075334
ENSMUSG00000040966
ENSMUSG00000026938
ENSMUSG00000039264
ENSMUSG00000078942
ENSMUSG00000052974
ENSMUSG00000115458
ENSMUSG00000064267
ENSMUSG00000027331
ENSMUSG00000050106
ENSMUSG00000026622
ENSMUSG00000003206
ENSMUSG00000103828
ENSMUSG00000022831
ENSMUSG00000033967
ENSMUSG00000073402
ENSMUSG00000056529
ENSMUSG00000100775
ENSMUSG00000061974
ENSMUSG00000067768
ENSMUSG00000110726
ENSMUSG00000111943
ENSMUSG00000051242
ENSMUSG00000111564
ENSMUSG00000075256
ENSMUSG00000050860
ENSMUSG00000039193
ENSMUSG00000054146
ENSMUSG00000032327
ENSMUSG00000027070
ENSMUSG00000050370
ENSMUSG00000012123
ENSMUSG00000019987
ENSMUSG00000022658
ENSMUSG00000116220
ENSMUSG00000115026
ENSMUSG00000092702
ENSMUSG00000081769
ENSMUSG00000037944
ENSMUSG00000068735
ENSMUSG00000071324
ENSMUSG00000035473
ENSMUSG00000028715
ENSMUSG00000089651
ENSMUSG00000054958
ENSMUSG00000118632
ENSMUSG00000084758
ENSMUSG00000028940
ENSMUSG00000020098
ENSMUSG00000102960
ENSMUSG00000024776
ENSMUSG00000106120
ENSMUSG00000004151
ENSMUSG00000033016

ENSMUSG00000087131
ENSMUSG00000090942
ENSMUSG00000095672
ENSMUSG00000051998
ENSMUSG00000000486
ENSMUSG00000063590
ENSMUSG00000055368
ENSMUSG00000030365
ENSMUSG00000058290
ENSMUSG00000029603
ENSMUSG00000022949
ENSMUSG00000116719
ENSMUSG00000095571
ENSMUSG00000027326
ENSMUSG00000031262
ENSMUSG00000110496
ENSMUSG00000003477
ENSMUSG00000024598
ENSMUSG00000031779
ENSMUSG00000114871
ENSMUSG00000034438
ENSMUSG00000103865
ENSMUSG00000036526
ENSMUSG00000108752
ENSMUSG00000090103
ENSMUSG00000037991
ENSMUSG00000043873
ENSMUSG00000027559
ENSMUSG00000029275
ENSMUSG00000101389
ENSMUSG00000074151
ENSMUSG00000051159
ENSMUSG00000113035
ENSMUSG00000021492
ENSMUSG00000083558
ENSMUSG00000083365
ENSMUSG00000006724
ENSMUSG00000056328
ENSMUSG00000034634
ENSMUSG00000033491
ENSMUSG00000116996
ENSMUSG00000070390
ENSMUSG00000045545
ENSMUSG00000074375
ENSMUSG00000078487
ENSMUSG00000104476
ENSMUSG00000001741
ENSMUSG00000050164
ENSMUSG00000050141
ENSMUSG00000031594
ENSMUSG00000022548
ENSMUSG00000033219
ENSMUSG00000089781
ENSMUSG00000074934
ENSMUSG00000015451
ENSMUSG00000029372
ENSMUSG00000053044
ENSMUSG00000117050
ENSMUSG00000118864
ENSMUSG00000109454
ENSMUSG00000098426
ENSMUSG00000078816
ENSMUSG00000031390
ENSMUSG00000075015
ENSMUSG00000119670
ENSMUSG00002076859
ENSMUSG00000116864
ENSMUSG00000088273
ENSMUSG00000030148
ENSMUSG00000030641
ENSMUSG00000039710
ENSMUSG00000106239
ENSMUSG00000053852
ENSMUSG00000024696
ENSMUSG00000028033
ENSMUSG00000001128
ENSMUSG00000034317
ENSMUSG00000022659
ENSMUSG00000036362
ENSMUSG00000106303
ENSMUSG00000117182
ENSMUSG00000021631
ENSMUSG00000038644
ENSMUSG00000067199
ENSMUSG00000048827
ENSMUSG00000044505
ENSMUSG00000035539
ENSMUSG00000062017
ENSMUSG00000082420
ENSMUSG00000116643
ENSMUSG00000083614
ENSMUSG00000064360
ENSMUSG00000030214
ENSMUSG00000046794
ENSMUSG00000002633
ENSMUSG00000051735
ENSMUSG00000074796
ENSMUSG00000031103
ENSMUSG00000085538
ENSMUSG00000035509
ENSMUSG00000109199
ENSMUSG00000090246
ENSMUSG00000006717
ENSMUSG00000076441
ENSMUSG00000026827
ENSMUSG00000037579
ENSMUSG00000025950
ENSMUSG00000037341
ENSMUSG00000063011
ENSMUSG00000028307
ENSMUSG00000081006
ENSMUSG00000062044
ENSMUSG00000029121
ENSMUSG00000100615
ENSMUSG00000029254
ENSMUSG00000050395
ENSMUSG00000028312
ENSMUSG00000105391
ENSMUSG00000035692
ENSMUSG00000073988

ENSMUSG00000047117
ENSMUSG00000040247
ENSMUSG00000039396
ENSMUSG00000076545
ENSMUSG00000075014
ENSMUSG00000059201
ENSMUSG00000118434
ENSMUSG00000117964
ENSMUSG00000069309
ENSMUSG00000108455
ENSMUSG00000034959
ENSMUSG00000039748
ENSMUSG00000081665
ENSMUSG00000035711
ENSMUSG00000037318
ENSMUSG00000026077
ENSMUSG00000048905
ENSMUSG00000024989
ENSMUSG00000076586
ENSMUSG00000000791
ENSMUSG00000015880
ENSMUSG00000047810
ENSMUSG00000021624
ENSMUSG00000032496
ENSMUSG00000028718
ENSMUSG00000118667
ENSMUSG00000031722
ENSMUSG00000096862
ENSMUSG00000115483
ENSMUSG00000070000
ENSMUSG00000045328
ENSMUSG00000104606
ENSMUSG00000094796
ENSMUSG00000052760
ENSMUSG00000061780
ENSMUSG00000024670
ENSMUSG00000070601
ENSMUSG00000061991
ENSMUSG00000110537
ENSMUSG00000069874
ENSMUSG00000030560
ENSMUSG00000029084
ENSMUSG00000026819
ENSMUSG00000028017
ENSMUSG00000078502
ENSMUSG00000075408
ENSMUSG00000012428
ENSMUSG00000108053
ENSMUSG00000026805
ENSMUSG00000098370
ENSMUSG00000091733
ENSMUSG00000026358
ENSMUSG00000020027
ENSMUSG00000025044
ENSMUSG00000038801
ENSMUSG00000037868
ENSMUSG00000047986
ENSMUSG00000077167
ENSMUSG00000092746
ENSMUSG00000028874
ENSMUSG00000118866
ENSMUSG00000118841
ENSMUSG00000001334
ENSMUSG00000040569
ENSMUSG00000039956
ENSMUSG00000092415
ENSMUSG00000064349
ENSMUSG00000116993
ENSMUSG00000118618
ENSMUSG00000108884
ENSMUSG00000025650
ENSMUSG00000024610
ENSMUSG00000089753
ENSMUSG00000036913
ENSMUSG00000064994
ENSMUSG00000033031
ENSMUSG00000103303
ENSMUSG00000032093
ENSMUSG00000094613
ENSMUSG00000032572
ENSMUSG00000046687
ENSMUSG00000020953
ENSMUSG00000109814
ENSMUSG00000027004
ENSMUSG00000028794
ENSMUSG00000022456
ENSMUSG00000031934
ENSMUSG00000078787
ENSMUSG00000048281
ENSMUSG00000019027
ENSMUSG00000023341
ENSMUSG00000078532
ENSMUSG00000089235
ENSMUSG00000037095
ENSMUSG00000114800
ENSMUSG00000027995
ENSMUSG00000022952
ENSMUSG00000023828
ENSMUSG00000004609
ENSMUSG00000036067
ENSMUSG00000054203
ENSMUSG00000064361
ENSMUSG00000109245
ENSMUSG00000072844
ENSMUSG00000027800
ENSMUSG00000082381
ENSMUSG00000029299
ENSMUSG00000108353
ENSMUSG00000032081
ENSMUSG00000116832
ENSMUSG00000041986
ENSMUSG00000037780
ENSMUSG00000029366
ENSMUSG00000024391
ENSMUSG00000043144
ENSMUSG00000063531
ENSMUSG00000087150
ENSMUSG00000050103
ENSMUSG00000109051
ENSMUSG00000046818

ENSMUSG00000025461	ENSMUSG00000007029	ENSMUSG00000090817
ENSMUSG00000044534	ENSMUSG00000055782	ENSMUSG00000020395
ENSMUSG00000033715	ENSMUSG00000024397	ENSMUSG00000117255
ENSMUSG00000034773	ENSMUSG00000091972	ENSMUSG00000055717
ENSMUSG00000095130	ENSMUSG00000030244	ENSMUSG00000037347
ENSMUSG00000052749	ENSMUSG00000037071	ENSMUSG00000115902
ENSMUSG00000117309	ENSMUSG00000048402	ENSMUSG00000046916
ENSMUSG00000090164	ENSMUSG00000055489	ENSMUSG00000040276
ENSMUSG00000098248	ENSMUSG00000105300	ENSMUSG00000027962
ENSMUSG00000037321	ENSMUSG00000113313	ENSMUSG00000023333
ENSMUSG00000030651	ENSMUSG00000044177	ENSMUSG00000096917
ENSMUSG00000024334	ENSMUSG00000000318	ENSMUSG00000082100
ENSMUSG00000025804	ENSMUSG00000061577	ENSMUSG00000002983
ENSMUSG00000101972	ENSMUSG00000104354	ENSMUSG00000030825
ENSMUSG00000027360	ENSMUSG00000069910	ENSMUSG00000031548
ENSMUSG00000009292	ENSMUSG00000021268	ENSMUSG00000018012
ENSMUSG00002076704	ENSMUSG00000017861	ENSMUSG00000049676
ENSMUSG00000071552	ENSMUSG00000021565	ENSMUSG00000025903
ENSMUSG00000035042	ENSMUSG00000044350	ENSMUSG00000029816
ENSMUSG00000014813	ENSMUSG00000058806	ENSMUSG00000049872
ENSMUSG00000026834	ENSMUSG00000090015	ENSMUSG00000103202
ENSMUSG00000114035	ENSMUSG00000032586	ENSMUSG00000117994
ENSMUSG00000101279	ENSMUSG00000026442	ENSMUSG00000097448
ENSMUSG00000024056	ENSMUSG00000119577	ENSMUSG00000065519
ENSMUSG00000096727	ENSMUSG00000032400	ENSMUSG00000071528
ENSMUSG00000091542	ENSMUSG00000013584	ENSMUSG00000050232
ENSMUSG00000027379	ENSMUSG00000004031	ENSMUSG00000037568
ENSMUSG00002076726	ENSMUSG00000065952	ENSMUSG00000024014
ENSMUSG00000069310	ENSMUSG00000058740	ENSMUSG00000026725
ENSMUSG00000051506	ENSMUSG00000022622	ENSMUSG00000031093
ENSMUSG00000021250	ENSMUSG00000009614	ENSMUSG00000036502
ENSMUSG00000038567	ENSMUSG00000098243	ENSMUSG00000084353
ENSMUSG00000059089	ENSMUSG00000030669	ENSMUSG00000105542
ENSMUSG00000053024	ENSMUSG00000041831	ENSMUSG00000079707
ENSMUSG00000005980	ENSMUSG00000002699	ENSMUSG00000107017
ENSMUSG00000097352	ENSMUSG00000097875	ENSMUSG00000074355
ENSMUSG00000071478	ENSMUSG00000024538	ENSMUSG00000072849
ENSMUSG00000071516	ENSMUSG00000021364	ENSMUSG00000029638
ENSMUSG00000022439	ENSMUSG00000055629	ENSMUSG00000001497
ENSMUSG00000027869	ENSMUSG00000021508	ENSMUSG00000052949

ENSMUSG00000049109	ENSMUSG00000112824	ENSMUSG00000030747
ENSMUSG00000099583	ENSMUSG00000053063	ENSMUSG00000030889
ENSMUSG00000101355	ENSMUSG00000060487	ENSMUSG00000044330
ENSMUSG00000031489	ENSMUSG00000039109	ENSMUSG00000030077
ENSMUSG00000022021	ENSMUSG00000027690	ENSMUSG00000113557
ENSMUSG00000108341	ENSMUSG00000093064	ENSMUSG00002075380
ENSMUSG00000055116	ENSMUSG00000073491	ENSMUSG00000115733
ENSMUSG00000030117	ENSMUSG00000115888	ENSMUSG00000037953
ENSMUSG00000030830	ENSMUSG00000032028	ENSMUSG00000028150
ENSMUSG00000026039	ENSMUSG00000116433	ENSMUSG00000048355
ENSMUSG00000026073	ENSMUSG00000069805	ENSMUSG00000061852
ENSMUSG00000069272	ENSMUSG00000033355	ENSMUSG00000077962
ENSMUSG00000086765	ENSMUSG00000104291	ENSMUSG00000086228
ENSMUSG00000023045	ENSMUSG00000093413	ENSMUSG00000115040
ENSMUSG00000025515	ENSMUSG00000071714	ENSMUSG00000027489
ENSMUSG00000016496	ENSMUSG00000047963	ENSMUSG00000072620
ENSMUSG00000083386	ENSMUSG00000037313	ENSMUSG00000007035
ENSMUSG00000080076	ENSMUSG00000104444	ENSMUSG00000102766
ENSMUSG00000099517	ENSMUSG00000022096	ENSMUSG00000022262
ENSMUSG00000071713	ENSMUSG00000040283	ENSMUSG00000003411
ENSMUSG00000054342	ENSMUSG00000005681	ENSMUSG00000056025
ENSMUSG00000004359	ENSMUSG00000051457	ENSMUSG00000097968
ENSMUSG00000073145	ENSMUSG00000021485	ENSMUSG00000015355
ENSMUSG00000043681	ENSMUSG00000023940	ENSMUSG00000054582
ENSMUSG00000061462	ENSMUSG00000000290	ENSMUSG00000106237
ENSMUSG00000087107	ENSMUSG00000016255	ENSMUSG00000092981
ENSMUSG00000033831	ENSMUSG00000023122	ENSMUSG00000103038
ENSMUSG00000050751	ENSMUSG00000074179	ENSMUSG00000081485
ENSMUSG00000105003	ENSMUSG00000024313	ENSMUSG00000115471
ENSMUSG00000107771	ENSMUSG00002076601	ENSMUSG00000084854
ENSMUSG00000043531	ENSMUSG00000113004	ENSMUSG00000020961
ENSMUSG00000035458	ENSMUSG00000022762	ENSMUSG00000112808
ENSMUSG00000053168	ENSMUSG00000024401	ENSMUSG00000109003
ENSMUSG00000094951	ENSMUSG00000040808	ENSMUSG00000050776
ENSMUSG00000066071	ENSMUSG00000098270	ENSMUSG00000037940
ENSMUSG00000064179	ENSMUSG00000024339	ENSMUSG00000110235
ENSMUSG00000076680	ENSMUSG00000024842	ENSMUSG00000105987
ENSMUSG00000061959	ENSMUSG00000061808	ENSMUSG00000100768
ENSMUSG00000074417	ENSMUSG00000102628	ENSMUSG00000051768
ENSMUSG00000034116	ENSMUSG00000062184	ENSMUSG00000106867

ENSMUSG00000108522	ENSMUSG00000060802	ENSMUSG00000064246
ENSMUSG00000065987	ENSMUSG00000020038	ENSMUSG00000020427
ENSMUSG00000034311	ENSMUSG00000115681	ENSMUSG00000065208
ENSMUSG00000030004	ENSMUSG00000054630	ENSMUSG00000062783
ENSMUSG00000035849	ENSMUSG00000028354	ENSMUSG00000107689
ENSMUSG00000115333	ENSMUSG00000082044	ENSMUSG00000114859
ENSMUSG00000034833	ENSMUSG00000072664	ENSMUSG00000117507
ENSMUSG00000018654	ENSMUSG00000042129	ENSMUSG00000105971
ENSMUSG00000071633	ENSMUSG00000109244	ENSMUSG00000056258
ENSMUSG00000089942	ENSMUSG00000044338	ENSMUSG00000091478
ENSMUSG00000069302	ENSMUSG00000006435	ENSMUSG00000032418
ENSMUSG00000012705	ENSMUSG00000090098	ENSMUSG00000041991
ENSMUSG00000106069	ENSMUSG00000050799	ENSMUSG00000047528
ENSMUSG00000050921	ENSMUSG00000055254	ENSMUSG00000095649
ENSMUSG00000084760	ENSMUSG00000006585	ENSMUSG00000087613
ENSMUSG00000042425	ENSMUSG00000112980	ENSMUSG00000048029
ENSMUSG00000042351	ENSMUSG00000053101	ENSMUSG00000104615
ENSMUSG00000030546	ENSMUSG00000102871	ENSMUSG00000027996
ENSMUSG00000095583	ENSMUSG00000097730	ENSMUSG00000031963
ENSMUSG00000109904	ENSMUSG00000032942	ENSMUSG00000042644
ENSMUSG00000038624	ENSMUSG00000058812	ENSMUSG00000041193
ENSMUSG00000007682	ENSMUSG00000056290	ENSMUSG00000083207
ENSMUSG00000073008	ENSMUSG00000021415	ENSMUSG00000118590
ENSMUSG00000028678	ENSMUSG00000034330	ENSMUSG00000038541
ENSMUSG00000038352	ENSMUSG00000026368	ENSMUSG00000042102
ENSMUSG00000076621	ENSMUSG00000025888	ENSMUSG00000061718
ENSMUSG00000069265	ENSMUSG00000117084	ENSMUSG00000031163
ENSMUSG00000096490	ENSMUSG00000070031	ENSMUSG00000067377
ENSMUSG00000069267	ENSMUSG00000064356	ENSMUSG00000038578
ENSMUSG00000021700	ENSMUSG00000022945	ENSMUSG00000027570
ENSMUSG00000039936	ENSMUSG00000109713	ENSMUSG00000065489
ENSMUSG00000006542	ENSMUSG00000089255	ENSMUSG00000026177
ENSMUSG00000069324	ENSMUSG00000026712	ENSMUSG00000108506
ENSMUSG00000076620	ENSMUSG00000027323	ENSMUSG00000101939
ENSMUSG00000073902	ENSMUSG00000046070	ENSMUSG00000003617
ENSMUSG00000075031	ENSMUSG00000108652	ENSMUSG00000043015
ENSMUSG00000014852	ENSMUSG00000000028	ENSMUSG00000029695
ENSMUSG00000022372	ENSMUSG00000035352	ENSMUSG00000039304
ENSMUSG00000070369	ENSMUSG00000053980	ENSMUSG00000034371
ENSMUSG00000040950	ENSMUSG00000031897	ENSMUSG00000061684

ENSMUSG00000041498	ENSMUSG00000039062	ENSMUSG00000028862
ENSMUSG00000037224	ENSMUSG00000006200	ENSMUSG00000028931
ENSMUSG00000046179	ENSMUSG00000074060	ENSMUSG00000022754
ENSMUSG00000030707	ENSMUSG00000017550	ENSMUSG00000059031
ENSMUSG00000036768	ENSMUSG00000031760	ENSMUSG00000013415
ENSMUSG00000042489	ENSMUSG00000118265	ENSMUSG00000012519
ENSMUSG00000091477	ENSMUSG00000051278	ENSMUSG00000035095
ENSMUSG00000024338	ENSMUSG00000027870	ENSMUSG00000078153
ENSMUSG00002075551	ENSMUSG00000032113	ENSMUSG00000021520
ENSMUSG00000020143	ENSMUSG00000099027	ENSMUSG00000027306
ENSMUSG00000027514	ENSMUSG00000026043	ENSMUSG00000070594
ENSMUSG00000019942	ENSMUSG00000030742	ENSMUSG00000027965
ENSMUSG00000023349	ENSMUSG00000084981	ENSMUSG00000029103
ENSMUSG00000023015	ENSMUSG00000011267	ENSMUSG00000057836
ENSMUSG00000037544	ENSMUSG00000001467	ENSMUSG00000118425
ENSMUSG00000000409	ENSMUSG00000114544	ENSMUSG00000055737
ENSMUSG00000082088	ENSMUSG00000073412	ENSMUSG00000030220
ENSMUSG00000043740	ENSMUSG00000087171	ENSMUSG00000044770
ENSMUSG00000037280	ENSMUSG00000043263	ENSMUSG00000049233
ENSMUSG00000010342	ENSMUSG00000032401	ENSMUSG00000029671
ENSMUSG00000061615	ENSMUSG00000026447	ENSMUSG00000003469
ENSMUSG00000096105	ENSMUSG00000119206	ENSMUSG00000062585
ENSMUSG00000021922	ENSMUSG00000035407	ENSMUSG00000091844
ENSMUSG00000099757	ENSMUSG00000095562	ENSMUSG00000041220
ENSMUSG00000024399	ENSMUSG00000026574	ENSMUSG00000118591
ENSMUSG00000035455	ENSMUSG00000106963	ENSMUSG00000038884
ENSMUSG00000063646	ENSMUSG00000024222	ENSMUSG00000106178
ENSMUSG00000053687	ENSMUSG00000119163	ENSMUSG00000020672
ENSMUSG00000035697	ENSMUSG00000049001	ENSMUSG00000101514
ENSMUSG00000090080	ENSMUSG00000117571	ENSMUSG00000118661
ENSMUSG00000099104	ENSMUSG00000078650	ENSMUSG00000036622
ENSMUSG00000003283	ENSMUSG00000029168	ENSMUSG00000081949
ENSMUSG00000078920	ENSMUSG00000078851	ENSMUSG00000022676
ENSMUSG00000030786	ENSMUSG00000037411	ENSMUSG00000024440
ENSMUSG00000038418	ENSMUSG00000081695	ENSMUSG00000034652
ENSMUSG00000044827	ENSMUSG00000051682	ENSMUSG00000051906
ENSMUSG00000070034	ENSMUSG00000033633	ENSMUSG00000108231
ENSMUSG00000059824	ENSMUSG00000037053	ENSMUSG00000047905
ENSMUSG00000040867	ENSMUSG00000069792	ENSMUSG00000032921
ENSMUSG00000057913	ENSMUSG00000002831	ENSMUSG00000079508

ENSMUSG00000110386
ENSMUSG00000030346
ENSMUSG00000041431
ENSMUSG00000026683
ENSMUSG00000021423
ENSMUSG00000028527
ENSMUSG00000069300
ENSMUSG00000079014
ENSMUSG00000024013
ENSMUSG00000105065
ENSMUSG00000097415
ENSMUSG00000027368
ENSMUSG00000076490
ENSMUSG00000001228
ENSMUSG00000020437
ENSMUSG00000008496
ENSMUSG00000021207
ENSMUSG00000027469
ENSMUSG00000022534
ENSMUSG00000078763
ENSMUSG00000089844
ENSMUSG00000083161
ENSMUSG00000048327
ENSMUSG00000043122
ENSMUSG00000034023
ENSMUSG00000108232
ENSMUSG00000017146
ENSMUSG00000038670
ENSMUSG00000109508
ENSMUSG00000025582
ENSMUSG00000007080
ENSMUSG00000119030
ENSMUSG00000010476
ENSMUSG00000001588
ENSMUSG00000064339
ENSMUSG00000118876
ENSMUSG00000055413
ENSMUSG00000004698
ENSMUSG00000033730
ENSMUSG00000021569
ENSMUSG00000024301
ENSMUSG00000029298
ENSMUSG00000117102
ENSMUSG00000118671
ENSMUSG00000109054
ENSMUSG00000030149
ENSMUSG00000049103
ENSMUSG00000091649
ENSMUSG00000064853
ENSMUSG00000074886
ENSMUSG00000049511
ENSMUSG00000075044
ENSMUSG00000063903
ENSMUSG00000027577
ENSMUSG00000064036
ENSMUSG00000027115
ENSMUSG00000104728
ENSMUSG00000021390
ENSMUSG00000047216
ENSMUSG00000057948
ENSMUSG00000066366
ENSMUSG00000025347
ENSMUSG00000042388
ENSMUSG00000052353
ENSMUSG00000021298
ENSMUSG00000053846
ENSMUSG00000022575
ENSMUSG00000026288
ENSMUSG00000037628
ENSMUSG00000041653
ENSMUSG00000024677
ENSMUSG00000022468
ENSMUSG00000044583
ENSMUSG00000070645
ENSMUSG00000057135
ENSMUSG00000085925
ENSMUSG00000030165
ENSMUSG00000119584
ENSMUSG00000025701
ENSMUSG00000036882
ENSMUSG00000025165
ENSMUSG00000110397
ENSMUSG00000082127
ENSMUSG00000025937
ENSMUSG00000022066
ENSMUSG00000028737
ENSMUSG00000023009
ENSMUSG00000049630
ENSMUSG00000032221
ENSMUSG00000023019
ENSMUSG00000077265
ENSMUSG00000033847
ENSMUSG00000088054
ENSMUSG00000089431
ENSMUSG00000083626
ENSMUSG00000032925
ENSMUSG00000059895
ENSMUSG00000001750
ENSMUSG00000049502
ENSMUSG00000059326
ENSMUSG00000031253
ENSMUSG00000073771
ENSMUSG00000057933
ENSMUSG00000031609
ENSMUSG00000025964
ENSMUSG00000035385
ENSMUSG00000057880
ENSMUSG00000074479
ENSMUSG00000084168
ENSMUSG00000031543
ENSMUSG00000006587
ENSMUSG00000045165
ENSMUSG00000087361
ENSMUSG00000064369
ENSMUSG00000031673
ENSMUSG00000017754
ENSMUSG00000000552
ENSMUSG00000060791
ENSMUSG00000020059
ENSMUSG00000099398

ENSMUSG00000046879	ENSMUSG00000049112	ENSMUSG00000096449
ENSMUSG00000056498	ENSMUSG00000022181	ENSMUSG00000091705
ENSMUSG00000038071	ENSMUSG00000056394	ENSMUSG00000078161
ENSMUSG00000009092	ENSMUSG00000031383	ENSMUSG00000110592
ENSMUSG00000024292	ENSMUSG00000036168	ENSMUSG00000039747
ENSMUSG00000072676	ENSMUSG00000036330	ENSMUSG00000055022
ENSMUSG00000075010	ENSMUSG00000020681	ENSMUSG00000037348
ENSMUSG00000108081	ENSMUSG00000071716	ENSMUSG00000112863
ENSMUSG00000046999	ENSMUSG00000022876	ENSMUSG00000034402
ENSMUSG00000031101	ENSMUSG00000030187	ENSMUSG00000028127
ENSMUSG00000033762	ENSMUSG00000039126	ENSMUSG00000021057
ENSMUSG00000034686	ENSMUSG00000113649	ENSMUSG00000003949
ENSMUSG00000055809	ENSMUSG00000019564	ENSMUSG00000024349
ENSMUSG00000091491	ENSMUSG00000045034	ENSMUSG00000102204
ENSMUSG00000040413	ENSMUSG00000052724	ENSMUSG00000115132
ENSMUSG00000052562	ENSMUSG00000087175	ENSMUSG00000025735
ENSMUSG00000034855	ENSMUSG00000072621	ENSMUSG00000038886
ENSMUSG00000034906	ENSMUSG00000025317	ENSMUSG00000083328
ENSMUSG00000030781	ENSMUSG00000111293	ENSMUSG00000087593
ENSMUSG00000098112	ENSMUSG00000078492	ENSMUSG00000031340
ENSMUSG00000105504	ENSMUSG00000030677	ENSMUSG00000096938
ENSMUSG00000074768	ENSMUSG00000039316	ENSMUSG00000073490
ENSMUSG00000097705	ENSMUSG00000024795	ENSMUSG00000030880
ENSMUSG00000020330	ENSMUSG00000037263	ENSMUSG00000061272
ENSMUSG00002075501	ENSMUSG00000092805	ENSMUSG00000039533
ENSMUSG00000079495	ENSMUSG00000104520	ENSMUSG00000101625
ENSMUSG00000052160	ENSMUSG00000055541	ENSMUSG00000002997
ENSMUSG00000004328	ENSMUSG00000006529	ENSMUSG00000052496
ENSMUSG00000015852	ENSMUSG00000042662	ENSMUSG00000042788
ENSMUSG00000119427	ENSMUSG00000033898	ENSMUSG00000028222
ENSMUSG00000119774	ENSMUSG00000038147	ENSMUSG00000082625
ENSMUSG00000118677	ENSMUSG00000023473	ENSMUSG00000040287
ENSMUSG00000100658	ENSMUSG00000033634	ENSMUSG00000031258
ENSMUSG00000118936	ENSMUSG00000020218	ENSMUSG00000037738
ENSMUSG00000118698	ENSMUSG00000045326	ENSMUSG00000002475
ENSMUSG00000068246	ENSMUSG00000061576	ENSMUSG00000103143
ENSMUSG00000079227	ENSMUSG00000045404	ENSMUSG00000021567
ENSMUSG00000038641	ENSMUSG00000023908	ENSMUSG00000048371
ENSMUSG00000073530	ENSMUSG00000034687	ENSMUSG00000033488
ENSMUSG00000038151	ENSMUSG00000026193	ENSMUSG00000017652

ENSMUSG00000019767	ENSMUSG00000007097	ENSMUSG00000087651
ENSMUSG00000020493	ENSMUSG00000022951	ENSMUSG00000116780
ENSMUSG00000030268	ENSMUSG00000026840	ENSMUSG00000054385
ENSMUSG00000027249	ENSMUSG00000106445	ENSMUSG00000040133
ENSMUSG00000024353	ENSMUSG00000069268	ENSMUSG00000028979
ENSMUSG00000048142	ENSMUSG00000092819	ENSMUSG00000056215
ENSMUSG00002074846	ENSMUSG00000062151	ENSMUSG00000028197
ENSMUSG00000040061	ENSMUSG00000024680	ENSMUSG00000049107
ENSMUSG00000046295	ENSMUSG00000053693	ENSMUSG00000116747
ENSMUSG00000037731	ENSMUSG00000031549	ENSMUSG00000028528
ENSMUSG00000057346	ENSMUSG00000022346	ENSMUSG00000104586
ENSMUSG00000026605	ENSMUSG00000106252	ENSMUSG00000021388
ENSMUSG00000062132	ENSMUSG00000097610	ENSMUSG00000064325
ENSMUSG00000108132	ENSMUSG00000015947	ENSMUSG00000010064
ENSMUSG00000082116	ENSMUSG00000061414	ENSMUSG00000030757
ENSMUSG00000085121	ENSMUSG00000084224	ENSMUSG00000092072
ENSMUSG00000099707	ENSMUSG00000034463	ENSMUSG00000021490
ENSMUSG00000061540	ENSMUSG00000084010	ENSMUSG00000035783
ENSMUSG00000027009	ENSMUSG00000045349	ENSMUSG00000051246
ENSMUSG00000058818	ENSMUSG00000048621	ENSMUSG00000028834
ENSMUSG00000029711	ENSMUSG00000098014	ENSMUSG00000097189
ENSMUSG00000093327	ENSMUSG00000103313	ENSMUSG00000058050
ENSMUSG00000097295	ENSMUSG00000074607	ENSMUSG00000069266
ENSMUSG00000064348	ENSMUSG00000026621	ENSMUSG00000040990
ENSMUSG00000024529	ENSMUSG00000035914	ENSMUSG00000085772
ENSMUSG00000020120	ENSMUSG00000040033	ENSMUSG00000079906
ENSMUSG00000020788	ENSMUSG00000114860	ENSMUSG00000047363
ENSMUSG00000044405	ENSMUSG00000022360	ENSMUSG00000024968
ENSMUSG00000000682	ENSMUSG00000102418	ENSMUSG00000038526
ENSMUSG00000026042	ENSMUSG00000111960	ENSMUSG00000105596
ENSMUSG00000051969	ENSMUSG00000019906	ENSMUSG00000066258
ENSMUSG00000119079	ENSMUSG00000035211	ENSMUSG00000034459
ENSMUSG00000029414	ENSMUSG00000049515	ENSMUSG00000028581
ENSMUSG00000020573	ENSMUSG00000048583	ENSMUSG00000055114
ENSMUSG00000027966	ENSMUSG00000094514	ENSMUSG00000028702
ENSMUSG00000039364	ENSMUSG00000021670	ENSMUSG00000039717
ENSMUSG00000087382	ENSMUSG00000020785	ENSMUSG00000071226
ENSMUSG00000049709	ENSMUSG00000073705	ENSMUSG00000003948
ENSMUSG00000020396	ENSMUSG00000006641	ENSMUSG00000026354
ENSMUSG00000045382	ENSMUSG00000105402	ENSMUSG00000054871

ENSMUSG00000028071	ENSMUSG00000087516	ENSMUSG00000082241
ENSMUSG00002075602	ENSMUSG00000049538	ENSMUSG00000063535
ENSMUSG00000015950	ENSMUSG00000095788	ENSMUSG00000067818
ENSMUSG00000097194	ENSMUSG00000027715	ENSMUSG00000068373
ENSMUSG00000024679	ENSMUSG00000023031	ENSMUSG00000107736
ENSMUSG00000079022	ENSMUSG00000046718	ENSMUSG00000094054
ENSMUSG00000095028	ENSMUSG00000110341	ENSMUSG00000101262
ENSMUSG00000024791	ENSMUSG00000089707	ENSMUSG00000082361
ENSMUSG00000044014	ENSMUSG00000046108	ENSMUSG00000029361
ENSMUSG00000032083	ENSMUSG00000024503	ENSMUSG00000065304
ENSMUSG00000057246	ENSMUSG00000059674	ENSMUSG00000097983
ENSMUSG00000048911	ENSMUSG00000028001	ENSMUSG00000021125
ENSMUSG00000028175	ENSMUSG00000024691	ENSMUSG00000108772
ENSMUSG00000031994	ENSMUSG00000026258	ENSMUSG00000052520
ENSMUSG00000092277	ENSMUSG00000027454	ENSMUSG00000086266
ENSMUSG00000035775	ENSMUSG00000002257	ENSMUSG00000074892
ENSMUSG00000081331	ENSMUSG00000035202	ENSMUSG00000075590
ENSMUSG00000044724	ENSMUSG00000030237	ENSMUSG00000096233
ENSMUSG00000064337	ENSMUSG00000031089	ENSMUSG00000030525
ENSMUSG00000039981	ENSMUSG00000115783	ENSMUSG00000108732
ENSMUSG00000118458	ENSMUSG00000022240	ENSMUSG00000074899
ENSMUSG00000029445	ENSMUSG00000086010	ENSMUSG00000085009
ENSMUSG00000074345	ENSMUSG00000044164	ENSMUSG00000079105
ENSMUSG00000085603	ENSMUSG00000028364	ENSMUSG00000031239
ENSMUSG00000017737	ENSMUSG00000049744	ENSMUSG00000102389
ENSMUSG00000108980	ENSMUSG00000106498	ENSMUSG00000097184
ENSMUSG00000052270	ENSMUSG00000022206	ENSMUSG00000035208
ENSMUSG00000015354	ENSMUSG00000106107	ENSMUSG00000102593
ENSMUSG00000026981	ENSMUSG00000113936	ENSMUSG00000056999
ENSMUSG00000022322	ENSMUSG00000003779	ENSMUSG00000049404
ENSMUSG00000079550	ENSMUSG00000022033	ENSMUSG00000069609
ENSMUSG00000118672	ENSMUSG00000090039	ENSMUSG00000107451
ENSMUSG00000069515	ENSMUSG00000049932	ENSMUSG00000026980
ENSMUSG00000047295	ENSMUSG00000021999	ENSMUSG00000074028
ENSMUSG00000041481	ENSMUSG00000089634	ENSMUSG00000031015
ENSMUSG00000061232	ENSMUSG00000060188	ENSMUSG00000043051
ENSMUSG00000073418	ENSMUSG00000112196	ENSMUSG00000024501
ENSMUSG00000093292	ENSMUSG00000022002	ENSMUSG00000022354
ENSMUSG00000040564	ENSMUSG00000024590	ENSMUSG00000060002
ENSMUSG00000118751	ENSMUSG00000038085	ENSMUSG00000102425

ENSMUSG00000064923	ENSMUSG00000065725	ENSMUSG00000027955
ENSMUSG00000035929	ENSMUSG00000058163	ENSMUSG00000061132
ENSMUSG00000064851	ENSMUSG00000104118	ENSMUSG00000054477
ENSMUSG00000028268	ENSMUSG00000010021	ENSMUSG00000094526
ENSMUSG00000040204	ENSMUSG00000002910	ENSMUSG00000085620
ENSMUSG00000023034	ENSMUSG00000032218	ENSMUSG00000030413
ENSMUSG00000030787	ENSMUSG00000036437	ENSMUSG00000011256
ENSMUSG00000028655	ENSMUSG00000096722	ENSMUSG00000095463
ENSMUSG00000028965	ENSMUSG00000038763	ENSMUSG00000028115
ENSMUSG00000024669	ENSMUSG00000064427	ENSMUSG00000024124
ENSMUSG00000028347	ENSMUSG00000025981	ENSMUSG00000105935
ENSMUSG00002076503	ENSMUSG00000046352	ENSMUSG00000102712
ENSMUSG00000062510	ENSMUSG00000024678	ENSMUSG00000044703
ENSMUSG00000036006	ENSMUSG00000048489	ENSMUSG00000109803
ENSMUSG00000119286	ENSMUSG00000021186	ENSMUSG00000048368
ENSMUSG00000097419	ENSMUSG00000002007	ENSMUSG00000107197
ENSMUSG00000118734	ENSMUSG00000113175	ENSMUSG00000035673
ENSMUSG00000025058	ENSMUSG00000041859	ENSMUSG00000019850
ENSMUSG00000079559	ENSMUSG00000102277	ENSMUSG00000036560
ENSMUSG00000054052	ENSMUSG00000022679	ENSMUSG00000026062
ENSMUSG00000034450	ENSMUSG00000031659	ENSMUSG00000032085
ENSMUSG00000025064	ENSMUSG00000113005	ENSMUSG00000035745
ENSMUSG00000114608	ENSMUSG00000002835	ENSMUSG00000115662
ENSMUSG00000023169	ENSMUSG00000053158	ENSMUSG00000026415
ENSMUSG00000119895	ENSMUSG00000044017	ENSMUSG00000013707
ENSMUSG00000075297	ENSMUSG00000089871	ENSMUSG00000020102
ENSMUSG00000094840	ENSMUSG00000086953	ENSMUSG00000064343
ENSMUSG00000058099	ENSMUSG00000024347	ENSMUSG00000082284
ENSMUSG00000073555	ENSMUSG00000055069	ENSMUSG00000024437
ENSMUSG00000021965	ENSMUSG00000037759	ENSMUSG00000002870
ENSMUSG00000048574	ENSMUSG00000041112	ENSMUSG00000030067
ENSMUSG00000065905	ENSMUSG00000073125	ENSMUSG00000026094
ENSMUSG00000030745	ENSMUSG00000019773	ENSMUSG00000029314
ENSMUSG00000026347	ENSMUSG00000106263	ENSMUSG00000070345
ENSMUSG00000030427	ENSMUSG00000085582	ENSMUSG00000078612
ENSMUSG00000025488	ENSMUSG00000048988	ENSMUSG00000035429
ENSMUSG00000064941	ENSMUSG00000109161	ENSMUSG00000028680
ENSMUSG00000045083	ENSMUSG00000118012	ENSMUSG00000104420
ENSMUSG00000119227	ENSMUSG00000074254	ENSMUSG00000067719
ENSMUSG00000095186	ENSMUSG00000034875	ENSMUSG00000037490

ENSMUSG00000031165
ENSMUSG00000031506
ENSMUSG00000035580
ENSMUSG00000029177
ENSMUSG00000004933
ENSMUSG00000104592
ENSMUSG00000041673
ENSMUSG00000001517
ENSMUSG00000024863
ENSMUSG00000038037
ENSMUSG00000037860
ENSMUSG00000048852
ENSMUSG00000025475
ENSMUSG00000051590
ENSMUSG00000009585
ENSMUSG00000048865
ENSMUSG00000085068
ENSMUSG00000022491
ENSMUSG00000021880
ENSMUSG00000054986
ENSMUSG00000086479
ENSMUSG00000083579
ENSMUSG00000033860
ENSMUSG00000054757
ENSMUSG00000000817
ENSMUSG00000024757
ENSMUSG00000031662
ENSMUSG00000070501
ENSMUSG00000091191
ENSMUSG00000105703
ENSMUSG00000033533
ENSMUSG00000074677
ENSMUSG00000113354
ENSMUSG00000037572
ENSMUSG00000084174
ENSMUSG00000086612
ENSMUSG00000026204
ENSMUSG00000022488
ENSMUSG00000075270
ENSMUSG00000055612
ENSMUSG00000028859
ENSMUSG00000047641
ENSMUSG00000113294
ENSMUSG00000050359
ENSMUSG00000025154
ENSMUSG00000043795
ENSMUSG00000089714
ENSMUSG00000086587
ENSMUSG00000048040
ENSMUSG00000032596
ENSMUSG00000109032
ENSMUSG00000023886
ENSMUSG00000097373
ENSMUSG00000015452
ENSMUSG00000079457
ENSMUSG00000112188
ENSMUSG00000036594
ENSMUSG00000034456
ENSMUSG00000019278
ENSMUSG00000026348
ENSMUSG00000068196
ENSMUSG00000022894
ENSMUSG00000006930
ENSMUSG00000002111
ENSMUSG00000074445
ENSMUSG00000118669
ENSMUSG00000038173
ENSMUSG00000042734
ENSMUSG00000041827
ENSMUSG00000028937
ENSMUSG00000040528
ENSMUSG00000032333
ENSMUSG00000084783
ENSMUSG00000015627
ENSMUSG00000111620
ENSMUSG00000118640
ENSMUSG00000091897
ENSMUSG00000106004
ENSMUSG00000032089
ENSMUSG00000023087
ENSMUSG00000048834
ENSMUSG00000058914
ENSMUSG00000086742
ENSMUSG00000059901
ENSMUSG00000083396
ENSMUSG00000083261
ENSMUSG00000031750
ENSMUSG00000027761
ENSMUSG00000111777
ENSMUSG00000117340
ENSMUSG00000032011
ENSMUSG00000080977
ENSMUSG00000064346
ENSMUSG00000089929
ENSMUSG00000104696
ENSMUSG00000084289
ENSMUSG00000086683
ENSMUSG00000097804
ENSMUSG00000021319
ENSMUSG00000028339
ENSMUSG00000007030
ENSMUSG00000041669
ENSMUSG00000021815
ENSMUSG00000040485
ENSMUSG00000021765
ENSMUSG00000099997
ENSMUSG00000041552
ENSMUSG00000055137
ENSMUSG00000043300
ENSMUSG00000108659
ENSMUSG00000031833
ENSMUSG00000006782
ENSMUSG00000069893
ENSMUSG00000030748
ENSMUSG00000042817
ENSMUSG00000026928
ENSMUSG00000027386
ENSMUSG00000085093
ENSMUSG00000017144
ENSMUSG00000109293

ENSMUSG00000022878	ENSMUSG00000021714	ENSMUSG00000114117
ENSMUSG00000086291	ENSMUSG00000111713	ENSMUSG00000032254
ENSMUSG00000026196	ENSMUSG00000000154	ENSMUSG00000058624
ENSMUSG00000021950	ENSMUSG00000079015	ENSMUSG00000090019
ENSMUSG00000100850	ENSMUSG00000045777	ENSMUSG00000099858
ENSMUSG00000075267	ENSMUSG00000049799	ENSMUSG00000062582
ENSMUSG00000030278	ENSMUSG00000031595	ENSMUSG00000077505
ENSMUSG00000029188	ENSMUSG00000030708	ENSMUSG00000045284
ENSMUSG00000114375	ENSMUSG00000040710	ENSMUSG00000001227
ENSMUSG00000017716	ENSMUSG00000004266	ENSMUSG00000079588
ENSMUSG00000086410	ENSMUSG00000061533	ENSMUSG00000035891
ENSMUSG00000079685	ENSMUSG00000034488	ENSMUSG00000097365
ENSMUSG00000056130	ENSMUSG00000022489	ENSMUSG00000066097
ENSMUSG00000030047	ENSMUSG00000031304	ENSMUSG00000069793
ENSMUSG00000056973	ENSMUSG00000026628	ENSMUSG00000022110
ENSMUSG00000020901	ENSMUSG00000029664	ENSMUSG00000005233
ENSMUSG00000034871	ENSMUSG00000052241	ENSMUSG00000030972
ENSMUSG00000041642	ENSMUSG00000105350	ENSMUSG00000041237
ENSMUSG00000007888	ENSMUSG00000038298	ENSMUSG00000034329
ENSMUSG00000039158	ENSMUSG00000039994	ENSMUSG00000081572
ENSMUSG00000078773	ENSMUSG00000111957	ENSMUSG00000022235
ENSMUSG00000019214	ENSMUSG00000032561	ENSMUSG00000058297
ENSMUSG00000043832	ENSMUSG00000070167	ENSMUSG00000021566
ENSMUSG00000081957	ENSMUSG00000042379	ENSMUSG00000029843
ENSMUSG00000090634	ENSMUSG00000019992	ENSMUSG00000089722
ENSMUSG00000032207	ENSMUSG00000031877	ENSMUSG00000055602
ENSMUSG00000028459	ENSMUSG00000081660	ENSMUSG00000041460
ENSMUSG00000027238	ENSMUSG00000027698	ENSMUSG00000078490
ENSMUSG00000029838	ENSMUSG00000117118	ENSMUSG00000070639
ENSMUSG00000025330	ENSMUSG00000025507	ENSMUSG00000062488
ENSMUSG00000091366	ENSMUSG00000094338	ENSMUSG00000035678
ENSMUSG00000038943	ENSMUSG00000041064	ENSMUSG00000023947
ENSMUSG00000072082	ENSMUSG00000064655	ENSMUSG00000021998
ENSMUSG00000053977	ENSMUSG00000084088	ENSMUSG00000030800
ENSMUSG00000064943	ENSMUSG00000042333	ENSMUSG00000062410
ENSMUSG00000070933	ENSMUSG00000038179	ENSMUSG00000091575
ENSMUSG00000083186	ENSMUSG00000044250	ENSMUSG00000029161
ENSMUSG00000076498	ENSMUSG00000058488	ENSMUSG00000114206
ENSMUSG00000052396	ENSMUSG00000089652	ENSMUSG00000063253
ENSMUSG00000030364	ENSMUSG00000060441	ENSMUSG00000116935

ENSMUSG00000040084	ENSMUSG00000102142	ENSMUSG00000035486
ENSMUSG00000074419	ENSMUSG00000032815	ENSMUSG00000026069
ENSMUSG00000030351	ENSMUSG00000022061	ENSMUSG00000040213
ENSMUSG00000028873	ENSMUSG00000072188	ENSMUSG00000109625
ENSMUSG00000111229	ENSMUSG00000020649	ENSMUSG00000030110
ENSMUSG00000061972	ENSMUSG00000066245	ENSMUSG00000027858
ENSMUSG00000069911	ENSMUSG00000057751	ENSMUSG00000052305
ENSMUSG00000052736	ENSMUSG00000049723	ENSMUSG00000045672
ENSMUSG00000030124	ENSMUSG00000021943	ENSMUSG00000046275
ENSMUSG00000117228	ENSMUSG00000025197	ENSMUSG00000102698
ENSMUSG00000100199	ENSMUSG00000091243	ENSMUSG00000048387
ENSMUSG00000095217	ENSMUSG00000067714	ENSMUSG00000022148
ENSMUSG00000035273	ENSMUSG00000116811	ENSMUSG00000020256
ENSMUSG00000040136	ENSMUSG00000024986	ENSMUSG00000026580
ENSMUSG00000023903	ENSMUSG00000005237	ENSMUSG00000026494
ENSMUSG00000069720	ENSMUSG00000114277	ENSMUSG00000068303
ENSMUSG00000024164	ENSMUSG00000029561	ENSMUSG00000026582
ENSMUSG00000115200	ENSMUSG00000014602	ENSMUSG00000046623
ENSMUSG00000040328	ENSMUSG00000075289	ENSMUSG00000030276
ENSMUSG00000065637	ENSMUSG00000110018	ENSMUSG00000116097
ENSMUSG00000045322	ENSMUSG00000110123	ENSMUSG00000067212
ENSMUSG00000069273	ENSMUSG00002075346	ENSMUSG00000085785
ENSMUSG00000015568	ENSMUSG00000049971	ENSMUSG00000117604
ENSMUSG00000104669	ENSMUSG00000024990	ENSMUSG00000110758
ENSMUSG00000046634	ENSMUSG00000048424	ENSMUSG00000074218
ENSMUSG00000089680	ENSMUSG00000064451	ENSMUSG00000064280
ENSMUSG00000034227	ENSMUSG00000019577	ENSMUSG00000105698
ENSMUSG00000064945	ENSMUSG00000109799	ENSMUSG00000083854
ENSMUSG00000032446	ENSMUSG00000094530	ENSMUSG00000073752
ENSMUSG00000110494	ENSMUSG00000108763	ENSMUSG00000030966
ENSMUSG00000112289	ENSMUSG00000025020	ENSMUSG00000002204
ENSMUSG00000089694	ENSMUSG00000022696	ENSMUSG00000028864
ENSMUSG00000036446	ENSMUSG00000097413	ENSMUSG00000058248
ENSMUSG00000026295	ENSMUSG00000029591	ENSMUSG00000043008
ENSMUSG00000079845	ENSMUSG00000074063	ENSMUSG00000088252
ENSMUSG00000039187	ENSMUSG00000108288	ENSMUSG00000062432
ENSMUSG00000117575	ENSMUSG00000040424	ENSMUSG00000085913
ENSMUSG00000061906	ENSMUSG00000032348	ENSMUSG00000051435
ENSMUSG00000065822	ENSMUSG00000047586	ENSMUSG00000070692
ENSMUSG00000080917	ENSMUSG00000041219	ENSMUSG00000031971

ENSMUSG00000072596	ENSMUSG00000047959	ENSMUSG00000040412
ENSMUSG00000036777	ENSMUSG00000082128	ENSMUSG00000032186
ENSMUSG00000034041	ENSMUSG00000036334	ENSMUSG00000081723
ENSMUSG00000060550	ENSMUSG00000020963	ENSMUSG00000090215
ENSMUSG00000108968	ENSMUSG00000103367	ENSMUSG00000047911
ENSMUSG00000004709	ENSMUSG00000031519	ENSMUSG00000105553
ENSMUSG00000113502	ENSMUSG00000057580	ENSMUSG00000110279
ENSMUSG00000019122	ENSMUSG00000024781	ENSMUSG00000080810
ENSMUSG00000026452	ENSMUSG00000065750	ENSMUSG00000069456
ENSMUSG00000021416	ENSMUSG00000116679	ENSMUSG00000049892
ENSMUSG00000069372	ENSMUSG00000040663	ENSMUSG00000028362
ENSMUSG00000065176	ENSMUSG00002075286	ENSMUSG00000044938
ENSMUSG00000109792	ENSMUSG00000043903	ENSMUSG00000027313
ENSMUSG00000031725	ENSMUSG00000022103	ENSMUSG00000032554
ENSMUSG00000030854	ENSMUSG00000020429	ENSMUSG00000108487
ENSMUSG00000075122	ENSMUSG00000059060	ENSMUSG00000083863
ENSMUSG00000100210	ENSMUSG00000109270	ENSMUSG00000025075
ENSMUSG00000074634	ENSMUSG00000068744	ENSMUSG00000039384
ENSMUSG00000036902	ENSMUSG00000080896	ENSMUSG00000040752
ENSMUSG00000066952	ENSMUSG00000087373	ENSMUSG00000079505
ENSMUSG00000084390	ENSMUSG00000086706	ENSMUSG00000001155
ENSMUSG00000033952	ENSMUSG00000095457	ENSMUSG00000046159
ENSMUSG00000085109	ENSMUSG00000024411	ENSMUSG00000027274
ENSMUSG00000027199	ENSMUSG00000040164	ENSMUSG00000015962
ENSMUSG00000024032	ENSMUSG00000039323	ENSMUSG00000022037
ENSMUSG00000030528	ENSMUSG00000005124	ENSMUSG00000027765
ENSMUSG00000037202	ENSMUSG00000038092	ENSMUSG00000010651
ENSMUSG00000054293	ENSMUSG00000043557	ENSMUSG00000074092
ENSMUSG00000004612	ENSMUSG00000042228	ENSMUSG00000108897
ENSMUSG00000113079	ENSMUSG00000101751	ENSMUSG00000090026
ENSMUSG00000029811	ENSMUSG00000035031	ENSMUSG00000101588
ENSMUSG00000028602	ENSMUSG00000020609	ENSMUSG00000032300
ENSMUSG00000081058	ENSMUSG00000085203	ENSMUSG00000068706
ENSMUSG00000046699	ENSMUSG00000026475	ENSMUSG00000081965
ENSMUSG00000051262	ENSMUSG00000083160	ENSMUSG00000028773
ENSMUSG00000027896	ENSMUSG00000005470	ENSMUSG00000039883
ENSMUSG00000082111	ENSMUSG00000103720	ENSMUSG00000100127
ENSMUSG00000024112	ENSMUSG00000045994	ENSMUSG00000029830
ENSMUSG00000059323	ENSMUSG00000059498	ENSMUSG00000027227
ENSMUSG00000099569	ENSMUSG00000032690	ENSMUSG00000081078

ENSMUSG00000016763
ENSMUSG00000098090
ENSMUSG00000045871
ENSMUSG00000052142
ENSMUSG00000025017
ENSMUSG00000047534
ENSMUSG00000003545
ENSMUSG00000073409
ENSMUSG00000036218
ENSMUSG00000017499
ENSMUSG00000087362
ENSMUSG00000050272
ENSMUSG00000008153
ENSMUSG00000052565
ENSMUSG00000022583
ENSMUSG00000102037
ENSMUSG00000085977
ENSMUSG00000081772
ENSMUSG00000097766
ENSMUSG00000082855
ENSMUSG00000051504
ENSMUSG00000067656
ENSMUSG00000037852
ENSMUSG00000080904
ENSMUSG00000034266
ENSMUSG00000092517
ENSMUSG00000015340
ENSMUSG00000036931
ENSMUSG00000024803
ENSMUSG00000087819
ENSMUSG00000091813
ENSMUSG00000023968
ENSMUSG00000045573
ENSMUSG00000022504
ENSMUSG00000033316
ENSMUSG00000001281
ENSMUSG00000032915
ENSMUSG00000047730
ENSMUSG00000074715
ENSMUSG00000086320
ENSMUSG00000050944
ENSMUSG00000103065
ENSMUSG00000117621
ENSMUSG00000071178
ENSMUSG00000021453
ENSMUSG00000104459
ENSMUSG00000113637
ENSMUSG00000027398
ENSMUSG00000021720
ENSMUSG00000099848
ENSMUSG00000035355
ENSMUSG00000027339
ENSMUSG00000065232
ENSMUSG00000083076
ENSMUSG00000036110
ENSMUSG00000029716
ENSMUSG00000037664
ENSMUSG00000024650
ENSMUSG00000020432
ENSMUSG00000112830
ENSMUSG00000062515
ENSMUSG00000070368
ENSMUSG00000017830
ENSMUSG00000114442
ENSMUSG00000041660
ENSMUSG00000049241
ENSMUSG00000060257
ENSMUSG00000003555
ENSMUSG00000038128
ENSMUSG00000012819
ENSMUSG00000042436
ENSMUSG00000083822
ENSMUSG00000112105
ENSMUSG00000085382
ENSMUSG00000118642
ENSMUSG00000084632
ENSMUSG00000002055
ENSMUSG00000025380
ENSMUSG00000034422
ENSMUSG00000045053
ENSMUSG00000020877
ENSMUSG00000038267
ENSMUSG00000020988
ENSMUSG00000005514
ENSMUSG00000010797
ENSMUSG00000069733
ENSMUSG00000042306
ENSMUSG00000014905
ENSMUSG00000058620
ENSMUSG00000053137
ENSMUSG00000058385
ENSMUSG00000039621
ENSMUSG00000061353
ENSMUSG00000037139
ENSMUSG00000095388
ENSMUSG00000057722
ENSMUSG00000038224
ENSMUSG00000061482
ENSMUSG00000071311
ENSMUSG00000027762
ENSMUSG00000035459
ENSMUSG00000117896
ENSMUSG00000002486
ENSMUSG00000060923
ENSMUSG00000102248
ENSMUSG00000107215
ENSMUSG00000106990
ENSMUSG00000027510
ENSMUSG00000051235
ENSMUSG00000015981
ENSMUSG00000030865
ENSMUSG00000095143
ENSMUSG00000037921
ENSMUSG00000027737
ENSMUSG00000045004
ENSMUSG00000029656
ENSMUSG00000025420
ENSMUSG00000083193
ENSMUSG00000028295
ENSMUSG00000118607

ENSMUSG00000015396	ENSMUSG00000052861	ENSMUSG00000029923
ENSMUSG00000035683	ENSMUSG00000100666	ENSMUSG00000028838
ENSMUSG00000016283	ENSMUSG00000029605	ENSMUSG00000031845

APPENDIX B BIOANALYZER DNA 1000 REPORT

Assay Class: DNA 1000
Data Path: C:\...2100 expert_DNA 1000_DE13805227_2022-04-22_11-42-21 (1).xad

Created: 2022-04-22 11:42:20 AM
Modified: 2022-04-29 11:45:36 AM

Electrophoresis File Run Summary

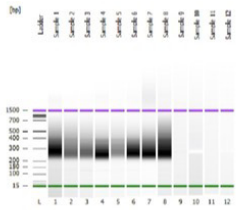

Instrument Information:

Instrument Name:	DE13805227	Firmware:	C.01.069
Serial#:	DE13805227	Type:	G2939A

Assay Information:

Assay Origin Path:	C:\Program Files (x86)\Agilent\2100 bioanalyzer\2100 expert\assays\dsDNA\DNA 1000 Series II.xsy
Assay Class:	DNA 1000
Version:	2.3
Assay Comments:	DNA Analysis 25 -1000 bp

Chip Information:

Chip Lot #:	
Reagent Kit Lot #:	
Chip Comments:	

Sample 1

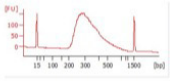

Sample 2

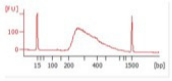

Sample 3

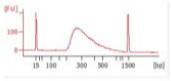

Sample 4

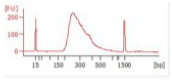

Sample 5

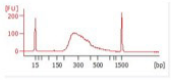

Sample 6

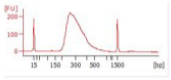

Sample 7

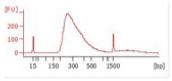

Sample 8

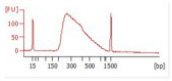

Sample 9

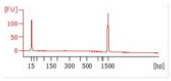

Sample 10

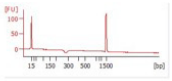

Sample 11

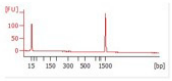

Sample 12

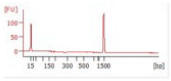

Assay Class: DNA 1000
Data Path: C:\...2100 expert_DNA 1000_DE13805227_2022-04-22_11-42-21 (1).xad

Created: 2022-04-22 11:42:20 AM
Modified: 2022-04-29 11:45:36 AM

Electrophoresis File Run Summary (Chip Summary)

Sample Name	Sample Comment	Rest. Digest	Status	Observation	Result Label	Result Color
Sample 1		☐	✓			
Sample 2		☐	✓			
Sample 3		☐	✓			
Sample 4		☐	✓			
Sample 5		☐	✓			
Sample 6		☐	✓			
Sample 7		☐	✓			
Sample 8		☐	✓			
Sample 9		☐	✓			
Sample 10		☐	✓			
Sample 11		☐	✓			
Sample 12		☐	✓			
Ladder		☐	✓			

Chip Lot # **Reagent Kit Lot #**

Chip Comments :

Assay Class: DNA 1000
Data Path: C:\...2100 expert_DNA 1000_DE13805227_2022-04-22_11-42-21 (1).xad

Created: 2022-04-22 11:42:20 AM
Modified: 2022-04-29 11:45:36 AM

Electrophoresis Assay Details

General Analysis Settings

Number of Available Sample and Ladder Wells (Max.) : 13
Minimum Visible Range [s] : 30
Maximum Visible Range [s] : 129
Start Analysis Time Range [s] : 30
End Analysis Time Range [s] : 128.95
Ladder Concentration [ng/µl] : 44
Uses Standard Area for Ladder Fragments
Lower Marker Concentration [ng/µl] : 4.2
Upper Marker Concentration [ng/µl] : 2.1
Used Upper Marker for Quantitation
Standard Curve Fit is Point to Point
Show Data Aligned to Lower and Upper Marker

Integrator Settings

Integration Start Time [s] : 30
Integration End Time [s] : 128.95
Slope Threshold : 0.5
Height Threshold [FU] : 20
Area Threshold : 0.1
Width Threshold [s] : 0.5
Baseline Plateau [s] : 0.5

Filter Settings

Filter Width [s] : 0.5
Polynomial Order : 4

Ladder

Ladder Peak	Size	Area
1	15	25
2	25	26
3	50	34
4	100	41
5	150	45
6	200	52
7	300	63
8	400	76
9	500	83
10	700	88
11	850	86
12	1000	90
13	1500	52

Assay Class: DNA 1000
Data Path: C:\...2100 expert_DNA 1000_DE13805227_2022-04-22_11-42-21 (1).xad

Created: 2022-04-22 11:42:20 AM
Modified: 2022-04-29 11:45:36 AM

Electropherogram Summary

Sample 1

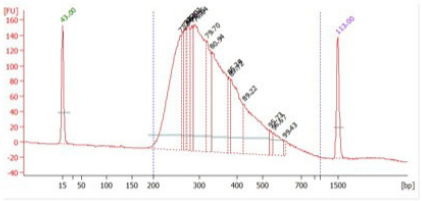

Overall Results for sample 1 : Sample 1

Number of peaks found:	14	Area 1:	3,037.6

Peak table for sample 1 : Sample 1

Peak	Size [bp]	Conc. [ng/µl]	Molarity [nmol/l]	Observations
1	15	4.20	424.2	Lower Marker
2	258	14.75	86.5	
3	265	2.28	13.1	
4	270	3.39	19.0	
5	276	4.31	23.6	
6	284	2.76	14.7	
7	291	13.40	69.9	
8	321	4.35	20.6	
9	333	11.65	53.0	
10	378	1.18	4.7	
11	383	5.92	23.4	
12	429	6.52	23.0	
13	539	0.54	1.5	
14	558	1.32	3.6	
15	613	0.20	0.5	
16	1,500	2.10	2.1	Upper Marker

Region table for sample 1 : Sample 1

From [bp]	To [bp]	Area	% of Total	Average Size [bp]	Size distribution in CV [%]	Conc. [ng/µl]	Color
200	1,000	3,037.6	99	343	29.0	73.50	

Assay Class: DNA 1000
Data Path: C:\...2100 expert_DNA 1000_DE13805227_2022-04-22_11-42-21 (1).xad

Created: 2022-04-22 11:42:20 AM
Modified: 2022-04-29 11:45:36 AM

Electropherogram Summary Continued ...

Sample 2

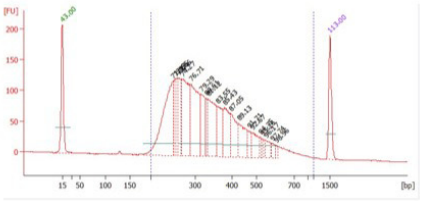

Overall Results for sample 2 : Sample 2

Number of peaks found:	19	Area 1:	2,418.6

Peak table for sample 2 : Sample 2

Peak	Size [bp]	Conc. [ng/µl]	Molarity [nmol/l]	Observations
1	15	4.20	424.2	Lower Marker
2	249	8.20	49.8	
3	256	1.74	10.3	
4	263	1.74	10.0	
5	270	5.82	32.6	
6	291	5.78	30.1	
7	316	2.18	10.5	
8	330	0.97	4.5	
9	335	4.01	18.1	
10	360	2.19	9.2	
11	380	2.40	9.6	
12	396	1.97	7.5	
13	427	2.04	7.2	
14	467	0.63	2.0	
15	483	1.18	3.7	
16	519	0.27	0.8	
17	529	0.30	0.9	
18	548	0.62	1.7	
19	579	0.37	1.0	
20	604	0.18	0.4	
21	1,500	2.10	2.1	Upper Marker

Region table for sample 2 : Sample 2

From [bp]	To [bp]	Area	% of Total	Average Size [bp]	Size distribution in CV [%]	Conc. [ng/µl]	Color
200	1,000	2,418.6	99	348	32.0	45.91	

Assay Class: DNA 1000
Data Path: C:\...2100 expert_DNA 1000_DE13805227_2022-04-22_11-42-21 (1).xad

Created: 2022-04-22 11:42:20 AM
Modified: 2022-04-29 11:45:36 AM

Electropherogram Summary Continued ...

Sample 3

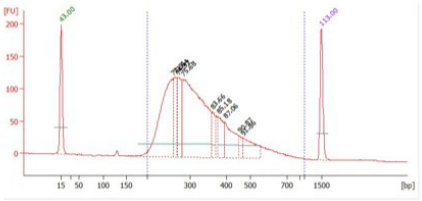

Overall Results for sample 3 : Sample 3

Number of peaks found:	9	Area 1:	2,077.5

Peak table for sample 3 : Sample 3

Peak	Size [bp]	Conc. [ng/µl]	Molarity [nmol/l]	Observations
1	15	4.20	424.2	Lower Marker
2	258	9.28	54.5	
3	265	2.23	12.8	
4	270	2.80	15.7	
5	282	14.68	78.8	
6	361	1.04	4.4	
7	377	1.67	6.7	
8	397	2.55	9.7	
9	454	0.45	1.5	
10	470	1.73	5.6	
11	1,500	2.10	2.1	Upper Marker

Region table for sample 3 : Sample 3

From [bp]	To [bp]	Area	% of Total	Average Size [bp]	Size distribution in CV [%]	Conc. [ng/µl]	Color
200	1,000	2,077.5	99	336	30.2	38.02	

Assay Class: DNA 1000
Data Path: C:\...2100 expert_DNA 1000_DE13805227_2022-04-22_11-42-21 (1).xad

Created: 2022-04-22 11:42:20 AM
Modified: 2022-04-29 11:45:36 AM

Electropherogram Summary Continued ...

Sample 4

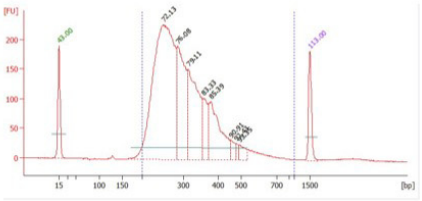

Overall Results for sample 4 : Sample 4

Number of peaks found:	8	Area 1:	3,119.4

Peak table for sample 4 : Sample 4

Peak	Size [bp]	Conc. [ng/µl]	Molarity [nmol/l]	Observations
1	15	4.20	424.2	Lower Marker
2	251	31.54	190.2	
3	286	9.71	51.5	
4	314	9.60	46.3	
5	358	2.65	11.2	
6	379	5.90	23.6	
7	455	0.62	2.1	
8	479	0.31	1.0	
9	493	0.77	2.4	
10	1,500	2.10	2.1	Upper Marker

Region table for sample 4 : Sample 4

From [bp]	To [bp]	Area	% of Total	Average Size [bp]	Size distribution in CV [%]	Conc. [ng/µl]	Color
200	1,000	3,119.4	98	312	27.8	61.31	

Assay Class: DNA 1000
Data Path: C:\...2100 expert_DNA 1000_DE13805227_2022-04-22_11-42-21 (1).xad

Created: 2022-04-22 11:42:20 AM
Modified: 2022-04-29 11:45:36 AM

Electropherogram Summary Continued ...

Sample 5

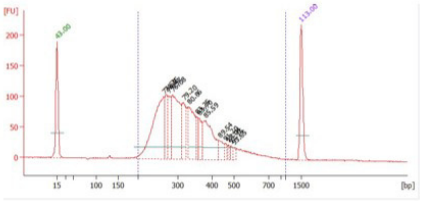

Overall Results for sample 5 : Sample 5

Number of peaks found:	14	Area 1:	1,618.2

Peak table for sample 5 : Sample 5

Peak	Size [bp]	Conc. [ng/µl]	Molarity [nmol/l]	Observations
1	15	4.20	424.2	Lower Marker
2	265	6.29	36.0	
3	270	1.59	8.9	
4	276	1.55	8.5	
5	286	4.43	23.5	
6	315	2.00	9.6	
7	333	2.62	12.0	
8	357	0.57	2.4	
9	362	0.97	4.1	
10	381	2.84	11.3	
11	434	0.64	2.2	
12	460	0.26	0.8	
13	473	0.19	0.6	
14	484	0.20	0.6	
15	498	0.20	0.6	
16	1,500	2.10	2.1	Upper Marker

Region table for sample 5 : Sample 5

From [bp]	To [bp]	Area	% of Total	Average Size [bp]	Size distribution in CV [%]	Conc. [ng/µl]	Color
200	1,000	1,618.2	98	339	29.4	26.41	

Assay Class: DNA 1000
Data Path: C:\...2100 expert_DNA 1000_DE13805227_2022-04-22_11-42-21 (1).xad

Created: 2022-04-22 11:42:20 AM
Modified: 2022-04-29 11:45:36 AM

Electropherogram Summary Continued ...

Sample 6

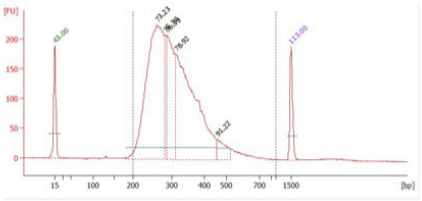

Overall Results for sample 6 : Sample 6

Number of peaks found:	5	Area 1:	2,956.6

Peak table for sample 6 : Sample 6

Peak	Size [bp]	Conc. [ng/µl]	Molarity [nmol/l]	Observations
1	15	4.20	424.2	Lower Marker
2	261	25.48	148.0	
3	282	2.42	13.0	
4	288	9.08	47.7	
5	312	21.35	103.5	
6	460	1.51	5.0	
7	1,500	2.10	2.1	Upper Marker

Region table for sample 6 : Sample 6

From [bp]	To [bp]	Area	% of Total	Average Size [bp]	Size distribution in CV [%]	Conc. [ng/µl]	Color
200	1,000	2,956.6	98	316	25.5	59.68	

Assay Class: DNA 1000
Data Path: C:\...2100 expert_DNA 1000_DE13805227_2022-04-22_11-42-21 (1).xad

Created: 2022-04-22 11:42:20 AM
Modified: 2022-04-29 11:45:36 AM

Electropherogram Summary Continued ...

Sample 7

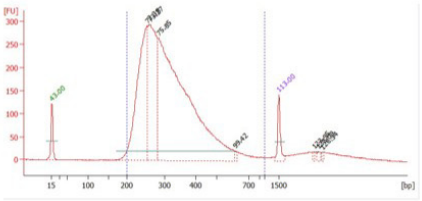

Overall Results for sample 7 : Sample 7

Number of peaks found:	4	Area 1:	4,041.1

Peak table for sample 7 : Sample 7

Peak	Size [bp]	Conc. [ng/µl]	Molarity [nmol/l]	Observations
1	15	4.20	424.2	Lower Marker
2	253	26.28	157.1	
3	261	21.80	126.4	
4	284	66.95	357.5	
5	613	0.29	0.7	
6	1,500	2.10	2.1	Upper Marker
7	2,741	0.00	0.0	
8	2,870	0.00	0.0	
9	3,012	0.00	0.0	

Region table for sample 7 : Sample 7

From [bp]	To [bp]	Area	% of Total	Average Size [bp]	Size distribution in CV [%]	Conc. [ng/µl]	Color
200	1,000	4,041.1	92	326	30.0	108.45	

Assay Class: DNA 1000
Data Path: C:\...2100 expert_DNA 1000_DE13805227_2022-04-22_11-42-21 (1).xad

Created: 2022-04-22 11:42:20 AM
Modified: 2022-04-29 11:45:36 AM

Electropherogram Summary Continued ...

Sample 8

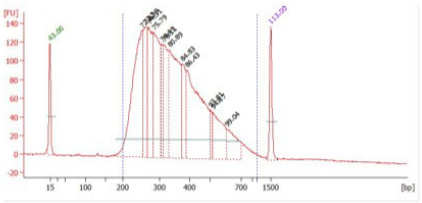

Overall Results for sample 8 : Sample 8

Number of peaks found:	12	Area 1:	2,479.8

Peak table for sample 8 : Sample 8

Peak	Size [bp]	Conc. [ng/µl]	Molarity [nmol/l]	Observations
1	15	4.20	424.2	Lower Marker
2	252	13.54	81.4	
3	262	5.98	34.6	
4	270	6.22	34.9	
5	283	7.97	42.7	
6	308	2.03	10.0	
7	314	4.62	22.3	
8	333	10.43	47.5	
9	374	3.18	12.9	
10	390	11.15	43.3	
11	500	0.79	2.4	
12	518	3.51	10.3	
13	605	2.26	5.6	
14	1,500	2.10	2.1	Upper Marker

Region table for sample 8 : Sample 8

From [bp]	To [bp]	Area	% of Total	Average Size [bp]	Size distribution in CV [%]	Conc. [ng/µl]	Color
200	1,000	2,479.8	97	361	34.0	72.45	

Assay Class: DNA 1000
Data Path: C:\...2100 expert_DNA 1000_DE13805227_2022-04-22_11-42-21 (1).xad

Created: 2022-04-22 11:42:20 AM
Modified: 2022-04-29 11:45:36 AM

Electropherogram Summary Continued ...

Sample 9

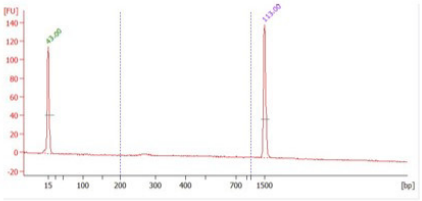

Overall Results for sample 9 : Sample 9

Number of peaks found:	0	Area 1:	16.9

Peak table for sample 9 : Sample 9

Peak	Size [bp]	Conc. [ng/µl]	Molarity [nmol/l]	Observations
1	15	4.20	424.2	Lower Marker
2	1,500	2.10	2.1	Upper Marker

Region table for sample 9 : Sample 9

From [bp]	To [bp]	Area	% of Total	Average Size [bp]	Size distribution in CV [%]	Conc. [ng/µl]	Color
200	1,000	16.9	54	520	37.9	0.47	

Assay Class: DNA 1000
Data Path: C:\...2100 expert_DNA 1000_DE13805227_2022-04-22_11-42-21 (1).xad

Created: 2022-04-22 11:42:20 AM
Modified: 2022-04-29 11:45:36 AM

Electropherogram Summary Continued ...

Sample 10

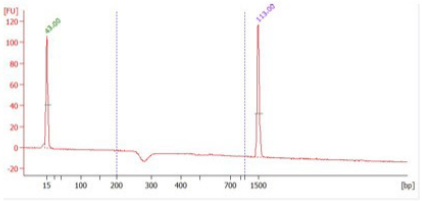

Overall Results for sample 10 : Sample 10

Number of peaks found:	0	Area 1:	2.8

Peak table for sample 10 : Sample 10

Peak	Size [bp]	Conc. [ng/µl]	Molarity [nmol/l]	Observations
1	15	4.20	424.2	Lower Marker
2	1,500	2.10	2.1	Upper Marker

Region table for sample 10 : Sample 10

From [bp]	To [bp]	Area	% of Total	Average Size [bp]	Size distribution in CV [%]	Conc. [ng/µl]	Color
200	1,000	2.8	30	229	14.4	0.12	

Assay Class: DNA 1000
Data Path: C:\...2100 expert_DNA 1000_DE13805227_2022-04-22_11-42-21 (1).xad

Created: 2022-04-22 11:42:20 AM
Modified: 2022-04-29 11:45:36 AM

Electropherogram Summary Continued ...

Sample 11

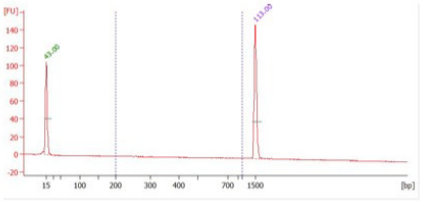

Overall Results for sample 11 : Sample 11

Number of peaks found:	0	Area 1:	1.5

Peak table for sample 11 : Sample 11

Peak	Size [bp]	Conc. [ng/µl]	Molarity [nmol/l]	Observations
1	15	4.20	424.2	Lower Marker
2	1,500	2.10	2.1	Upper Marker

Region table for sample 11 : Sample 11

From [bp]	To [bp]	Area	% of Total	Average Size [bp]	Size distribution in CV [%]	Conc. [ng/µl]	Color
200	1,000	1.5	17	641	26.1	0.03	

Assay Class: DNA 1000
Data Path: C:\...2100 expert_DNA 1000_DE13805227_2022-04-22_11-42-21 (1).xad

Created: 2022-04-22 11:42:20 AM
Modified: 2022-04-29 11:45:36 AM

Electropherogram Summary Continued ...

Sample 12

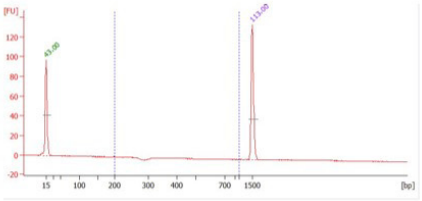

Overall Results for sample 12 : Sample 12

Number of peaks found:	0	Area 1:	0.0

Peak table for sample 12 : Sample 12

Peak	Size [bp]	Conc. [ng/µl]	Molarity [nmol/l]	Observations
1	15	4.20	424.2	Lower Marker
2	1,500	2.10	2.1	Upper Marker

Region table for sample 12 : Sample 12

From [bp]	To [bp]	Area	% of Total	Average Size [bp]	Size distribution in CV [%]	Conc. [ng/µl]	Color
200	1,000	0.0	0	0	0.0	0.00	

Assay Class: DNA 1000
Data Path: C:\...2100 expert_DNA 1000_DE13805227_2022-04-22_11-42-21 (1).xad

Created: 2022-04-22 11:42:20 AM
Modified: 2022-04-29 11:45:36 AM

Gel Image

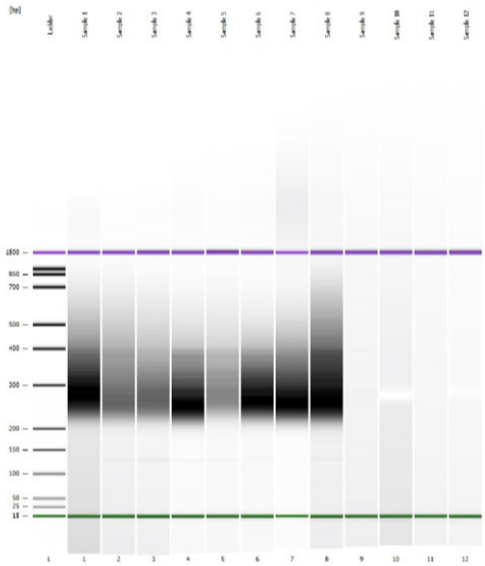

Assay Class: DNA 1000
Data Path: C:\...2100 expert_DNA 1000_DE13805227_2022-04-22_11-42-21 (1).xad

Created: 2022-04-22 11:42:20 AM
Modified: 2022-04-29 11:45:36 AM

Run Logbook

Description	Number	Source	Category	Sub Category	Time	Time Zone	User	Host
Run ended on port 6 (Number of wells acquired: 13)		Instrument	Run		2022-04-22 12:24:09 PM	(GMT --03:00) Atlantic Standard Time	LaRoche's Lab	DEBANY-IDEAP AD3
Run started on port 6 (File: C:\Program Files (x86)\Agilent\2100 bioanalyzer\2100 expert\Data\2022-04-22\2100 expert_DNA 1000_DE13805227_2022-04-22_11-42-21.xad)		Instrument	Run		2022-04-22 11:42:26 AM	(GMT --03:00) Atlantic Standard Time	LaRoche's Lab	DEBANY-IDEAP AD3
Product Number : G2939A		Instrument	Run		2022-04-22 11:42:26 AM	(GMT --03:00) Atlantic Standard Time	LaRoche's Lab	DEBANY-IDEAP AD3
Name :		Instrument	Run		2022-04-22 11:42:26 AM	(GMT --03:00) Atlantic Standard Time	LaRoche's Lab	DEBANY-IDEAP AD3
Vendor : Agilent Technologies		Instrument	Run		2022-04-22 11:42:26 AM	(GMT --03:00) Atlantic Standard Time	LaRoche's Lab	DEBANY-IDEAP AD3
Serial# : DE13805227		Instrument	Run		2022-04-22 11:42:26 AM	(GMT --03:00) Atlantic Standard Time	LaRoche's Lab	DEBANY-IDEAP AD3
Firmware : C.01.069		Instrument	Run		2022-04-22 11:42:26 AM	(GMT --03:00) Atlantic Standard Time	LaRoche's Lab	DEBANY-IDEAP AD3
Cartridge : Electrode		Instrument	Run		2022-04-22 11:42:26 AM	(GMT --03:00) Atlantic Standard Time	LaRoche's Lab	DEBANY-IDEAP AD3

BIBLIOGRAPHY

1. Sims-Gould, J. *et al.* A national intervention to support frail older adults in primary care: a protocol for an adapted implementation framework. *BMC Geriatr* **21**, 453 (2021).

2. Kojima, G. Frailty as a Predictor of Future Falls Among Community-Dwelling Older People: A Systematic Review and Meta-Analysis. *Journal of the American Medical Directors Association* **16**, 1027–1033 (2015).

3. Kojima, G. Frailty as a predictor of disabilities among community-dwelling older people: a systematic review and meta-analysis. *https://doi.org/10.1080/09638288.2016.1212282* **39**, 1897–1908 (2016).

4. Kojima, G., Taniguchi, Y., Iliffe, S. & Walters, K. Frailty as a Predictor of Alzheimer Disease, Vascular Dementia, and All Dementia Among Community-Dwelling Older People: A Systematic Review and Meta-Analysis. *Journal of the American Medical Directors Association* **17**, 881–888 (2016).

5. Kojima, G., Iliffe, S. & Walters, K. Frailty index as a predictor of mortality: a systematic review and meta-analysis. *Age and Ageing* **47**, 193–200 (2018).

6. Kojima, G. Frailty as a Predictor of Nursing Home Placement Among Community-Dwelling Older Adults: A Systematic Review and Meta-analysis. *Journal of geriatric physical therapy (2001)* **41**, 42–48 (2018).

7. Kojima, G. Frailty as a predictor of hospitalisation among community-dwelling older people: a systematic review and meta-analysis. *Journal of epidemiology and community health* **70**, 722–729 (2016).

8. Kojima, G., Iliffe, S., Jivraj, S. & Walters, K. Association between frailty and quality of life among community-dwelling older people: a systematic review and meta-analysis. *Journal of epidemiology and community health* **70**, 716–721 (2016).

9. Bisset, E. S. & Howlett, S. E. The biology of frailty in humans and animals: Understanding frailty and promoting translation. *Aging Medicine* **2**, 27 (2019).

10. Fried, L. P. *et al.* Frailty in older adults: evidence for a phenotype. *J Gerontol A Biol Sci Med Sci* **56**, M146-156 (2001).

11. Mitnitski, A. B., Mogilner, A. J. & Rockwood, K. Accumulation of Deficits as a Proxy Measure of Aging. **1**, 323–336 (2001).

12. Howlett, S. E., Rockwood, M. R. H., Mitnitski, A. & Rockwood, K. Standard laboratory tests to identify older adults at increased risk of death. *BMC Medicine* **12**, (2014).

13. Sepúlveda, M. *et al.* Frailty in Aging and the Search for the Optimal Biomarker: A Review. *Biomedicines* **10**, (2022).

14. Clegg, A., Young, J., Iliffe, S., Rikkert, M. O. & Rockwood, K. Frailty in elderly people. *The Lancet* **381**, 752–762 (2013).

15. Calimport, S. R. G. *et al.* To help aging populations, classify organismal senescence: Comprehensive disease classification and staging is required to address unmet needs of aging populations. *Science (New York, N.Y.)* **366**, 576 (2019).

16. Wang, M. *et al.* Frailty and the risk of kidney function decline in the elderly population: the Rugao Longevity and Ageing Study. *Nephrology Dialysis Transplantation* (2021) doi:10.1093/ndt/gfaa323.

17. Wang, X., Bonventre, J. V. & Parrish, A. R. The Aging Kidney: Increased Susceptibility to Nephrotoxicity. *Int. J. Mol. Sci* **15**, 15358–15376 (2014).

18. Worthen, G. & Tennankore, K. Frailty Screening in Chronic Kidney Disease: Current Perspectives. *International journal of nephrology and renovascular disease* **12**, 229–239 (2019).

19. Rockwood, K. & Howlett, S. E. Fifteen years of progress in understanding frailty and health in aging. *BMC Medicine* **16**, 1–4 (2018).

20. Al Saedi, A., Feehan, J., Phu, S. & Duque, G. Current and emerging biomarkers of frailty in the elderly. *Clinical Interventions in Aging* **14**, 389 (2019).

21. Song, X., Mitnitski, A. & Rockwood, K. Prevalence and 10-Year Outcomes of Frailty in Older Adults in Relation to Deficit Accumulation. *Journal of the American Geriatrics Society* **58**, 681–687 (2010).

22. Kojima, G., Liljas, A. E. M. & Iliffe, S. Frailty syndrome: Implications and challenges for health care policy. *Risk Management and Healthcare Policy* **12**, 23–30 (2019).

23. Travers, J., Romero-Ortuno, R., Bailey, J. & Cooney, M. T. Delaying and reversing frailty: a systematic review of primary care interventions. *British Journal of General Practice* **69**, e61–e69 (2019).

24. Gray, S. L. *et al.* Angiotensin-Converting Enzyme Inhibitor Use and Incident Frailty in Women Aged 65 and Older: Prospective Findings from the Women's Health Initiative Observational Study. *Journal of the American Geriatrics Society* **57**, 297–303 (2009).

25. Onder, G. *et al.* Relation between use of angiotensin-converting enzyme inhibitors and muscle strength and physical function in older women: An observational study. *Lancet* **359**, 926–930 (2002).

26. Sumukadas, D., Witham, M. D., Struthers, A. D. & McMurdo, M. E. T. Effect of perindopril on physical function in elderly people with functional impairment: a randomized controlled trial. *CMAJ : Canadian Medical Association journal = journal de l'Association medicale canadienne* **177**, 867–874 (2007).

27. Keller, K., Kane, A., Heinze-Milne, S., Grandy, S. A. & Howlett, S. E. Chronic Treatment With the ACE Inhibitor Enalapril Attenuates the Development of Frailty and Differentially Modifies Pro- and Anti-inflammatory Cytokines in Aging Male and Female C57BL/6 Mice. *The Journals of Gerontology Series A: Biological Sciences and Medical Sciences* **74**, 1149 (2019).

28. Cappe, M., Laterre, P. F. & Dechamps, M. Preoperative frailty screening, assessment and management. *Current Opinion in Anaesthesiology* **36**, 83–88 (2023).

29. Imamura, K. *et al.* Comparison of the association between six different frailty scales and clinical events in patients on hemodialysis. *Nephrology Dialysis Transplantation* **38**, 455–462 (2023).

30. Wennberg, A. M. *et al.* Comparison of two different frailty scales in the longitudinal Swedish Adoption/Twin Study of Aging (SATSA). *Scandinavian Journal of Public Health* (2021) doi:10.1177/14034948211059958.

31. Cohen, C. I., Benyaminov, R., Rahman, M., Ngu, D. & Reinhardt, M. Frailty: A Multidimensional Biopsychosocial Syndrome. *Medical Clinics of North America* **107**, 183–197 (2023).

32. Gobbens, R. J. J. & Uchmanowicz, I. Frailty Viewed From a Nursing Perspective. *https://doi.org/10.1177/23779608221150598* **9**, (2023).

33. Pilotto, A. *et al.* A multidimensional approach to frailty in older people. *Ageing Research Reviews* **60**, 101047 (2020).

34. Rockwood, K. *et al.* A global clinical measure of fitness and frailty in elderly people. *CMAJ* **173**, 489–495 (2005).

35. Heinze-Milne, S. D., Banga, S. & Howlett, S. E. Frailty Assessment in Animal Models. *Gerontology* **65**, 610–619 (2019).

36. Ribeiro, A. R., Howlett, S. E. & Fernandes, A. Frailty—A promising concept to evaluate disease vulnerability. *Mechanisms of Ageing and Development* **187**, 111217 (2020).

37. Bennett, J. A., Winters-Stone, K. M., Dobek, J. & Nail, L. M. Frailty in Older Breast Cancer Survivors: Age, Prevalence, and Associated Factors. doi:10.1188/13.ONF.E126-E134.

38. García-Esquinas, E. *et al.* Diabetes and Risk of Frailty and Its Potential Mechanisms: A Prospective Cohort Study of Older Adults. *Journal of the American Medical Directors Association* **16**, 748–754 (2015).

39. Laube, R. *et al.* Frailty in advanced liver disease. *Liver international : official journal of the International Association for the Study of the Liver* **38**, 2117–2128 (2018).

40. Lorenz, E. C. *et al.* Frailty in CKD and Transplantation. *Kidney International Reports* **6**, 2270–2280 (2021).

41. Rech, R. S. *et al.* Factors associated with frailty in patients with neurodegenerative diseases. *CoDAS* **34**, e20200214 (2022).

42. Singh, M., Stewart, R. & White, H. Importance of frailty in patients with cardiovascular disease. *European heart journal* **35**, (2014).

43. Freer, K. & Wallington, S. L. Social frailty: the importance of social and environmental factors in predicting frailty in older adults. *https://doi.org/10.12968/bjcn.2019.24.10.486* **24**, 486–492 (2019).

44. Wang, X., Hu, J. & Wu, D. Risk factors for frailty in older adults. *Medicine* **101**, E30169 (2022).

45. Cesari, M. *et al.* Frailty syndrome and skeletal muscle: results from the Invecchiare in Chianti study. *The American journal of clinical nutrition* **83**, 1142–1148 (2006).

46. Feridooni, H. A. *et al.* The impact of age and frailty on ventricular structure and function in C57BL/6J mice. *The Physiological Society J Physiol* **595**, 12 (2017).

47. Kant, I. M. J. *et al.* The association between brain volume, cortical brain infarcts, and physical frailty. (2018) doi:10.1016/j.neurobiolaging.2018.06.032.

48. Moghtadaei, M. *et al.* The impacts of age and frailty on heart rate and sinoatrial node function. *The Journal of Physiology C 2016 The Authors. The Journal of Physiology C* **594**, 7105–7126 (2016).

49. Rosaria Rizzo, M. *et al.* Functional Connectivity Disruption in Frail Older Adults Without Global Cognitive Deficits. *Frontiers in Medicine | www.frontiersin.org* **1**, 322 (2020).

50. Wilson, D., Jackson, T., Sapey, E. & Lord, J. M. Frailty and sarcopenia: The potential role of an aged immune system. *Ageing Research Reviews* **36**, 1–10 (2017).

51. Harman, D. Aging: Overview. *Annals of the New York Academy of Sciences* **928**, 1–21 (2001).

52. Fedarko, N. S. The Biology of Aging and Frailty. *Clinics in Geriatric Medicine* **27**, 27–37 (2011).

53. Kulminski, A. M. *et al.* Cumulative Deficits Better Characterize Susceptibility to Death in the Elderly than Phenotypic Frailty: Lessons from the Cardiovascular Health Study. *Journal of the American Geriatrics Society* **56**, 898 (2008).

54. Searle, S. D., Mitnitski, A., Gahbauer, E. A., Gill, T. M. & Rockwood, K. A standard procedure for creating a frailty index. *BMC Geriatrics* **8**, 1–10 (2008).

55. Cesari, M., Gambassi, G., Van Kan, G. A. & Vellas, B. The frailty phenotype and the frailty index: different instruments for different purposes. *Age and Ageing* **43**, 10–12 (2014).

56. Blodgett, J. M., Theou, O., Howlett, S. E. & Rockwood, K. A frailty index from common clinical and laboratory tests predicts increased risk of death across the life course. *GeroScience* **39**, 447 (2017).

57. Azzu, V. & Valencak, T. G. E-Mail Experimental Section / Mini-Review Energy Metabolism and Ageing in the Mouse: A Mini-Review. *Gerontology* **63**, 327–336 (2017).

58. Liu, H., Graber, T. G., Ferguson-Stegall, L. & Thompson, L. V. Clinically relevant frailty index for mice. *The journals of gerontology. Series A, Biological sciences and medical sciences* **69**, 1485–1491 (2014).

59. Miller, M. G., Thangthaeng, N. & Shukitt-Hale, B. A Clinically Relevant Frailty Index for Aging Rats. *The journals of gerontology. Series A, Biological sciences and medical sciences* **72**, 892–896 (2017).

60. Hua, J. *et al.* Assessment of frailty in aged dogs. *American Journal of Veterinary Research* **77**, 1357–1365 (2016).

61. Walston, J. *et al.* The Physical and Biological Characterization of a Frail Mouse Model. *The journals of gerontology. Series A, Biological sciences and medical sciences* **63**, 391 (2008).

62. Parks, R. J. *et al.* A Procedure for Creating a Frailty Index Based on Deficit Accumulation in Aging Mice. *The Journals of Gerontology: Series A* **67A**, 217–227 (2012).

63. Whitehead, J. C. *et al.* A clinical frailty index in aging mice: Comparisons with frailty index data in humans. *Journals of Gerontology - Series A Biological Sciences and Medical Sciences* **69**, 621–632 (2014).

64. Yorke, A., Kane, A. E., Hancock Friesen, C. L., Howlett, S. E. & O'Blenes, S. Development of a Rat Clinical Frailty Index. *The Journals of Gerontology Series A: Biological Sciences and Medical Sciences* **72**, 897 (2017).

65. Kane, A. E., Keller, K. M., Heinze-Milne, S., Grandy, S. A. & Howlett, S. E. A Murine Frailty Index Based on Clinical and Laboratory Measurements: Links Between Frailty and Pro-inflammatory Cytokines Differ in a Sex-Specific Manner. *The journals of gerontology. Series A, Biological sciences and medical sciences* **74**, 275–282 (2019).

66. Kane, A. E. *et al.* Impact of Longevity Interventions on a Validated Mouse Clinical Frailty Index. *The journals of gerontology. Series A, Biological sciences and medical sciences* **71**, 333–339 (2016).

67. Antoch, M. P. *et al.* Physiological frailty index (PFI): quantitative in-life estimate of individual biological age in mice. *Aging (Albany NY)* **9**, 615 (2017).

68. Baumann, C. W., Kwak, D. & Thompson, L. D. V. Sex-specific components of frailty in C57BL/6 mice. *Aging (Albany NY)* **11**, 5206 (2019).

69. Herrera, M. L. *et al.* Sex frailty differences in ageing mice: Neuropathologies and therapeutic projections. *European Journal of Neuroscience* **52**, 2827–2837 (2020).

70. Kane, A. E. & Howlett, S. E. Sex differences in frailty: Comparisons between humans and preclinical models. *Mechanisms of Ageing and Development* **198**, 111546 (2021).

71. Puntmann, V. O. How-to guide on biomarkers: biomarker definitions, validation and applications with examples from cardiovascular disease. *Postgraduate medical journal* **85**, 538–545 (2009).

72. Kane, A. E. & Sinclair, D. A. Frailty biomarkers in humans and rodents: Current approaches and future advances. *Mechanisms of Ageing and Development* **180**, 117–128 (2019).

73. Wang, J., Maxwell, C. A. & Yu, F. Biological Processes and Biomarkers Related to Frailty in Older Adults: A State-of-the-Science Literature Review. *Biological Research for Nursing* **21**, 80–106 (2019).

74. Collerton, J. *et al.* Frailty and the role of inflammation, immunosenescence and cellular ageing in the very old: Cross-sectional findings from the Newcastle 85+ Study. *Mechanisms of Ageing and Development* **133**, 456–466 (2012).

75. Hubbard, R. E., O'Mahony, M. S., Savva, G. M., Calver, B. L. & Woodhouse, K. W. Inflammation and frailty measures in older people. *Journal of Cellular and Molecular Medicine* **13**, 3103–3109 (2009).

76. Puts, M. T. E., Visser, M., Twisk, J. W. R., Deeg, D. J. H. & Lips, P. Endocrine and inflammatory markers as predictors of frailty. *Clinical Endocrinology* **63**, 403–411 (2005).

77. Leng, S. X., Xue, Q. L., Tian, J., Walston, J. D. & Fried, L. P. Inflammation and Frailty in Older Women. *Journal of the American Geriatrics Society* **55**, 864–871 (2007).

78. Baylis, D. *et al.* Immune-endocrine biomarkers as predictors of frailty and mortality: a 10-year longitudinal study in community-dwelling older people. *Age* **35**, 963 (2013).

79. Leng, S. X. *et al.* White blood cell counts, insulin-like growth factor-1 levels, and frailty in community-dwelling older women. *The journals of gerontology. Series A, Biological sciences and medical sciences* **64**, 499–502 (2009).

80. Leng, S. X. *et al.* IL-6-independent association of elevated serum neopterin levels with prevalent frailty in community-dwelling older adults. *Age and Ageing* **40**, 475 (2011).

81. Walston, J. *et al.* Frailty and Activation of the Inflammation and Coagulation Systems With and Without Clinical Comorbidities: Results From the Cardiovascular Health Study. *Archives of Internal Medicine* **162**, 2333–2341 (2002).

82. Fontana, L. *et al.* Identification of a metabolic signature for multidimensional impairment and mortality risk in hospitalized older patients. *Aging Cell* **12**, 459–466 (2013).

83. Erlandson, K. M. *et al.* Inflammation, Immune Activation, Immunosenescence, and Hormonal Biomarkers in the Frailty-Related Phenotype of Men With or at Risk for HIV Infection. *The Journal of Infectious Diseases* **215**, 228–237 (2017).

84. Carcaillon, L. *et al.* Higher Levels of Endogenous Estradiol are Associated with Frailty in Postmenopausal Women from the Toledo Study for Healthy Aging. *The Journal of Clinical Endocrinology & Metabolism* **97**, 2898–2906 (2012).

85. Lu, Y. *et al.* Inflammatory and immune markers associated with physical frailty syndrome: findings from Singapore longitudinal aging studies. *Oncotarget* **7**, 28783 (2016).

86. Tsai, J. S. *et al.* Plasma Adiponectin Levels Correlate Positively with an Increasing Number of Components of Frailty in Male Elders. *PLoS ONE* **8**, 56250 (2013).

87. Leng, S. X. *et al.* Serum levels of insulin-like growth factor-I (IGF-I) and dehydroepiandrosterone sulfate (DHEA-S), and their relationships with serum interleukin-6, in the geriatric syndrome of frailty. *Aging Clinical and Experimental Research* **16**, 153–157 (2004).

88. Guan, B. *et al.* Association between thyroid hormone levels and frailty in the community-dwelling oldest-old: a cross-sectional study. *Chin Med J (Engl)* **135**, 1962–1968 (2022).

89. Howard, C. *et al.* Oxidative protein damage is associated with poor grip strength among older women living in the community. *Journal of applied physiology (Bethesda, Md. : 1985)* **103**, 17 (2007).

90. Liu, C. K. *et al.* Biomarkers of oxidative stress are associated with frailty: the Framingham Offspring Study. *AGE* **38**, 1–10 (2016).

91. Inglés, M. *et al.* Oxidative Stress Is Related to Frailty, Not to Age or Sex, in a Geriatric Population: Lipid and Protein Oxidation as Biomarkers of Frailty. *J Am Geriatr Soc* **62**, 1324–1328 (2014).

92. Serviddio, G. *et al.* Frailty syndrome is associated with altered circulating redox balance and increased markers of oxidative stress. *International Journal of Immunopathology and Pharmacology* **22**, 819–827 (2009).

93. Saum, K. U. *et al.* Association between Oxidative Stress and Frailty in an Elderly German Population: Results from the ESTHER Cohort Study. *Gerontology* **61**, 407–415 (2015).

94. Wu, I. C., Shiesh, S. C., Kuo, P. H. & Lin, X. Z. High oxidative stress is correlated with frailty in elderly chinese. *Journal of the American Geriatrics Society* **57**, 1666–1671 (2009).

95. Almeida, O. P., Norman, P. E., Van Bockxmeer, F. M., Hankey, G. J. & Flicker, L. CRP 1846G>A polymorphism increases risk of frailty. *Maturitas* **71**, 261–266 (2012).

96. Matteini, A. M. *et al.* Transcobalamin-II variants, decreased vitamin b12 availability and increased risk of frailty. *The journal of nutrition, health & aging* **14**, 73 (2010).

97. Mekli, K., Marshall, A., Nazroo, J., Vanhoutte, B. & Pendleton, N. Genetic variant of Interleukin-18 gene is associated with the Frailty Index in the English Longitudinal Study of Ageing. *Age and Ageing* **44**, 938 (2015).

98. Mekli, K., Nazroo, J. Y., Marshall, A. D., Kumari, M. & Pendleton, N. Proinflammatory genotype is associated with the frailty phenotype in the English Longitudinal Study of Ageing. *Aging Clinical and Experimental Research* **28**, 413 (2016).

99. Brault, M. E. *et al.* Telomere length and the clinical phenotype of frailty in older adults undergoing cardiac surgery. *Journal of the American Geriatrics Society* **62**, 2205–2207 (2014).

100. Pathai, S. *et al.* Accelerated biological ageing in HIV-infected individuals in South Africa: a case-control study. *AIDS (London, England)* **27**, 2375–2384 (2013).

101. Marzetti, E. *et al.* Shorter Telomeres in Peripheral Blood Mononuclear Cells from Older Persons with Sarcopenia: Results from an Exploratory Study. *Frontiers in Aging Neuroscience* **6**, 1–31 (2014).

102. Saum, K. U. *et al.* Frailty and telomere length: cross-sectional analysis in 3537 older adults from the ESTHER cohort. *Experimental gerontology* **58**, 250–255 (2014).

103. Yu, R., Tang, N., Leung, J. & Woo, J. Telomere length is not associated with frailty in older Chinese elderly: Cross-sectional and longitudinal analysis. *Mechanisms of ageing and development* **152**, 74–79 (2015).

104. Collerton, J. *et al.* Acquisition of aberrant DNA methylation is associated with frailty in the very old: findings from the Newcastle 85+ Study. *Biogerontology* **15**, 317–328 (2014).

105. Bellizzi, D. *et al.* Global DNA methylation in old subjects is correlated with frailty. *Age* **34**, 169 (2012).

106. Valdiglesias, V. *et al.* Exploring Genetic Outcomes as Frailty Biomarkers. *The journals of gerontology. Series A, Biological sciences and medical sciences* **74**, 168–175 (2019).

107. Darvin, K. *et al.* Plasma protein biomarkers of the geriatric syndrome of frailty. *The journals of gerontology. Series A, Biological sciences and medical sciences* **69**, 182–186 (2014).

108. Reiner, A. P. *et al.* Inflammation and thrombosis biomarkers and incident frailty in postmenopausal women. *The American journal of medicine* **122**, 947–954 (2009).

109. Sanchis, J. *et al.* Usefulness of Clinical Data and Biomarkers for the Identification of Frailty After Acute Coronary Syndromes. *The Canadian journal of cardiology* **31**, 1462–1468 (2015).

110. Kuro-o, M. Klotho and aging. *Biochimica et biophysica acta* **1790**, 1049–1058 (2009).

111. Shardell, M. *et al.* Plasma Klotho and Frailty in Older Adults: Findings From the InCHIANTI Study. *The journals of gerontology. Series A, Biological sciences and medical sciences* **74**, 1052–1058 (2019).

112. Pan, Y., Ji, T., Li, Y. & Ma, L. Omics biomarkers for frailty in older adults. *Clinica Chimica Acta* **510**, 363–372 (2020).

113. Ramakrishnan, P. *et al.* A systematic review of studies comparing potential biochemical biomarkers of frailty with frailty assessments. *European Geriatric Medicine* **8**, 397–407 (2017).

114. Nishimoto, N. *et al.* Mechanisms and pathologic significances in increase in serum interleukin-6 (IL-6) and soluble IL-6 receptor after administration of an anti–IL-6 receptor antibody, tocilizumab, in patients with rheumatoid arthritis and Castleman disease. *Blood* **112**, 3959–3964 (2008).

115. Heinze-Milne, S. D., Banga, S. & Howlett, S. E. Frailty and cytokines in preclinical models: Comparisons with humans. *Mechanisms of Ageing and Development* **206**, 111706 (2022).

116. Gonçalves, R. S. dos S. A., Maciel, Á. C. C., Rolland, Y., Vellas, B. & de Souto Barreto, P. Frailty biomarkers under the perspective of geroscience: A narrative review. *Ageing Research Reviews* **81**, 101737 (2022).

117. Franceschi, C. *et al.* Inflamm-aging: An Evolutionary Perspective on Immunosenescence. *Annals of the New York Academy of Sciences* **908**, 244–254 (2000).

118. Ferrucci, L. & Fabbri, E. Inflammageing: chronic inflammation in ageing, cardiovascular disease, and frailty. (2018) doi:10.1038/s41569-018-0064-2.

119. Moinuddin, Z. & Dhanda, R. Anatomy of the kidney and ureter. *Anaesthesia & Intensive Care Medicine* **16**, 247–252 (2015).

120. Eckardt, K. U. *et al.* Evolving importance of kidney disease: from subspecialty to global health burden. *Lancet (London, England)* **382**, 158–169 (2013).

121. Acharya, V. & Olivero, J. The Kidney as an Endocrine Organ. *METHODIST DEBAKEY CARDIOVASC J* | **14**, (2018).

122. Wallace, M. A. Anatomy and Physiology of the Kidney. *AORN Journal* **68**, 799–820 (1998).

123. Gounden, V., Bhatt, H. & Jialal, I. Renal Function Tests. *StatPearls* (2022).

124. Bjornstad, P., Karger, A. B. & Maahs, D. M. Measured GFR in Routine Clinical Practice – The Promise of Dried Blood Spots. *Advances in chronic kidney disease* **25**, 76 (2018).

125. Ferguson, M. A. & Waikar, S. S. Established and Emerging Markers of Kidney Function. *Clinical Chemistry* **58**, 680–689 (2012).

126. Smith, H. W. *The Kidney: Structure and Function in Health and Disease*. (Oxford University Press, 1951).

127. Filler, G. *et al.* Cystatin C as a marker of GFR--history, indications, and future research. *Clinical biochemistry* **38**, 1–8 (2005).

128. Van Der Velde, M. *et al.* Lower estimated glomerular filtration rate and higher albuminuria are associated with all-cause and cardiovascular mortality. A collaborative meta-analysis of high-risk population cohorts. *Kidney international* **79**, 1341–1352 (2011).

129. Garza, A. Z., Park, S. B. & Kocz, R. *Drug Elimination*. (StatPearls, 2023).

130. Miners, J. O., Yang, X., Knights, K. M. & Zhang, L. The Role of the Kidney in Drug Elimination: Transport, Metabolism, and the Impact of Kidney Disease on Drug Clearance. *Clinical Pharmacology and Therapeutics* **102**, 436–449 (2017).

131. Knights, K. M., Rowland, A. & Miners, J. O. Renal drug metabolism in humans: The potential for drug-endobiotic interactions involving cytochrome P450 (CYP) and UDP-glucuronosyltransferase (UGT). *British Journal of Clinical Pharmacology* **76**, 587–602 (2013).

132. Denic, A., Glassock, R. J. & Rule, A. D. Structural and Functional Changes With the Aging Kidney. *Advances in Chronic Kidney Disease* **23**, 19–28 (2016).

133. Melsom, T. *et al.* Sex Differences in Age-Related Loss of Kidney Function. *Journal of the American Society of Nephrology* **33**, 1891–1902 (2022).

134. Rule, A. D. *et al.* Measured and estimated GFR in healthy potential kidney donors. *American Journal of Kidney Diseases* **43**, 112–119 (2004).

135. Glassock, R. J. & Winearls, C. Ageing and the Glomerular Filtration Rate: Truths and Consequences. *Transactions of the American Clinical and Climatological Association* **120**, 419 (2009).

136. Kellum, J. A. *et al.* Acute kidney injury. *Nature reviews. Disease primers* **7**, (2021).

137. Romagnani, P. *et al.* Chronic kidney disease. *Nature Reviews Disease Primers 2017 3:1* **3**, 1–24 (2017).

138. Chen, T. K., Knicely, D. H. & Grams, M. E. Chronic Kidney Disease Diagnosis and Management: A Review. *JAMA* **322**, 1294–1304 (2019).

139. Pannu, N. Bidirectional relationships between acute kidney injury and chronic kidney disease. *Current Opinion in Nephrology and Hypertension* **22**, 351–356 (2013).

140. Iseki, K. Factors influencing the development of end-stage renal disease. *Clinical and Experimental Nephrology* **9**, 5–14 (2005).

141. Maher, D., Ailabouni, N., Mangoni, A. A., Wiese, M. D. & Reeve, E. Alterations in drug disposition in older adults: a focus on geriatric syndromes. *Expert Opinion on Drug Metabolism & Toxicology* **17**, 41–52 (2021).

142. Mühlberg, W. & Platt, D. Age-Dependent Changes of the Kidneys: Pharmacological Implications. *Gerontology* **45**, 243–253 (1999).

143. Kinirons, M. T. & O'Mahony, M. S. Drug metabolism and ageing. *British Journal of Clinical Pharmacology* **57**, 540–544 (2004).

144. Miners, J. O. & Mackenzie, P. I. Drug glucuronidation in humans. *Pharmacology & Therapeutics* **51**, 347–369 (1991).

145. Levey, A. S., Astor, B. C., Stevens, L. A. & Coresh, J. Chronic kidney disease, diabetes, and hypertension: what's in a name? *Kidney International* **78**, 19–22 (2010).

146. Prasad, R. Metabolic syndrome and chronic kidney disease: Current status and future directions. *World J Nephrol* **3**, 210–219 (2014).

147. Takemon, Y. *et al.* Proteomic and transcriptomic profiling reveal different aspects of aging in the kidney. *eLife* **10**, (2021).

148. GEO Accession viewer. https://www.ncbi.nlm.nih.gov/geo/query/acc.cgi?acc=GSE121330.

149. Schroeder, A. *et al.* The RIN: An RNA integrity number for assigning integrity values to RNA measurements. *BMC Molecular Biology* **7**, 1–14 (2006).

150. Dobin, A. *et al.* STAR: ultrafast universal RNA-seq aligner. *Bioinformatics* **29**, 15 (2013).

151. Williams, A. G., Thomas, S., Wyman, S. K. & Holloway, A. K. RNA-seq Data: Challenges in and Recommendations for Experimental Design and Analysis. *Current protocols in human genetics / editorial board, Jonathan L. Haines ... [et al.]* **83**, 11.13.1 (2014).

152. Dobin, A. & Gingeras, T. R. Optimizing RNA-seq mapping with STAR. *Methods in Molecular Biology* **1415**, 245–262 (2016).

153. Mus_musculus - Ensembl genome browser 109. https://useast.ensembl.org/Mus_musculus/Info/Annotation.

154. Putri, G. H., Anders, S., Pyl, P. T., Pimanda, J. E. & Zanini, F. Analysing high-throughput sequencing data in Python with HTSeq 2.0. *Bioinformatics* **38**, 2943–2945.

155. Gentleman, R. C. *et al.* Bioconductor: open software development for computational biology and bioinformatics. *Genome Biology 2004 5:10* **5**, 1–16 (2004).

156. Robinson, M. D. & Oshlack, A. A scaling normalization method for differential expression analysis of RNA-seq data. *Genome Biology* **11**, 1–9 (2010).

157. Kanehisa, M. & Goto, S. KEGG: Kyoto Encyclopedia of Genes and Genomes. *Nucleic Acids Research* **28**, 27–30 (2000).

158. Smyth, G. K. Linear models and empirical bayes methods for assessing differential expression in microarray experiments. *Statistical Applications in Genetics and Molecular Biology* **3**, (2004).

159. Law, C. W. *et al.* A guide to creating design matrices for gene expression experiments. *F1000Research* **9**, (2020).

160. Smyth, G. K. *et al.* RNA-seq analysis is easy as 1-2-3 with limma, Glimma and edgeR. *F1000Research* **5**, (2016).

161. Benjamini, Y. & Hochberg, Y. Controlling the False Discovery Rate: A Practical and Powerful Approach to Multiple Testing. *Journal of the Royal Statistical Society: Series B (Methodological)* **57**, 289–300 (1995).

162. Storey, J. D. The positive false discovery rate: a Bayesian interpretation and the q-value. *https://doi.org/10.1214/aos/1074290335* **31**, 2013–2035 (2003).

163. Yokoyama, T. *et al.* Identification of reference genes for quantitative PCR analyses in developing mouse gonads. doi:10.1292/jvms.18-0417.

164. Validated Antibodies, cDNA Clones, Lentivirus, RNAi | OriGene. https://www.origene.com/.

165. Ming, Y. N. *et al.* Liquid chromatography mass spectrometry-based profiling of phosphatidylcholine and phosphatidylethanolamine in the plasma and liver of acetaminophen-induced liver injured mice. *Lipids in Health and Disease 2017 16:1* **16**, 1–11 (2017).

166. Ye, J. *et al.* Primer-BLAST: a tool to design target-specific primers for polymerase chain reaction. *BMC bioinformatics* **13**, 134 (2012).

167. Yue, F. *et al.* A comparative encyclopedia of DNA elements in the mouse genome. *Nature* **515**, 355–364 (2014).

168. Taylor, S., Wakem, M., Dijkman, G., Alsarraj, M. & Nguyen, M. A practical approach to RT-qPCR—Publishing data that conform to the MIQE guidelines. *Methods* **50**, S1–S5 (2010).

169. Davarinejad, H. Quantifications of Western Blots with ImageJ.

170. Desjardins, P. & Conklin, D. NanoDrop Microvolume Quantitation of Nucleic Acids. *JoVE (Journal of Visualized Experiments)* e2565 (2010) doi:10.3791/2565.

171. Puchta, M., Boczkowska, M. & Groszyk, J. Low RIN Value for RNA-Seq Library Construction from Long-Term Stored Seeds: A Case Study of Barley Seeds. *Genes* **11**, 1–15 (2020).

172. Imbeaud, S. *et al.* Towards standardization of RNA quality assessment using user-independent classifiers of microcapillary electrophoresis traces. *Nucleic acids research* **33**, 1–12 (2005).

173. Wang, L. *et al.* Measure transcript integrity using RNA-seq data. *BMC bioinformatics* **17**, (2016).

174. Dalman, M. R., Deeter, A., Nimishakavi, G. & Duan, Z. H. Fold change and p-value cutoffs significantly alter microarray interpretations. *BMC bioinformatics* **13 Suppl 2**, 1–4 (2012).

175. Tuttle, A. H., Philip, V. M., Chesler, E. J. & Mogil, J. S. Comparing phenotypic variation between inbred and outbred mice. *Nat Methods* **15**, 994–996 (2018).

176. Rogers-Broadway, K. R. & Karteris, E. Amplification efficiency and thermal stability of qPCR instrumentation: Current landscape and future perspectives. *Experimental and Therapeutic Medicine* **10**, 1261–1264 (2015).

177. Kalyani, R. R., Varadhan, R., Weiss, C. O., Fried, L. P. & Cappola, A. R. Frailty Status and Altered Glucose-Insulin Dynamics. *The Journals of Gerontology: Series A* **67**, 1300–1306 (2012).

178. Goulet, E. D. B. *et al.* Frailty in the elderly is associated with insulin resistance of glucose metabolism in the postabsorptive state only in the presence of increased abdominal fat. *Experimental Gerontology* **44**, 740–744 (2009).

179. Parker, J. *et al.* Levels of vitamin D and cardiometabolic disorders: Systematic review and meta-analysis. *Maturitas* **65**, 225–236 (2010).

180. Tang, Z. *et al.* Co-occurrence of cardiometabolic diseases and frailty in older Chinese adults in the Beijing Longitudinal Study of Ageing. *Age and Ageing* **42**, 346–351 (2013).

181. Chevalier, S., Gougeon, R., Nayar, K. & Morais, J. A. Frailty amplifies the effects of aging on protein metabolism: role of protein intake. *The American Journal of Clinical Nutrition* **78**, 422–429 (2003).

182. Evans, W. J. *et al.* Frailty and muscle metabolism dysregulation in the elderly. doi:10.1007/s10522-010-9297-0.

183. Rattray, N. J. W. *et al.* Metabolic dysregulation in vitamin E and carnitine shuttle energy mechanisms associate with human frailty. *Nature Communications 2019 10:1* **10**, 1–12 (2019).

184. Sheetz, T. & Lee, C. T. Frailty and geriatric assessment in urologic oncology. *Current Opinion in Urology* **28**, 233–242 (2018).

185. Fassett, R. G. *et al.* Biomarkers in chronic kidney disease: a review. *Kidney International* **80**, 806–821 (2011).

186. Morrissey, J. J., London, A. N., Luo, J. & Kharasch, E. D. Urinary biomarkers for the early diagnosis of kidney cancer. *Mayo Clinic proceedings* **85**, 413–421 (2010).

187. Kim, K. *et al.* Urine metabolomic analysis identifies potential biomarkers and pathogenic pathways in kidney cancer. *OMICS A Journal of Integrative Biology* **15**, 293–303 (2011).

188. Campi, R. *et al.* Novel Liquid Biomarkers and Innovative Imaging for Kidney Cancer Diagnosis: What Can Be Implemented in Our Practice Today? A Systematic Review of the Literature. *European Urology Oncology* **4**, 22–41 (2021).

189. Huang, H., Li, Y., Liang, J. & Finkelman, F. D. Molecular regulation of histamine synthesis. *Frontiers in Immunology* **9**, 355220 (2018).

190. Hirasawa, N. Expression of Histidine Decarboxylase and Its Roles in Inflammation. *International journal of molecular sciences* **20**, (2019).

191. Grange, C. *et al.* Histamine in the kidneys: what is its role in renal pathophysiology? *British Journal of Pharmacology* **177**, 503–515 (2020).

192. Banks, R. O., Inscho, E. W. & Jacobson, E. D. Histamine H1 receptor antagonists inhibit autoregulation of renal blood flow in the dog. *Circulation research* **54**, 527–535 (1984).

193. Laight, D. W., Woodward, B. & Waterfall, J. F. Renal vasodilation to histamine in vitro: Roles of nitric oxide, cyclo-oxygenase products and H2 receptors. *Inflamm Res* **44**, 116–120 (1995).

194. Pini, A. *et al.* Histamine H4 receptor antagonism prevents the progression of diabetic nephropathy in male DBA2/J mice. *Pharmacological research* **128**, 18–28 (2018).

195. Veglia, E. *et al.* Histamine type 1-receptor activation by low dose of histamine undermines human glomerular slit diaphragm integrity. *Pharmacological research* **114**, 27–38 (2016).

196. Noguchi, K. *et al.* Histamine receptor agonist alleviates severe cardiorenal damages by eliciting anti-inflammatory programming. *Proceedings of the National Academy of Sciences of the United States of America* **117**, 3150–3156 (2020).

197. Hass, C., Panda, B. P., Khanam, R., Najmi, A. K. & Akhtar, M. Histamine H3 Receptor Agonist Imetit Attenuated Isoproterenol Induced Renin Angiotensin System and Sympathetic Nervous System Overactivity in Myocardial Infarction of Rats. *Drug research* **66**, 324–329 (2016).

198. Yamasaki, T., Tamai, I. & Matsumura, Y. Activation of histamine H3 receptors inhibits renal noradrenergic neurotransmission in anesthetized dogs. *American journal of physiology. Regulatory, integrative and comparative physiology* **280**, (2001).

199. Shimada, H., Miura, K. & Imamura, Y. Characteristics and inhibition by flavonoids of 20α-hydroxysteroid dehydrogenase activity in mouse tissues. *Life Sciences* **78**, 2931–2936 (2006).

200. Imamura, Y., Ohtaguro, M. & Shimada, H. Several distinct enzymes catalyze 20-hydroxysteroid dehydrogenase activity in mouse liver and kidney. *Journal of Steroid Biochemistry & Molecular Biology* **107**, 120–126 (2007).

201. Vergnes, L., Phan, J., Stolz, A. & Reue, K. A cluster of eight hydroxysteroid dehydrogenase genes belonging to the aldo-keto reductase supergene family on mouse chromosome 13. *Journal of Lipid Research* **44**, 503–511 (2003).

202. Barski, O. A., Tipparaju, S. M. & Bhatnagar, A. The aldo-keto reductase superfamily and its role in drug metabolism and detoxification. *Drug metabolism reviews* **40**, 553–624 (2008).

203. Piekorz, R. P., Gingras, S., Hoffmeyer, A., Ihle, J. N. & Weinstein, Y. Regulation of Progesterone Levels during Pregnancy and Parturition by Signal Transducer and Activator of Transcription 5 and 20α-Hydroxysteroid Dehydrogenase. *Molecular Endocrinology* **19**, 431–440 (2005).

204. Stolz, A. *et al.* cDNA cloning and expression of the human hepatic bile acid-binding protein. A member of the monomeric reductase gene family. *Journal of Biological Chemistry* **268**, 10448–10457 (1993).

205. Penning, T. M., Wangtrakuldee, P. & Auchus, R. J. Structural and Functional Biology of Aldo-Keto Reductase Steroid-Transforming Enzymes. *Endocr Rev* **40**, 447–475 (2018).

206. Deyashiki, Y. *et al.* Molecular cloning and characterization of mouse estradiol 17β-dehydrogenase (A-specific), a member of the aldoketoreductase family. *Journal of Biological Chemistry* **270**, 10461–10467 (1995).

207. Suzuki-Yamamoto, T. *et al.* cDNA cloning, expression and characterization of human prostaglandin F synthase. *FEBS Letters* **462**, 335–340 (1999).

208. Jez, J. M. & Penning, T. M. The aldo-keto reductase (AKR) superfamily: An update. *Chemico-Biological Interactions* **130–132**, 499–525 (2001).

209. Mindnich, R. D. & Penning, T. M. Aldo-keto reductase (AKR) superfamily: genomics and annotation. *Human genomics* **3**, 362–370 (2009).

210. Henderson, B. E. & Feigelson, H. S. Hormonal carcinogenesis The key distinction between this ‘cell proliferation’ model. *Carcinogenesis* **21**, 427–433 (2000).

211. Rižner, T. L. & Penning, T. M. Role of aldo-keto reductase family 1 (AKR1) enzymes in human steroid metabolism. (2013) doi:10.1016/j.steroids.2013.10.012.

212. Huang, K.-H. *et al.* Overexpression of aldo-keto reductase 1C2 is associated with disease progression in patients with prostatic cancer. *Histopathology* **57**, 384–394 (2010).

213. Ji, Q. *et al.* Selective Loss of AKR1C1 and AKR1C2 in Breast Cancer and Their Potential Effect on Progesterone Signaling. *Cancer Research* **64**, 7610–7617 (2004).

214. Kljun, J. *et al.* Ruthenium complexes show potent inhibition of AKR1C1, AKR1C2, and AKR1C3 enzymes and anti-proliferative action against chemoresistant ovarian cancer cell line. (2022) doi:10.3389/fphar.2022.920379.

215. Rižner, T. L., Tinašmuc, T. T., Rupreht, R., Jasnašinkovec, J. J. & Penning, T. M. AKR1C1 and AKR1C3 may determine progesterone and estrogen ratios in endometrial cancer. *Molecular and Cellular Endocrinology* **248**, 126–135 (2006).

216. Thierer, J. H. *et al.* Pla2g12b is Essential for Expansion of Nascent Lipoprotein Particles. *bioRxiv* 2022.08.02.502564 (2022) doi:10.1101/2022.08.02.502564.

217. Rouault, M., Bollinger, J. G., Lazdunski, M., Gelb, M. H. & Lambeau, G. Novel Mammalian Group XII Secreted Phospholipase A 2 Lacking Enzymatic Activity †, ‡. (2003) doi:10.1021/bi0349930.

218. Six, D. A. & Dennis, E. A. The expanding superfamily of phospholipase A 2 enzymes: classi¢cation and characterization.

219. Guan, M., Qu, L., Tan, W., Chen, L. & Wong, C.-W. Hepatocyte Nuclear Factor-4 Alpha Regulates Liver Triglyceride Metabolism in Part Through Secreted Phospholipase A 2 GXIIB. *HEPATOLOGY* **53**, 458–466 (2011).

220. Aljakna, A. *et al.* Pla2g12b and Hpn are genes identified by mouse ENU mutagenesis that affect HDL cholesterol. *PloS one* **7**, (2012).

221. Liu, Q. *et al.* Activation of farnesoid X receptor promotes triglycerides lowering by suppressing phospholipase A2 G12B expression. *Mol Cell Endocrinol* **436**, 93–101 (2016).

222. Chen, L. *et al.* Estrogen-related receptor γ regulates hepatic triglyceride metabolism through phospholipase A2 G12B. *FASEB J* **33**, 7942–7952 (2019).

223. Huang, F., Wang, K. & Shen, J. Lipoprotein-associated phospholipase A2: The story continues. *Medicinal Research Reviews* **40**, 79–134 (2020).

224. Gai, Z. *et al.* Lipid Accumulation and Chronic Kidney Disease. *Nutrients* **11**, (2019).

225. De Vries, A. P. J. *et al.* Fatty kidney: emerging role of ectopic lipid in obesity-related renal disease. *The Lancet Diabetes & Endocrinology* **2**, 417–426 (2014).

226. Muller, D. N. *et al.* Mouse Cyp4a isoforms: enzymatic properties, gender- and strain-specific expression, and role in renal 20-hydroxyeicosatetraenoic acid formation. *Biochemical Journal* **403**, 109 (2007).

227. Heng, Y. M. *et al.* A novel murine P-450 gene, Cyp4a14, is part of a cluster of Cyp4a and Cyp4b, but not of CYP4F, genes in mouse and humans. *Biochemical Journal* **325**, 741 (1997).

228. Holla, V. R. *et al.* Alterations in the regulation of androgen-sensitive Cyp 4a monooxygenases cause hypertension. *Proceedings of the National Academy of Sciences of the United States of America* **98**, 5211–5216 (2001).

229. Brouillette, J., Rivard, K., Lizotte, E. & Fiset, C. Sex and strain differences in adult mouse cardiac repolarization: Importance of androgens. *Cardiovascular Research* **65**, 148–157 (2005).

230. Simpson, A. E. C. M. The cytochrome P450 4 (CYP4) family. *General Pharmacology: The Vascular System* **28**, 351–359 (1997).

231. Bellamine, A. *et al.* Characterization of the CYP4A11 gene, a second CYP4A gene in humans. *Archives of Biochemistry and Biophysics* **409**, 221–227 (2003).

232. Gainer, J. V. *et al.* Functional variant of CYP4A11 20-hydroxyeicosatetraenoic acid synthase is associated with essential hypertension. *Circulation* **111**, 63–69 (2005).

233. Capdevila, J. H., Falck, J. R. & Imig, J. D. Roles of the cytochrome P450 arachidonic acid monooxygenases in the control of systemic blood pressure and experimental hypertension. *Kidney International* **72**, 683–689 (2007).

234. Dordea, A. C. *et al.* Androgen-sensitive hypertension associated with soluble guanylate cyclase-α1 deficiency is mediated by 20-HETE. *American Journal of Physiology - Heart and Circulatory Physiology* **310**, H1790–H1800 (2016).

235. Zhang, C. *et al.* Conflicting roles of 20-HETE in hypertension and renal end organ damage. doi:10.1016/j.ejphar.2018.06.010.

236. Lasker, J. M. *et al.* Formation of 20-hydroxyeicosatetraenoic acid, a vasoactive and natriuretic eicosanoid, in human kidney. Role of Cyp4F2 and Cyp4A11. *The Journal of biological chemistry* **275**, 4118–4126 (2000).

237. Pichai, E. & Lakshmanan, M. Drug Elimination. *Introduction to Basics of Pharmacology and Toxicology: Volume 1: General and Molecular Pharmacology: Principles of Drug Action* 117–129 (2022) doi:10.1007/978-981-32-9779-1_8.

238. Miners, J. O., MacKenzie, P. I. & Knights, K. M. The prediction of drug-glucuronidation parameters in humans: UDP-glucuronosyltransferase enzyme-selective substrate and inhibitor probes for reaction phenotyping and in vitro-in vivo extrapolation of drug clearance and drug-drug interaction potential. *Drug metabolism reviews* **42**, 196–208 (2010).

239. ALEXANIAN, A., MILLER, B., ROMAN, R. J. & SOROKIN, A. 20-HETE-producing Enzymes Are Up-regulated in Human Cancers. *Cancer Genomics & Proteomics* **9**, (2012).

240. Capdevila, J. H. & Falck, J. R. Biochemical and molecular characteristics of the cytochrome P450 arachidonic acid monooxygenase. *Prostaglandins and Other Lipid Mediators* **62**, 271–292 (2000).

241. McGiff, J. C. & Quilley, J. 20-HETE and the kidney: resolution of old problems and new beginnings. *The American journal of physiology* **277**, (1999).

242. Roman, R. J. P-450 metabolites of arachidonic acid in the control of cardiovascular function. *Physiological reviews* **82**, 131–185 (2002).

243. Wu, C. C., Gupta, T., Garcia, V., Ding, Y. & Schwartzman, M. L. 20-HETE and Blood Pressure Regulation: Clinical Implications. *Cardiology in review* **22**, 1 (2014).

244. Lin, F., Abraham, N. G. & Schwartzman, M. L. Cytochrome P450 arachidonic acid omega-hydroxylation in the proximal tubule of the rat kidney. *Annals of the New York Academy of Sciences* **744**, 11–24 (1994).

245. Roman, R. J. & Alonso-Galicia, M. P-450 eicosanoids: A novel signaling pathway regulating renal function. *News in Physiological Sciences* **14**, 238–242 (1999).

246. Arima, S., Omata, K., Ito, S., Tsunoda, K. & Abe, K. 20-HETE Requires Increased Vascular Tone to Constrict Rabbit Afferent Arterioles. *Hypertension* **27**, 781–785 (1996).

247. Garcia, V. *et al.* 20-HETE Signals Through G-Protein-Coupled Receptor GPR75 (Gq) to Affect Vascular Function and Trigger Hypertension. *Circulation research* **120**, 1776–1788 (2017).

248. Barden, A. E. *et al.* N-3 fatty acids reduce plasma 20-hydroxyeicosatetraenoic acid and blood pressure in patients with chronic kidney disease. *Journal of Hypertension* **33**, 1947–1953 (2015).

249. Dunn, K. M. *et al.* Elevated production of 20-HETE in the cerebral vasculature contributes to severity of ischemic stroke and oxidative stress in spontaneously hypertensive rats. *American Journal of Physiology - Heart and Circulatory Physiology* **295**, 2455–2465 (2008).

250. Gilani, A. *et al.* 20-HETE interferes with insulin signaling and contributes to obesity-driven insulin resistance. *Prostaglandins & Other Lipid Mediators* **152**, 106485 (2021).

251. Park, F., Sweeney, W. E., Jia, G., Roman, R. J. & Avner, E. D. 20-HETE mediates proliferation of renal epithelial cells in polycystic kidney disease. *Journal of the American Society of Nephrology* **19**, 1929–1939 (2008).

252. Mackenzie, P. I. *et al.* Nomenclature update for the mammalian UDP glycosyltransferase (UGT) gene superfamily. *Pharmacogenetics and Genomics* **15**, 677 (2005).

253. Buckley, D. B. & Klaassen, C. D. Tissue- and gender-specific mRNA expression of UDP-glucuronosyltransferases (UGTs) in mice. *Drug metabolism and disposition: the biological fate of chemicals* **35**, 121–127 (2007).

254. Kojima, A., Nadai, M. & Katoh, M. Species and tissue differences in regorafenib glucuronidation. *https://doi.org/10.1080/00498254.2022.2055507* **52**, 129–133 (2022).

255. Oda, S., Nakajima, M., Hatakeyama, M., Fukami, T. & Yokoi, T. Preparation of a Specific Monoclonal Antibody against Human UDP-Glucuronosyltransferase (UGT) 1A9 and Evaluation of UGT1A9 Protein Levels in Human Tissues. *Drug Metabolism and Disposition* **40**, 1620–1627 (2012).

256. Matsumoto, J. *et al.* Significance of UGT1A6, UGT1A9, and UGT2B7 genetic variants and their mRNA expression in the clinical outcome of renal cell carcinoma. *Molecular and Cellular Biochemistry* **478**, 1779–1790 (2023).

257. Margaillan, G. *et al.* Quantitative Profiling of Human Renal UDP-glucuronosyltransferases and Glucuronidation Activity: A Comparison of Normal and Tumoral Kidney Tissues. *Drug Metabolism and Disposition* **43**, 611–619 (2015).

258. Buckley, D. B. & Klaassen, C. D. Induction of Mouse UDP-Glucuronosyltransferase mRNA Expression in Liver and Intestine by Activators of Aryl-Hydrocarbon Receptor, Constitutive Androstane Receptor, Pregnane X Receptor, Peroxisome Proliferator-Activated Receptor α, and Nuclear Factor Erythroid 2-Related Factor 2. *Drug Metabolism and Disposition* **37**, 847 (2009).

259. Jarrar, Y. B. *et al.* Determination of major UDP-glucuronosyltransferase enzymes and their genotypes responsible for 20-HETE glucuronidation. *Journal of Lipid Research* **55**, 2334 (2014).

260. Turgeon, D. *et al.* Glucuronidation of arachidonic and linoleic acid metabolites by human UDP-glucuronosyltransferases. *Journal of Lipid Research* **44**, 1182–1191 (2003).

261. Rowland, A., Miners, J. O. & Mackenzie, P. I. The UDP-glucuronosyltransferases: Their role in drug metabolism and detoxification. *The International Journal of Biochemistry & Cell Biology* **45**, 1121–1132 (2013).

262. Ito, O., Omata, K., Ito, S., Hoagland, K. M. & Roman, R. J. Effects of converting enzyme inhibitors on renal P-450 metabolism of arachidonic acid. *American journal of physiology. Regulatory, integrative and comparative physiology* **280**, (2001).

263. Everaert, C. *et al.* Benchmarking of RNA-sequencing analysis workflows using whole-transcriptome RT-qPCR expression data. *Scientific Reports* **7**, (2017).

264. Goodrick, C. L. Life-span and the inheritance of longevity of inbred mice. *J Gerontol* **30**, 257–263 (1975).

265. Kõks, S. *et al.* Mouse models of ageing and their relevance to disease. *Mechanisms of Ageing and Development* **160**, 41–53 (2016).

266. Wang, J., Wu, G., Chen, L. & Zhang, W. Integrated analysis of transcriptomic and proteomic datasets reveals information on protein expressivity and factors affecting translational efficiency. *Methods in Molecular Biology* **1375**, 123–136 (2016).

267. Labbadia, J. & Morimoto, R. I. The Biology of Proteostasis in Aging and Disease. *https://doi.org/10.1146/annurev-biochem-060614-033955* **84**, 435–464 (2015).

268. Wang, T. *et al.* Arachidonic Acid Metabolism and Kidney Inflammation. *International Journal of Molecular Sciences 2019, Vol. 20, Page 3683* **20**, 3683 (2019).

269. Elshenawy, O. H., Shoieb, S. M., Mohamed, A. & El-Kadi, A. O. S. Clinical Implications of 20-Hydroxyeicosatetraenoic Acid in the Kidney, Liver, Lung and Brain: An Emerging Therapeutic Target. *Pharmaceutics* **9**, (2017).

270. Aprahamian, I. *et al.* Hypertension and frailty in older adults. *The Journal of Clinical Hypertension* **20**, 186–192 (2018).

271. Schmieder, R. E. End Organ Damage In Hypertension. *Deutsches Ärzteblatt International* **107**, 866 (2010).

272. Hollenberg, P. F. Characteristics and common properties of inhibitors, inducers, and activators of CYP enzymes. *https://doi.org/10.1081/DMR-120001387* **34**, 17–35 (2002).

273. Patterson, A. D., Gonzalez, F. J. & Idle, J. R. XENOBIOTIC METABOLISM – A VIEW THROUGH THE METABOLOMETER. *Chemical research in toxicology* **23**, 851 (2010).

274. Zhao, M. *et al.* Cytochrome P450 Enzymes and Drug Metabolism in Humans. *Int J Mol Sci* **22**, 12808 (2021).

275. Ward, N. C. *et al.* Urinary 20-Hydroxyeicosatetraenoic Acid Is Associated With Endothelial Dysfunction in Humans. *Circulation* **110**, 438–443 (2004).

276. Hilmer, S. N. & Kirkpatrick, C. M. J. New Horizons in the impact of frailty on pharmacokinetics: latest developments. *Age and Ageing* **50**, 1054–1063 (2021).

277. Masnoon, N., Shakib, S., Kalisch-Ellett, L. & Caughey, G. E. What is polypharmacy? A systematic review of definitions. *BMC Geriatrics* **17**, 1–10 (2017).

278. Alshogran, O. Y. Pharmacogenetics of aldo-keto reductase 1C (AKR1C) enzymes. *https://doi.org/10.1080/17425255.2017.1376648* **13**, 1063–1073 (2017).

279. Court, M. H. Interindividual variability in hepatic drug glucuronidation: studies into the role of age, sex, enzyme inducers, and genetic polymorphism using the human liver bank as a model system. *http://dx.doi.org/10.3109/03602530903209288* **42**, 209–224 (2010).

280. Graham, M. J. & Lake, B. G. Induction of drug metabolism: Species differences and toxicological relevance. *Toxicology* **254**, 184–191 (2008).

281. Scheen, A. J. Drug-drug interactions with sodium-glucose cotransporters type 2 (SGLT2) inhibitors, new oral glucose-lowering agents for the management of type 2 diabetes mellitus. *Clinical Pharmacokinetics* **53**, 295–304 (2014).